

**DEVELOPING A METHODOLOGY TO ACCOUNT FOR COMMERCIAL MOTOR  
VEHICLES USING MICROSCOPIC TRAFFIC SIMULATION MODELS**

A Dissertation

by

GRANT GEORGE SCHULTZ

Submitted to the Office of Graduate Studies of  
Texas A&M University  
in partial fulfillment of the requirements for the degree of

DOCTOR OF PHILOSOPHY

December 2003

Major Subject: Civil Engineering

**DEVELOPING A METHODOLOGY TO ACCOUNT FOR COMMERCIAL MOTOR  
VEHICLES USING MICROSCOPIC TRAFFIC SIMULATION MODELS**

A Dissertation

by

GRANT GEORGE SCHULTZ

Submitted to Texas A&M University  
in partial fulfillment of the requirements  
for the degree of

DOCTOR OF PHILOSOPHY

Approved as to style and content by:

---

Laurence R. Rilett  
(Chair of Committee)

---

Mark W. Burris  
(Member)

---

Timothy J. Lomax  
(Member)

---

Clifford H. Spiegelman  
(Member)

---

Paul N. Roschke  
(Interim Head of Department)

December 2003

Major Subject: Civil Engineering

## ABSTRACT

Developing a Methodology to Account for Commercial Motor Vehicles Using Microscopic Traffic Simulation Models. (December 2003)

Grant George Schultz, B.S., Brigham Young University;

M.S., Brigham Young University

Chair of Advisory Committee: Dr. Laurence R. Rilett

The collection and interpretation of data is a critical component of traffic and transportation engineering used to establish baseline performance measures and to forecast future conditions. One important source of traffic data is commercial motor vehicle (CMV) weight and classification data used as input to critical tasks in transportation design, operations, and planning. The evolution of Intelligent Transportation System (ITS) technologies has been providing transportation engineers and planners with an increased availability of CMV data. The primary sources of these data are automatic vehicle classification (AVC) and weigh-in-motion (WIM).

Microscopic traffic simulation models have been used extensively to model the dynamic and stochastic nature of transportation systems including vehicle composition. One aspect of effective microscopic traffic simulation models that has received increased attention in recent years is the calibration of these models, which has traditionally been concerned with identifying the “best” parameter set from a range of acceptable values. Recent research has begun the process of automating the calibration process in an effort to accurately reflect the components of the transportation system being analyzed.

The objective of this research is to develop a methodology in which the effects of CMVs can be included in the calibration of microscopic traffic simulation models. The research examines the ITS data available on weight and operating characteristics of CMVs and incorporates this data in the calibration of microscopic traffic simulation models. The research develops a methodology to model CMVs using microscopic traffic simulation models and then utilizes the output of these models to generate the data necessary to quantify the impacts of CMVs on infrastructure, travel time, and emissions.

The research uses advanced statistical tools including principal component analysis (PCA) and recursive partitioning to identify relationships between data collection sites

(i.e., WIM, AVC) such that the data collected at WIM sites can be utilized to estimate weight and length distributions at AVC sites. The research also examines methodologies to include the distribution or measures of central tendency and dispersion (i.e., mean, variance) into the calibration process. The approach is applied using the CORSIM model and calibrated utilizing an automated genetic algorithm methodology.

## **DEDICATION**

This dissertation is dedicated to my family for the support they provided to help me achieve my goal. First, to the one who stands by my side and shares in all of my challenges and success. To the one who encouraged me to continue on and who strengthened me along the way. To my wife, Karen, thanks for your love, your patience, your belief in me, and your endurance with me to the end. And to my children, Jessica, Courtney, and Tyler. Thank you for your encouragement and understanding when Daddy wasn't always there. For your support and love, I will forever be indebted. I love you.

## ACKNOWLEDGEMENTS

I would like to begin by expressing my sincere appreciation to Dr. Larry Rilett, my advisor and chair of my committee for his guidance and support both academically and personally during my time at Texas A&M University. His vision and direction provided the support necessary to achieve my goals.

I would also like to thank my committee members, Dr. Mark Burris, Dr. Tim Lomax, and Dr. Cliff Spiegelman for their guidance, insights, and direction, and for taking the time to work with me and to provide technical expertise to achieve my objectives.

I would like to thank Dr. Kyu-Ok Kim for his willingness to share his ideas and knowledge of the subject matter. I would like to thank Seung-Jun Kim, Srikar Doddi, and Ivan Lorenz for their technical assistance. And to Dr. Josias Zietsman, Dr. William Eisele, and Dr. Paul Carlson, thanks for your insights and the guidance you provided to help me make it through.

I would like to thank the research sponsor, the Texas Higher Education Board, as well as the TransLink<sup>®</sup> Research Program at the Texas Transportation Institute, Texas A&M University for providing the facilities to complete this research.

I would like to thank the Texas Department of Transportation (TxDOT) Transportation Planning and Programming Division (TPP) for the data provided to accomplish this research, especially Ms. Betty Hohensee for all of her help with obtaining the data needed.

Finally, I would like to thank my family. First, to my parents, George and Jean Schultz, thank you for teaching me the value of hard work and always encouraging me to set goals and to work hard to achieve them. And most of all, thanks to my wife Karen, and to my children, Jessica, Courtney, and Tyler for your encouragement, your love, your patience, and your willingness to share me with my research, I am forever grateful.

## TABLE OF CONTENTS

	Page
1. INTRODUCTION.....	1
1.1 Background .....	2
1.1.1 Commercial Motor Vehicles and the Transportation System .....	2
1.1.2 Microscopic Traffic Simulation Models .....	4
1.1.3 Calibration of Microscopic Traffic Simulation Models .....	5
1.1.4 The Connection between Vehicle Composition and Traffic Simulation Models.....	7
1.2 Problem Statement .....	8
1.2.1 Need to Incorporate CMV Weight and Classification ITS Data into Microscopic Traffic Simulation Models .....	8
1.2.2 Need to Develop a Methodology to Calibrate Microscopic Traffic Simulation Models to Account for CMVs.....	8
1.2.3 Need to Generate Accurate Disaggregate Input Data for use in CMV Infrastructure, Travel Time, and Emissions Analyses .....	9
1.3 Research Objectives .....	9
1.4 Statement of Work .....	10
1.4.1 Perform Literature Review.....	10
1.4.2 Identify Data Collection Methodologies .....	10
1.4.3 Analyze Data Collected Using Advanced Statistical Methodologies .....	10
1.4.4 Outline the Relationship between CMVs and Microscopic Traffic Simulation Models.....	11
1.4.5 Develop an Automated Calibration Methodology to Model CMVs and Perform Analysis of Results.....	11
1.4.6 Perform Sensitivity Analysis of Calibrated Models.....	11
1.4.7 Identify Conclusions and Areas for Future Research.....	12
1.5 Contribution of the Research .....	12
1.6 Organization of the Dissertation .....	12
2. LITERATURE REVIEW.....	14
2.1 North America Free Trade Agreement.....	14
2.2 Motor Vehicle Operating Characteristics.....	18
2.2.1 Resistant Forces .....	18
2.2.2 Tractive Effort.....	22
2.2.3 Acceleration Performance.....	25
2.2.4 Deceleration Characteristics.....	27
2.3 Data Collection Methodologies.....	30
2.3.1 Traffic Volume Counts .....	31
2.3.2 Vehicle Classification Counts .....	34
2.3.3 Truck Weight Monitoring .....	41
2.3.4 Weigh-in-Motion Technology .....	47
2.3.5 WIM System Installation and Calibration.....	56
2.4 Statistical Analysis Tools.....	61

	Page
2.4.1 Principal Component Analysis.....	62
2.4.2 Recursive Partitioning.....	68
2.5 Microscopic Traffic Simulation Modeling.....	73
2.5.1 Microscopic Traffic Simulation Models .....	74
2.5.2 Benefits of Microscopic Traffic Simulation Models.....	76
2.5.3 Challenges of Microscopic Traffic Simulation Models .....	76
2.5.4 The Connection between Vehicle Composition and Traffic Simulation Models.....	77
2.6 Optimization Algorithms .....	78
2.6.1 Background on Genetic Algorithm .....	78
2.6.2 Overall Parameter Representation.....	79
2.6.3 Operating Rules for Genetic Algorithms .....	81
2.7 Concluding Remarks .....	83
<b>3. TEXAS CMV DATA COLLECTION.....</b>	<b>85</b>
3.1 Texas Department of Transportation Data Collection Process .....	85
3.1.1 Automatic Traffic Recorder Volume Data.....	87
3.1.2 Accumulative Count Recorder Traffic Data .....	87
3.1.3 Vehicle Classification Data.....	88
3.1.4 Border Trend Traffic Data .....	89
3.1.5 Texas WIM Data Collection Process .....	91
3.2 Texas CMV Size and Weight Regulations.....	93
3.3 Texas WIM Dataset.....	95
3.3.1 Aggregate Dataset Background Analysis.....	98
3.3.2 Disaggregate Data Collection Sites.....	104
3.4 Concluding Remarks .....	110
<b>4. STATISTICAL ANALYSIS OF DATA.....</b>	<b>112</b>
4.1 Principal Component Analysis.....	112
4.1.1 Preliminary Analysis of Data.....	113
4.1.2 Spatial Analysis of Data.....	118
4.1.3 Temporal Analysis of Data .....	130
4.1.4 Summary of Principal Component Analysis Dataset.....	136
4.1.5 Analysis of Vehicle Classification .....	140
4.2 Recursive Partitioning.....	145
4.2.1 Dataset Analysis.....	146
4.2.2 Final Results—FHWA Classification .....	152
4.2.3 Final Results—Texas 6 Classification .....	154
4.3 Concluding Remarks .....	155
<b>5. CMV MICROSCOPIC TRAFFIC SIMULATION .....</b>	<b>157</b>
5.1 Calibration of Microscopic Traffic Simulation Models .....	157
5.2 CORSIM Application of Proposed Methodology .....	161

	Page
5.2.1 Test Network.....	161
5.2.2 Network Coding.....	164
5.3 CORSIM Calibration Parameters.....	167
5.3.1 General Calibration Parameters .....	167
5.3.2 Vehicle Type Calibration Parameters .....	181
5.4 Concluding Remarks .....	197
<b>6. AUTOMATED CALIBRATION METHODOLOGY .....</b>	<b>199</b>
6.1 Genetic Algorithm Calibration Code .....	199
6.2 Parameter Distribution Alternatives.....	201
6.2.1 Lognormal Distribution.....	202
6.2.2 Normal Distribution .....	205
6.3 Evaluation Criteria .....	208
6.3.1 Calibration Data Sources.....	208
6.3.2 Identification of Fitness Function .....	210
6.4 Genetic Algorithm Application Methodology .....	214
6.4.1 Step 1: Initialization of the GA Parameters and Selection of Parent Population .....	214
6.4.2 Step 2: Microscopic Traffic Simulation Model.....	216
6.4.3 Step 3: Evaluate Model Output and Select “New” Parameter Set .....	216
6.4.4 Step 4: Check Stopping Rules.....	216
6.4.5 Step 5: Perform Crossover and Mutation Operations .....	216
6.5 Model Sensitivity Analysis .....	217
6.5.1 Maximum Generation and Population Size .....	218
6.5.2 Probability of Crossover .....	219
6.5.3 Probability of Mutation.....	219
6.5.4 Fitness Function Coefficients.....	220
6.5.5 Origin-Destination Model Selection .....	223
6.5.6 Car-Following Sensitivity Distribution Model Selection.....	225
6.6 Network Calibration.....	229
6.7 Concluding Remarks .....	233
<b>7. SENSITIVITY OF SIMULATION RESULTS .....</b>	<b>235</b>
7.1 Sensitivity Analysis Alternatives .....	235
7.1.1 Calibrated Model (Base) .....	236
7.1.2 Default Parameter Set No Trucks (Alternative 1).....	236
7.1.3 Default Parameter Set Calibrated Distribution (Alternative 2).....	236
7.1.4 Calibrated Parameter Set Default Distribution (Alternative 3).....	237
7.1.5 Calibrated Parameter Set Semi-Trailer Truck with Medium Load (Alternative 4).....	237
7.1.6 Calibrated Parameter Set Semi-Trailer Truck with Full Load (Alternative 5).....	237
7.2 Verification of Simulated Vehicle Distribution .....	237
7.2.1 Background on Verification Process.....	238

	Page
7.2.2	Verification of Analysis Results ..... 239
7.2.3	Conversion to Full Distribution ..... 240
7.3	CMV Sensitivity Analysis..... 242
7.3.1	Objective Function Analysis ..... 242
7.3.2	Volume, Travel Time, and Delay ..... 245
7.3.3	CMV Sensitivity Analysis Results..... 247
7.4	Emissions Analysis ..... 248
7.4.1	Comprehensive Modal Emissions Model Background ..... 248
7.4.2	Emissions Input Data Process ..... 249
7.4.3	Emissions Output Data Process ..... 251
7.4.4	Emissions Analysis Results..... 252
7.5	CMV Growth Sensitivity Analysis ..... 256
7.5.1	Traffic Volume Trends..... 256
7.5.2	Vehicle Composition Trends..... 257
7.5.3	Constant Growth Analysis Results..... 258
7.6	Concluding Remarks ..... 262
8.	CONCLUSIONS AND FUTURE RESEARCH..... 264
8.1	Summary ..... 264
8.1.1	Incorporating CMV ITS Data into Microscopic Traffic Simulation Models... 264
8.1.2	Calibrating Microscopic Traffic Simulation Models to Account for CMVs ... 265
8.1.3	Sensitivity Analysis of CMV Impacts..... 268
8.2	Conclusions ..... 269
8.3	Future Research..... 271
	REFERENCES..... 273
	APPENDIX A GLOSSARY OF FREQUENTLY USED TERMS AND ACRONYMS ..... 288
	APPENDIX B PRELIMINARY ANALYSIS RESULTS ..... 292
	APPENDIX C STATISTICAL ANALYSIS RESULTS ..... 302
	APPENDIX D MICROSCOPIC TRAFFIC SIMULATION ..... 319
	APPENDIX E SENSITIVITY ANALYSIS RESULTS ..... 330
	VITA ..... 332

## LIST OF FIGURES

		Page
FIGURE 1.1	Microscopic traffic simulation model input architecture .....	5
FIGURE 2.1	1990–2001 border truck crossings .....	17
FIGURE 2.2	1990–2001 border vehicle crossings .....	17
FIGURE 2.3	Forces acting on a vehicle .....	19
FIGURE 2.4	Tractive effort, speed, and resistance relationships.....	26
FIGURE 2.5	Speed-distance relationships by vehicle type.....	27
FIGURE 2.6	Typical inductive loop detector design .....	33
FIGURE 2.7	Typical traffic variation by time-of-day .....	35
FIGURE 2.8	Typical traffic variation by day-of-week .....	36
FIGURE 2.9	FHWA vehicle classification scheme .....	38
FIGURE 2.10	Static versus dynamic vehicle weight .....	49
FIGURE 2.11	Typical piezoelectric WIM system design .....	52
FIGURE 2.12	Typical bending plate WIM system design.....	54
FIGURE 2.13	Typical single load cell WIM system design .....	56
FIGURE 2.14	Example scree plot.....	68
FIGURE 2.15	Basic CART regression tree structure.....	70
FIGURE 3.1	Texas 6 vehicle classification.....	90
FIGURE 3.2	TxDOT WIM 2001 operational data collection sites .....	97
FIGURE 3.3	2001 aggregate dataset site distribution .....	99
FIGURE 3.4	2001 aggregate dataset hourly distribution .....	100
FIGURE 3.5	FHWA classification count .....	101
FIGURE 3.6	Texas 6 classification count .....	101
FIGURE 3.7	Aggregate dataset total weight distribution.....	102

	Page
FIGURE 3.8 Aggregate dataset total spacing distribution .....	103
FIGURE 3.9 PZ-074 (US 77) total weight distribution.....	105
FIGURE 3.10 PZ-074 (US 77) total spacing distribution .....	105
FIGURE 3.11 PZ-502 (IH-10) total weight distribution .....	106
FIGURE 3.12 PZ-502 (IH-10) total spacing distribution.....	107
FIGURE 3.13 LW-512 (IH-37) total weight distribution.....	108
FIGURE 3.14 LW-522 (US 281) total weight distribution .....	108
FIGURE 3.15 LW-512 (IH-37) total spacing distribution .....	109
FIGURE 3.16 LW-522 (US 281) total spacing distribution.....	110
FIGURE 4.1 Preliminary analysis PC one score versus PC two score .....	117
FIGURE 4.2 Spatial data analysis PC two score versus PC three score .....	122
FIGURE 4.3 Spatial data analysis box-plot results .....	123
FIGURE 4.4 Spatial data analysis error bar chart .....	126
FIGURE 4.5 Group one box-plot results.....	129
FIGURE 4.6 Group two box-plot results.....	130
FIGURE 4.7 Group one temporal data analysis box-plot results .....	132
FIGURE 4.8 Group two temporal data analysis box-plot results.....	132
FIGURE 4.9 Group one temporal data analysis error bar chart .....	134
FIGURE 4.10 Group two temporal data analysis error bar chart.....	135
FIGURE 4.11 Vehicle classification analysis box-plot results .....	141
FIGURE 4.12 Vehicle classification analysis error bar chart.....	142
FIGURE 4.13 Full dataset relative error results .....	147
FIGURE 4.14 Full dataset three terminal node tree results.....	148
FIGURE 4.15 Full dataset four terminal node tree results .....	148

	Page
FIGURE 4.16 Full dataset five terminal node tree results.....	149
FIGURE 4.17 Full dataset three terminal node box-plot results .....	150
FIGURE 4.18 Full dataset four terminal node box-plot results.....	150
FIGURE 4.19 Full dataset five terminal node box-plot results .....	151
FIGURE 4.20 Final distribution results.....	155
FIGURE 5.1 Proposed calibration methodology.....	160
FIGURE 5.2 Test network locations .....	162
FIGURE 5.3 IH-10 Houston, Texas, test network.....	163
FIGURE 5.4 US 290 Houston, Texas, test network.....	164
FIGURE 5.5 CORSIM car-following headway .....	170
FIGURE 5.6 Space headway sensitivity analysis.....	172
FIGURE 5.7 Time headway sensitivity analysis.....	172
FIGURE 5.8 Lane-change parameters.....	175
FIGURE 5.9 Group A total spacing histogram with normal distribution displayed .....	188
FIGURE 5.10 Group B total spacing histogram with normal distribution displayed.....	188
FIGURE 5.11 Group C total spacing histogram with normal distribution displayed.....	189
FIGURE 5.12 Group A total weight histogram with normal distribution displayed.....	191
FIGURE 5.13 Group B total weight histogram with normal distribution displayed.....	192
FIGURE 5.14 Group C total weight histogram with normal distribution displayed.....	192
FIGURE 5.15 Subgroup C1 total weight histogram with normal distribution displayed.....	194
FIGURE 5.16 Subgroup C2 total weight histogram with normal distribution displayed.....	194
FIGURE 6.1 Lognormal cumulative distribution function.....	204
FIGURE 6.2 Genetic algorithm calibration methodology.....	215
FIGURE 6.3 GA maximum generation and population size sensitivity analysis.....	218

	Page
FIGURE 6.4 GA probability of crossover ( $P_c$ ) sensitivity analysis .....	219
FIGURE 6.5 GA probability of mutation ( $P_m$ ) sensitivity analysis.....	220
FIGURE 6.6 AM peak period $\beta_2$ traffic volume sensitivity analysis .....	222
FIGURE 6.7 AM peak period $\beta_2$ travel time sensitivity analysis.....	223
FIGURE 6.8 Traffic volume analysis—volume only calibration.....	227
FIGURE 6.9 Traffic volume analysis—volume and travel time calibration.....	227
FIGURE 6.10 Discrete distribution analysis results—volume only calibration.....	228
FIGURE 6.11 Discrete distribution analysis results—volume and travel time calibration.....	228
FIGURE 7.1 MAER sensitivity analysis results .....	244
FIGURE 7.2 Fitness value sensitivity analysis results .....	244
FIGURE 7.3 Volume sensitivity analysis results .....	246
FIGURE 7.4 Travel time sensitivity analysis results.....	246
FIGURE 7.5 Constant growth volume sensitivity analysis (AM peak period) .....	259
FIGURE 7.6 Constant growth travel time sensitivity analysis (AM peak period).....	259
FIGURE 7.7 Constant growth volume sensitivity analysis (off peak period).....	261

## LIST OF TABLES

		Page
TABLE 2.1	1990–2001 Border Truck Crossings .....	16
TABLE 2.2	1990–2001 Border Vehicle Crossings .....	16
TABLE 2.3	Truck Deceleration Rates for Use in Highway Design .....	29
TABLE 2.4	FHWA Vehicle Classification Scheme .....	37
TABLE 2.5	ASTM WIM System Classification Summary .....	50
TABLE 2.6	Functional Performance Requirements for WIM Systems.....	50
TABLE 2.7	WIM System Performance and Cost Comparison .....	55
TABLE 3.1	Texas 6 Vehicle Classification Code .....	89
TABLE 3.2	Texas Weigh-in-Motion Site Locations .....	92
TABLE 3.3	State of Texas Legal Length Limits .....	93
TABLE 3.4	State of Texas Legal Height Limits .....	94
TABLE 3.5	State of Texas Permissible Weight Table .....	94
TABLE 3.6	Texas Weigh-in-Motion 2001 Operational Site Locations .....	98
TABLE 4.1	Preliminary Dataset Total Variance Explained.....	115
TABLE 4.2	Preliminary PCA Data Component Matrix .....	116
TABLE 4.3	Example Class 9 Row Entry .....	119
TABLE 4.4	Spatial Data Analysis Total Variance Explained .....	120
TABLE 4.5	Spatial Data Analysis Component Matrix.....	120
TABLE 4.6	Spatial Data Analysis One-Way ANOVA Results .....	125
TABLE 4.7	Spatial Data Analysis Robust Tests of Equality of Variance.....	125
TABLE 4.8	Spatial Data Analysis Pairwise Comparison Results .....	127
TABLE 4.9	Peak Period Categories .....	131
TABLE 4.10	Group One Temporal Data Analysis One-Way ANOVA Results .....	133

	Page
TABLE 4.11	Group Two Temporal Data Analysis One-Way ANOVA Results..... 133
TABLE 4.12	Group One Temporal Data Analysis Pairwise Comparison Results..... 136
TABLE 4.13	Group Two Temporal Data Analysis Pairwise Comparison Results ..... 136
TABLE 4.14	Group One Descriptive Statistics ..... 137
TABLE 4.15	Group Two Descriptive Statistics ..... 137
TABLE 4.16	Group One versus Group Two <i>t</i> -test Equality of Means..... 139
TABLE 4.17	Vehicle Classification Analysis Pairwise Comparison—Full Final Dataset.... 143
TABLE 4.18	Vehicle Classification Analysis Pairwise Comparison—AM Peak..... 143
TABLE 4.19	Vehicle Classification Analysis Pairwise Comparison—Midday Peak ..... 143
TABLE 4.20	Vehicle Classification Analysis Pairwise Comparison—PM Peak..... 144
TABLE 4.21	Vehicle Classification Analysis Pairwise Comparison—Night Peak ..... 144
TABLE 4.22	CART Analysis Results—1 S.E. of Minimum Cost Tree..... 147
TABLE 4.23	Relative Error Comparison—Three Node versus Full Tree..... 151
TABLE 4.24	FHWA Classification Groupings ..... 152
TABLE 4.25	Full Analysis Final Distributions ..... 153
TABLE 4.26	Group A Final Distributions—Full Analysis ..... 153
TABLE 4.27	Group B Final Distributions—Full Analysis ..... 153
TABLE 4.28	Group C Final Distributions—Full Analysis ..... 154
TABLE 4.29	Texas 6 Classification Groupings ..... 154
TABLE 5.1	CORSIM General Calibration Parameters ..... 168
TABLE 5.2	Default Distribution of Car-Following Sensitivity Factors..... 169
TABLE 5.3	Default CORSIM Fleet and Vehicle Types..... 181
TABLE 5.4	CORSIM Vehicle Type Calibration Parameters ..... 182

	Page
TABLE 5.5	INTRAS Calibration Normal Acceleration Rates, $g$ (ft/sec <sup>2</sup> ) by Vehicle Type ..... 184
TABLE 5.6	CORSIM Maximum Acceleration Rate, $g$ (ft/sec <sup>2</sup> ) by Performance Index ..... 184
TABLE 5.7	CORSIM Performance Index Definitions ..... 185
TABLE 5.8	Summary of Total Spacing Distributions for Full Analysis ..... 187
TABLE 5.9	Summary of Total Spacing Distributions ..... 190
TABLE 5.10	Group C Final Distribution Disaggregate Analysis Results ..... 193
TABLE 5.11	Final Distribution for CORSIM Analysis ..... 195
TABLE 5.12	Total Truck Percentage 2001 ..... 197
TABLE 5.13	Truck Percentage by Distribution ..... 197
TABLE 6.1	Calibration Parameter Set ..... 200
TABLE 6.2	Standard Normal Random Variables ..... 207
TABLE 6.3	US 290 Link Travel Time and Speed Data ..... 210
TABLE 6.4	IH-10 Eastbound Link Travel Time and Speed Data ..... 210
TABLE 6.5	Travel Time Fitness Function Sensitivity Analysis Results ..... 221
TABLE 6.6	Origin-Destination Sensitivity Analysis Results ..... 224
TABLE 6.7	Car-Following Sensitivity Analysis Results ..... 225
TABLE 6.8	Base Calibration Model Analysis Results ..... 231
TABLE 6.9	Full Calibration Model Analysis Results ..... 232
TABLE 6.10	Default Calibration Parameter Analysis Results ..... 233
TABLE 7.1	Calibrated Vehicle Distribution Verification Results ..... 239
TABLE 7.2	Default Vehicle Distribution Verification Results ..... 239
TABLE 7.3	Simulated Distribution Results ..... 240
TABLE 7.4	Simulated FHWA Distribution Results ..... 241

	Page
TABLE 7.5 Objective Function Analysis Results .....	243
TABLE 7.6 Network Delay Time Analysis Results .....	245
TABLE 7.7 Vehicle/Technology Modeled Categories .....	251
TABLE 7.8 One-Hour Aggregate Emissions Summary Data—Node 19 to Node 20 .....	252
TABLE 7.9 One-Hour Emissions Descriptive Statistics—Node 19 to Node 20 .....	253
TABLE 7.10 HC Emission Results Pairwise Analysis .....	255
TABLE 7.11 CO Emission Results Pairwise Analysis .....	255
TABLE 7.12 NO <sub>x</sub> Emission Results Pairwise Analysis .....	255
TABLE 7.13 Fuel Emission Results Pairwise Analysis .....	255
TABLE 7.14 IH-10 Katy Freeway Vehicle Composition Trends 1997–2001 .....	258
TABLE 7.15 IH-10 Katy Freeway Truck Distribution Trends 1997–2001 .....	258
TABLE 7.16 Constant Growth Network Delay Results (AM Peak Period) .....	260
TABLE 7.17 Constant Growth Network Delay Results (Off Peak Period) .....	261

## 1. INTRODUCTION

There have been a number of changes over the last decade across the United States that have had a direct effect on the transportation system. One of the most pronounced impacts has occurred as a result of the signing of the North America Free Trade Agreement (NAFTA), which has substantially increased the size and volume of large trucks on the nation's highway system (1). With the signing and subsequent implementation of NAFTA, the need for reliable and accurate estimates of commercial motor vehicles (CMVs) and their effect on the transportation system has become increasingly important. Data on trade between the United States, Canada, and Mexico indicate that from 1993 (the year preceding NAFTA implementation) to 2001, trade among the NAFTA nations increased 109 percent, from \$297 billion to \$622 billion. This equates to nearly \$1.7 billion in trilateral trade every day (1, 2, 3). It is expected that this trend will continue as the NAFTA nations continue to expand their trade relationships, resulting in a continual increase in the number of CMVs on the transportation system.

Microscopic traffic simulation models have been used extensively over the years to model both the dynamic and stochastic nature of transportation systems. Microscopic traffic simulation models that focus on individual vehicles (i.e., CORSIM and VISSIM) are used in transportation operations analyses to analyze the vehicle-to-vehicle and vehicle-to-traffic control interactions. Microscopic traffic simulation models have also more recently been adopted for use in transportation planning applications to provide a more thorough analysis of traffic interaction. This is particularly apparent with the development of the TRansportation ANalysis SIMulation System (TRANSIMS) model developed at the Los Alamos National Laboratory, in Los Alamos, New Mexico, as part of the Travel Model Improvement Program (TMIP).

One of the critical aspects of effective microscopic traffic simulation models is the calibration and validation of the models. Researchers have repeatedly pointed to the need to accurately represent observed traffic conditions in both traffic operations and transportation planning applications as essential to improve not only engineers' and planners' perceptions of the model, but the public perception as well (4, 5, 6, 7, 8, 9). The proper calibration is essential if the model is to accurately replicate both supply and demand characteristics, as well as their interaction.

---

This dissertation follows the style and format of the *Transportation Research Record*.

Recent research has begun the process of automating the calibration process in microscopic traffic simulation models (9). This research, however, has been targeted at automobile traffic and has not included CMVs, a main component of the traffic stream. One of the main reasons for this has been the lack of available data for use in calibration purposes. This has been augmented recently, however, with developments in intelligent transportation system (ITS) technologies that have resulted in the deployment of a number of data collection systems including weigh-in-motion (WIM) to collect data on CMVs. These data collection systems have been utilized to some extent in the existing automated procedures but have not generally included CMV characteristics.

The objective of this dissertation is to develop a methodology in which the effects of CMV characteristics and operations can be included in the calibration and application of microscopic traffic simulation models. This methodology will provide an approach to better represent existing and projected conditions in both transportation planning and traffic operations analyses. The proposed research will examine the ITS data available on weight and operating characteristics of CMVs and will incorporate these data into microscopic traffic simulation models. In addition, the research will develop a methodology to calibrate microscopic traffic simulation models to account for CMVs aiding in quantifying the impacts caused by these vehicles on infrastructure, travel time, and emissions. The methodology was tested on two urban freeway systems in the state of Texas using the microscopic traffic simulation model CORSIM.

## **1.1 Background**

### *1.1.1 Commercial Motor Vehicles and the Transportation System*

A number of changes over the past several years across the United States have had a direct effect on the transportation system. Perhaps one of the biggest was the signing of NAFTA, which substantially increased the size and volume of large trucks on the nation's highway system. With the signing of NAFTA, and the subsequent implementation of this agreement on January 1, 1994, the need for reliable and accurate estimates of CMVs and their effect on the transportation system has become increasingly important. NAFTA opened the borders to a wide range of trade and industry between the United States, Mexico, and Canada. The implementation of NAFTA created the world's largest free trade area, linking nearly 410 million people and producing over \$11 trillion worth of goods and services (1, 2, 3).

The majority of the value of trade that occurs between the United States, Mexico, and Canada is delivered between the three countries through the use of the highway network. The U.S. Department of Transportation (USDOT), Bureau of Transportation Statistics (BTS) reported that in 1999 trucks transported approximately 69 percent of the value of NAFTA merchandise trade, rail transported approximately 14 percent of the share, and air and water modes accounted for approximately 4 to 6 percent (10). More specifically, truck traffic has increased substantially since the implementation of NAFTA, particularly at United States border crossing locations with both Canada and Mexico. In the state of Texas, for example, total truck crossings into Mexico from Texas have increased from 974,017 in 1993 to 2,184,441 in 2001, an overall increase of 124 percent (11). Total truck crossings into Texas from Mexico have also increased during this time from 509,477 in 1993 to 2,239,313 in 2001, an overall increase of 340 percent (12). During the same time as truck crossings were increasing, vehicles crossings into Texas from Mexico only increased by 32 percent, from 30,868,637 in 1993 to 40,723,627 in 2001 (13). Vehicle crossings into Mexico from Texas increased by 26 percent, from 29,853,781 in 1993 to 37,543,677 in 2001, compared to the 124 percent increase in truck traffic (11, 14).

The substantial increase in truck traffic at the Texas–Mexico border points to a need to pay particular attention to CMVs in transportation planning and traffic operations analyses, particularly in Texas and other border states. This is especially true when considering that the origins (destinations) of the trucks exiting (entering) at a specific port of entry are often outside of the port state. The USDOT BTS estimates that over 70 percent of the shipments that cross through the ports of Laredo, Texas, and Buffalo, New York, for example, have their respective origins or destinations outside of Texas or New York (10). This information further increases the need to evaluate the impacts of CMVs on the nation’s highways.

Researchers as early as the 1940s began to recognize the need to pay attention to CMVs, particularly in terms of highway operations. Extensive studies of truck performance have been conducted over the years to determine the separate and combined effects of roadway grade, tractive effort, and gross vehicle weight (GVW). Early research combined with more recent studies have laid the foundation for the investigation of the impact of vehicle weight on tractive effort, acceleration/deceleration, and overall infrastructure investment (15, 16, 17, 18, 19, 20, 21). With the improvements that have been made over the years to improve the weight/power ratio of CMVs, the impact of CMVs operationally has been reduced somewhat; however, the

overall impact of CMVs on infrastructure, travel time characteristics, and emissions must continue to be researched.

Research performed by Eisele and Rilett, for example, on the use of ITS data to estimate travel time mean and variance characteristics, investigated the statistical comparison of CMVs and ITS travel time estimates. In this study, researchers utilized automatic vehicle identification (AVI) data in Houston, Texas, and inductance loop detector (ILD) data in San Antonio, Texas, to compare travel times between the AVI and ILD data to that of CMVs along the same 2.0-mile stretch of the corridor. The results indicated that there was a statistically significant difference between automobile and CMV travel time. In Houston, the average travel time estimates for CMVs were approximately 6 percent higher than the AVI travel time estimates, while in San Antonio, the CMV travel times were approximately 3 percent higher than the ILD travel time estimates. Eisele and Rilett point out that although the mean travel time differences between the vehicular data and the CMVs do not seem large, this difference may become more significant along longer corridors, raising questions about the impacts on just-in-time delivery and fleet operations that operate under strict arrival constraints (22, 23).

### *1.1.2 Microscopic Traffic Simulation Models*

One of the methodologies available to look more closely at the impacts of CMVs on the transportation system is the use of microscopic traffic simulation models. A wide range of microscopic traffic simulation models are readily available to traffic engineers and planners, including models such as CORSIM, TRANSIMS, VISSIM, and others. These models are effective in transportation analyses because of their ability to model the stochastic and dynamic nature of traffic systems. These models are used to estimate and forecast traffic conditions and can be used to provide realistic vehicle trajectories, aiding engineers and planners with more accurate estimates of future network conditions, which can, in turn, lead to better planning of transportation facilities, including roadway improvements and other infrastructure needs.

The basic architecture of microscopic traffic simulation models includes input on the supply and demand of the transportation network as illustrated in Figure 1.1. The supply input includes the links, nodes, and traffic control system. Link attributes include length, grade, and any other distinguishing features of the link (i.e., number of driveways, location of bus stops). Node attributes include x,y location, approach characteristics of the node (i.e., number of lanes, lane width), and so forth. The traffic control system includes the type of intersection control

(i.e., signal control, stop sign control, uncontrolled) and the appropriate attributes of each control type (i.e., signal location, signal timing, stop control). The demand input includes the origin–destination (OD) information or the base traffic volume information necessary for the generation of traffic within the simulation model, and the vehicle routes.

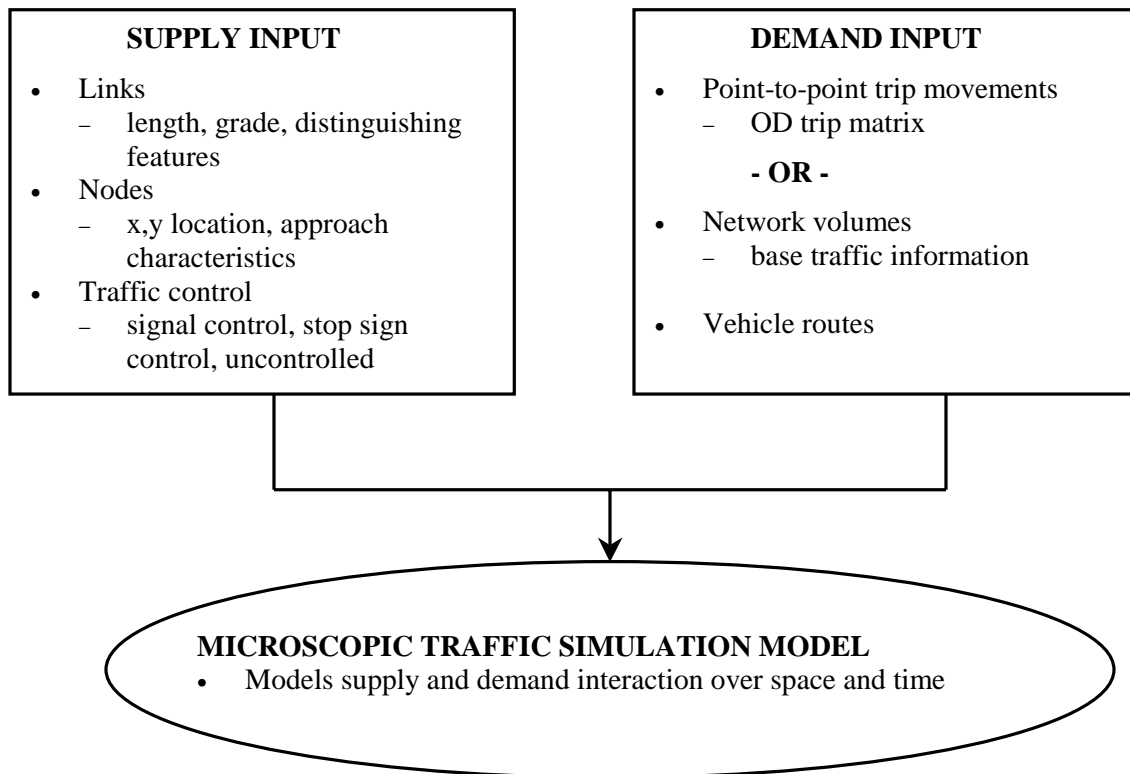


**FIGURE 1.1** Microscopic traffic simulation model input architecture

### 1.1.3 Calibration of Microscopic Traffic Simulation Models

Some of the key components in developing a successful microscopic traffic simulation model are the calibration and subsequent validation of the model. Model calibration is generally defined as the process in which the model parameters are adjusted, such that the model accurately reflects specific components of the system being modeled. Model calibration is essential since engineers and planners utilize these models to accurately portray existing and future conditions through the

proper replication of both supply and demand characteristics, as well as their interactions. Once the model has been calibrated, it can then be validated by utilizing the calibrated model to determine if it provides an accurate representation of field-collected data not used in the calibration process.

Several authors have performed validation and calibration tests on microscopic traffic simulation models to test the validity of the data. Bloomberg and Dale, for example, compare the microscopic simulation models CORSIM and VISSIM on a congested network. The authors indicate that the calibration of the data is key to overcoming potential skepticism regarding the models. While the authors do not include a calibration procedure that takes into account the vehicular composition of the network, they conclude by indicating that a sensitivity analysis of performance measures (i.e., delay, travel time) based on various traffic compositions should be conducted in the future (4). Other reports provide similar results, offering a calibration procedure that does not explicitly account for vehicle composition, while indicating the need for calibration and validation of the models to accurately represent the observed traffic conditions, and to increase not only the engineer and planner perception of the model, but the public perception as well (5, 6, 7, 8, 9).

One of the aspects of calibration of microscopic traffic simulation models is the vehicular composition of the traffic stream and the ability of the model to accurately represent this information. This can be particularly critical in areas where a high percentage of truck traffic exists on a given interstate or arterial roadway (i.e., NAFTA corridor). Research efforts to date appear to have focused primarily on the calibration and subsequent simulation of automobile traffic, rather than focusing on a mixture of vehicle types. When calibrating microscopic traffic simulation models, analysts have generally treated all vehicles equal, or more common yet have relied on default parameters in the model, rather than calibrating the model for existing conditions. One of the reasons for this tendency to exclude calibration by vehicle type could be related to the historic lack of available data necessary to perform this calibration. These data include: 1) an OD estimate for the CMVs that is generally assumed to be different than that of automobile traffic although rarely treated this way; 2) the operating characteristics of the CMV (i.e., tractive effort, resistance, power) and the effect of these characteristics on acceleration, deceleration, and driving behavior; and 3) data on the weight characteristics of the CMVs. Weight characteristics are related to the operating characteristics (i.e., heavier vehicles have slower acceleration); however, they are separate in terms of infrastructure impacts,

primarily the impacts to bridges and pavements as a result of the load factors, and their respective equivalent single-axle load (ESAL) characteristics (24, 25).

With the improvements that have been made in technology and in microscopic traffic simulation modeling in general over the past decade, the importance of calibrating microscopic traffic simulation models is ever increasing, while the technology and availability of data that have come as a result of this technology have made this effort more attainable. In recent research by Kim, for example, an automated calibration methodology for a microscopic traffic simulation model was developed to select the “best” parameter set based on observed ITS data and optimized algorithms (9). Research such as this begins to open the doors for more automated calibration methods in microscopic traffic simulation models, including the opportunity to develop a methodology to make the connection between the ITS data, vehicle characteristics, and the calibration of microscopic traffic simulation models.

#### *1.1.4 The Connection between Vehicle Composition and Traffic Simulation Models*

It is clear that the inclusion of CMVs and their interaction with automobile traffic has become increasingly important in transportation analyses. Additionally, researchers have consistently shown that microscopic traffic simulation models are an important and useful tool in providing information to engineers and planners for both existing and future transportation planning and traffic operational needs. The problem that tends to exist, however, is that these two have not been integrated in the past. Users of microscopic traffic simulation models tend to use default values in their analyses, and when calibration does occur, it does not generally include provisions for vehicle composition. It is assumed that this has been the case in the past due to a paucity of available data, as well as a tendency toward utilizing default parameters, providing more of a comparison across scenarios, rather than an analysis of actual conditions. Several researchers have addressed the need for a more thorough sensitivity analysis of performance measures (i.e., delay and travel time) based on various traffic compositions; however, the methodologies that have been developed to date base calibration primarily on existing characteristics of automobile traffic (5, 7, 8, 9, 26, 27).

The lack of research and guidelines on the connection and interaction between vehicle composition and microscopic traffic simulation models raises some concern about whether the impact CMVs have on the calibration of these models, particularly on corridors with a high percentage of truck volumes, is being adequately addressed. It is anticipated that in areas where

large numbers of trucks are present (i.e., NAFTA corridors), the impact of CMVs and the significant difference in both mean and variance of CMV travel times could have a significant impact on overall model calibration and future planning along these corridors. Additional impacts are also anticipated, including infrastructure impacts as a result of increased frequency and magnitude of axle weights, and environmental impacts due to variations in emissions output that result from different vehicle compositions. The mere fact that current calibration procedures do not include a provision for the analysis of vehicle composition raises the question as to whether or not this should be included as automated calibration procedures are continually improved. The data and literature clearly point to a need to investigate the connection between vehicle composition and microscopic traffic simulation models, and towards the development of a methodology to include CMVs in the calibration of these models.

## **1.2 Problem Statement**

### *1.2.1 Need to Incorporate CMV Weight and Classification ITS Data into Microscopic Traffic Simulation Models*

Researchers have begun to develop procedures to utilize ITS data to develop microscopic traffic simulation models, particularly in the calibration effort (9). This research has focused primarily on the utilization of automobile-related ITS data and has not generally included provision for CMVs or overall vehicle composition. As ITS data are continually made available for both research and application, the opportunities exist to utilize these data in calibration procedures, particularly in terms of CMV weight and classification ITS data. WIM sites, for example, are continually being implemented with higher and higher levels of accuracy (28, 29). With this availability of data comes the need to incorporate CMV ITS data into microscopic traffic simulation models.

### *1.2.2 Need to Develop a Methodology to Calibrate Microscopic Traffic Simulation Models to Account for CMVs*

Once the CMV ITS data are collected, the requirement to determine how to best utilize these data in the calibration of microscopic traffic simulation models needs to be addressed. ITS technologies provide a vast amount of data that can be used for modeling purposes. WIM data, for example, include a wealth of information including data on axle weight, axle spacing,

classification, volume, vehicle composition, and vehicle speed (28, 29, 30). To utilize these data, the information must first be converted to useful truck data, validated based on actual conditions, and then utilized in the model and calibrated according to some known parameter(s). The results of the model can then be used to examine the effects of the vehicle composition on infrastructure (i.e., ESALs), travel time characteristics (i.e., traffic volume, vehicle speed), and emissions. Before this can occur, however, there is a need to develop a systematic methodology to account for CMVs using microscopic traffic simulation models.

### *1.2.3 Need to Generate Accurate Disaggregate Input Data for use in CMV Infrastructure, Travel Time, and Emissions Analyses*

As was stated previously, once the methodology for modeling CMVs in microscopic traffic simulation models has been developed, it then becomes possible to generate disaggregate data that can be used as input to analyze and quantify both the temporal and spatial effects of these vehicles on infrastructure (24), travel time characteristics (22, 23), and emissions. The results of this analysis can then be utilized in both transportation planning and traffic operations analyses. While this dissertation does not specifically examine the impacts, it does provide the input necessary to meet this need.

## **1.3 Research Objectives**

The objective of this research is to develop a methodology in which the effects of CMVs can be included in the calibration and application of microscopic traffic simulation models. The research examines the ITS data available on weight and operating characteristics of CMVs and incorporates these data in the calibration of microscopic traffic simulation models. In addition, the research develops a methodology to model CMVs in microscopic traffic simulation models and to generate the required simulation output necessary to quantify the impacts of these vehicles on infrastructure, travel time characteristics, and emissions. The research provides needed information in the areas of:

- utilization of ITS technologies including WIM, automatic vehicle classification (AVC), automatic traffic recorder (ATR) site, and permanent weigh station data to provide travel time, volume, and weight data necessary for the analysis of CMVs;

- development of a methodology to calibrate microscopic traffic simulation models to account for CMVs; and
- development of accurate disaggregate input necessary to analyze the infrastructure, travel time characteristics, and emissions impacts caused by CMVs.

## **1.4 Statement of Work**

### *1.4.1 Perform Literature Review*

The first task involved the completion of a comprehensive literature review on aspects related to microscopic traffic simulation models and CMVs. The primary areas of focus for the literature review include: 1) NAFTA initiatives and their impact on CMVs, particularly in the state of Texas; 2) operating characteristics of passenger cars and CMVs; 3) data collection methodologies available to aid in the collection of automobile and CMV traffic data; 4) statistical tools to analyze multivariate datasets and make inferences about the analysis results; 5) the use of microscopic traffic simulation models to model the effect of CMVs; and 6) optimization algorithms to calibrate microscopic traffic simulation models. The purpose of this task was to ensure that no research that may contribute to this study is overlooked or unnecessarily duplicated.

### *1.4.2 Identify Data Collection Methodologies*

The purpose of this task was to identify the data collection methodologies and techniques in the state of Texas for the collection of CMV volume, weight, and classification data. Currently, the Texas Department of Transportation (TxDOT) maintains 21 permanent WIM sites within the state of Texas. In addition to the WIM sites, classification data are collected at 650 to 750 locations across the state each year (30, 31). Once the sites were identified, the relationships that exist within these data were explored, primarily through an analysis of data trends found within the Texas WIM dataset.

### *1.4.3 Analyze Data Collected Using Advanced Statistical Methodologies*

The purpose of this task was to utilize advanced statistical analysis tools to explore the relationships that exist in the TxDOT WIM dataset, and to develop a distribution of vehicle

weight and length that adequately represents the data. The statistical analysis tools utilized in this task included primarily: 1) principal component analysis (PCA) and 2) the data-mining tool, Classification and Regression Trees (CART), with additional tools introduced in the analysis as appropriate.

#### *1.4.4 Outline the Relationship between CMVs and Microscopic Traffic Simulation Models*

The purpose of this task was to identify the parameters available in microscopic traffic simulation models to address the needs of both passenger cars and CMVs. To accomplish this purpose, this task included three specific subtasks. The first provided a discussion on the calibration of microscopic traffic simulation models, including a proposed calibration methodology. The second outlined an application of the methodology using the microscopic traffic simulation model CORSIM applied to two specific test networks in Houston, Texas, during the AM peak period, off peak period, and PM peak period. The third subtask identified the calibration parameters available within the microscopic traffic simulation model and provided a methodology to calibrate the parameters based on observed conditions.

#### *1.4.5 Develop an Automated Calibration Methodology to Model CMVs and Perform Analysis of Results*

With the development of the microscopic traffic simulation models, the next task was to implement a calibration optimization methodology and perform a thorough analysis of the simulation results. The purpose of this task was not to develop the calibration optimization methodology itself but to utilize previous calibration research, build upon this research, and provide a methodology to accommodate CMV calibration utilizing microscopic traffic simulation models and automated calibration methodologies. A number of simulation runs were conducted using default parameters in each of the microscopic traffic simulation models and then calibrated based on the optimization methodology chosen for the analysis. Calibration was conducted at a macroscopic level, with analysis of the results conducted at a microscopic level to ensure a consistent, thorough, systematic approach to the analysis.

#### *1.4.6 Perform Sensitivity Analysis of Calibrated Models*

The next task in the analysis was to examine and verify the output from the optimization process in comparison with different calibration parameters and vehicle distributions, and to perform

sensitivity analyses on the objective functions, the operational characteristics (i.e., volume, travel time, delay), and the emissions output for each alternative. In addition, this task included a sensitivity analysis based on forecasted traffic volumes and distributions to examine the impacts of calibration on future analyses.

#### *1.4.7 Identify Conclusions and Areas for Future Research*

The final task of the research work was to identify conclusions and recommendations based upon observations and analysis in each of the tasks above. This task also includes the identification of areas that require additional research.

### **1.5 Contribution of the Research**

This research provides a systematic methodology to modeling CMVs using microscopic traffic simulation models. The approach included the use of ITS data to obtain both vehicle composition and calibration parameters for the model. Some of the main contributions of this research include: 1) an analysis of the impacts of CMVs in the state of Texas, the application of which can be applied to any state; 2) the development of a methodology to identify relationships between data collection sites (i.e., WIM and AVC), such that the data collected at WIM sites can be used to estimate weight and length distributions at AVC sites, increasing the total number of representative sites for critical design, operations, and planning applications; 3) utilization of an automated calibration approach to analyze the effects of CMVs in the traffic stream; 4) provision of an alternative methodology to model the distribution of car-following sensitivity factors in microscopic traffic simulation models using lognormal and normal distributions; and 5) development of an overall methodology for CMV analysis that, although it was applied to a series of highway networks, can be applied to a variety of network alternatives.

### **1.6 Organization of the Dissertation**

The dissertation is organized into eight sections. Section 1 provides an introduction to the research and includes discussion on the background, problem statement, research objectives, statement of work, contribution of the research, and organization of the dissertation. Section 2 provides a detailed literature review outlining the state of the practice of the main topics associated with this research. These topics include a discussion of NAFTA, motor vehicle operating characteristics, data collection methodologies, statistical analysis tools, microscopic

traffic simulation models including the benefits and challenges of using these models, and background on optimization algorithms for use with microscopic traffic simulation models. Section 3 outlines the Texas CMV data collection process and includes an analysis of the Texas WIM dataset. Section 4 outlines a detailed statistical analysis of the WIM dataset including a preliminary analysis of the raw dataset, a spatial analysis of the data, temporal analysis of data, and an analysis of vehicle classification using both PCA and CART. The results of this section identify a distribution of vehicle size and weight characteristics that can be utilized for further analyses. Section 5 identifies the conceptualization of a methodology for the calibration of microscopic traffic simulation models to account for CMVs. The methodology is then applied to two freeway networks in Houston, Texas, using the CORSIM microscopic traffic simulation model. The results of this section identify both general and vehicle-specific calibration parameters for use in CMV simulation. Section 6 outlines a proposed automated calibration methodology to apply to the CORSIM model outlined in Section 5. This analysis includes the adaptation of a genetic algorithm calibration code to account for the additional calibration parameters identified for CMV application. In addition, Section 6 outlines two alternatives for the distribution of car-following sensitivity factors using both lognormal and normal distributions. Finally, this section identifies the sensitivity of calibration optimization parameters and provides final calibrated models for each of the corridors and travel times analyzed. Section 7 includes a sensitivity analysis of the simulation results by comparing the calibrated base model with five alternatives. Each of the alternatives is comprised of different combinations of calibrated parameters and vehicle distributions. This analysis includes a comparison of volume, travel time, and emissions analyses, as well as a discussion of constant growth scenarios. Section 8 provides the summary, conclusions, and recommendations for future research.

In addition to the eight sections, this dissertation also includes five appendices. Appendix A provides a glossary of terms and acronyms used in this dissertation. Appendix B provides summary tables of WIM data collection sites. Appendix C provides statistical analysis results, while Appendix D provides results from the microscopic traffic simulation analyses. Finally, Appendix E summarizes the future trends used in the constant growth scenario sensitivity analysis.

## 2. LITERATURE REVIEW

The problem statement in Section 1 identified three specific needs deemed necessary to account for CMVs using microscopic traffic simulation models. To meet these needs, a detailed statement of work was developed. This section provides a comprehensive literature review on the state-of-the-practice for microscopic traffic simulation models and CMVs necessary to address these needs and to provide the background necessary to accomplish the statement of work. The primary areas of focus for the literature review were: 1) NAFTA initiatives and their impact on CMVs, particularly in the state of Texas; 2) operating characteristics of passenger cars and CMVs; 3) data collection methodologies available to aid in the collection of automobile and CMV traffic data; 4) statistical tools to analyze the data and make inferences about the analysis results; 5) the use of microscopic traffic simulation models to analyze transportation networks; and 6) optimization algorithms to calibrate microscopic traffic simulation models. Each of these topics will be discussed in more detail in the following sections.

### 2.1 North America Free Trade Agreement

As outlined in Section 1, there have been a number of changes over the years across the United States that have had a direct effect on the nation's transportation system, particularly with regard to CMVs and their impact on border states. Research suggests that the United States experienced a nearly five-fold increase in the overall number of CMVs traveling to and from Mexico during the years from 1984 to 2000 (32). The primary influences in this increase were the maquiladora Mexican assembly and manufacturing export operations (33), the General Agreement on Tariffs and Trade (GATT), and NAFTA (32). Arguably, one of the biggest impacts was the signing of NAFTA, which substantially increased the size and volume of large trucks on the nation's highway system. The signing and subsequent implementation of this agreement on January 1, 1994, increased the need for reliable and accurate estimates of CMVs and their effect on the transportation system. NAFTA's implementation created the world's largest free trade area, linking nearly 410 million people and producing over \$11 trillion worth of goods and services. From 1993 (the year preceding NAFTA implementation) to 2001, trade among the NAFTA nations increased 109 percent, from \$297 billion to \$622 billion, nearly \$1.7 billion in trilateral trade every day (1, 2, 3).

When considering the impacts of NAFTA on the transportation system, it is important to note that the USDOT BTS reports that in 1999, trucks transported approximately 69 percent of the value of NAFTA merchandise trade (10). More specifically in the state of Texas, total truck crossings into Mexico from Texas have increased from 974,017 in 1993 to 2,184,441 in 2001, an overall increase of 124 percent, or an average increase of approximately 16 percent per year. Prior to the implementation of NAFTA, truck crossings into Mexico from Texas increased from 553,682 in 1990 (earliest year data are available) to 974,017 in 1993, an overall increase of 76 percent, or approximately 25 percent per year (11). These trends indicate that truck traffic into Mexico from Texas has been increasing both with and without NAFTA in place but that the increase has been even more substantial since NAFTA was signed. During the same time as truck crossings were increasing, vehicle crossings into Mexico from Texas increased by 26 percent overall, or approximately 3 percent per year from 29,853,781 in 1993 to 37,543,677 in 2001. Prior to NAFTA, vehicle crossings into Mexico from Texas increased by 21 percent (7 percent per year) from 24,595,166 in 1990 to 29,853,781 in 1993 (14).

While total truck crossings into Mexico from Texas have not increased as dramatically since the implementation of NAFTA, total truck crossings into Texas from Mexico have increased substantially, completely reversing earlier trends in the data. As reported in Section 1.1.1, total truck crossings into Texas from Mexico have increased from 509,477 in 1993 to 2,239,313 in 2001, an overall increase of 340 percent, or approximately 42 percent per year. The most substantial increase in trucks crossing into Texas from Mexico occurred between 1997 and 1998 when truck crossings jumped from 959,796 to 2,045,136, an increase of 113 percent. Prior to the implementation of NAFTA, truck crossings into Texas from Mexico decreased from 725,784 in 1990 to 509,477 in 1993, a decrease of 30 percent, or 10 percent per year (12). Vehicle crossings into Texas from Mexico increased 32 percent (4 percent per year), from 30,868,637 in 1993 to 40,723,627 in 2001. Prior to NAFTA, vehicle crossings into Texas from Mexico increased by 32 percent (11 percent per year) from 23,371,955 in 1990 to 30,868,637 in 1993 (13). These trends indicate a substantial impact in truck crossings into Texas from Mexico immediately following implementation of NAFTA.

A summary of 1990–2001 border truck crossings both into Texas from Mexico and into Mexico from Texas is provided in Table 2.1, while a summary of 1990–2001 border vehicle crossings both into Texas from Mexico and into Mexico from Texas is provided in Table 2.2. A visual representation of these data is provided in Figure 2.1 for 1990–2001 border truck

crossings and in Figure 2.2 for 1990–2001 border vehicle crossings. It is important to note when comparing Figures 2.1 and 2.2 that the y-axis in Figure 2.2 has a much larger scale and does not include zero in the axis. This is important in considering the slope of the graph and the relationship between the data.

**TABLE 2.1 1990–2001 Border Truck Crossings**

Year	Total Number of Truck Crossings	
	South (into Mexico from Texas)	North (into Texas from Mexico)
1990	553,682	725,784
1991	669,861	674,818
1992	805,706	453,519
1993	974,017	509,477
1994	1,102,446	659,949
1995	909,266	739,981
1996	1,063,643	924,374
1997	1,268,229	959,796
1998	1,945,868	2,045,136
1999	2,114,421	2,314,938
2000	2,253,459	2,383,923
2001	2,184,441	2,239,313

**TABLE 2.2 1990–2001 Border Vehicle Crossings**

Year	Total Number of Vehicle Crossings	
	South (into Mexico from Texas)	North (into Texas from Mexico)
1990	24,595,166	23,371,955
1991	26,289,478	27,341,157
1992	28,145,801	30,213,842
1993	29,853,781	30,868,637
1994	31,000,798	32,222,118
1995	29,093,456	31,688,723
1996	31,697,421	34,305,727
1997	32,958,414	35,663,847
1998	35,464,628	36,979,285
1999	37,880,259	41,329,311
2000	38,579,196	42,168,970
2001	37,553,677	40,723,627

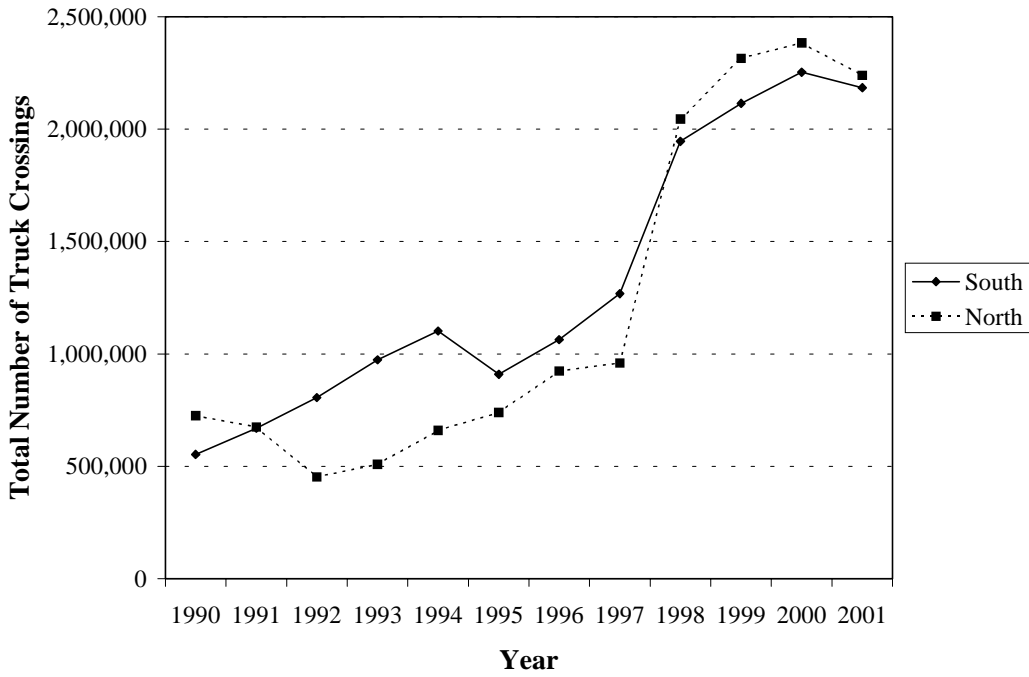


FIGURE 2.1 1990–2001 border truck crossings

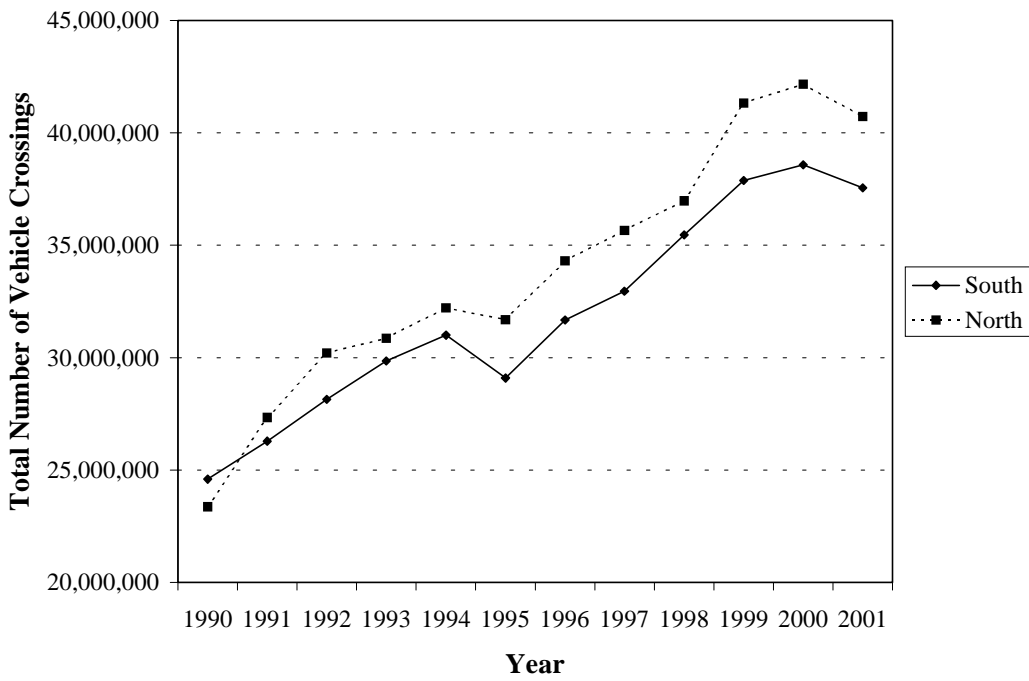


FIGURE 2.2 1990–2001 border vehicle crossings

It can be seen from these tables and figures that the total number of vehicles entering the United States from Mexico has been steadily increasing since the implementation of NAFTA, particularly the number of CMVs. It is projected that these trends will continue, with CMV traffic expected to double by the year 2020 (34), increasing the level of congestion and the need to examine the impacts of CMVs on the transportation network.

## 2.2 Motor Vehicle Operating Characteristics

The overall performance of motor vehicles is critical in both design and operations of any traffic analysis. Vehicle performance, or in particular CMV performance, affects design aspects such as roadway width to accommodate vehicle off-tracking, the length of freeway and arterial acceleration and deceleration lanes, driveway spacing to allow adequate stopping sight distance, climbing lanes, and critical length of grade to accommodate heavy vehicles, as well as superelevation and runoff length criteria. Vehicle performance is also a major consideration in the selection of traffic control devices, traffic signal design and coordination, and safe speed determination. Understanding the impact of vehicle performance provides insight into highway design and traffic operations, while forming the basis on which to assess the impact of advancing vehicle technologies and vehicle performance characteristics (35, 36).

The two primary opposing forces that are evaluated in the performance of road vehicles are tractive effort and resistance. Tractive effort is defined as the force available at the roadway surface to perform work and is typically expressed in pounds (lb) or Newtons (N). Resistance is the opposing force impeding the vehicles motion and is also typically expressed in pounds or Newtons (35, 36).

### 2.2.1 Resistant Forces

For a vehicle to move it must overcome four primary resistant forces: 1) aerodynamic resistance ( $R_a$ ); 2) rolling resistance ( $R_r$ ); 3) grade or gravitational resistance ( $R_g$ ); and 4) inertial resistance ( $R_i$ ) (15, 35, 36). These basic forces are illustrated graphically in Figure 2.3 (15). In addition to the resistant forces, additional parameters including the gross vehicle weight,  $W$ ; the height of the grade,  $H$ ; the length of the grade,  $L$ ; the slope angle,  $\theta$ ; and the standard x,y coordinates are also included in this figure.

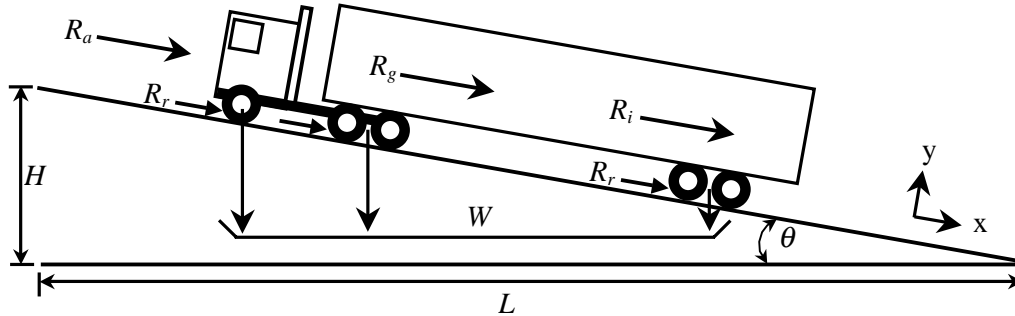


**FIGURE 2.3 Forces acting on a vehicle (adapted from 15)**

Summing the forces along the x-axis provides the basic equation of a vehicle in motion as outlined in Equation 2.1. It is important to note here that the sign for the grade resistance and inertial resistance changes depending on whether the grade is positive (uphill) or negative (downhill). A brief explanation of each of these four forces will be discussed in the following sections.

$$R = R_a + R_r + R_g + R_i \quad (2.1)$$

where:  $R$  = sum of resistant forces (lb);  
 $R_a$  = aerodynamic resistance (lb);  
 $R_r$  = rolling resistance (lb);  
 $R_g$  = grade resistance (lb);  
 $R_i$  = inertial resistance (lb); and

1 pound (lb) = 4.448 Newton (N).

**2.2.1.1 Aerodynamic Resistance** Aerodynamic resistance is the combination of the direct effect of air pressure in the pathway of the vehicle and can have a significant impact on vehicle performance. Aerodynamic resistance has been documented to originate from a number of sources. The primary source of aerodynamic resistance (approximately 85 percent) is the result of the turbulent flow of air around the vehicle body and is primarily a function of the shape of the vehicle. The second source (approximately 12 percent) is a result of the friction of air passing over the body of the vehicle, while the final source (accounting for the remaining

3 percent) is generally attributed to airflow through the vehicle in components such as radiators and air vents (35, 36).

The general equation for determining aerodynamic resistance is summarized in Equation 2.2 (35, 37). In this equation, the density of air at sea level and 59 degrees Fahrenheit is approximately 0.002378 slugs per cubic foot, and the aerodynamic drag coefficient ( $C_D$ ) varies by vehicle type with a range of 0.25 to 0.55 for an average automobile and as high as 1.3 for tractor-trailer units. Varying ranges for the parameters outlined in this equation can be obtained in the literature (35, 36).

$$R_a = \frac{\rho}{2} C_D A_f V^2 \quad (2.2)$$

where:  $\rho$  = density of air (slugs/ft<sup>3</sup>);  
 $C_D$  = aerodynamic drag coefficient;  
 $A_f$  = frontal cross-sectional area (ft<sup>2</sup>); and  
 $V$  = vehicle speed relative to the prevailing wind speed (ft/sec).

**2.2.1.2 Rolling Resistance** Rolling resistance occurs as a result of the frictional force between the tire and the pavement surfaces, including resistance due to the flexing of the tire rubber at the contact point, deformation due to particles on the roadway (i.e., rocks or debris), climbing from roadway depressions, and pushing wheels through mud, sand, or snow (38). The primary source of rolling resistance (approximately 90 percent) occurs as a result of the deformation of the tire as it passes over the roadway surface, while the penetration of the tire into the surface and the corresponding surface compression accounts for an additional 4 percent of the resistance. The final source of rolling resistance (accounting for the remaining 6 percent) is frictional motion that occurs as a result of the slippage of the tire on the roadway, combined with air circulation around the tire (35, 36).

One equation for calculating the rolling resistance for a passenger car on a relatively smooth pavement surface is provided in Equation 2.3 (37, 39). Several additional methodologies have been developed to estimate rolling resistance due to the wide range of factors involved in the calculation of the constant values. An alternative methodology approximates the rolling resistance according to Equation 2.4 (35). Both equations provide very comparable results for calculating rolling resistance and can be used interchangeably.

$$R_r = (C_{rs} + C_{rv}V^2)W \quad (2.3)$$

$$R_r = f_r W \quad (2.4)$$

where:  $C_{rs}$  = constant (typically 0.012 for passenger cars);  
 $C_{rv}$  = constant (typically 6.5 E-07 sec<sup>2</sup>/ft<sup>2</sup> for passenger cars);  
 $W$  = gross vehicle weight (lb); and  
 $f_r$  = coefficient of rolling resistance calculated as:

$$f_r = 0.01 \left( 1 + \frac{V}{147} \right)$$

Empirical studies have shown that the rolling resistance of trucks varies from that of passenger cars. A separate and alternate method, therefore, is used to calculate the rolling resistance for trucks as outlined in Equation 2.5 (39).

$$R_r = (C_a + C_b V)W \quad (2.5)$$

where:  $C_a$  = constant (typically 0.2445 for trucks) and  
 $C_b$  = constant (typically 4.4 E-04 sec/ft for trucks).

**2.2.1.3 Gradient Resistance** The gradient resistance occurs as a result of the gravitational force acting on the vehicle and is equal to the vector component of the vehicle total weight acting down on the grade. Equation 2.6 provides the general equation to account for gradient resistance. Because highway grades are usually small, the value of  $\sin \theta$  is approximately equal to the value of  $\tan \theta$ ; thus, the equation can be rewritten according to Equation 2.7 (35). Note that the force is negative (positive) for downhill (uphill) grades.

$$R_g = W \sin \theta \quad (2.6)$$

$$R_g = W \frac{G}{100} \quad (2.7)$$

where:  $\theta$  = slope angle and  
 $G$  = gradient (percent).

**2.2.1.4 Inertial Resistance** The final resistance force identified is the inertial resistance, or the force that must be overcome to allow a vehicle to change speed. Inertial resistance is a function of the vehicle weight and the instantaneous rate of acceleration (or deceleration). Inertial resistance can be calculated according to Equation 2.8 (39).

$$R_i = \frac{Wa}{g} \quad (2.8)$$

where:  $a$  = instantaneous rate of acceleration (ft/sec<sup>2</sup>) and  
 $g$  = acceleration of gravity (32.2 ft/sec<sup>2</sup>).

## 2.2.2 Tractive Effort

To overcome the effects of the resistant forces, the total available engine-generated tractive effort ( $F_e$ ) must be considered. The maximum tractive effort available to overcome the resistant forces is a function of a variety of engine and design factors, including the shape of the combustion chamber, the air intake in the combustion chamber, fuel type, and others (35, 36). For practical considerations, the tractive effort of a vehicle to overcome the resistant forces is generally represented as a function of the vehicle's power requirements, or the weight/power ratio. Each of these topics will be discussed in the following sections.

**2.2.2.1 Power Requirements** The two most commonly used measures of engine output are torque and power. Torque is a measure of the twisting moment, or work generated by the engine, expressed in foot-pounds (ft-lb) (35). Power is defined as the rate of doing work and is generally expressed in units of horsepower (hp) or kilowatts (kW) (1 hp = 0.746 kW). Power is related to engine torque according to Equation 2.9 (35), while the power used by a motor vehicle for propulsion, as a function of the resistant forces, can be determined using Equation 2.10 (38).

$$P_e = \frac{2\pi M_e n_e}{33000} \quad (2.9)$$

where:  $P_e$  = engine power (hp);  
 $M_e$  = engine torque (ft-lb);  
 $n_e$  = engine speed (rpm); and  
1 hp = 550 ft-lb/sec.

$$P = 0.00392RV \quad (2.10)$$

where:  $P$  = power actually used (hp) (lb).

The maximum power output that is available at any given engine speed for propulsion of the vehicle is equal to the difference between the maximum gross brake power available at the flywheel and the power consumption necessary to operate vehicle accessories (i.e., alternative, automatic transmission, air conditioner, power steering). Typical maximum power available for passenger car propulsion at 60 miles per hour is approximately 50 percent of the manufacturer's nominal engine power rating, while large trucks have approximately 94 percent of the manufacturer's rated power available for propulsion (39). The vehicle propulsion rates can be used to examine maximum acceleration rates and maximum speeds on grades based on nominal engine power (39).

The final item of consideration for engine power requirements in this discussion is the need for gear reduction to generate maximum power. The tractive effort needed to provide adequate acceleration characteristics is greatest at low vehicle speeds, while maximum engine torque is developed at high engine speeds. Because of this incompatibility in providing maximum tractive effort and torque, gear reductions are used to provide the mechanical advantage necessary for acceptable acceleration characteristics. Two factors play a key role in the development of gear reduction: 1) efficiency of the gear reduction device and 2) overall gear reduction ratio (35). The efficiency of the gear reduction device (i.e., transmission, differential) is necessary since an estimated 10 to 25 percent of the tractive effort generated by the engine is lost in the gear reduction devices. This corresponds to a mechanical efficient ( $\eta_r$ ) of 0.75 to 0.90 (35). The gear reduction ratio ( $\epsilon_0$ ) also plays a key role in the determination of tractive effort by defining the relationship between the engine revolutions and road revolutions. For example, if the gear reduction ratio is equal to five ( $\epsilon_0 = 5$ ), the engine will turn five revolutions for every one revolution of the road wheel (35). The resulting engine-generated tractive effort that reaches the drive wheel can therefore be calculated according to Equation 2.11 (35).

$$F_e = \frac{M_e \varepsilon_0 \eta_t}{r} \quad (2.11)$$

where:  $F_e$  = engine-generated tractive effort (lb);  
 $\varepsilon_0$  = gear reduction ratio;  
 $\eta_t$  = mechanical efficiency; and  
 $r$  = radius of the wheel (ft).

The final determination as to whether or not the engine-generated tractive effort is sufficient for propulsion depends on the sum of the resistant forces outlined in the previous sections. The engine-generated tractive effort provides the supply end of the equation, while the demand is a function of the resistant forces and efficiencies outlined. The demand changes based on environmental conditions (i.e., wind speed), operating conditions (i.e., velocity), roadway conditions (i.e., roadway grade), and so forth. The supply, however, remains relatively constant for a specific vehicle. The difference between the supply and the demand affects the overall operating characteristics of the vehicle.

**2.2.2.2 Weight/Power Ratio** The second indicator for representing vehicle performance is the weight/power ratio. The weight/power ratio is calculated by dividing of the weight of the vehicle by the power and measures the ability of a vehicle to accelerate or maintain speed on upgrades. High weight/power ratios provide poorer acceleration performance, while low weight/power ratios provide better performance due to the low ratio of motion resistance to power capacity (38). Weight/power ratios are especially critical in the evaluation of CMV performance and have been shown to vary widely, particularly when analyzed over the years. Although vehicle sizes and weights have increased, weight/power ratios have steadily decreased due to an increase in the engine power, transmission arrangement, and engine speed. As a result, weight/power ratios used in design have decreased with current warrants for truck climbing lanes based on a design truck with a weight/power ratio of 200 pounds per horsepower in 2001 (15), compared with weight/power ratios of 300 pounds per horsepower in 1994 (40). The weight/power ratio is important in defining the hill climbing and speed maintenance characteristics of a vehicle, as well as acceleration performance, a topic that will be discussed in more detail in the next subsection.

### 2.2.3 Acceleration Performance

As the previous sections have indicated, available tractive effort, power requirements, and weight/power ratios can be used to determine a number of vehicle performance characteristics, one of which is vehicle acceleration. Vehicle acceleration is related to tractive effort and power requirements as outlined in Equation 2.12 (35).

$$a = \frac{F_e - R}{\gamma_m m} \quad (2.12)$$

where:  $\gamma_m$  = mass factor, calculated as:

$$\gamma_m = 1.04 + 0.0025\varepsilon_0^2$$

It can be seen from this equation that acceleration is a function of the tractive effort available to accelerate ( $F_e - R$ ) and the mass of the vehicle ( $m$ ). The basic relationship between the net force available to accelerate ( $F_{net}$ ), the available tractive effort ( $F_e$ ), and the resistance forces ( $R$ ) is provided graphically in Figure 2.4 (35). In this figure, the net force available to accelerate ( $F_{net}$ ) is measured as the distance between the lesser of the maximum tractive effort ( $F_{max}$ ) and the engine-generated tractive effort ( $F_e$ ), and the total resistance ( $R$ ). The engine-generated tractive effort in this illustration represents the tractive effort available with gear reduction for a four-speed transmission. An example of the net force available to accelerate is provided in the figure ( $F_{net}$ ) and is the difference between the engine-generated tractive effort in third gear and the sum of the resistant forces ( $R$ ) at that particular speed. Also illustrated in the figure is the maximum attainable speed as a function of the resistant forces and the engine-generated tractive effort. At the maximum speed ( $V_{max}$ ), the sum of the available tractive effort is equal to the resistant forces; as a result, acceleration is equal to zero (35).

Acceleration characteristics play a major role in the determination of vehicle operations, including speed, lane-change, and merge characteristics, as well as implications on roadway geometric design. To illustrate the difference in operating conditions for trucks (12,000 pound, single-unit truck) and passenger cars on level grade, 6 percent grade, and 10 percent grade, the relationship between distance traveled and speed achieved based on maximum acceleration rates from stopped conditions is shown in Figure 2.5 (41). Although operating characteristics of vehicles (i.e., weight/power ratios) have improved since the data for this graphic was recorded,

the fact still remains that trucks perform differently than passenger cars, primarily as a result of their lower acceleration characteristics that must be considered in design.

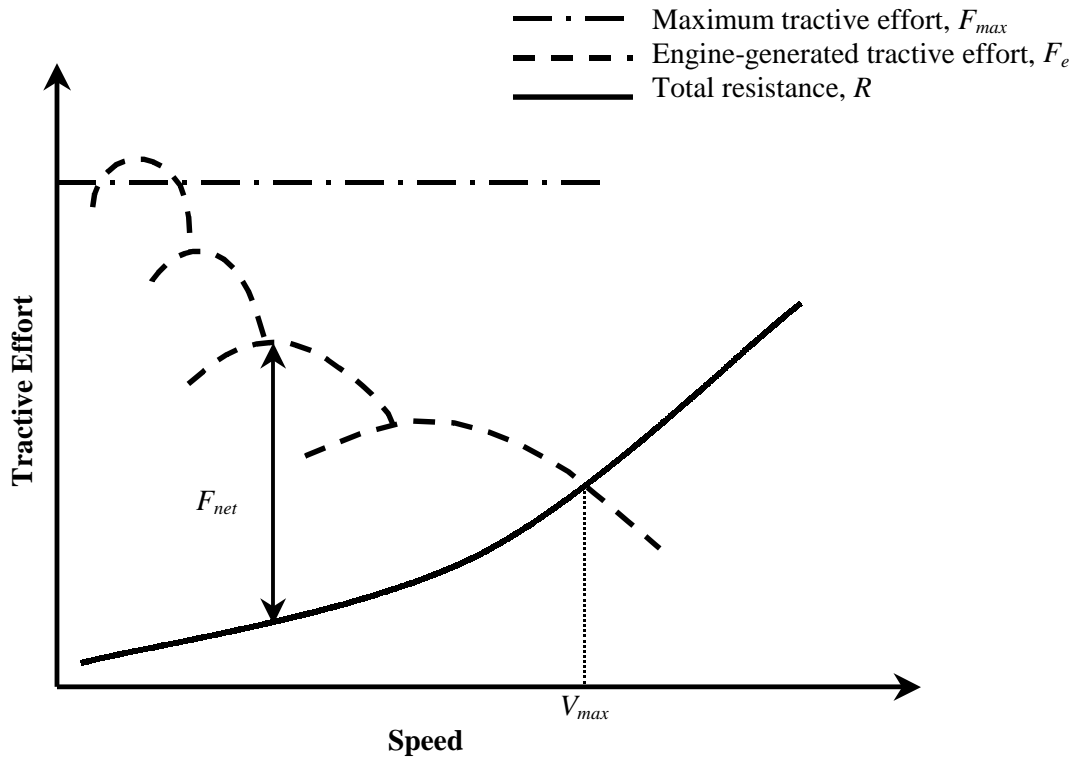


**FIGURE 2.4** Tractive effort, speed, and resistance relationships (adapted from 35)

The primary operating characteristics of interest in this dissertation are acceleration and deceleration characteristics of different vehicle types and the impact that these rates have on overall operations. A detailed discussion of the characteristics of deceleration for both passenger cars and trucks is provided in the next section, while the relationship between acceleration and deceleration of vehicles in the calibration and validation of microscopic traffic simulation models will be discussed in some detail in later sections.

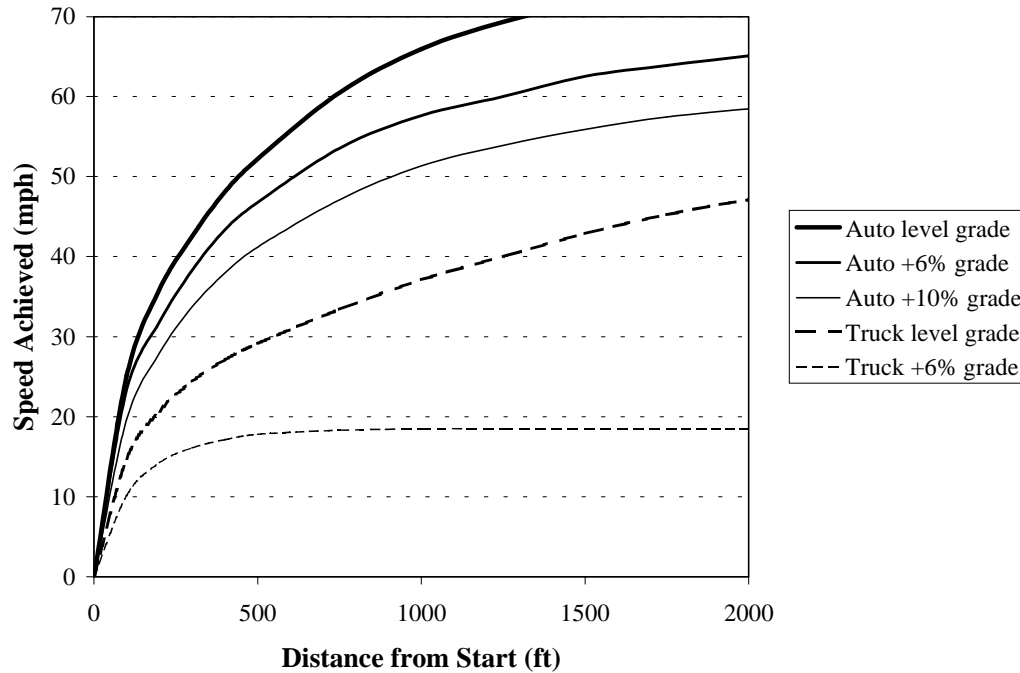


**FIGURE 2.5** Speed-distance relationships by vehicle type (adapted from 41)

#### 2.2.4 Deceleration Characteristics

The basic deceleration characteristics of a moving vehicle determine braking distance and have historically been determined based on the friction factor of the pavement surface. Equation 2.13 outlines the braking distance equation as a function of the coefficient of friction between tires and roadways, while Equation 2.14 provides the basic dynamic relationship for braking distance as a function of speed and deceleration (15, 42).

$$d = \frac{V_{mph}^2}{30f} \quad (2.13)$$

$$d = 1.075 \frac{V_{mph}^2}{a} \quad (2.14)$$

where:  $d$  = braking distance (ft);  
 $V_{mph}$  = initial speed (mph); and  
 $f$  = coefficient of friction between tires and roadways.

The coefficient of friction between the tire and roadway is a dynamic factor that changes based on vehicle speed as well as physical elements such as air pressure of tires, composition of tires, tire tread, condition of pavement surface, and the presence of snow or ice. As a result, friction factors vary considerably depending on the given condition. These values generally fall within the range of 0.28 and 0.80, corresponding to deceleration rates between 0.28g (9.0 feet per second squared) and 0.80g (25.8 feet per second squared) (42).

The purpose of this section is to outline research on the deceleration characteristics of both passenger cars and trucks. To accomplish this purpose, this section has been divided into two subsections. The first discusses passenger car deceleration rates, while the second provides background information on CMV deceleration rates.

**2.2.4.1 Passenger Car Deceleration Rates** The 1950 edition of the Institute of Traffic Engineers *Traffic Engineering Handbook* indicated that the highest rates of deceleration are 0.93g (30 feet per second squared), a rate that occurs just prior to the vehicle coming to rest. According to the handbook, deceleration rates above 0.68g (22 feet per second squared) require occupants to brace for the stop or be pulled out of their seats. At a deceleration rate of 0.43g (14 feet per second squared), packages will slide off of seats and occupants will find the deceleration uncomfortable, rates of 0.34g (11 feet per second squared) are undesirable but not alarming to the passenger, while rates of 0.26g to 0.28g (8.5 to 9 feet per second squared) are comfortable (43).

Based on the research in the 1950 *Traffic Engineering Handbook*, Gazis et al. analyzed amber phasing and dilemmas zones based on deceleration rates of 0.33g (10.7 feet per second squared) and 0.5g (16.1 feet per second squared). In this analysis, the authors indicate that a deceleration rate of 0.33g is feasible but fairly high and not desirable in normal driving, while 0.5g was referred to as a “very hard stop” (44). The Institute of Transportation Engineers (ITE) second edition of the *Transportation and Traffic Engineering Handbook* in 1982 (41), as well as the 1992 fourth edition and 1999 fifth edition of the *Traffic Engineering Handbook* (38, 39), all indicate that a comfortable deceleration rate for use in design is 0.31g (10 feet per second squared), while a maximum locked wheel deceleration rate of 0.5g (16.1 feet per second squared) was identified as an undesirable braking rate. The fourth edition of the handbook further identified a minimum deceleration rate of 0.1g (3.2 feet per second squared) at speeds of 70 mph due only to the removal of a driver’s foot from the accelerator pedal (39).

Several research projects between 1976 and 1982 examined the impacts of different deceleration rates and estimated deceleration rates based on actual driving conditions (45, 46, 47, 48, 49). These analyses provided deceleration rates that range between 0.22g and 0.43g (7.0 and 13.9 feet per second squared), with average deceleration rates generally observed between 0.30g and 0.36g (9.7 and 11.6 feet per second squared).

**2.2.4.2 CMV Deceleration Rates** Several research projects have also been conducted over the years to analyze the effects of deceleration of CMVs as this relates to stopping sight distance. The first such study was conducted in 1984 as part of a National Cooperative Highway Research Program (NCHRP) project. NCHRP Report 270 begins to analyze the differences between car and truck stopping distances. The field results from this study for loaded truck average deceleration rates indicated deceleration rates between 0.20g (6.5 feet per second squared) and 0.42g (13.6 feet per second squared) (50). Further analysis performed by Harwood et al. (51) identified truck deceleration rates and braking distances for use in highway design based on the 1984 American Association of State Highway and Transportation Officials (AASHTO) *A Policy on Geometric Design of Highways and Streets* (AASHTO Green Book) (52). The results of this analysis are provided in Table 2.3 (51).

**TABLE 2.3 Truck Deceleration Rates for Use in Highway Design**

Vehicle Speed (mph)	AASHTO Policy	Deceleration Rate, $g$ (ft/sec <sup>2</sup> ) <sup>1</sup>		
		Worst-Performance Driver <sup>2</sup>	Best-Performance Driver <sup>3</sup>	Antilock Brake System
20	0.40 (12.9)	0.17 (5.5)	0.28 (9.0)	0.36 (11.6)
30	0.35 (11.3)	0.16 (5.2)	0.26 (8.4)	0.34 (11.0)
40	0.32 (10.3)	0.16 (5.2)	0.25 (8.1)	0.31 (10.0)
50	0.30 (9.7)	0.16 (5.2)	0.25 (8.1)	0.31 (10.0)
60	0.29 (9.3)	0.16 (5.2)	0.26 (8.4)	0.32 (10.3)
70	0.28 (9.0)	0.16 (5.2)	0.26 (8.4)	0.32 (10.3)

<sup>1</sup> Based on an empty tractor-trailer truck on wet pavement

<sup>2</sup> Based on driver control efficiency of 0.62

<sup>3</sup> Based on driver control efficiency of 1.00

The results of the Harwood study are reiterated in a February 1992 ITE report (53), and again in NCHRP Report 400 (54). NCHRP Report 400 provides additional analysis on

passenger car and light truck deceleration characteristics and summarizes the results of this analysis by indicating that drivers generate maximum deceleration rates that range between  $0.7g$  (22.5 feet per second squared) and  $0.9g$  (30.0 feet per second squared), with 95 percent of all drivers exhibiting constant decelerations of at least  $0.29g$  (9.3 feet per second squared) under wet conditions and  $0.41g$  (13.2 feet per second squared) on dry pavements. The research provides recommendations for design deceleration rates by indicating that most drivers choose deceleration rates in excess of  $0.57g$  (18.4 feet per second squared) when confronted with the need to stop for an unexpected object in the roadway, and that approximately 90 percent of all drivers choose a deceleration rate in excess of  $0.35g$  (11.2 feet per second squared) (54). This rate is determined comfortable for most drivers and is recommended as the deceleration threshold for determining required sight distance regardless of initial speed. This rate is subsequently utilized in the 2001 AASHTO Green Book for design purposes (15).

The results presented in the previous two sections can be summarized to provide guidance on both maximum non-emergency and emergency deceleration rates for both passenger cars and trucks. Based on the research outlined, maximum non-emergency deceleration rates for passenger cars and light trucks appear to fall within a range of  $0.22g$  (7 feet per second squared) and  $0.37g$  (12 feet per second squared), with a comfortable deceleration for most drivers set at  $0.35g$  (11.2 feet per second squared). Truck deceleration rates are slightly lower than that of passenger cars and light trucks, primarily for trucks that are not currently equipped with antilock brakes. Most studies indicate that trucks equipped with antilock brakes appear to exhibit characteristics very similar to passenger car deceleration rates. The range of deceleration rates observed for trucks appears to fall between approximately  $0.16g$  (5.15 feet per second squared) and  $0.28g$  (9.02 feet per second squared) for vehicles without antilock brakes, and  $0.31g$  to  $0.36g$  (10.0 to 11.6 feet per second squared) for vehicles equipped with antilock brakes. A minimum deceleration rate of  $0.1g$  (3.2 feet per second squared) caused by the removal of the driver's foot from the accelerator was also noted in the research.

### **2.3 Data Collection Methodologies**

Several sources are available to aid in the collection of traffic data. The most commonly used source is the *Traffic Monitoring Guide* (TMG), published by the USDOT, Federal Highway Administration (FHWA), Office of Highway Policy Information (55). The TMG was developed

to provide information and guidance to state and local highway agencies and metropolitan planning organizations (MPOs) and was designed with three main objectives in mind (55):

1. to relate the intensity of the monitoring effort to the quality of the information being reported in an effort to meet user defined needs;
2. to provide an emphasis on ways in which traffic volume counts, vehicle classification counts and truck weight monitoring form a related set of traffic characteristic monitoring functions; and
3. to highlight the need to incorporate non-traditional data sources with more traditional sources to improve the traffic estimates available to users and to reduce the amount of traditional data collection in a geographic area.

The three primary data monitoring techniques covered by the TMG include the three techniques outlined in the objectives: 1) traffic volume counts; 2) vehicle classification counts; and 3) truck weight monitoring. A background discussion on each of these data collection topics is provided in the following sections.

### *2.3.1 Traffic Volume Counts*

The fundamental relationship between traffic volume (flow rate), density, and speed is essential in understanding the operating characteristics of a roadway. Knowledge of these relationships and the analytical techniques associated with traffic flow characteristics is essential in planning, design, and operations of transportation facilities (38, 56, 57). To accurately estimate these relationships, traffic counts need to be collected for use in traffic analysis procedures (55).

Although a variety of traffic volume statistics are utilized in traffic analysis procedures, the TMG outlines the two primary statistics of interest to develop a successful statewide traffic monitoring program as: 1) annual average daily traffic (AADT) and 2) average daily vehicle distance traveled (DVDT) (i.e., annual vehicle miles of travel [AVMT]). Because, by definition, DVDT is calculated as the product of AADT and the length of the roadway segment, the primary goal of the traffic monitoring program is to develop estimates of AADT that can be used to estimate DVDT and other design criteria (55, 58). To achieve the goal of collecting accurate AADT estimates, the TMG has recommended that traffic monitoring programs consist of two basic components: 1) a continuous count program and 2) a short-duration count program (55).

**2.3.1.1 Continuous Count Program** One of the most critical aspects of a data collection program is the ability to obtain access to continuous count data. These data are essential to understanding temporal changes in traffic volumes, including time-of-day, day-of-week, and seasonal variations that can be used to improve the accuracy of traffic estimates and subsequent traffic analyses (55). In addition, the data can be used to understand the spatial changes in traffic volumes along a corridor or throughout a transportation network.

Some of the more common ITS continuous traffic monitoring data collection techniques available for use today include: 1) ATR; 2) AVC; 3) continuously operating WIM devices; and 3) volume and speed monitoring stations. Continuous traffic volume data are generally collected by state highway agencies using permanently installed, continuous traffic counters. The technology for these counters (ATRs) has been in place for many years, with ILDs the most common sensor used in ATR applications. ILDs vary in size and shape, with 5-foot or 6-foot square loops, 6-foot diameter round loops, and rectangular configurations with a 6-foot width and variable length comprising the most common configurations (59). ILDs are generally embedded in a shallow cut (generally 1 inch to 2 inches deep and 1 inch to 2 inches wide) in the pavement surface and are placed in the travel lane with a conduit to curb, pull-box, lead-in conduit, and controller cabinet. A typical 6-foot square ILD installation design is provided in Figure 2.6 (59).

The loops embedded in the roadway function as an inductive element in conjunction with an electronics unit in the controller cabinet. When a vehicle stops on or passes over the loop, the inductance of the loop is decreased, which in turn increases the oscillation frequency and causes the electronics unit to send a pulse to the controller, signaling the presence or passage of a vehicle. The operation of inductive loop sensors can be used to determine vehicle passage, presence, count, and occupancy. Additional parameters such as speed, headway, and gap can also be determined using a two-loop design in conjunction with an algorithm that includes loop length, spacing, and average vehicle length to calculate the required parameters (59).

Other technologies utilized for continuous traffic volume data include magnetometers, magnetic induction coil technology, microwave radar, active and passive infrared, ultrasonic detection, acoustic arrays, and video image processing. Details on the methodology behind each of these technologies can be found in the literature (59).

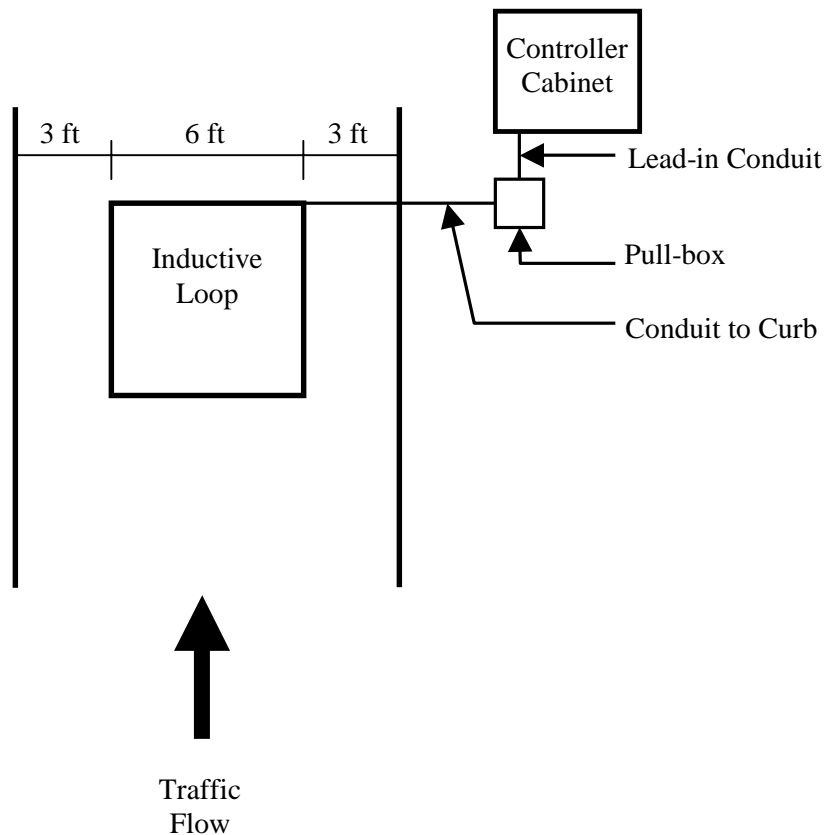


**FIGURE 2.6** Typical inductive loop detector design (adapted from 59)

**2.3.1.2 Short-Duration Count Program** The short-duration count program is designed to provide traffic data coverage over a wide geographic area on a cyclical basis. This program provides data that can be used to define the traffic demand on specific roadway segments and subsequently to set standards for design, maintenance, and long-term management.

The primary differences between the continuous count program and short-duration count program are the frequency and duration that data are collected. The location of short-duration counts is revised on a regular basis, providing much-needed information on a wide range of facilities across a region. Some locations are counted on a regular basis (every one to three years), while others are counted much less frequently. The TMG recommends short-duration count data be collected for 48-hour periods with counters that record hourly data increments. Contrasting this to the continuous count program, data are collected for a much shorter duration,

necessitating adjustments to the data to represent annual conditions. The recommended adjustments include (55):

- axle correction (for counts taken with single-axle sensors);
- day-of-week adjustments (for counts taken over a timeframe of less than one-week); and
- month-of-year adjustments (to account for seasonal variations).

### 2.3.2 *Vehicle Classification Counts*

The variation in traffic volume becomes even more apparent when considering specific vehicle classification schemes on a given roadway. The same sources of variation that are present in traditional traffic streams (i.e., time-of-day, day-of-week, season) have also been observed to vary by vehicle classification scheme. Research performed by Hallenbeck et al. identified significant variation of truck volumes by time-of-day and day-of-week when compared to car volumes (60, 61). When analyzing the time-of-day variations, the researchers classified truck travel and car travel into one of two basic time-of-day patterns. The two patterns, however, were not the same for cars as they were for trucks, with variations existing between the different vehicle types as illustrated in Figure 2.7 (55). Cars tended to follow either the traditional urban commute pattern (i.e., urban car) or more of a single hump commonly seen in more rural areas (i.e., rural car). Trucks, on the other hand, tended to follow either a single hump pattern with peaking occurring in the morning for urban local trucks (i.e., local truck) or a long-haul through-truck pattern that tended to be relatively stable throughout the day (i.e., through truck) (55, 60, 61).

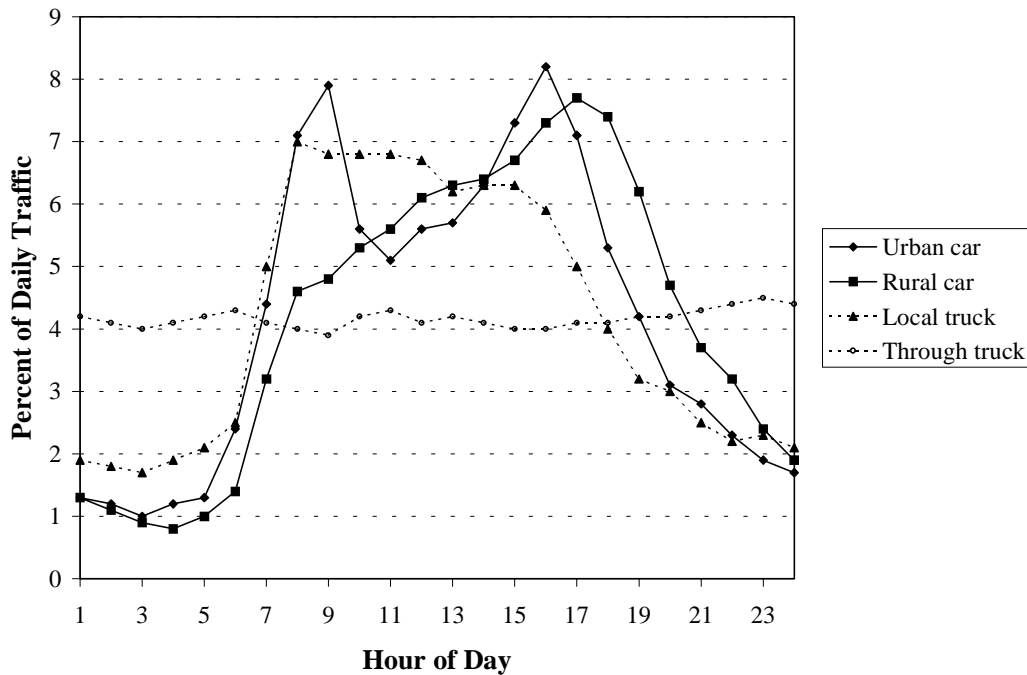


**FIGURE 2.7** Typical traffic variation by time-of-day (adapted from 55)

When analyzing day-of-week variations, the researchers again classified truck travel and car travel into one of two basic day-of-week patterns. Again, the patterns varied from truck travel to car travel as illustrated in Figure 2.8 (55). In this comparison, cars tended to follow either a traditional pattern where volumes were fairly constant during weekdays and then declined slightly on the weekends (i.e., traditional car), or a more recreational pattern where weekday traffic is again constant, with a slight increase in weekend travel (i.e., recreational car). In this application, trucks also showed two patterns, influenced primarily by business delivery needs. Most trucks tended to follow an exaggerated version of the traditional car pattern where the truck volumes were fairly constant during weekdays and then dropped off considerably during the weekend due to the drop in business activity (i.e., typical truck), while the remainder of the trucks followed a very different and more constant day-of-week pattern as they were not concerned with local business travel rather they were influenced by interstate trips that are generally unaffected by a typical work week (i.e., through truck) (55, 60, 61).

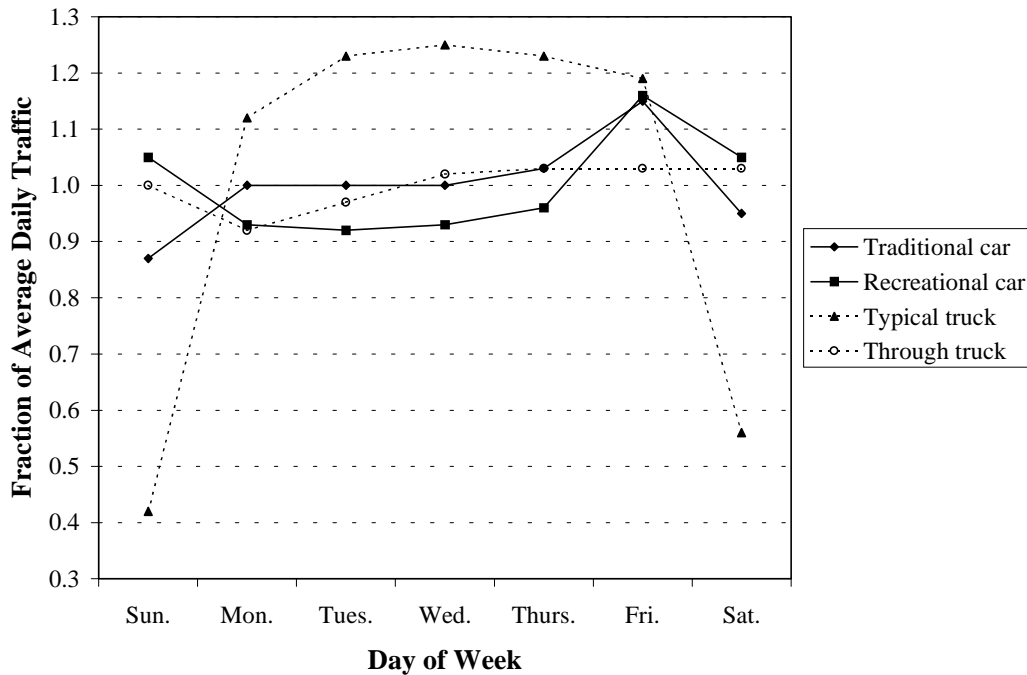


**FIGURE 2.8** Typical traffic variation by day-of-week (adapted from 55)

To aid in the classification of vehicles, the FHWA developed a 13-category classification scheme in the 1980s. A summary of the FHWA vehicle classification scheme is provided in Table 2.4 (30), with a graphical representation provided in Figure 2.9 (30). While most agencies have adopted this scheme for their analysis, some continue to use a variation of the FHWA scheme and then aggregate or disaggregate their results to FHWA standards for reporting purposes. The FHWA scheme was developed as somewhat of a compromise among several factors, including (55):

- the manual (vision-based) classification schemes used before that time;
- the need to create a nationally consistent classification scheme;
- the automated counters being developed at the time; and
- the need to provide the basic information on different truck types as input to a variety of policy issues.

**TABLE 2.4 FHWA Vehicle Classification Scheme**

<b>Class Code</b>	<b>Vehicle Type</b>
1	Motorcycles
2	Passenger vehicles
3	Other two-axle, four-tire single-unit vehicles
4	Buses
5	Two-axle, six-tire, single-unit trucks
6	Three-axle single-unit trucks
7	Four or more axle single-unit trucks
8	Four or fewer axle single-trailer trucks (i.e., 2S1, 2S2, 3S1)
9	Five-axle single-trailer trucks (i.e., 3S2, 2S3)
10	Six or more axle single-trailer trucks (i.e., 3S3, 3S4)
11	Five or fewer axle multi-trailer trucks (i.e., 2S1-2)
12	Six-axle multi-trailer trucks (i.e., 2S2-2, 3S1-2)
13	Seven or more axle multi-trailer trucks (i.e., 3S2-2)

To effectively capture the variations that occur over time and space for different vehicle classes, the recommended structure for vehicle classification counts parallels that of the traditional traffic volume count, with recommendations for: 1) permanent continuous classification counts and 2) short-duration classification counts. The primary purpose for the permanent continuous classification counts is to provide needed information on temporal variations in the data to convert short-duration counts into annual estimates by assuming that the same general patterns are consistent across the sites, while the short-duration classification counts provide geographic coverage of classification data that cannot be achieved economically by permanent continuous classification count locations (55). A brief summary of each of these data collection methodologies is provided in the following sections.

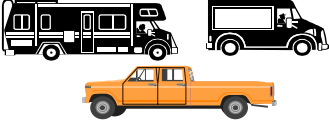
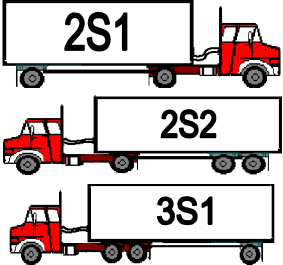
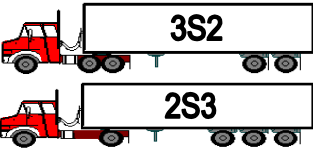
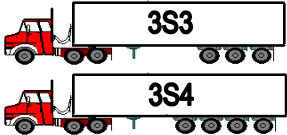
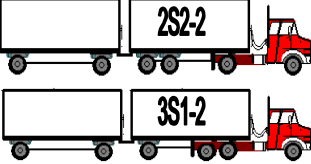
 <p>FHWA Class 1 Motorcycles</p>	 <p>FHWA Class 2 Passenger Vehicles</p>
 <p>FHWA Class 3 Other Two-Axle, Four-Tire Single-Unit Vehicles</p>	 <p>FHWA Class 4 Buses</p>
 <p>FHWA Class 5 Two-Axle, Six-Tire, Single-Unit Trucks</p>	 <p>FHWA Class 6 Three-Axle Single-Unit Trucks</p>
 <p>FHWA Class 7 Four or More Axle Single-Unit Trucks</p>	 <p>FHWA Class 8 Four or Fewer Axle Single-Trailer Trucks</p>
 <p>FHWA Class 9 Five-Axle Single-Trailer Trucks</p>	
 <p>FHWA Class 10 Six or More Axle Single-Trailer Trucks</p>	 <p>FHWA Class 11 Five or Fewer Axle Multi-trailer Trucks</p>
 <p>FHWA Class 12 Six-Axle Multi-trailer Trucks</p>	 <p>FHWA Class 13 Seven or More Axle Multi-trailer Trucks</p>

FIGURE 2.9 FHWA vehicle classification scheme

**2.3.2.1 Permanent Continuous Classification Counts** The primary purpose of the permanent continuous classification count program is to collect data that can be used to develop factors needed to estimate annual average daily truck traffic (AADTT) from short-duration classification counts. As illustrated in the previous section, researchers have identified significant variation in truck volumes by time-of-day and day-of-week, with local truck traffic volumes ranging from less than 2 percent of daily traffic volumes in late evening and early morning hours to as high as 7 percent during the morning commute period (55, 60, 61). This research, combined with the analysis of continuously collected data, indicates that truck volumes can change both temporally and spatially, thus necessitating the need for continuously operating classification counters to monitor truck flows and to detect patterns for use in engineering and planning analyses.

As a result of the variation in traffic volumes by vehicle classification, the TMG outlines four primary purposes for installing and operating permanent continuously operating vehicle classification counters. These include the need to: 1) provide a highly accurate measure of truck volumes at a limited number of specific sites around the state; 2) track the changes in volumes over time with a high degree of accuracy; 3) determine the travel patterns of different truck types on different roadways across the state; and 4) create adjustment factors and factor groups that allow application of the factors for converting short-duration classification counts into annual average estimates of volume by vehicle type. (55)

Although the base technology for traffic data collection has been available since the early 1950s, the added technology to provide for continuous vehicle classification counts (i.e., AVCs) using this base technology has only been available since the mid-1980s. In 1990, the number of permanent continuous classification counters began to increase across the nation as a result of the data collection requirements for the Strategic Highway Research Program (SHRP) Long Term Pavement Performance (LTPP) project. As a result of the increased need to collect data associated with the SHRP and LTPP projects, many states added permanent continuous classification counters, while at the same time converting many of their old and outdated ATR locations to this new technology. Data collected through this program have continued to provide justification for the differences in time-of-day, day-of-week, and seasonal variations for truck traffic (55).

The primary technology utilized for AVC data collection is two-loop ILLDs in conjunction with a vehicle classification algorithm that provides detailed information on loop design, loop spacing, and ranges of vehicle lengths necessary to classify vehicles (59). The base

design is equivalent to that of a typical ILD outlined previously with the addition of a second loop in the travel lane and a detailed classification algorithm based on typical vehicle design. Additional technologies for classification counts include microwave radar, active infrared, and video image processor units. More details on each of these technologies can be found in the literature (59).

**2.3.2.2 Short-Duration Classification Counts** The primary objective of the short-duration classification count program is to provide geographic coverage of classification data that cannot be achieved economically by permanent continuous classification count locations, and to ensure that highway agencies have valid truck information for all highways under their jurisdiction. Short-duration classification counts should be performed regularly to monitor the movement of truck traffic on the transportation network; these counts should be collected by equipment capable of providing hourly volume summaries and disaggregate data by lane and direction at each site. The TMG recommends that 25 to 30 percent of the coverage volume counts should be classification counts and that a coverage program over a six-year cycle should be implemented. When performing classification counts, it is recommended that the counts be performed for a minimum duration of 48 hours and, where possible, should classify according to the standard FHWA vehicle classification scheme (55).

The short-duration classification count data collection effort is necessary to develop basic truck traffic statistics including the geographic variability of truck movement and time-of-day distribution at a variety of locations. These data will then serve as the starting point for other statistics needed, including truck vehicle miles of travel (VMT), freight flows (tonnage), and traffic load design statistics (ESAL and axle load distributions). These data must then be adjusted based on the permanent continuous classification counts in the area to eliminate potential bias in the estimates (55).

It is important to note that vehicle classification counts (both permanent continuous and short-duration) should not be considered separate from the traffic volume counts traditionally performed. To meet the stated objectives of the TMG, they should be integrated to provide both classification and total volume information. This can be accomplished by replacing traditional volume counts with classification counts wherever possible, thus reducing duplication and error. As indicated, the TMG recommends that state highway agencies initially aim to take 25 to

30 percent of their short-duration coverage counts with classification counting equipment, and that higher coverage should be provided whenever possible (55).

### 2.3.3 *Truck Weight Monitoring*

The final traffic monitoring activity is truck weight monitoring. The gathering of truck weight data is the most difficult and expensive of the three data collection activities outlined in the TMG. In many respects, truck weight data are the most important to collect, as the data are used as input to some of the state highway agency's most critical transportation engineering and planning tasks, including but not limited to (55):

- pavement and bridge design, maintenance, and loading restrictions;
- economic analyses, including the development of equitable tax structures;
- CMV weight law enforcement actions;
- geometric design considerations; and
- safety improvement analyses.

The truck weight monitoring systems are generally designed to provide the following information on GVW per vehicle (usually by vehicle class), axle load distribution (by type of axle) for specific vehicle types, and ESALs for specific vehicle types (55). The basic statistics (GVW and ESALs) for a specified vehicle classification can then be expressed as distributions, mean values, or mean values with confidence intervals, depending on data collection needs. GVW provides actual weight data that can be used to compare freight flows for different geographic locations within a state, or that can be multiplied by the number of trucks within a given class to yield the total number of tons applied by that class on a roadway. This statistic is often used to develop traffic volume flow maps that effectively illustrate high volume and weight corridors. ESAL values can also be used to compare freight flows along corridors within a geographic area by calculating the total ESAL load for a specific type and weight range of axles, where one ESAL is defined as the cumulative number of applications of an 18,000 pound single-axle load applied to the pavement on two sets of dual tires inflated to 70 pounds per square inch (psi) (62, 63). ESAL values are typically computed using the AASHTO axle load equivalence factors for single, tandem, and tridem axles, which are available for both flexible or rigid pavements (64, 65, 66).

**2.3.3.1 Commercial Motor Vehicle Size and Weight Regulations** Federal and state regulations govern the use of CMVs by limiting the weight and dimensions of trucks, buses, and trailers on U.S. highways. These regulations have important economic consequences because the trucking industry accounts for 80 percent of total freight transportation expenditures nationwide. The size and weight of CMVs has a very pronounced impact on costs associated with freight movement as well as a noticeable impact on highway construction costs, maintenance costs, and highway safety issues (67).

The federal government began to regulate CMV size and weight limits in 1956 by imposing maximum vehicle weight and width limits in the Federal-Aid Highway Act of 1956. Since before World War I, states had regulated the size and weight of vehicles operating on state highways, but with the investment that was taking place with the Interstate Highway System in the late 1950s, the federal government determined a need to become more involved with the size and weight regulations. The regulations imposed under the original Act of 1956 placed a maximum GVW limit of 73,280 pounds along with maximum weights of 18,000 pounds on single axles and 32,000 pounds on tandem axles. Regulations were also set for a maximum vehicle width of 96 inches on interstate highways, with length and height limits to remain under the regulation of the state. States that had regulations in place on July 1, 1956, for vehicle width or weight that exceeded the federal limits were allowed to retain these higher limits under a grandfather clause (68, 69, 70).

The federal requirements were changed with the Federal-Aid Highway Amendments of 1974. These amendments increased the GVW limit on interstate highways to 80,000 pounds, with single-axle limits increased to 20,000 pounds and tandem-axle limits to 34,000 pounds. At the same time, Congress enacted the bridge formula to further limit the weight on groups of axles in an attempt to reduce risk of damage to highway bridges. The bridge formula set allowable weight limits depending on the number of axles on a vehicle combined with the spacing between these axles, as outlined in Equation 2.15 (67, 69, 70).

$$W = 500 \left( \frac{LN}{N-1} + 12N + 36 \right) \quad (2.15)$$

where:  $W$  = maximum weight in pounds that can be carried on a group of two or more axles to the nearest 500 pounds;  
 $L$  = distance in feet between the outer axles of any two or more consecutive axles; and  
 $N$  = number of axles being considered.

Initially, not all states adopted the new 80,000 pound limit, which began to place barriers on long-distance travel. As a result of the inconsistency across the nation, a study called for by the Surface Transportation Assistance Act (STAA) of 1978 addressed the need to find a solution to this and other issues. In the STAA of 1982, Congress required all states to adopt the federal weight limits on interstate highways, including the bridge formula. In addition, Congress required states to allow vehicles with certain minimum dimensions on what was termed a National Network (NN) for STAA vehicles that was to be designated by the Secretary of Transportation in consultation with the states. One of the dimensions adopted in the STAA of 1982 was an increase in maximum vehicle width for all CMVs to 102 inches (68, 70).

Since 1982 only minor changes to the federal size and weight limitations have been imposed, the most significant of which was a freeze on longer combination vehicle (LCV) operations, which was imposed as part of the Intermodal Surface Transportation Efficiency Act of 1991 (ISTEA) and extended in the Transportation Equity Act for the 21<sup>st</sup> Century (TEA-21). A summary of the current federal regulations on vehicle dimensions for the interstate system is as follows (67, 70):

- maximum GVW shall be 80,000 pounds except where lower GVW is dictated by the bridge formula;
- maximum gross weight upon any one axle, including any one axle of a group of axles, or a vehicle is 20,000 pounds;
- maximum gross weight on tandem axles is 34,000 pounds;
- maximum vehicle width shall be 102 inches on the NN for STAA vehicles;
- minimum vehicle length is 48 feet for a semi-trailer operating in a truck-tractor/semi-trailer combination; and
- minimum vehicle length is 28 feet for a semi-trailer or trailer operating in a truck-tractor/semi-trailer/trailer combination.

Since the federal size and weight regulations were established in 1982, several proposals have been made to make changes to these regulations. To explore these proposals, research studies have been conducted to reassess the current CMV size and weight regulations. The two most recent studies were the *U.S. Department of Transportation's Comprehensive Truck Size and Weight Study (70)* published in 2000 and the Transportation Research Board (TRB) Special Report 267, *Regulation of Weights, Lengths, and Widths of Commercial Motor Vehicles (67)* published in 2002. Both documents provide discussions of the existing regulations along with recommendations on ways to improve CMV size and weight regulations through modification of the existing framework, as well as modifications outside of the existing framework or changes to the structure of the regulation. A brief description of the results of these studies is provided in the following sections.

#### *2.3.3.1.1 U.S. Department of Transportation's Comprehensive Truck Size and Weight Study*

The *U.S. Department of Transportation's Comprehensive Truck Size and Weight Study* outlines five truck size and weight scenarios to illustrate the nature and relative magnitude of impacts on safety, productivity, infrastructure, the environment, traffic operations, and railroads. Each of the scenarios was characterized by the weight and length that the vehicle would be able to operate under, the networks of highways upon which the vehicles would operate, and the federal truck size and weight limitations that would apply. The five scenarios included: 1) uniformity scenario; 2) North American trade scenarios; 3) longer combination vehicles nationwide scenario; 4) H.R. 551 scenario; and 5) triples nationwide scenario. The findings of this study indicated that significant productivity benefits would be expected for each scenario that allows heavier vehicle weights, primarily from the use of LCVs, but that nationwide use of these vehicles would entail significant infrastructure costs, adverse impacts on railroads, and potentially negative safety impacts (70).

#### *2.3.3.1.2 TRB Special Report 267*

The TRB Special Report 267 outlines seven conclusions and six recommendations for further study as outlined in the following statements (67).

1. Opportunities exist for improving the efficiency of the highway system through reform of federal truck size and weight regulations. Such reform may entail allowing larger trucks to operate.

2. Appropriate objectives for federal truck size and weight regulations are to facilitate safe and efficient freight transportation and interstate commerce, to establish highway design parameters, and to manage consumption of public infrastructure assets.
3. Changes in truck size and weight regulations made in coordination with complementary changes in the management of the highway system offer the greatest potential to improve the functioning of the system.
4. The methods used in past studies have not produced satisfactory estimates of the effect of changes in truck weights on bridge costs.
5. It is not possible to predict the outcomes of regulatory changes with high confidence.
6. It is essential to examine the safety consequences of size and weight regulation. Research and monitoring needed to understand the relationship of truck characteristics and truck regulations to safety and other highway costs are not being conducted today.
7. Although violations of size and weight regulations may be an expensive problem, monitoring of compliance with the regulations is too unsystematic to allow the costs involved to be estimated.

The specific recommendations that have been suggested as a result of this study include, first, the creation of an independent public organization with a charter to observe and evaluate CMV performance and the effects of size and weight regulation. Secondly, it was recommended that Congress authorize the Secretary of Transportation to approve pilot studies to evaluate the consequences of changes in truck size and weight regulations. The third recommendation calls for federal law that would allow states to participate in a federally supervised permit program that would allow vehicles to operate with heavier loads than the present federal limits, with restrictions outlined in the document (67). The fourth recommendation calls for federal law to allow the operation of longer combination vehicles under the same restrictions as the third recommendation, while the fifth recommendation addresses the routes and roads to which federal standards should apply. The sixth and final recommendation calls for research on three specific topics: 1) systematic monitoring of truck traffic and truck costs to evaluate regulatory effectiveness; 2) basic research on the relationship of truck characteristics to highway costs; and 3) pilot studies to test new vehicles (67).

**2.3.3.2 Traffic Monitoring Guide Data Collection Focus** The TMG has recently changed the focus of truck weight monitoring from collecting data at a random number of locations to adjusting the number of locations to fit the level of variability in truck weights and thus data collection needs. The objective of this new direction is to ensure that each agency (i.e., state transportation department) collects adequate truck weight data to meet their specific needs. This methodology allows agencies to collect data at a relatively small number of sites that represent a much larger group of roadways according to the following four activities (55).

1. Define “truck weight roadway groups” to ensure that each road within a group experiences truck weights that are similar across the entire group.
2. Collect weight data at a minimum of six sites within each group, at least one of which should operate continuously throughout the year and the remainder of which should operate no less than 24 consecutive hours, preferably one-week at a time.
3. Collect data on day-of-week and seasonal changes within each group and develop estimates of average GVW by vehicle class and axle load distributions by type of axle (i.e., single, tandem, tridem).
4. Place heavy emphasis on the calibration of WIM data collection equipment, where quality information is more important than quantity of data collected.

The core objective of the truck weight data collection program as defined by the TMG is “to obtain a reliable estimate of the distribution of vehicle and axle loads per vehicle for truck categories within defined roadway groups” (55). To accomplish this objective, the TMG has provided guidelines to follow in generating the truck weight groups and in determining which vehicles fall within each of the groups. Once the number and characteristics of each group have been established, specific guidelines are provided to determine the quality of the groups, the precision of estimates necessary for each group, the number of WIM sites to provide for each group, the number of days that should be counted at each WIM site, installation and site selection criteria, and the total size of the weight data collection program.

The structure for collecting truck weight data parallels traditional traffic volume counts and classification counts by referencing the need for both permanent weight data collection combined with short-duration weight data collection. The primary purpose of the permanent weight data collection is again to provide needed information on temporal variations in the data

that are necessary to aid in the conversion of short-duration counts into more accurate estimates, while the short-duration (temporary) weight data collection provides the geographic coverage of data that cannot be achieved economically by permanent weight data locations. The difference in this application, however, is the duration of data collection for the permanent locations.

Although permanent weight data collection locations are in place in most states throughout the nation, these locations do not generally collect data on a continuous basis. Rather, these sites provide data collection at select increments, generally quarterly, for durations that range from a minimum of 48 hours to one-week. The most recent version of the TMG, however, has recommended that at least one permanent weight data collection location for each truck weight group should collect data on a continuous basis (365 days per year). The new TMG further recommends that permanent weight data collection locations that do not provide continuous data should provide data for a period of seven continuous days. The short-duration (temporary) weight data collection is then accomplished using temporary data collection devices at a number of locations throughout the geographic region at shorter (generally 48-hour to one-week) time intervals (55).

Both the permanent weight data collection locations and the temporary short-duration data collection locations are generally accomplished using WIM technology, a technology that will be discussed in the following subsection.

#### 2.3.4 *Weigh-in-Motion Technology*

WIM technology had its beginnings in the early 1950s when the U.S. Bureau of Public Roads, the Virginia State Department of Highways, and the Williams Construction Company installed a load cell WIM system on the Henry G. Shirley Memorial Highway. This technology spread across the nation in the 1960s, when the California Department of Transportation (Caltrans) became actively involved in WIM research and application. From these early beginnings, WIM technology and application continued to advance through the early 1980s. The first national WIM conference was held in 1983 as a starting point in the process to formalize WIM technology and needs on a more standardized level (71). Shortly after this conference, the American Society for Testing and Materials (ASTM) published the first *Standard Specification for Highway Weigh-in-Motion (WIM) Systems with User Requirements and Test Methods* (Designation: E 1318-90) in 1990. This document was revised in 1994, and again in 2002 to the version (Designation: E 1318-02) that is used today (62).

ASTM Designation: E 1318-02 describes WIM as “the process of measuring the dynamic tire forces of a moving vehicle and estimating the corresponding tire loads of the static vehicle” (62). In addition to the collection of dynamic tire forces, a variety of ancillary traffic data can also be obtained through the use of WIM systems. These data include traffic volume, speed, directional distribution, lane distribution, date and time of passage, axle spacing, and vehicle classification. Of all data collection methodologies, WIM data collection requires the most sophisticated technology for data collection sensors, as well as the most controlled operating environment (smooth, level pavement) and the highest equipment set-up and calibration costs.

The primary reason for the needed sophistication in technology and the relatively high equipment set-up and calibration costs comes from a need to determine static weight from a dynamic measurement. In standard weigh scale application, vehicles are stopped on a static scale and are measured without any interaction between the vehicle and the roadway. In WIM applications, a variety of forces are acting on the vehicle, including the force of gravity as well as dynamic effects of influences such as (62):

- roadway roughness;
- vehicle speed;
- vehicle acceleration and deceleration;
- out of balance tires and wheels;
- tire inflation pressure;
- suspension;
- aerodynamics and wind; and
- other dynamic factors.

As a vehicle travels along the roadway, these dynamic forces cause the measured weight of the vehicle to vary, thus necessitating the need for a sophisticated calibration process. An illustration of the effects of weighing a vehicle dynamically at high speeds versus weighing a vehicle in a static manner is provided in Figure 2.10 (72). In this figure,  $W_s$  represents the static weight of a vehicle, while  $W_d$  represents the dynamic weight at the WIM location. The oscillating line represents the variation in the dynamic weight of the vehicle due to the factors outlined (55, 72).

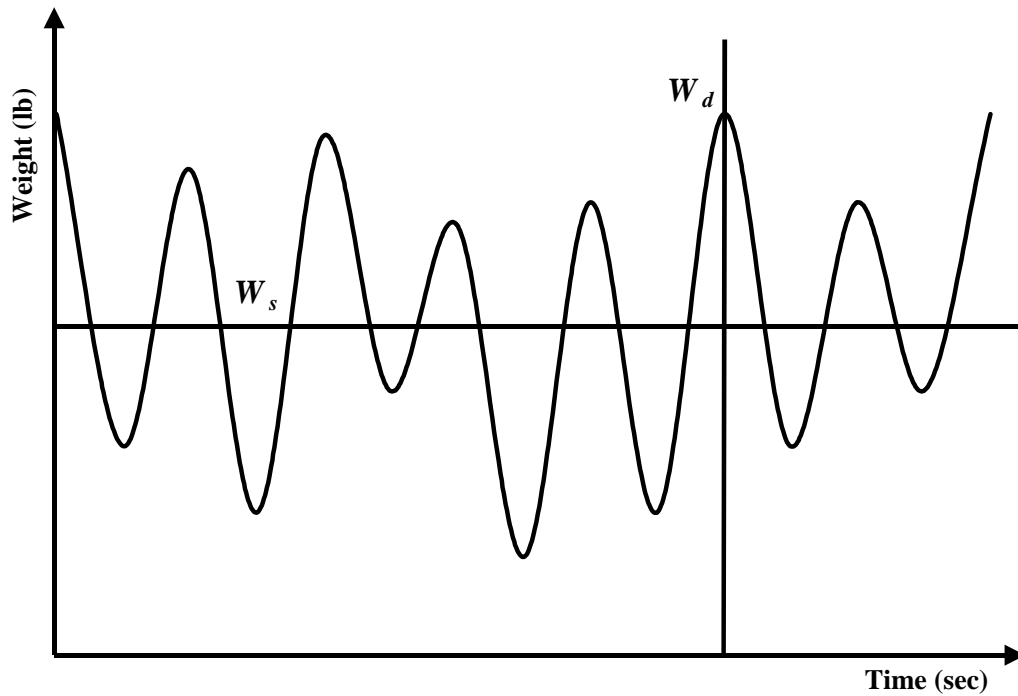


**FIGURE 2.10** Static versus dynamic vehicle weight (adapted from 55, 72)

ASTM Standard Designation: E 1318-02 has designated four specific types (Type I, II, III, and IV) of WIM systems based on application and performance requirements for data collection. The standard provides specific guidelines and user requirements that must be met for each of the specific WIM type designations and should be consulted in the set-up and installation of any WIM system. The standard also refers to Section 2.20 of the *Specifications, Tolerances, and Other Technical Requirements for Weighing and Measuring Devices, National Institute of Standards and Technology (NIST) Handbook 44, 2003 Edition (73)* for definitions and standards for each weighing device.

In general terms, each of the different types of WIM systems are designed to accommodate highway vehicles at a range of speeds, with data collection produced for a variety of weight, speed, and classification metrics. A summary of the operating characteristics and data collection metrics that can be accommodated by each of the four types of WIM systems included in Table 2.5, where traffic data collection refers to weight, classification, and volume data collection (62, 74).

**TABLE 2.5 ASTM WIM System Classification Summary**

	Classification of WIM System <sup>1</sup>			
	Type I	Type II	Type III	Type IV
Speed Range	10–80 mph	15–80 mph	10–80 mph	2–10 mph
Application	Traffic data collection	Traffic data collection	Weight enforcement	Weight enforcement
Bending Plate	X	X	X	X
Piezoelectric Sensor	X	X		
Load Cell	X	X	X	X
Wheel Load	X		X	X
Axle Load	X	X	X	X
Axle-Group Load	X	X	X	X
Gross-Vehicle Weight	X	X	X	X
Speed	X	X	X	X
Axle Spacing	X	X	X	X
Vehicle Classification	X	X		
Site Identification Code	X	X	X	X
Lane/Direction of Travel	X	X	X	
Date/Time of Passage	X	X	X	X
Vehicle Record Number	X	X	X	X
Wheelbase <sup>2</sup>	X	X		
ESALs	X	X		
Violation Code	X	X	X	X

<sup>1</sup> Cells designated with “X” indicate that the WIM system can accommodate the specified data collection

<sup>2</sup> Measured from front axle to rear axle

**TABLE 2.6 Functional Performance Requirements for WIM Systems**

Function	Tolerance for 95% Probability of Conformity				
	Type I	Type II	Type III	Type IV	
				Value $\geq$ lb <sup>1</sup>	$\pm$ lb
Wheel Load	$\pm 25\%$		$\pm 20\%$	5,000	300
Axle Load	$\pm 20\%$	$\pm 30\%$	$\pm 15\%$	12,000	500
Axle-Load Group	$\pm 15\%$	$\pm 20\%$	$\pm 10\%$	25,000	1200
GVW	$\pm 10\%$	$\pm 15\%$	$\pm 6\%$	60,000	2,500
Speed	$\pm 1$ mph				
Axle Spacing	$\pm 0.5$ ft				

<sup>1</sup> Lower values are not usually a concern for enforcement

Each type of WIM system has been specified to perform its indicated functions within specific tolerances. The ASTM standard has outlined the functional performance requirements for WIM systems summarized in Table 2.6 (62). When vehicle classification data are collected

by WIM systems, it is recommended that the classification be recorded according to the axle arrangements of the FHWA vehicle classification schemes discussed previously.

Several different technologies are available for WIM data collection systems (31, 74, 75, 76). The three most commonly used are piezoelectric, bending plate, and load cell (74). The following subsections provide a brief summary of each of these three technologies.

**2.3.4.1 Piezoelectric WIM Technology** Piezoelectric WIM systems are the most common WIM sensor for data collection purposes and have been used for highway data collection since the 1970s. Piezoelectric WIM systems are categorized as either Type I or II according to the ASTM Designation: E 1318-02 classification system (62). The basic construction of a piezoelectric sensor includes a copper central conductor coated with piezoelectric material and then covered by an outer copper sheath. These sensors are generally encapsulated in an aluminum channel to protect the piezoelectric cable and maintain its position. When pressure is applied to the piezoelectric material, an electrical charge is created. The value of the electrical charge is used to estimate the dynamic load of the axle. The dynamic load and associated calibration parameters are then utilized to estimate the static load of the axle or wheel (31, 72, 74, 77).

Piezoelectric sensors are embedded in the pavement and generally consist of one or more sensors placed across a traffic lane. The installation of the piezoelectric system allows it to conform to the profile of the roadway, thus utilizing the characteristics of the pavement to carry the signal. Installation of the piezoelectric sensor is relatively easy and involves only a small cut (generally 1 inch to 2 inches deep and 1 inch to 2 inches wide) in the pavement surface. This minimizes the impact to the pavement and allows the system to be installed in a short timeframe with minimal disruption to traffic during installation (31, 72, 74, 77).

A typical piezoelectric WIM system consists of at least one sensor and one inductive loop. It is common, however, to install two piezoelectric sensors and two inductive loops in each lane that is being monitored. The sensors are placed in the travel lane perpendicular to the direction of travel, with inductive loops placed both upstream and downstream of the detectors as illustrated in Figure 2.11 (77). The upstream loop is used to detect vehicles and alert the system of an approaching vehicle, while the downstream loop is used to determine the speed and axle spacing based on the time it takes to travel between loops (31, 72, 74, 77).

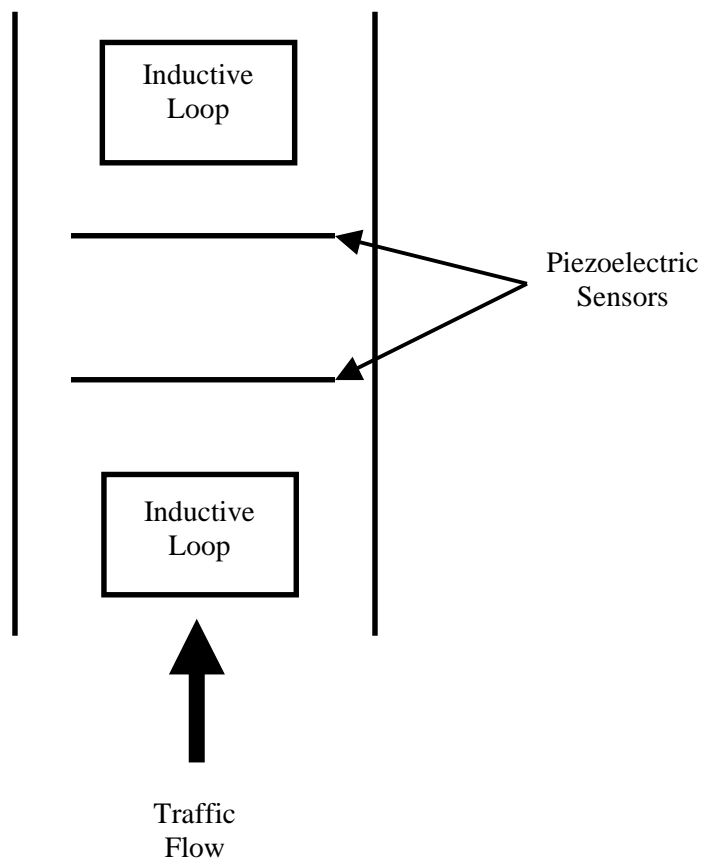


**FIGURE 2.11** Typical piezoelectric WIM system design (adapted from 77)

Piezoelectric WIM systems generally provide results of GVW within approximately 10 to 15 percent of the static vehicle weight for 95 percent of the vehicles measured at highway speeds. The estimated initial cost per lane for a fully installed piezoelectric WIM system is approximately \$9,000 to \$9,500 (72, 74, 77).

**2.3.4.2 Bending Plate WIM Technology** The second type of WIM technology is the bending plate, or bending plate with strain gauge technology. Bending plate WIM systems can be categorized based on the intended use of the device and the number of scales placed in a given lane as Type I, II, III or IV according to the ASTM Designation: E 1318-02 classification system (62, 74). The basic construction of a bending plate system consists of two high strength, thin steel plates—2 feet wide by 6 feet long—placed adjacent to each other, or staggered 16 feet, to

cover a typical 12-foot lane. The plates are equipped with wire strain gauges bonded to the underside to measure the strain in the steel plate as vehicles pass over the system. The strain measured in the plates is used to calculate the dynamic load, while the static load is estimated based on the measured dynamic load and the associated calibration parameters of the system (31, 72, 74, 77).

There are two basic installation methods for a bending plate scale. The first is referred to as a “quick installation” and is used in concrete roadways where sufficient depth exists to install the system in a shallow excavation of the surface of the roadway. The scale frame is then anchored in place using epoxy and anchoring bars. Where sufficient depth does not exist for the quick installation, a concrete foundation and support frame must be installed to create a secure foundation or “vault,” for the scale. The vault is typically designed in a pit 2 feet 6 inches deep by 4 feet 10 inches wide and 13 feet 10 inches long (72, 77).

The typical bending plate WIM system consists of at least one scale and either two inductive loops, or one inductive loop and one axle sensor. The scales are placed in the travel lane perpendicular to the direction of travel, with inductive loops placed upstream and downstream of the detectors (similar to the piezoelectric design). The upstream loop is used to detect vehicles and alert the system of an approaching vehicle, while the downstream loop is used to calculate the speed and axle spacing of the vehicle (72, 74, 77). The vehicle speed and axle spacing can be found three different ways, depending on the set-up of the system. The first method uses the time traveled from the weigh pad to the downstream inductive loop, the second is from the weigh pad to an axle sensor, and the third is from weigh pad to weigh pad (assuming the weigh pads are staggered) (74). If an axle sensor is utilized in the installation, it is placed downstream of the weigh pad as illustrated in Figure 2.12 (77).

Bending plate WIM systems generally provide GVW within approximately 5 to 10 percent of the static weight for 95 percent of the vehicles measured at highway speeds. The estimated cost per lane for a fully installed bending plate system varies between approximately \$18,900 and \$21,500 (72, 74, 77).

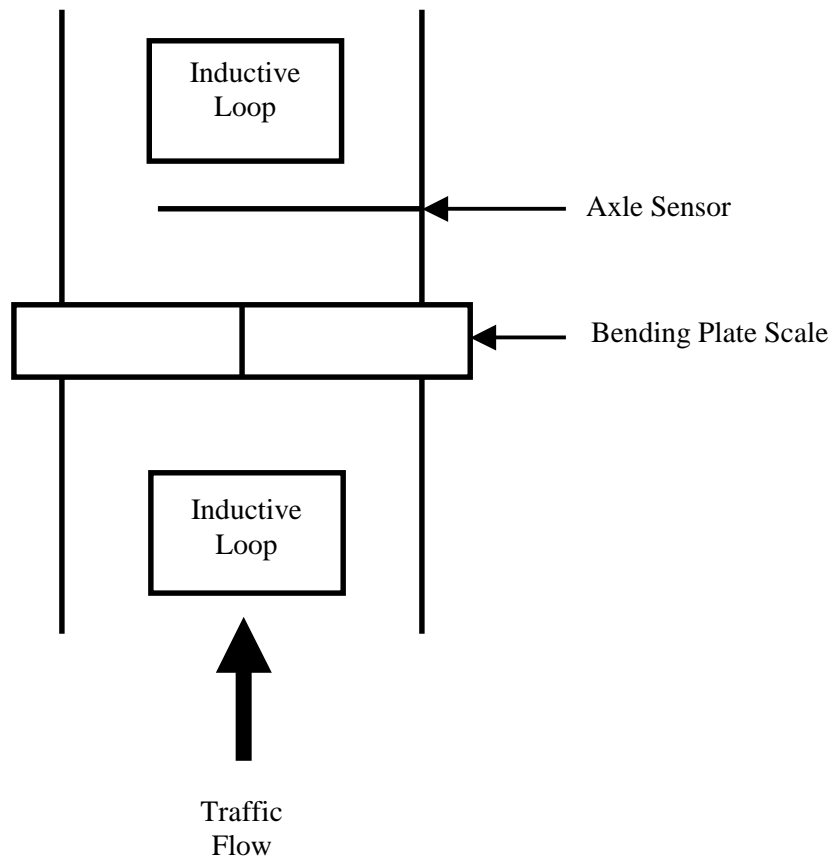


**FIGURE 2.12** Typical bending plate WIM system design (adapted from 77)

**2.3.4.3 Load Cell WIM Technology** The final WIM technology is the load cell scale design. Load cell scales are categorized as either single or multiple load cell scales. As with the bending plate WIM, load cell systems are categorized based on the site design as Type I, II, III, or IV according to the ASTM Designation: E 1318-02 classification system (74). The single load cell scale incorporates two weighing platforms—3 feet 2 inches wide by 6 feet long—placed adjacent to each other to cover a typical 12-foot lane. Each plate is instrumented with a single hydraulic load cell at the center of the platform to measure the force applied to the scale. The force, or hydraulic pressure, is measured to calculate the dynamic load, while the static load is estimated based on the calculated dynamic load and the associated calibration parameters of the system (31, 72, 74, 77). The multiple load cell is a similar design with one main difference. Rather than including only one load cell per weighing platform, the multiple load cell design utilizes as many as four load cells per platform for improved accuracy in the measurement.

The installation of a single load cell requires the use of a concrete vault to form a pit for the hydraulic load cell. The size of the vault required for the load cell design is slightly larger than that used in the bending plate vault design, with a typical vault measuring 3 feet 2 inches deep by 4 feet 10 inches wide and 13 feet 9 inches long (72, 77).

The load cell WIM system is installed in a lane with at least one inductive loop and one axle sensor. Typically, the system is installed with two inductive loops and one axle sensor to provide accurate vehicle length and axle spacing information. The load cell is placed in the travel lane perpendicular to the direction of travel, with an inductive loop placed upstream of the load cell to detect vehicles and alert the system of an approaching vehicle. If a second inductive loop is used, it is placed downstream of the load cell to determine axle spacing, which is then used to calculate vehicle speed. The axle sensor is also placed downstream of the load cell to determine axle spacing and speed as illustrated in Figure 2.13 (74, 77).

Load cell WIM systems generally provide GVW within approximately 3 to 6 percent of the static weight for 95 percent of the vehicles measured at highway speeds. The approximate cost per lane for a fully installed load cell system varies between approximately \$48,700 and \$52,500 (72, 74, 77).

A summary of the performance levels and cost comparison of different WIM systems is provided in Table 2.7 (72, 74, 78). It is apparent from the data contained in this table that the load cell technology is the most accurate of all systems, with the highest overall installation and life cycle cost. The piezoelectric system has the lowest performance level of all systems, as well as the lowest estimated installation and life cycle cost, and is the most common system in use today.

**TABLE 2.7 WIM System Performance and Cost Comparison**

<b>WIM System</b>	<b>Performance (Percent Error on GVW at Highway Speeds)</b>	<b>Estimated Initial Cost per Lane (Equipment and Installation)</b>	<b>Estimated Average Cost per Lane (12-Year Life Span)</b>
Piezoelectric Sensor	±15%	\$9,000–\$9,500	\$4,224–\$4,750
Bending Plate Scale	±10%	\$18,900–\$21,500	\$4,990–\$6,400
Load Cell Scale	±6%	\$48,700–\$52,500	\$7,296–\$8,300

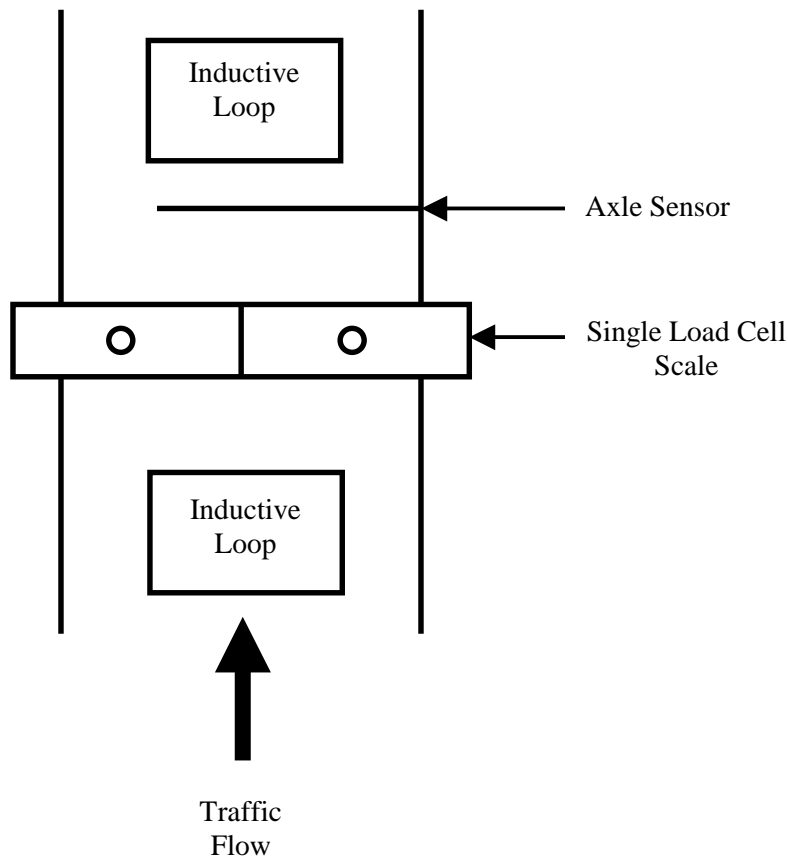


**FIGURE 2.13** Typical single load cell WIM system design (adapted from 77)

### 2.3.5 WIM System Installation and Calibration

Regardless of the WIM technology utilized, an adequate operating environment for the sensors and instruments must be provided to perform properly. As mentioned previously, of all data collection systems, WIM requires the most controlled operating environment. The accuracy and performance of the WIM system depends upon the quality of the sensors and their prevailing operating environment. ASTM Designation: E 1318-02 provides detailed requirements and recommended tolerances for horizontal alignment, longitudinal alignment, cross slope, lane width and markings, surface smoothness, pavement structure, instrument environment, power, data communication, and temperature range and should be referred to in site design (62). Some of the basic requirements that must be met to install a successful WIM site are as follows (55):

- pavement that is smooth, flat (in all planes), in good condition, and strong enough to adequately support axle weight sensors;
- constant vehicle speeds over the sensors; and
- convenient access to power and communications (although these can be supplied from solar panels and through various forms of wireless communications).

Because the success of a WIM system depends upon the conversion of a dynamic weight to that of a static vehicle weight, it is essential that the system be calibrated regularly to offset the site conditions outlined previously (i.e., roadway roughness, vehicle speed) that can have a detrimental effect on the weight estimated by the system, and to ensure that specified tolerances are being met and accurate data collected. These effects are even more critical when utilizing WIM data to calculate ESALs for use in pavement design. The current AASHTO ESAL design procedure involves a fourth-order relationship between damage and axle weight. As a result, the effects of poor calibration of a WIM system can be magnified considerably in the actual loading application (64). The relationship is often simplified by stating that the damage from a single-axle can be calculated based on the relationship outlined in Equation 2.16 (55).

$$D = \left( \frac{W_a}{18,000} \right)^4 \quad (2.16)$$

where:  $D$  = damage from a single-axle and  
 $W_a$  = axle weight (lb).

In a 1998 USDOT FHWA publication it was recorded that for every 1 percent that a WIM scale is under calibrated, a 3 percent under-estimation of the true ESAL value results. In addition, for every 1 percent that axle weights are over-calibrated, a 4.5 percent over-estimated value of ESALs will result. Based on this relationship, a 10 percent over-calibration of vehicle weight results in a 45 percent over-estimation in ESAL calculation (55, 78). This relationship further emphasizes the need for proper calibration of WIM systems.

To account for the calibration of WIM systems, two key issues must be addressed: 1) the calibration of the WIM equipment and 2) the monitoring of the data that are generated by the WIM system to detect sudden changes in the data, as well as drift in the data results, that

could indicate a loss of calibration of the WIM sensors. Each of these two items will be discussed in the following subsections.

**2.3.5.1 WIM Sensor Calibration** A number of attempts have been made over the years to develop an inexpensive yet accurate WIM calibration procedure. Two such attempts were made by NCHRP projects, both of which have not been as widely adopted as originally anticipated due to their cost and complexity (55, 79, 80). A third technique that has been widely adopted for use is outlined in ASTM Designation: E 1318-02. This process involves the use of test trucks of known weight used to compare the estimated weight from the WIM system. Multiple passes are made with the test trucks over the WIM scale, and adjustments are made to the scale's calibration based on the results of the pass. Additional passes are then made to confirm that the performance of the scale has improved to the level of accuracy desired. Although this methodology is not as robust as the NCHRP procedures, the process has been far more widely accepted than any other calibration procedure (55, 62, 74).

The test truck procedure generally involves the use of two loaded pre-weighed and measured test vehicles that each make multiple runs over the WIM system sensors in each lane at specified speeds. Based on the ASTM standard, one of the loaded vehicles should be an FHWA Class 5 vehicle, while the second vehicle is generally an FHWA Class 9 vehicle. The test vehicles are recommended to have a suspension system that is representative of the majority of vehicles on the highway being tested, and they should be loaded to at least 90 percent of the registered GVW with a non-shifting symmetric load. It is important that the vehicles are in good operating condition and that the tires are inflated to the recommended pressure (62).

The test procedure begins by adjusting all WIM system settings to the vendor's recommendations or to the best estimate of the proper setting based upon previous experience. The test proceeds with each test vehicle making a series of three or more runs over the WIM system sensors at the minimum and maximum speed specified by the user within the acceptable limits of the WIM system type (Type I, II, or III). The maximum specified speed is recommended to be less than the legal speed limit of the site, and the maximum and minimum speeds are recommended to differ by at least 20 mph. In addition, each test truck should also pass over the sensors three or more times at an intermediate speed that is representative of the prevailing speed of the roadway. Each of the three runs is recommended to occur at a different location in the lane (i.e., left edge, right edge, middle), with all data recorded for each run. Once

the calibration runs have been completed for each test vehicle, the difference in the WIM system estimate and the respective reference value for the test vehicles for each speed, wheel load, axle load, tandem axle load, GVW, and axle-spacing value should be calculated as a percent difference in weight. From these differences, a mean value for the difference for each set of values should be calculated. Using this difference, appropriate changes to the WIM system calibration settings should be conducted in accordance with the manufacturer's recommendations to adjust the mean value of the respective difference for each value to equal approximately zero (62).

The standard test procedure is not without bias, however, since the test truck will have a dynamic interaction with the roadway that may or may not be the same as other vehicles on the system. The relationship between the dynamic and static weight of a vehicle was outlined previously, indicating the importance of calibration and the interaction that occurs between the vehicle and the roadway. The oscillation presented earlier may or may not be unique for each vehicle on a given roadway. When the calibration procedure is completed using only one vehicle, the range of dynamic interactions possible on the roadway may not be represented. This can be compensated using any of the following five alternatives to improve the accuracy with which calibration is accomplished (55).

1. A scale sensor can be used to physically measure the truck weight for a long enough time period as to be able to account for the truck's dynamic motion.
2. Multiple sensors can be used to weigh the truck at different points in its dynamic motion, either to average out the dynamic motion or to provide enough data to predict the dynamic motion.
3. The relationship of the test truck to all other trucks can be determined by mathematically modeling the dynamic motion of the truck being weighed to predict where in the dynamic cycle it is when it reaches the scale.
4. More than one type of test truck can be used in the calibration effort to get a sample of the vehicle dynamic effects at that point in the roadway.
5. Independent measurements can be used to ensure that the data being collected are not biased as a result of the test truck being used.

Each of these alternatives has pros and cons associated with its implementation, and each has been experimented with in some form or another. The first two techniques are somewhat similar and in many aspects have the best chance for long-term success. A new technique that has been tested that relates to this alternative is the addition of an artificial neural network to “teach” a WIM system to better estimate vehicle weight (81). The biggest downside to these alternatives is the capital costs associated with the installation of multiple sensors. The third technique has strong theoretical backing but can be difficult to measure in the field due to the dynamic interaction of the vehicle. This technique is currently being researched through the use of vehicle simulation programs such as VESYM (82). The fourth approach is the most widely used approach and is the recommendation of the FHWA LTPP projects (55). The fifth and final approach is also used frequently by agencies such as Caltrans and utilizes independent measurements, including speed variations, expected truck weights, and the front axle weight of FHWA Class 9 trucks (55, 74).

**2.3.5.2 Monitoring of WIM Data Output** Once a WIM system has been calibrated and is in full operation, a number of techniques can be utilized to monitor the “health” of the WIM system and to determine whether a site is in need of recalibration. The FHWA Class 9 vehicle is by far the most common classification of vehicle on the highway. As a result, the data that are collected for this vehicle class are generally very consistent and thus have been used as the main source of monitoring WIM data output. The most common statistics utilized in the monitoring of a WIM system are as follows (55):

1. the front axle weight of five-axle, tractor semi-trailer trucks (FHWA Class 9);
2. the GVW distribution of five-axle, tractor semi-trailer trucks (FHWA Class 9);
3. the spacing of tandem axles on five-axle, tractor semi-trailer trucks (FHWA Class 9); and
4. traffic volumes for various vehicle classes, with particular emphasis on the percentage of vehicles that fall within each FHWA vehicle classification.

The first of these statistics, the front axle weight of an FHWA Class 9 vehicle, is tested based on a rolling average of the last 100 front axle weights for this vehicle configuration. Due to the general stability of this vehicle type, the front axle weight of the FHWA Class 9 vehicle is generally very consistent. If this mean value changes by more than a specified amount

(generally determined as a function of the site-specific variability of the road being tested), the scale calibration is in question and should be investigated further.

The second statistic is that of the GVW of FHWA Class 9 vehicles. This technique has been adopted by the LTPP program and is accomplished by generating a histogram plot (generally a 4,000 pound bin) of the weights of the FHWA Class 9 vehicles. The underlying logic of this analysis is to examine the histograms and to observe the peaking characteristics of the GVW. History has shown that the peaks in the GVW histogram should remain relatively constant, with the first peak occurring between 28,000 and 36,000 pounds GVW (unloaded or empty vehicles) and the second peak occurring between 72,000 and 80,000 pounds GVW (loaded vehicles). If the peaks are shifted from the expected values, this could mean that the scale is out of calibration (if both peaks are shifted) or some other scale error may be in place, particularly if only one peak has shifted. The histogram will also show if vehicles are being measured at weights higher than the legal limit for the state (generally 80,000 pounds GVW), thus bringing into question the reliability of the data and the scale calibration (55).

The third measure used to monitor the health of a WIM system is the changes in tandem axle spacing, particularly for FHWA Class 9 vehicles. The mean axle spacing of the drive tandems on an FHWA Class 9 vehicle is generally constant. If the axle spacing for the tandem axles are not constant, or are not within acceptable ranges, the calibration of the system may again be in question (55).

The final monitoring device for WIM system health is to compare the expected truck volumes by classification with the actual volumes measured. This is generally done in terms of total volume of trucks by classification and percentage of trucks within each classification. This type of monitoring can be very useful for catching calibration problems early to avoid collecting large numbers of inaccurate data (55).

## **2.4 Statistical Analysis Tools**

The primary objective for the field of statistics is “to make inferences about a population from information contained in a sample” (83). Oftentimes the data that are contained in the sample include observations on more than one variable where there is some type of interdependence between the variables. This type of statistical analysis is referred to as the analysis of multiple variables, or simply multivariate analysis (84).

The interdependence between variables in multivariate datasets often makes it possible to reduce the total number of variables in the analysis while retaining the accuracy of the statistical sample. Several different methodologies exist wherein the number of variables of multivariate datasets can be reduced for ease of analysis. Some of these include principal component analysis, factor analysis, canonical correlations, and partial least squares. In addition to reducing the total number of variables in the analysis, additional methodologies to better understand the relationships that exist between multivariate datasets are also available. One of the most universal of these methodologies is recursive partitioning. Several different techniques are available for the analysis of data using recursive partitioning, or “data mining,” methodologies. Two of the more common techniques are CART (85) and FIRM (86).

The two primary statistical tools utilized in this dissertation to explore the relationships in a multivariate dataset include: 1) PCA and 2) the recursive partitioning tool CART. A background discussion on each of these statistical tools is provided in the following subsections.

#### *2.4.1 Principal Component Analysis*

The concept of PCA had its beginnings in the early part of the 20<sup>th</sup> century in papers by Pearson (87) and Hotelling (88, 89). In 1975, Bryant and Atchley (90) compiled their work and that of several others into a collection of papers on multivariate statistics. Hotelling’s research set the stage for the standard algebraic derivation of PCA, while Pearson was more concerned with finding lines and planes which best fit a set of points in  $p$ -dimensional space, leading to the concept of principal components (PCs). Hotelling’s motivation for this research was based upon the fundamental theory that there may be a smaller set of independent variables that determine the values of the original variables. In this work, Hotelling introduces the term “components” to describe the variables that come as a result of the analysis, rather than using the term “factor” to avoid confusion with uses of the word factor in mathematics (91).

The central idea of PCA is to reduce the dimensionality of a multivariate dataset while retaining as much of the variation in the data as possible. This is accomplished by transforming the data to a new set of variables, the PCs, which are uncorrelated and ordered linear transformations of the original set of variables. The PCs are ordered so that the first few retain most of the variation present in all of the original set of variables (91). The following subsections provide background on the definition and derivation of PCA, followed by discussion

on methodologies available to determine the total number of PCs to adequately represent the total variation in a dataset.

**2.4.1.1 Definition and Derivation of Principal Component Analysis** Consider  $\mathbf{x}$ , a vector matrix of  $p$  random variables where the variances of the random variables as well as the structure of the covariances or correlations between the random variables are of interest. To explore the variances and correlations between variables, it is not always helpful to simply look at the  $p$  variances and all of the  $0.5p(p - 1)$  correlations or covariances between the variables, unless the number of random variables is relatively small. An alternative approach is to look for a few variables that can preserve most of the information given by the variances, correlations, or covariances of the data, where the number of new variables is much less than the original vector of  $p$  random variables ( $\ll p$ ) (91).

Although PCA concentrates on variances, it does not ignore covariances and correlations completely. The first step in beginning to analyze the PCA is to look for a linear combination or linear function  $\alpha'_1 \mathbf{x}$  of the components or variables  $\mathbf{x}$  with maximum variance. In this scenario,  $\alpha_1$  represents a vector of  $p$  constants,  $\alpha_{11}, \alpha_{12}, \dots, \alpha_{1p}$ , and the prime denotes the transpose of the matrix forming the relationship outlined in Equation 2.17 (91).

$$\alpha'_1 \mathbf{x} = \alpha_{11}x_1 + \alpha_{12}x_2 + \dots + \alpha_{1p}x_p = \sum_{j=1}^p \alpha_{1j}x_j \quad (2.17)$$

where:  $\alpha'_1$  = transposed vector of  $p$  constants ( $\alpha_{11}, \alpha_{12}, \dots, \alpha_{1p}$ );  
 $\mathbf{x}$  = vector of  $p$  random variables ( $x_1, x_2, \dots, x_p$ ); and  
 $p$  = random variable.

The next step is to look for a linear function  $\alpha'_2 \mathbf{x}$  that is uncorrelated or orthogonal with  $\alpha'_1 \mathbf{x}$  and that has maximum variance, followed by a linear function  $\alpha'_3 \mathbf{x}$ , uncorrelated or orthogonal with  $\alpha'_1 \mathbf{x}$  and  $\alpha'_2 \mathbf{x}$ , and so on. Each of these functions are linear combinations of the original variables, and the process is continued so that at the  $k^{\text{th}}$  iteration, a linear function is found that has maximum variance subject to being uncorrelated with  $\alpha'_1 \mathbf{x}, \alpha'_2 \mathbf{x}, \dots, \alpha'_{k-1} \mathbf{x}$ . This  $k^{\text{th}}$ -derived variable  $\alpha'_k \mathbf{x}$  is the  $k^{\text{th}}$  PC, where up to  $p$  PCs are possible. The objective of the PCA is to show that most of the variation in  $\mathbf{x}$  will be accounted for by  $m$  PCs, where  $m$  is much smaller than  $p$  ( $m \ll p$ ) (91).

To begin the PCA, the properties of the variance of the PCs must be known or assumed. In the first case, the vector of random variables  $\mathbf{x}$  has known properties in which  $\mathbf{x} \sim (\mu, \Sigma)$ . It is generally assumed in this case that the data are mean centered with  $\mu$  equal to zero, and that the covariance matrix, or the correlation among the columns,  $\Sigma$ , is known. In this matrix, the  $(i, j)^{\text{th}}$  element is the known covariance between the  $i^{\text{th}}$  and  $j^{\text{th}}$  elements of  $\mathbf{x}$  when  $i \neq j$ . In the case where  $\Sigma$  is unknown, the sample covariance matrix  $\mathbf{S}$ , can be used to replace  $\Sigma$  (84, 91). For the case in which  $k = 1, 2, \dots, p$ , the  $k^{\text{th}}$  PC is given by  $z_k = \alpha_k' \mathbf{x}$ , where  $\alpha_k$  is an eigenvector of  $\Sigma$  corresponding to its  $k^{\text{th}}$  largest eigenvalue  $\lambda_k$ . In addition, by normalizing  $\alpha_k$  to have a unit length of one ( $\alpha_k' \alpha_k = 1$ ), the variance of  $z_k$  is equal to  $\lambda_k$  (91).

If it is assumed that  $\alpha$  is a  $p$  component column vector, normalized such that  $\alpha_k' \alpha_k = 1$  (i.e., the sum of the squares of elements of  $\alpha_1$  equals one), PCs can be derived to maximize  $\alpha_1' \Sigma \alpha_1$ , subject to  $\alpha_k' \alpha_k = 1$ , using the technique of Lagrange multipliers. The Lagrange multipliers ( $\lambda$ ) place bounds on  $\alpha$  to avoid potential maximization at infinity, with the resulting maximization function represented by Equation 2.18 (91).

$$\phi_1 = \alpha_1' \Sigma \alpha_1 - \lambda (\alpha_1' \alpha_1 - 1) \quad (2.18)$$

where:  $\phi_1$  = maximization function;  
 $\Sigma$  = covariance matrix; and  
 $\lambda$  = Lagrange multiplier.

Differentiating  $\phi_1$  with respect to  $\alpha_1$  ( $\partial \phi_1 / \partial \alpha_1$ ), and setting this equation equal to zero to maximize the function, Equation 2.19 and Equation 2.20 are obtained (91).

$$\Sigma \alpha_1 - \lambda \alpha_1 = \mathbf{0} \quad (2.19)$$

or

$$(\Sigma - \lambda \mathbf{I}_p) \alpha_1 = \mathbf{0} \quad (2.20)$$

where:  $\mathbf{I}_p$  = ( $p$  by  $p$ ) identity matrix and  
 $\mathbf{0}$  = zero matrix.

From this analysis it can be seen that  $\lambda$  is an eigenvalue of  $\Sigma$  and  $\alpha_1$  is the corresponding eigenvector. To determine which of the  $p$  possible eigenvectors maximizes the value of  $\alpha_1$ , the quantity to be maximized is  $\lambda$ , according to the relationships outlined previously and summarized in Equation 2.21. Thus,  $\alpha_1$  is the eigenvector corresponding to the largest eigenvalue of  $\Sigma$ , and  $\text{var}(\alpha_1' \mathbf{x}) = \alpha_1' \Sigma \alpha_1 = \lambda_1$  is the largest eigenvalue. In general terms, therefore, the  $k^{\text{th}}$  PC of  $\mathbf{x}$  is  $\alpha_k' \mathbf{x}$  and  $\text{var}(\alpha_k' \mathbf{x}) = \lambda_k$ , where  $\lambda_k$  is the  $k^{\text{th}}$  largest eigenvalue of  $\Sigma$  and  $\alpha_k$  is the corresponding eigenvector (91).

$$\alpha_1' \Sigma \alpha_1 = \alpha_1' \lambda \alpha_1 = \lambda \alpha_1' \alpha_1 = \lambda \quad (2.21)$$

Because  $\alpha_p$  cannot equal  $\mathbf{0}$ , it is necessary that  $|(\Sigma - \lambda \mathbf{I}_p)| = \mathbf{0}$ , where  $|(\Sigma - \lambda \mathbf{I}_p)|$  is a polynomial of degree  $p$  in  $\lambda$  and the  $p$  roots are  $\lambda_1 \geq \dots \geq \lambda_p$ . The successive vectors  $\alpha_k$  that solve  $|(\Sigma - \lambda \mathbf{I}_p)| = \mathbf{0}$  are orthogonal and are called the PCs of  $\mathbf{x}$ . The number of PCs,  $m$ , where  $m \ll p$ , that are necessary to explain the overall variance of the parameters must be determined as outlined in the next subsection.

**2.4.1.2 Choosing the Number of Principal Components** A number of methodologies exist to determine the total number of PCs,  $m$ , necessary to adequately represent most of the variation in a multivariate dataset,  $\mathbf{x}$ , containing  $p$  random variables. The most common methodologies that exist for choosing  $m$  are often referred to as *ad hoc* rules of thumb, justified primarily in terms of their intuitiveness and ability to work well in practice, while several other more statistical methods are also available. The common methodologies include: 1) cumulative percentage of total variation; 2) size of variances of PCs; and 3) scree plots. These methodologies have been utilized in the analysis discussed in this dissertation and will be described in more detail in the following subsections. Further information on additional statistical methodologies may be found in the literature (84, 90, 91, 92).

**2.4.1.2.1 Cumulative Percentage of Total Variation** Probably the most widely used criterion to determine the number of PCs,  $m$ , is to select a cut-off value for the percentage of total variation to be accounted for by the PCs. Depending on the dataset to be analyzed, this value can range

anywhere from approximately 75 percent to as high as 95 percent. In some instances, this value may be less than 75 percent, depending on the accumulation of variation that is accounted for, as more and more PCs are included. Once this cut-off value has been determined, the number of PCs is the smallest value of  $m$  in which the chosen value is exceeded (91).

To calculate the percentage of the variance that is accounted for by the first  $k$  PCs, a number of relationships must hold true. First, by definition, PCs are successively chosen to have the largest possible variance ( $\lambda_1 \geq \dots \geq \lambda_p$ ). When analyzing a sample of data, the variance of the  $j^{\text{th}}$  PC is referred to as  $l_j$ . In addition, the sum of the variances of all PCs is equal to the sum of the variances of all elements  $p$ , in  $\mathbf{x}$  ( $s_{jj}$ ), according to the relationship  $\sum_{j=1}^p l_j = \sum_{j=1}^p s_{jj}$ . The percentage of variation accounted for by the first  $k$  PCs, therefore, can be summarized as outlined in Equation 2.22, with a reduced version of this equation provided in Equation 2.23 for the case of a correlation matrix (91).

$$t_k = 100 \frac{\sum_{j=1}^k l_j}{\sum_{j=1}^p s_{jj}} = 100 \frac{\sum_{j=1}^k l_j}{\sum_{j=1}^p l_j} \quad (2.22)$$

$$t_k = \frac{100}{p} \sum_{j=1}^k l_j \quad (2.23)$$

where:  $t_k$  = cumulative percent of variation for  $k$  PCs;  
 $l_j$  = variance of the  $j^{\text{th}}$  PC;  
 $s_{jj}$  = sum of variances of all elements  $p$ , in  $\mathbf{x}$ ; and  
 $k$  = number of PCs ( $k \leq p$ ).

Choosing a cut-off value,  $t^*$  in the range of 70 percent to 90 percent and retaining  $m$  PCs, where  $m$  is the smallest integer,  $k$ , in which  $t_k > t^*$ , provides a situation in which the first  $m$  PCs are able to preserve the majority of the variation in  $\mathbf{x}$ . In general, the cut-off value for  $t^*$  will become smaller as  $p$  increases, or as the number of observations,  $n$ , increases (91).

*2.4.1.2.2 Size of Variances of Principal Components* The second methodology, mentioned only briefly here, is constructed primarily for use with correlation matrices and indicates that if all elements of  $\mathbf{x}$  are independent, then the PCs are the same as the original variables and have unit

variances. Thus, any of the PCs with variance less than one contain less information than the original variables and are, therefore, not worth retaining (91). This rule is also referred to as Kaiser's rule (93), which retains only those PCs whose variances,  $l_k$ , are greater than or equal to one.

It has been argued that a cut-off value of  $l_k = 1$  may retain too few variables and that other cut-off values ( $l_k^*$ ) should be considered. Jolliffe (94) has suggested that a cut-off value of 0.7 is roughly the correct level to use based on simulation studies. An alternative to this is to consider looking at the size of individual variances through the use of the "broken stick model." This model indicates that if we have a stick of unit length, broken at random into  $p$  segments, then the expected length of the  $k^{\text{th}}$  longest segment can be identified according to Equation 2.24. Using this equation, PCs for which the proportion exceeds  $l_k^*$  are retained, while all others are deleted (91).

$$l_k^* = \frac{1}{p} \sum_{j=k}^p \frac{1}{j} \quad (2.24)$$

where:  $l_k^*$  = proportion of PC variance to be retained.

**2.4.1.2.3 Scree Plots** The final methodology discussed is that of the scree plot. The scree plot, or scree graph, was first discussed and named by Cattell (95) and is used in common statistical computer programs today, such as SPSS (96), to determine cut-off levels for PCs. The scree plot is created by graphing the eigenvalues corresponding to each of the variances ( $l_k$ ) against  $k$  and determining from this plot the point  $k$ , at which the slope of lines adjoining the plotted points are "steep" to the left and "not steep" to the right. This value of  $k$  is then determined to be the number of components to be retained,  $m$ .

The methodology to determine the point where the slope changes from "steep" to "not steep" is generally described as the point beyond which the scree plot defines a straight line, not necessarily a horizontal one. The first point on the straight line is taken to be the last component to be retained. If there are two or more straight lines formed by the lower eigenvalues, the cut-off point is generally chosen to be the upper (left-hand) end of the left-most straight line (91). An example of a scree plot is provided in Figure 2.14. In this example, a definable point where the slope changes from "steep" to "not steep" occurs at component four. The results of the scree plot analysis can be used in combination with other methodologies by comparing the eigenvalue,

evaluating the cumulative percentage of total variation, and then comparing these cut-off points with the scree plot.

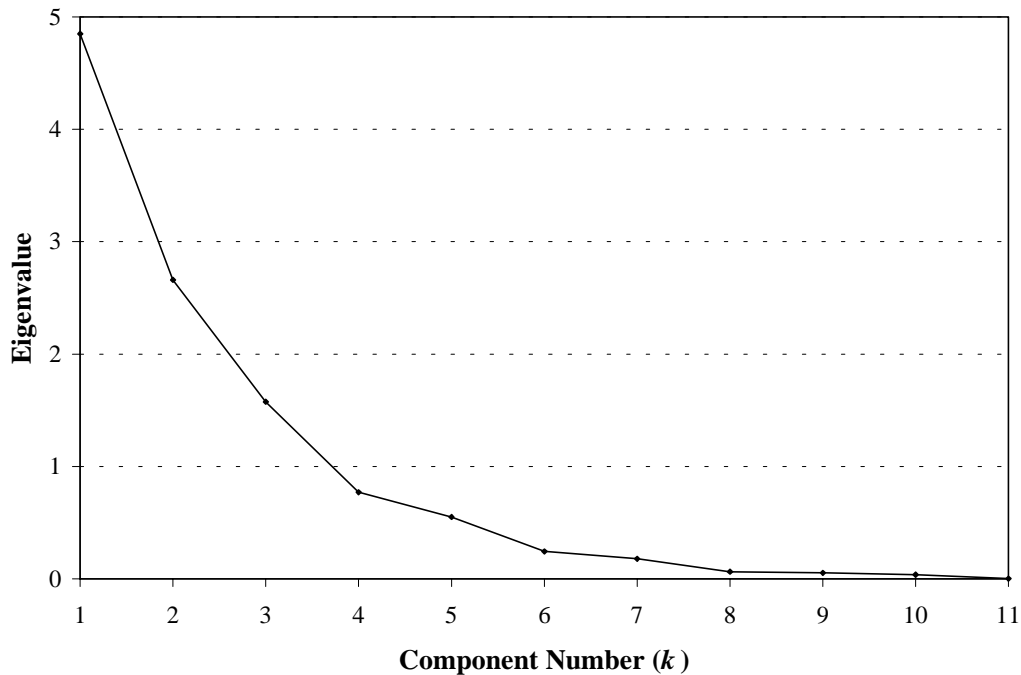


**FIGURE 2.14** Example scree plot

#### 2.4.2 Recursive Partitioning

Recursive partitioning is an effective alternative, primarily in large multivariate datasets, to analyze the relationship between a simple dependent variable and a set of predictor variables. Recursive partitioning continually asks the same questions about the data, only on different groups of data. As these questions are answered and analyzed, the results are disaggregated to show how the data can be organized and grouped. Recursive partitioning methodologies can be applied to both interval-scale (regression) and categorical dependent (classification) variables (86). The analysis for the current dataset is limited to interval-scale (regression) analysis.

Recursive partitioning and the use of regression trees dates back to the early 1960s and the Automatic Interaction Detection (AID) program developed by Morgan and Sonquist at the University of Michigan Institute for Social Research (97, 98, 99, 100). Since this initial

development, a number of methodologies have been proposed to analyze data using the recursive partitioning “data mining” technique. The most familiar and presumably the most utilized methodology available today is CART procedure outlined by Breiman et al. (85). A second highly effective methodology is the FIRM technique developed by Hawkins (86). Other methodologies exist in a variety of software packages, including the SAS JMP product (101). The methodology utilized in this dissertation was the CART algorithm. More detailed information on the CART algorithm, tree structured regression, and pruning and estimating are provided in the following subsections.

**2.4.2.1 CART Algorithm** In regression analysis, the CART algorithm provides an analysis of data  $(\mathbf{x}, y)$ , where  $\mathbf{x}$  refers to the independent variables (in matrix form for multivariate analysis) defined on the measurement space  $\chi$ , and the variable  $y$  refers to the response or dependent variable. A prediction rule or predictor is a function  $d(\mathbf{x})$  defined on  $\mathbf{x}$  taking real values. In regression analysis, the predictor  $d(\mathbf{x})$  is estimated in order to: 1) predict the response variable corresponding to future measurements and 2) to understand the relationships between the response and the measured variables (85).

In the tree structured regression methodology, each node  $t$ , is split into two sub-nodes,  $t_n$ . Each sub-node is then split into two more sub-nodes, and the process continues until some criterion is met. Once this criterion is met, the tree is pruned to obtain the minimum allowable error. An example of this methodology is provided in Figure 2.15. The number of possible splits varies for continuous variables and discrete variables. For continuous variables, the total number of splits is  $n-1$ , where  $n$  is the number of distinct values. For a discrete variable, the total number of splits is more complex, being defined as  $2^{(J-1)}-1$ , where  $J$  is the number of categories (85).

**2.4.2.2 Tree Structured Regression** Several important relationships are necessary in understanding and developing the CART tree structured regression methodology. The first of these relationships is the average mean squared error, used in regression to measure the accuracy of response and predicted variables. The basic equation for the average mean squared error is provided in Equation 2.25 (85).

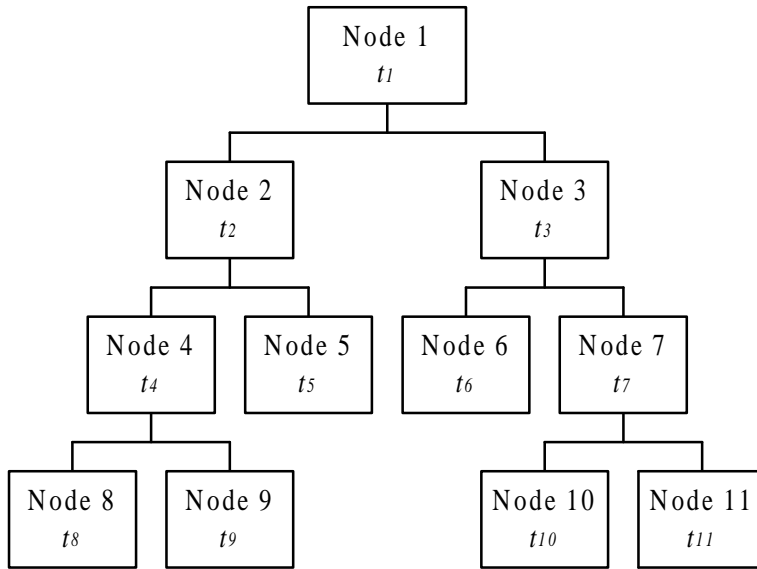


**FIGURE 2.15 Basic CART regression tree structure**

$$R(d) = \frac{1}{N} \sum_{n=1}^N (y_n - d(\mathbf{x}_n))^2 \quad (2.25)$$

where:  $R(d)$  = average mean squared error;  
 $y_n$  = value of the response variable;  
 $d(\mathbf{x}_n)$  = value of the predictor variable;  
 $n$  = case number; and  
 $N$  = total number of cases.

To determine the best possible outcome for this equation, it is necessary to choose a function  $y(t)$ , to minimize  $R(d)$ . The value of  $y(t)$  that will minimize  $R(d)$  is the average of  $y_n$  for all cases  $(\mathbf{x}_n, y_n)$  that fall in the node  $t$ . This relationship is summarized in Equation 2.26 (85).

$$\bar{y}(t) = \frac{1}{N(t)} \sum_{\mathbf{x}_n \in t} y_n \quad (2.26)$$

where:  $\bar{y}(t)$  = average value of all response variables in node  $t$ ;  
 $t$  = node number; and  
 $N(t)$  = total number of cases in  $t$ .

Similarly, for any subset  $y_{n'}$  of the  $y_n$ , the number that minimizes  $R(d)$  is the average of the  $y_{n'}$ . Based on Equation 2.26, the predicted value in any node  $t$  can be referred to as  $\bar{y}(t)$ . The mean squared error can then be defined by Equation 2.27 (85).

$$R(T) = \frac{1}{N} \sum_{t \in \tilde{T}} \sum_{x_n \in t} (y_n - \bar{y}(t))^2 \quad (2.27)$$

where:  $R(T)$  = total mean squared error of all nodes,  $T$  and

$\tilde{T}$  = set of terminal nodes in  $T$ .

The simple interpretation of this equation indicates that for every node  $t$ , the within node sum of squares is defined as  $\sum_{x_n \in t} (y_n - \bar{y}(t))^2$ . Summing this value over all  $t$  in the set  $\tilde{T}$  provides the total within node sum of squares, and dividing this by  $N$  gives the average value (85).

The next step in the analysis is to determine the best split  $s^*$  of  $t$ , given any set of splits  $S$  of a current terminal node  $t$  in  $\tilde{T}$ . By definition, the best split  $s^*$  of  $t$  is that split in  $S$  that most decreases the value of the objective function  $R(T)$ , as outlined in Equation 2.28. The regression tree, therefore, is formed by iteratively splitting nodes, while maximizing the decrease in  $R(T)$  (85).

$$\Delta R(s^*, t) = \max_{s \in S} \Delta R(s, t) \quad (2.28)$$

where:  $\Delta R$  = change in value of the objective function (decrease);

$s$  = current split of  $t$ ;

$s^*$  = best split of  $t$ ; and

$S$  = set of all splits.

Given the nature of the relationship between the nodes, a simplified alternative form of the objective function can be considered. Letting  $p(t) = N(t)/N$  equal the estimate for the probability that a case chosen at random falls into node  $t$ , then the sample variance of the  $y_n$  values in the node  $t$  can be determined as identified in Equation 2.29 (85).

$$s^2(t) = \frac{1}{N(t)} \sum_{x_n \in t} (y_n - \bar{y}(t))^2 \quad (2.29)$$

where:  $s^2(t)$  = sample variance of node  $t$ .

In this scenario,  $R(t) = s^2(t)p(t)$ , with the total mean squared error calculated according to Equation 2.30. The best split of  $t$  is the one that minimizes the sum of the proportion of the cases that go to the left multiplied by the sample variance, and the proportion of cases that go to the right multiplied by the sample variance of these cases as outlined in Equation 2.31 (85). This relationship provides the basis for the splitting criteria in the CART algorithm.

$$R(T) = \sum_{t \in T} s^2(t)p(t) \quad (2.30)$$

$$\min [p_L s^2(t_L) + p_R s^2(t_R)] \quad (2.31)$$

where:  $p(t)$  = proportion of cases in  $t$ ;  
 $p_L$  = proportion of cases that go to the left;  
 $p_R$  = proportion of cases that go to the right;  
 $s^2(t_L)$  = sample variance of the cases that go to the left; and  
 $s^2(t_R)$  = sample variance of the cases that go to the right.

**2.4.2.3 Pruning and Estimating** The final step that must occur in the recursive partitioning process is the pruning and estimating of the dataset to determine whether or not a node has reached its stopping criteria and should be declared terminal. One of the most general criteria to use in making this determination for a categorical analysis is the homogeneity of a node. For regression trees, the decision criterion is more complex, with a variety of alternatives available for determining where the cut-off should be.

In the original AID program, the terminal criterion was met if the value of the objective function at the maximum split was less than or equal to 0.6 percent of the objective function of the initial node. This criterion was followed by the use of re-substitution estimates  $R(T)$  or  $1 - RE(T)$  as a measure of accuracy, where  $RE(T) = R(T)/R(\mu)$ . In general, however, using these methodologies, the trees grown were not the right size, resulting in estimates that were overly

optimistic. In addition, the error measure  $R(t)$  has the property that for any split of  $t$  into  $t_L$  and  $t_R$  that  $R(t) \geq R(t_L) + R(t_R)$ ; thus, the more splitting that is done, the better  $RE(T)$  appears.

In the CART algorithm, a large tree ( $T_{max}$ ) is grown by successively splitting to maximize  $R(T)$  until for every  $t \in \tilde{T}_{max}$ , the number of nodes in the sample is less than or equal to a pre-defined minimum node size ( $N_{min}$ ). In most cases,  $N_{min}$  was taken to be five; however, this value can vary depending on the size of the dataset and the number of categories in the predictor variables. Oftentimes, therefore, the tree would over-fit the data and would then be pruned back to accomplish the desired objective, which in the case of this dissertation is to provide a distribution of truck weight as a function of vehicles classification that best represents the data, as will be presented in Section 4. In many cases the user can determine the level of detail necessary to accomplish the desired objective, paying particular attention to the  $RE(T)$  for each successive split (85).

## 2.5 Microscopic Traffic Simulation Modeling

Section 1.1.2 identified microscopic traffic simulation models such as CORSIM, TRANSIMS, VISSIM, and others as effective transportation analysis tools due to their ability to model the stochastic and dynamic nature of transportation systems, including vehicle composition. These models are used to estimate and forecast traffic conditions and can be used to provide realistic vehicle trajectories, aiding engineers and planners with more accurate estimates of future volumes, which can then lead to better planning of transportation facilities including roadway improvements and infrastructure needs. While in theory microscopic traffic simulation models can be effective for modeling the impacts of CMVs on traffic flow, infrastructure, safety, and other criteria, in practice there has been little research to analyze how best to accomplish this task.

The next three subsections outline briefly the background on the three models introduced in Section 1.1.2 followed by discussions on the benefits of microscopic traffic simulation models, the challenges associated with these models, and the connection that exists between vehicle composition and microscopic traffic simulation models, in an attempt to begin the discussion of how to effectively model CMVs.

### 2.5.1 *Microscopic Traffic Simulation Models*

Three specific models were introduced in Section 1.1.2 to model the dynamic and stochastic nature of transportation systems, while several additional microscopic traffic simulation models are also readily available for this same purpose. The three models outlined in Section 1.1.2 chosen for discussion in this dissertation include CORSIM, TRANSIMS, and VISSIM. A brief description of each of these models will be provided in the following subsections.

**2.5.1.1 CORSIM** CORSIM is one of the most widely used microscopic traffic simulation models in the United States. CORSIM was developed by the FHWA at the Turner-Fairbank Highway Research Center in McLean, Virginia, and consists of an integrated set of two microscopic traffic simulation models, NETSIM and FRESIM. NETSIM represents the traffic on urban streets, while FRESIM provides a representation of traffic on freeways. The CORSIM model is currently operated in a Windows<sup>®</sup> environment through the use of the Traffic Software Integration System (TSIS). CORSIM is a stochastic model, applying a time-step simulation to describe traffic operations, randomly assigning driver and vehicle characteristics to the decision-making process. Each vehicle is modeled individually and can be uniquely identified as one of nine different types of vehicles comprising four vehicle fleets (102). The CORSIM model is considered a medium scale model because it is designed primarily for the analysis of freeway and arterial networks, and can also be classified as a high fidelity model because of its design to represent the spatial interaction of drivers on a continuous, rather than a discrete, basis (26).

**2.5.1.2 TRANSIMS** The TRANSIMS model is another tool that has recently been developed to model transportation systems. The TRANSIMS model departs somewhat from the traditional demand forecasting and traffic simulation models, operating based on input from five integrated modules. These modules include the population synthesizer, activity generator, route planner, traffic microsimulator, and emissions estimator. In addition to these five modules, a selector/iteration database is also included in the model. Utilizing each of these components, TRANSIMS estimates activities for individuals and households, plans trips according to the activities generated, assigns these trips to routes, and then creates a microsimulation of the vehicles within the transportation system. Emissions estimates are then generated based on the microsimulation results, and the process is repeated based on the selector/iteration database (27, 103).

TRANSIMS is defined to be “microscopic” in terms of the resolution of the model because it allows the identification and modeling of individual vehicles (104). The resolution of the model can also be categorized as “fine” because of the ability of the model to represent each individual vehicle in a discrete manner, while the model is large-scale because it is capable of modeling large networks and low fidelity because it uses a minimal representation of road traffic (26, 27, 104). Since the TRANSIMS model allows the identification and modeling of individual vehicles, it is possible to model CMVs using the TRANSIMS model. This is accomplished by generating trip tables for different types of vehicles. The tables can then be transformed into TRANSIMS activities by creating drivers from individuals not created as part of the synthetic populations, choosing the starting and ending point of the trip based on the zones specified in the trip tables, and creating one vehicle for each trip in the trip table. With the known origins and destinations for the CMV trips, the route planner can then generate the routes of the trips for use in the traffic microsimulator phase of the model (103).

**2.5.1.3 VISSIM** VISSIM was developed at the University of Karlsruhe in Karlsruhe, Germany, during the 1970s, with commercial distribution commencing in 1993. VISSIM is a microscopic, time-step and behavior-based simulation model that has been developed to analyze the full range of functionally classified roadway and public transportation operations. VISSIM can model integrated roadway networks found in a typical corridor as well as various modes of transportation and vehicle compositions (4, 105, 106).

The VISSIM model consists of two primary components: 1) the traffic simulator and 2) the signal state generator. The traffic simulator is a microscopic traffic flow simulation model including car-following and lane-change logic. The signal state generator is signal control software that uses detector information from the traffic simulator on a discrete time-step basis as input. The signal state generator then determines the signal status for the following second and returns this information to the traffic simulator. The traffic simulation model for VISSIM uses the psycho-physical driver behavior model developed by Wiedemann (105, 107) to create an iterative process of acceleration and deceleration. VISSIM simulates traffic flow by assigning each driver, and their respective behavioral characteristics, to a specific vehicle. As a consequence, the driver behavior corresponds to the technical capabilities of the vehicle and is consistent across the simulation. This allows the VISSIM model to provide an analysis of a variety of vehicle and driver compositions in the traffic stream (105).

### 2.5.2 *Benefits of Microscopic Traffic Simulation Models*

Several benefits have been identified for microscopic traffic simulation models, probably the most widely publicized of which is the ability of the models to evaluate different alternatives for transportation projects. With the use of a microscopic traffic simulation model, engineers and planners can control the experimental environment of their study area and apply a range of alternative transportation systems to this area to determine overall effectiveness. Another benefit is the ability of these models to test new designs without the expense of construction and potential user costs. In addition, their ability to optimize traffic systems—and provide engineers, planners, and technicians with training and solutions—is also very useful (108).

A related benefit of microscopic traffic simulation models is the ability to model an existing transportation network and to subsequently display the results of this network visually through the use of animation files. This is especially useful when working with governing bodies to aid in decision making for transportation alternatives. With the improvements in computing technology, it has become increasingly important to perform sensitivity analyses on a variety of transportation alternatives and to compare each of these alternatives both statistically through the model output and visually through the use of the animation files.

Microscopic traffic simulation models also provide an opportunity to analyze vehicle composition and to determine the effects of different vehicle compositions on roadway networks. For example, changes can be made to CMV distributions, and the effect of this change on traffic operations can be estimated with the model. As has been explained in previous sections of this dissertation, the need to consider CMVs in the planning and operations analysis is increasing. Microscopic traffic simulation models provide an opportunity to analyze the impacts of these different vehicle compositions and to compare the impacts on traffic flow, infrastructure, safety, and other criteria through both statistical and visual methods.

### 2.5.3 *Challenges of Microscopic Traffic Simulation Models*

One of the challenges identified for microscopic traffic simulation models is the potential lack of understanding of the theory behind the model and the ability to operate the model in its intended manner. For example, Nagel et al. in an analysis of the TRANSIMS model, indicate, “One could probably reach agreement that the traffic flow behavior of traffic simulation models should be well documented. Yet, in practice, this turns out to be somewhat difficult. Many traffic simulation models are under continuous development, and the traffic flow dynamics documented

in a certain publication is often a ‘snapshot,’ valid at the time of writing, but no longer the true state of the model” (104). May et al., in an analysis of freeway systems research and the CORSIM model, concluded, “Direct relationships between desired capacity estimates and CORSIM input parameter(s) were not clear. Research is needed to determine the relationships between the appropriate CORSIM model input parameter(s) and obtaining the desired segment capacity output” (109). Sometimes this lack of documentation and parameter definition makes it difficult to adequately understand the model and make informed decisions utilizing the output.

Another challenge of the microscopic traffic simulation models related to the user of the model is the lack of formal and consistent guidelines regarding the development and application of such models, as well as the lack of consistency in model calibration, validation, and verification. This lack of consistency at times leads to models that are not representative of existing conditions and, therefore, may not adequately project future conditions along the network, which in turn leads to misconceptions, misunderstanding, and an overall lack of trust in the “black box” technology (5, 6, 7).

#### *2.5.4 The Connection between Vehicle Composition and Traffic Simulation Models*

As was pointed out in Section 1.1.4, CMVs and their interaction with automobile traffic appear to be an important aspect of the overall vehicle composition of the nation’s highway system. Additionally, microscopic traffic simulation models have been identified as an important and useful tool in providing information to engineers and planners on both existing and future transportation planning and traffic operational needs. The problem that tends to exist, however, is that these two are not generally connected. Users of microscopic traffic simulation models tend to use default values in their analysis, and when calibration does occur, it does not generally include provisions for vehicle composition. As mentioned earlier, Bloomberg and Dale have recommended that a sensitivity analysis of performance measures (i.e., delay, travel time) based on various traffic compositions should be conducted in the future (4). Earlier research has begun to address this relationship but has been based primarily on volume and travel time characteristics of vehicles, with calibration based primarily on existing characteristics of automobile traffic (4, 5, 7, 8, 9, 26, 27).

The questions that need to be asked as this technology evolves and a methodology for calibration of microscopic traffic simulation models emerge are, first, is it necessary to include a breakdown of vehicle composition in the calibration process and, second, can microscopic traffic

simulation models effectively model truck traffic, and, if so, can these models be calibrated according to data on a mixture of vehicle types. This is particularly true in a border state such as Texas where a 340 percent increase in total truck crossings from Mexico between 1993 and 2001 has been observed (12). Needless to say, in order to examine the effect on traffic flow, infrastructure, safety, and other criteria, accurate information on CMV characteristics (i.e., weight, length, acceleration) are required.

## **2.6 Optimization Algorithms**

A number of optimization algorithms are available for use in calibration of microscopic traffic simulation models. Two of the more commonly used optimization algorithms are the simplex algorithm (SA) and the genetic algorithm (GA) (9). The tool that has been selected for this dissertation is the GA. The purpose of this subsection is: 1) to outline the background of the GA methodology; 2) to identify the overall method for parameter representation in the GA, and 3) to discuss the operating rules for GAs.

### *2.6.1 Background on Genetic Algorithm*

The GA can be generalized as a search method based on the mechanics of natural selection and natural genetics (110). GAs were first developed by Holland in the early 1970s at the University of Michigan (111) and, since that time, have been used for a wide range of applications, including traffic signal timing (112, 113, 114, 115, 116, 117), pavement and bridge maintenance planning (118, 119), ITS applications (120), transit route planning (121, 122), and traffic simulation modeling (9, 123, 124, 125, 126). While the detailed theory behind the GA can be found in the literature (110, 111, 127, 128), a general understanding of the GA methodology and logic is necessary to understand the simulation and calibration results.

In the basic GA procedure, individuals (i.e., calibration parameters) are encoded as strings of chromosomes that are uniquely mapped to each of the parameters. Each chromosome is utilized to represent the decision variable domain and to assess the performance, or “fitness,” of the parameter string. During the analysis phase of the algorithm, the fitness value is calculated based on a predetermined fitness function to evaluate the performance of the chromosome. The fitness value is used during the reproduction phase to determine the probability of being selected for reproduction. The chromosomes whose fitness value is high have a much higher probability of being selected for the next generation and being used to

generate new chromosomes from the “best” chromosomes within the population. In summary, GAs utilize the genetic rules of reproduction, crossover, and mutation to generate populations that include the best parameters to meet the fitness objective.

### 2.6.2 Overall Parameter Representation

In the basic GA procedure, individuals (i.e., calibration parameters) are encoded as strings of chromosomes that are uniquely mapped to each of the parameters. Each chromosome is utilized to represent the decision variable domain and to assess the performance, or “fitness,” of the parameter string. The first step in setting up the GA problem is the determination of a representation scheme for the strings of chromosomes in the analysis. Chipperfield has indicated in a paper on the introduction to genetic algorithms that the most common representation scheme for a string of chromosomes is the binary alphabet, although others including ternary, integer, real-value, etc., can also be used (127). In a review of the literature and GA application, binary encoding has been used almost exclusively and will be utilized in this analysis. A discussion of the binary encoding methodology as well as the initialization of the parameter set is provided in the following subsections.

**2.6.2.1 Binary Encoding Methodology** The basic equations necessary to develop the binary encoding for the GA include a determination of the level of precision necessary for analysis, along with the encoding and mapping of each individual parameter to a binary string, and the resultant overall binary string to represent the set of parameters. If  $x_{ij}$  represents the real value of parameter  $j$  for chromosome  $i$  with a domain in the set  $[x_{min}, x_{max}]$ , the length of the binary string can be calculated by solving the inequality in Equation 2.32, while the mapping of the binary string to a real variable  $x_{ij}$  can be found utilizing Equation 2.33 (9).

$$B_j \geq \log_2 \left( \frac{x_j^{\max} - x_j^{\min}}{D_j} + 1 \right) \quad \forall j = 1, NP \quad (2.32)$$

where:  $B_j$  = length of binary string required to represent parameter  $j$  (integer);  
 $x_j^{\max}$  = maximum value of parameter  $j$  (integer or real);  
 $x_j^{\min}$  = minimum value of parameter  $j$  (integer or real);  
 $D_j$  = desired precision of parameter  $j$  (integer or real);  
 $j$  = parameter in a chromosome (integer or real); and  
 $NP$  = number of parameters.

$$x_{ij} = x_j^{\min} + A_{ij} \times \frac{x_j^{\max} - x_j^{\min}}{2^{B_j} - 1} \quad \forall i = 1, N \quad (2.33)$$

where:  $x_{ij}$  = real valued variable of parameter  $j$  for chromosome  $i$ ;  
 $A_{ij}$  = value of binary string to base 10 of parameter  $j$  for chromosome  $i$ ;  
 $i$  = individual or chromosome (integer or real); and  
 $N$  = number of chromosomes.

The best way to illustrate the application of the above equations is through the use of an example. If a parameter,  $x_{ij}$ , in the range of 30 to 150 (car-following sensitivity factor), with integer precision is considered, the length of the binary string is the minimum integer value that satisfies the following inequality:

$$B_j \geq \log_2 \left( \frac{150 - 30}{1} + 1 \right) = 6.92$$

The required number of bits for this parameter, therefore, must be seven and the parameter can be mapped using a binary string of length seven bits. Suppose further that the parameter  $j$  of chromosome  $i$  is set to a binary string such that:

$$x_{ij} \text{ of Chromosome } i = (0 \ 1 \ 0 \ 1 \ 0 \ 0 \ 1)$$

Then, the base 10 value corresponding to the value of  $x_{ij}$  can be calculated according to:

$$2^5 + 2^3 + 2^0 = 41$$

Finally, the parameter value can be mapped to the real number system using Equation 2.33, as illustrated in this example:

$$x_{ij} = 30 + 41 \times \frac{150 - 30}{2^7 - 1} = 69$$

**2.6.2.2 Initialization of Parameter Set** The first step in the GA algorithm is the initialization of the parameter set and the subsequent identification of the initial population. The primary operators for the GA include the population size ( $P$ ), the maximum number of iterations or generations ( $T$ ), the crossover probability ( $P_c$ ), and the probability of mutation ( $P_m$ ). Based on the format of the binary string and identification of the primary operators, an initial population ( $P$ ) can be generated utilizing a random process. In this process, each of the chromosomes is randomly assigned a value of one or zero, with equal probability for each choice. Each of these operators will be discussed in more detail in the next subsections and again later in this dissertation.

### 2.6.3 Operating Rules for Genetic Algorithms

The basic GA methodology hinges upon the genetic reproduction of the “best” parameter set based on the fitness of the parameter string. To generate the best parameter set and to provide opportunities to modify the best parent chromosomes to produce ideal offspring requires three primary applications. These include crossover, mutation, and the application of specific stopping criteria. Each of these topics will be discussed in the following subsections.

**2.6.3.1 Crossover** The crossover operation is utilized in the GA to enlarge the parameter set by producing additional offspring chromosomes from the parent chromosome set through the exchange of genetic material or genes. The model has been developed such that there are  $P/2$  crossover operations performed at each generation. During the crossover operation, a uniform random number in the range  $[0,1]$  is generated. If the value of the random number generated is less than the crossover probability,  $P_c$ , then a crossover operation is performed. The crossover probability is selected *a priori* following a sensitivity analysis of various probabilities. In the crossover operation, two parent chromosomes,  $q$  and  $r$ , are selected at random based on the probability that the chromosome is selected in the crossover operation ( $p_i$ ). The crossover selection in the algorithm is determined based on a roulette wheel selection (110). In the roulette

wheel selection, each chromosome in the population is assigned a roulette wheel slot sized in proportion to its fitness. As a result, the chromosomes with the highest fitness values have the highest probability of being selected for the crossover operation and, therefore, the highest probability of passing their genes on to the next generation.

Once the parent chromosomes,  $q$  and  $r$ , are selected, the crossover locations ( $k$  and  $k'$ ) are selected randomly along the chromosome bit string. The genes are then switched or “crossed over” to produce two new offspring chromosomes  $q'$  and  $r'$  carrying the basic genetic material from the parent chromosomes, only now slightly altered at the crossover point. An example of the initial chromosomes ( $X_q$  and  $X_r$ ) along with the resulting offspring chromosomes ( $X_{q'}$  and  $X_{r'}$ ) are shown below:

Initial Chromosomes:

Chromosome $X_q$ :	(101001001...101100101...110	00101...101010001)
Chromosome $X_r$ :	(101101110...100011110...110	11001...100111001)
	$k^{th}$ cell	$k'^{th}$ cell

Offspring Chromosomes:

Chromosome $X_{q'}$ :	(101001001...101100101...110	11001...100111001)
Chromosome $X_{r'}$ :	(101101110...100011110...110	00101...101010001)
	$k^{th}$ cell	$k'^{th}$ cell

Both the parent and offspring chromosomes are added to the new set of chromosomes for analysis of the resulting mean absolute error ratio (MAER) and fitness function. A total of  $O_I$  offspring are generated in this step, where  $O_I \leq P/2$  (9).

**2.6.3.2 Mutation** The mutation operation is similar in concept to the crossover operation since the overall goal in both mutation and crossover is to increase the sample space utilizing the “best” chromosomes from the previous generation. The mutation operation is performed  $P$  times, where every chromosome has an equal chance of selection. During each iteration a parent chromosome is selected and a random number sampled in the range  $[0,1]$ . If the random number

is less than the probability of mutation,  $P_m$ , then a mutation operation is performed. As with the crossover probability, the probability of mutation is selected *a priori* following a sensitivity analysis. If the parent chromosome is selected for mutation, a location within the chromosome is identified randomly and the value of the binary cell at that location is changed from a 1 (0) to a 0 (1). At the end of the mutation step, a total of  $O_2$  offspring are created, where  $O_2 \leq P$  (9). As a result of the mutation and crossover, the maximum number of offspring that can be created is  $1.5P$ .

**2.6.3.3 Stopping Rules** The elitist selection method (129) has been utilized to maintain the best chromosome set at the end of each generation. In the elitist methodology, the best chromosomes from each generation are maintained and passed along to the next generation. As a result, as the generations increase, the best chromosomes are kept and used in the mutation and crossover of subsequent generations. A variety of stopping criteria can be selected for use with the GA algorithm, including minimum objective function, maximum fitness value, and minimum change in fitness from one generation to the next. The typical stopping criterion is based on a selection of maximum number of generations,  $T$ , identified *a priori*. This number is generally set based on a sensitivity analysis to identify the generation in which fitness values converge to maximum rates.

## 2.7 Concluding Remarks

This section has provided the background information necessary to analyze the effects of CMVs on the transportation system and to develop a methodology to account for these vehicles using microscopic traffic simulation models. A variety of topics have been covered in this section, including: 1) NAFTA initiatives and their impact on CMVs, particularly in the state of Texas; 2) operating characteristics of passenger cars and CMVs; 3) data collection methodologies available to aid in the collection of automobile and CMV traffic data; 4) statistical tools to analyze the data and make inferences about the analysis results; 5) the use of microscopic traffic simulation models to analyze transportation networks; and 6) optimization algorithms to calibrate microscopic traffic simulation models to aid in this analysis.

The literature review begins by outlining the trends in CMV traffic in the state of Texas, particularly as a result of NAFTA. This analysis provides border crossing trends for CMV traffic between the years 1993 and 2001. These trends include an average growth rate of

16 percent per year in total truck crossings into Mexico from Texas, and an average 25 percent per year increase in total truck crossings into Texas from Mexico. Although the trends show a slight decline in growth from 2000 to 2001, the overall increased growth trend is expected to continue well into the future. This increase in CMV traffic, especially in the state of Texas, provides the basis to evaluate the impacts of CMV traffic on the transportation network and to model these impacts using microscopic traffic simulation models.

The second subsection focuses on CMV impacts by identifying key operational characteristics for both automobile and CMV traffic that should be considered in transportation analyses. The overall performance of vehicles is critical in both design and operations of any transportation network and must be considered for existing and future design considerations. This section leads to a discussion on the data collection methodologies available to collect: 1) traffic volume counts; 2) vehicle classification counts; and 3) truck weight monitoring data. These data can be used in the analysis of CMVs to determine both the impact of these vehicles on the transportation network and to develop relationships between the types of data collected that can be used in critical design analyses. Several statistical analysis tools were then introduced to analyze the data collected and to make inferences about the data collected.

The next topic of interest in the literature review is the use of microscopic traffic simulation models as an effective transportation analysis tool due to their ability to model the stochastic and dynamic nature of transportation systems, including vehicle composition. Three different models were introduced that have successfully been used to estimate and forecast traffic conditions, providing realistic vehicle trajectories to aid in more accurate estimates of future traffic conditions. The analyses of these future traffic conditions are then used for planning of transportation facilities, including roadway improvements and infrastructure needs. Finally genetic algorithms were introduced as an optimization tool to aid in the calibration of microscopic traffic simulation models for use in CMV analysis.

The tools and background information identified in this section will be used throughout this dissertation to fulfill the needs identified in Section 1.2, and to successfully develop a methodology to account for CMVs using microscopic traffic simulation models. The first step in this process is the identification of the dataset for use in this analysis, a topic that will be discussed in the next section.

### 3. TEXAS CMV DATA COLLECTION

The collection of traffic data is a critical component of traffic and transportation engineering that can be used to establish baseline performance measures and to forecast future traffic conditions. Beginning in the 1930s, statewide highway planning surveys were conducted to collect traffic data including parameters such as traffic volume, vehicle type, and truck weight. These surveys provided the background for the establishment of planning programs at both the state and federal level (55). These programs have continued to evolve and over the years have provided transportation engineers with an influx of data. As was outlined previously, one of the more recent advancements in technology that has greatly enhanced these programs and their associated data collection efforts is the implementation of ITS. Transportation analysis that was once difficult to perform objectively due to a paucity of available data is now made easier with the introduction of ITS data collection methods.

Some of the most important sources of traffic data are CMV volume, classification, and weight data. These data are used as input to some of the most critical tasks in transportation engineering and planning, included, but not limited to: 1) pavement and bridge design, maintenance, and loading restrictions; 2) economic analyses, including the development of equitable tax structures; 3) CMV weight enforcement actions; 4) geometric design considerations; and 5) safety improvement analyses (55). The purpose of this section, therefore, is to identify the data collection methodologies and techniques in the state of Texas for the collection of CMV volume, classification, and weight data. Once these have been identified, the relationships that exist within these data will be explored, primarily through an analysis of data trends found within the Texas WIM dataset.

To accomplish this purpose, this section has been divided into four subsections. The first subsection outlines the TxDOT data collection process, the second summarizes the Texas CMV size and weight regulations, and the third outlines the Texas WIM dataset and identifies data trends for both the aggregate and disaggregate data. Finally, the fourth subsection provides concluding remarks based on the data collection methodologies.

#### 3.1 Texas Department of Transportation Data Collection Process

In 1917 the Texas Legislature established the Texas Highway Department to administer federal highway funds for transportation and maintenance. In 1975 the responsibilities of the highway

department were increased when the Legislature merged the agency with the Texas Mass Transportation Commission to form the State Department of Highways and Public Transportation. In 1991, the Legislature combined the State Department of Highways and Public Transportation, the Department of Aviation, and the Texas Motor Vehicle Commission to create what is currently known as TxDOT. The transportation system maintained by TxDOT includes more than 79,000 centerline miles of roadway that are traversed by the more than 18.7 million motor vehicles registered within the state (130). In addition to the maintenance of existing infrastructure and the design of current projects, TxDOT also provides estimation and forecasting of traffic data across the state to aid in future planning statewide through their Transportation Planning and Programming (TPP) Division.

Based upon the principles of the TMG outlined in Section 2.3, the *Traffic Data and Analysis Manual* published by TxDOT provides guidelines for traffic data collection, traffic estimation, and traffic forecasting for use across the state (30). The process of traffic estimation and forecasting includes coordination between TxDOT, the MPOs, and local government entities. The data collected by TxDOT are utilized by transportation professionals both within and outside of the department for a variety of activities, including: 1) estimation and forecasting of traffic volumes in transportation plans and programs; 2) analysis of project alternatives; 3) environmental analyses; 4) roadway geometric, intersection, and pavement design; and 5) selection of projects for funding from alternatives under consideration (30).

According to the *Traffic Data and Analysis Manual*, TxDOT collects data on a continuous basis using a variety of data collection techniques. Some of the more common techniques include (30):

- ATR volume data,
- accumulative count recorder (ACR) traffic data,
- highway performance monitoring system (HPMS) traffic data,
- five-year count program,
- vehicle classification data,
- truck WIM data,
- vehicle speed data,
- LTPP data, and
- border trend traffic data.

The data collected is used to support the planning, design, and programming functions of TxDOT, MPOs, and local government agencies. The data collection efforts that are most applicable to the analysis of CMVs and their impact on the current and future infrastructure include: 1) ATR volume data; 2) ACR traffic data; 3) vehicle classification data; 4) border trend traffic data; and 5) WIM data.

A summary of each of these data collection efforts within the state is provided in the following subsections.

### *3.1.1 Automatic Traffic Recorder Volume Data*

Traffic volume data are collected by TPP using permanent ATR equipment at approximately 160 permanent sites across the state. The ATR sites collect data for each lane 24 hours a day, 365 days a year, and record the traffic volumes in terms of daily and directional traffic at each station. The data are retrieved daily (Monday through Sunday) and are compared to patterns identified in archived data to develop adjustment factors for daily and seasonal variation, directional distribution factors, k-factors, and AADT volumes, and to estimate variations in VMT. The information is summarized in both monthly reports within TxDOT and in year-end reports that include information on annual average hourly volumes by days of the week, highest hours of the year, average daily traffic by month, day and season, AADT percent variation by years, and AADT. These data are then made available for use in planning and design (30).

### *3.1.2 Accumulative Count Recorder Traffic Data*

ACR data collection includes short-term traffic volume counts conducted under the direction of TPP. ACR counts are performed at 60,000 to 80,000 sites each year and include HPMS samples, on-system roads (annually), and off-system locations on county roads and in urbanized areas (five-year cycles). TPP determines the count locations, which include HPMS site samples, all on-system road sites annually, off-system road sites based on a five-year cycle, and special request locations received annually through TxDOT district offices. ACR data recorders collect axle counts in 24-hour samples at each data collection location. Counted or estimated vehicle classification data are then used to determine the axle-to-vehicle ratio for each axle count. The ACR recorded count volumes are then converted into the total number of vehicles by dividing the total axles by the axle count ratios. TPP typically maintains a database of 10 years of historic data to provide background at the ACR locations (30).

### 3.1.3 Vehicle Classification Data

Vehicle classification counts are performed at 650 to 750 different locations across the state of Texas each year. The total number of sites where data are collected varies based on the condition of the AVC hardware installed at the sites, the number of special requests received by each district for classification data, construction at the site, and potential problems with the equipment that require either the repair of the equipment or the use of a visual classification contract to collect the data. At the AVC sites, TPP has installed sensors and loops in the roadway infrastructure with a cabinet and pedestal to house the electronics, loop, and piezoelectric sensor leads similar to the standard configurations identified in Section 2.3.2 (30).

In general, three types of classification data are collected on the Texas system (30):

- AVC at approximately 250 sites with 48-hour data collection;
- contract visual manual classification (MC) counts at approximately 400 sites with 24-hour data collection; and
- AVC at 25 border crossing sites with data collection 365 days a year.

Vehicles are classified into 14 categories according to the Texas 6 Vehicle Classification Code. The Texas 6 Classification Code is summarized in Table 3.1 (30), with graphical representation of the vehicle classification code provided in Figure 3.1 (30). The classification system utilized by TxDOT is slightly different from that utilized by the FHWA, a summary of which was provided previously in Section 2.3.2. The primary difference between the Texas and FHWA classification occurs in relation to the Texas 6 Class 1 and Class 2, as well as Texas 6 Class 7 and Class 8. Texas 6 Class 1 is disaggregated by the FHWA classification scheme into a specific classification for motorcycles (FHWA Class 1) and a separate classification for passenger cars (FHWA Class 2). These two classifications are combined in the Texas 6 class system. Furthermore, the Texas 6 Class 7 (three axles, single trailer) and Texas 6 Class 8 (four axles, single trailer) are aggregated by FHWA into one classification, FHWA Class 8 (three to four axles, single trailer). The remaining classification codes are comparable between Texas 6 and FHWA, although the code numbers are slightly offset through Class 8 due to the different combinations found in the early class codes.

**TABLE 3.1 Texas 6 Vehicle Classification Code**

<b>Class Code</b>	<b>Vehicle Type</b>
1	Motorcycles and passenger vehicles
2	Other two-axle, four-tire, single-unit vehicles
3	Buses
4	Two-axle, six-tire, single-unit trucks
5	Three-axle single-unit trucks
6	Four or more axle single-unit trucks
7	Three-axle single-trailer trucks (i.e., 2S1)
8	Four-axle single-trailer trucks (i.e., 2S2, 3S1)
9	Five-axle single-trailer trucks (i.e., 3S2, 2S3)
10	Six or more axle single-trailer trucks (i.e., 3S3, 3S4)
11	Five or fewer axle multi-trailer trucks (i.e., 2S1-2)
12	Six-axle multi-trailer trucks (i.e., 2S2-2, 3S1-2)
13	Seven or more axle multi-trailer trucks (i.e., 3S2-2)

#### *3.1.4 Border Trend Traffic Data*

NAFTA introduced data collection requirements for the state of Texas to aid in the planning and maintenance of the highway system in areas that are directly affected by the agreement. Traffic data are collected at these locations and categorized into the Texas 6 vehicle classification scheme. The data are compiled by the Department of Public Safety (DPS) and are used to measure the growth at border crossing locations. The data include monthly average truck traffic, monthly station trend summaries for past years, monthly average number of vehicles, annual summaries of station and directions for past years, and detailed vehicle classification and directional flow data by station (30).

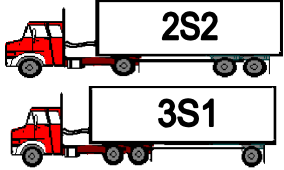
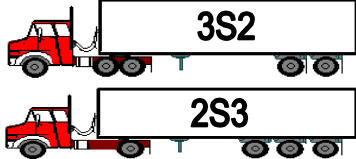
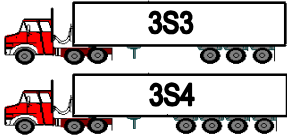
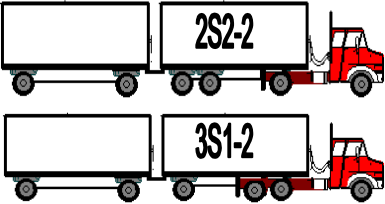
 <p>Texas 6 Class 1 Motorcycles and Passenger Vehicles</p>	 <p>Texas 6 Class 2 Other Two-Axle, Four-Tire, Single-Unit Vehicles</p>
 <p>Texas 6 Class 3 Buses</p>	
 <p>Texas 6 Class 4 Two Axle, Six-Tire, Single-Unit Trucks</p>	 <p>Texas 6 Class 5 Three Axle Single-Unit Trucks</p>
 <p>Texas 6 Class 6 Four or More Axle Single-Unit Trucks</p>	 <p>Texas 6 Class 7 Three-Axle Single-Trailer Trucks</p>
 <p>Texas 6 Class 8 Four-Axle Single Trailer Trucks</p>	 <p>Texas 6 Class 9 Five-Axle Single Trailer Trucks</p>
 <p>Texas 6 Class 10 Six or More Axle Single-Trailer Trucks</p>	 <p>Texas 6 Class 11 Five or Fewer Axle Multi-trailer Trucks</p>
 <p>Texas 6 Class 12 Six-Axle Multi-trailer Trucks</p>	 <p>Texas 6 Class 13 Seven or More Axle Multi-trailer Trucks</p>

FIGURE 3.1 Texas 6 vehicle classification

### 3.1.5 Texas WIM Data Collection Process

As discussed in Section 2.3.4, ASTM Designation: E 1318-02 describes WIM as “the process of measuring the dynamic tire forces of a moving vehicle and estimating the corresponding tire loads of the static vehicle” (62). WIM equipment has the ability to estimate the static weight of vehicles with a wide variety of axle configurations at both low (10 mph) and high (80 mph) speeds. The equipment collects traffic volumes by vehicle classification and weight, while also including the date, time, vehicle length by axle spacing, speed, and axle weight (30, 31).

The concept of weighing vehicles in motion began to be studied in the state of Texas in the early 1960s. The original study was one in which portable electronic scales for weighing each wheel of vehicles moving at highway speeds was developed (131). Later, additional research projects led to a plan to utilize WIM at a number of permanent locations as an alternative to the conventional static weigh sites that were currently in operation throughout the state. This study determined that the number of weigh sites could be reduced from 21 conventional sites to a recommended six original WIM stations to detect timewise variation in truck data (132).

Over the years the original WIM locations have gone in and out of service depending on construction, equipment failure, and the ability of the highway in which they were installed to support the roadway sensors. In addition, sites have been added and upgraded through the years, with a majority of the sites being converted from bending plate to piezoelectric technology. TPP currently uses piezoelectric Type II and bending plate Type I technology to collect data at 21 permanent WIM sites across the state of Texas listed in Table 3.2. Data are collected at each of the operational sites for 48 hours during each quarter of the year. The number of operational sites at which WIM data are collected each year varies due to factors such as construction, road conditions, and WIM hardware.

As was discussed in Section 2.3, the most recent edition of the TMG provides recommendations for total size of the weight data collection program in a given state. The TMG concludes that the size of a weight data collection program within a state is a function of the variability of the truck weights in the state and the accuracy and precision desired to monitor and report these weights. For a state the size of Texas, the TMG estimates that the number of truck weight road groups may be as high as 10 to 15. The TMG recommends that six data collection sites per group should be used in developing trends in traffic weight data. Based on this recommendation, as many as 60 to 90 data collection sites are required to categorize the traffic

weight data characteristics in a large state such as Texas (55). To conform to the TMG, therefore, would require providing additional weigh sites throughout the state distributed by area type (rural or urban) and by functional classification (31). The state of Texas is currently evaluating their data collection process based on the recent edition of the TMG and is expected to modify the collection of data based on the new recommendations.

**TABLE 3.2 Texas Weigh-in-Motion Site Locations**

Site # <sup>1</sup>	District	County	Hwy.	Location
PZ-010	El Paso	El Paso	IH-10	2.0 mi E of FM 1281
PZ-071	San Antonio	McMullen	SH-16	1.1 mi S of SH 72
PZ-074	Pharr	Kenedy	US-77	0.1 mi N of Sarita
PZ-077	Pharr	Cameron	US-77	0.6 mi N of SH 100
PZ-181	Pharr	Cameron	SH-48	3.6 mi W of FM 511
PZ-502	San Antonio	Guadalupe	IH-10	0.4 mi E of FM 775
LW-504	Abilene	Nolan	IH-20	0.7 mi E of US 84
LW-506	Wichita Falls	Wichita	US-287	1.5 mi W of LP 11
PZ-507	Bryan	Walker	IH-45	2.6 mi S of PR 40
PZ-509	Paris	Hunt	IH-30	2.5 mi W of SH 50
PZ-510	El Paso	El Paso	IH-10	2.4 mi W of LP 375
LW-512	Corpus Christi	Live Oak	IH-37	0.7 mi S of FM 2049
LW-513	Waco	Bell	IH-35	0.9 mi N of Williamson County line
PZ-514	Dallas	Kaufman	IH-20	0.7 mi W of SH 429
LW-516	San Antonio	Bexar	IH-35	5.3 mi S of LP 1604
LW-517	Pharr	Hidalgo	US-83	0.2 mi W of FM 1426
PZ-518	San Antonio	Kerr	IH-10	5.7 mi E of US 290
PZ-519	Abilene	Mitchell	IH-20	2.1 mi W of FM 2836
PZ-520	Amarillo	Randall	IH-27	0.5 mi S of SH 217
LW-521	El Paso	El Paso	US-54	At Delta just N of Customs
LW-522	Pharr	Hidalgo	US-281	9.3 mi N of SH 186

<sup>1</sup> PZ is used to designate piezoelectric sites, while LW designates bending plate sites

Also discussed in Section 2.3 was the importance of calibration in the WIM data collection process. Calibration is an essential part of WIM data collection due to the variability in the traffic stream and the added challenge of converting dynamic traffic loads to static traffic loads. TxDOT utilizes a technique similar to that outlined in ASTM Designation: E 1318-02, which involves the use of test trucks of known weight to determine the performance of the WIM system (62). The test trucks used by TxDOT are generally two-, three-, and five-axle trucks, with the majority of the calibration data based on a 3S2 (FHWA Class 9) vehicle. As outlined in

ASTM Designation: E 1318-02, the reference truck makes multiple passes over the weight pad equipment at low, high, and intermediate speeds, and the equipment is adjusted according to manufacturer specifications (31, 62). TxDOT has determined that calibration is acceptable when the difference between the expected axle weight and the actual axle weight of the test vehicle is within 6 percent (31).

### 3.2 Texas CMV Size and Weight Regulations

The state of Texas has established CMV size and weight regulations very similar to the federal requirements. The state has developed guidelines for legal width limits of 102 inches, length limits listed in Table 3.3, height limits listed in Table 3.4, and weight limits based on the bridge formula listed in Table 3.5 (133). The size and weight regulations established for the state of Texas are equivalent to federal regulations and are applicable when operating on state-maintained roads and bridges as well as the NN and interstate system.

**TABLE 3.3 State of Texas Legal Length Limits**

Vehicle(s) Type	Legal Length Limit	Maximum Permit Length
Truck or Single Vehicle	45 ft	75 ft
Truck and trailer combination	65 ft	180 ft
Commercial Truck and Semi-Trailer Combination Transporting Automobiles or Boats	Overall length unlimited, trailer limited to 59 ft	-
Combinations such as Truck, Travel Trailer and Boat or Motorhome, Boat, and Towing a Car	65 ft	-
Truck and Trailer Combination Hauling Oilfield Equipment	Overall length unlimited, trailer limited to 59 ft	180 ft
Truck-Tractor	Unlimited	Unlimited
Truck-Tractor Combination	Overall length unlimited, trailer limited to 59 ft	180 ft
Single-Unit Semi-trailer	59 ft	-
2 Trailer Semi-trailer	28.5 ft	-
Front Overhang	3 ft	25 ft
Rear Overhang	4 ft	30 ft
Maximum Overall Length	180 ft	
Maximum Length Permitted Without Route, Traffic Study, and Route Certification by Application on File	125 ft	

**TABLE 3.4 State of Texas Legal Height Limits**

Explanation	Height Limit
Legal Height Limit	14 ft
Maximum Height Permitted on Holidays	16 ft
Maximum Height Permitted Without Route, Traffic Study, and Route Certification	< 19 ft

**TABLE 3.5 State of Texas Permissible Weight Table**

Axle Spacing (ft)	2 axles	3 axles	4 axles	5 axles	6 axles	7 axles
4	34,000					
5	34,000					
6	34,000					
7	34,000					
8	34,000	34,000				
8+	38,000	42,000				
9	39,000	42,500				
10	40,000	43,500				
11		44,500				
12		45,000	50,000			
13		45,500	50,500			
14		46,500	51,500			
15		47,500	52,000			
16		48,000	52,500	58,000		
17		48,500	53,500	58,500		
18		49,900	54,000	59,000		
19		51,400	54,500	60,000		
20		52,800	55,500	60,500	66,000	
21		54,000	56,000	61,000	66,500	
22		54,000	56,500	61,500	67,000	
23		54,000	57,500	62,500	68,000	
24		54,000	58,700	63,000	68,500	74,000
25		54,500	59,650	63,500	69,000	74,500
26		55,500	60,600	64,000	69,500	75,000
27		56,000	61,550	65,000	70,000	75,500
28		57,000	62,500	65,500	71,000	76,500
29		57,500	63,450	66,000	71,500	77,000
30		58,500	64,000	66,500	72,000	77,500
31		59,000	65,350	67,500	72,500	78,000
32		60,000	66,300	68,500	73,000	78,500
33			67,250	68,500	74,000	79,000
34			68,200	69,000	74,500	80,000
35			69,150	70,000	75,000	
36			70,100	70,500	75,500	
37			71,050	71,050	76,000	

**TABLE 3.5** Continued

Axle Spacing (ft)	2 axles	3 axles	4 axles	5 axles	6 axles	7 axles
38			72,000	72,000	77,000	
39			72,000	72,500	77,500	
40			72,000	73,000	78,000	
41			72,000	73,500	78,500	
42			72,000	74,000	79,000	
43			72,000	75,000	80,000	
44			72,000	75,500		
45			72,000	76,000		
46			72,500	76,500		
47			73,500	77,500		
48			74,000	78,000		
49			74,500	78,500		
50			75,500	79,000		
51			76,000	80,000		

### 3.3 Texas WIM Dataset

WIM data are summarized and stored by TxDOT's TPP in a database for analysis and distribution between the department and other users. The data collected include a listing of time and date for each vehicle, as well as detailed classification data, aggregate axle spacing, aggregate vehicle weight, disaggregate axle spacing, and disaggregate axle weight for each vehicle that crosses the WIM location. The original WIM dataset obtained from TxDOT for this analysis was modified slightly from its original condition to aid in analysis. The first modification involved the conversion of the vehicle classification codes from the standard FHWA six-digit coding to TxDOT and FHWA standard classification codes (1 through 13). In addition, the lower limit weight threshold was modified in the background analysis for the bending plate sites from a minimum of 4,900 pounds to a minimum of 8,000 pounds to be consistent with the piezoelectric scale calibration parameters. This modification left the following columns for analysis:

- CSN—county station number (site number);
- dir—direction (1 = N, 2 = NE, 3 = E, 4 = SE, 5 = S, 6 = SW, 7 = W, 8 = NW);
- date—date data were captured;
- hr—hour data were captured (i.e., 0 = 12:00–12:59 a.m., 1 = 1:00–1:59 a.m., etc.);

- FHWA class—FHWA vehicle classification scheme (Class 1 through 13);
- TxDOT class—Texas 6 vehicle classification scheme (Class 1 through 13);
- ttl wgt—total weight of all axles for the vehicle (lb);
- A—weight of the first axle (lb);
- B—weight of the second axle (lb);
- C—weight of the third axle (lb);
- D—weight of the fourth axle (lb);
- E—weight of the fifth axle (lb);
- F—weight of the sixth axle (lb);
- G—weight of the seventh axle (lb);
- H—weight of the eighth axle (lb);
- I—weight of the ninth axle (lb);
- A-B—axle spacing of the first axle to the second axle (ft);
- B-C—axle spacing of the second axle to the third axle (ft);
- C-D—axle spacing of the third axle to the fourth axle (ft);
- D-E—axle spacing of the fourth axle to the fifth axle (ft);
- E-F—axle spacing of the fifth axle to the sixth axle (ft);
- F-G—axle spacing of the sixth axle to the seventh axle (ft);
- G-H—axle spacing of the seventh axle to the eighth axle (ft);
- H-I—axle spacing of the eighth axle to the ninth axle (ft); and
- ttl spc—total spacing from first axle to last axle (ft).

The dataset used in the analysis of Texas data includes all TxDOT WIM data collection sites that were operational in the state during 2001. Of the 21 existing WIM data collection sites, nine sites were operational during the year and provided data for this analysis. These nine operational sites are shown graphically in Figure 3.2 and listed in Table 3.6. Of the nine data locations, five of the sites collected data using piezoelectric Type II WIM technology, and the remaining four sites collected data using bending plate Type I technology.

The data collected at each of the nine operational WIM sites exhibit somewhat different characteristics depending on the location and type of WIM technology used to collect data at their respective locations. To illustrate the variations in both the aggregate and disaggregate data

collection site locations, a background analysis of the data collected across the sites will be discussed in the following subsections.

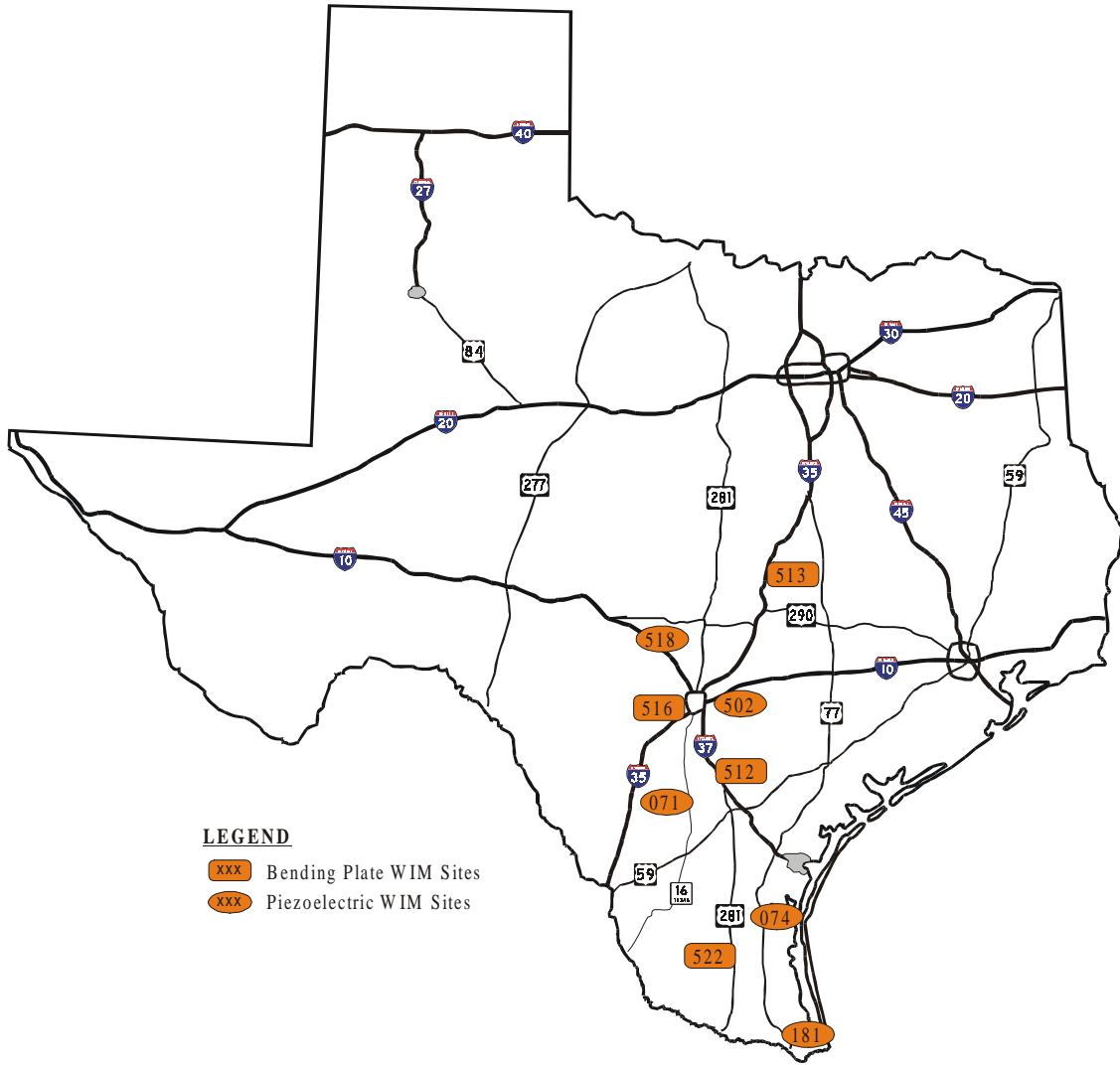


**FIGURE 3.2** TxDOT WIM 2001 operational data collection sites

**TABLE 3.6 Texas Weigh-in-Motion 2001 Operational Site Locations**

Site # <sup>1</sup>	District	County	Hwy.	Location
PZ-071	San Antonio	McMullen	SH 16	1.1 mi S of SH 72
PZ-074	Pharr	Kenedy	US 77	0.1 mi N of Sarita
PZ-181	Pharr	Cameron	SH 48	3.6 mi W of FM 511
PZ-502	San Antonio	Guadalupe	IH-10	0.4 mi E of FM 775
PZ-518	San Antonio	Kerr	IH-10	5.7 mi E of US 290
LW-512	Corpus Christi	Live Oak	IH-37	0.7 mi S of FM 2049
LW-513	Waco	Bell	IH-35	0.9 mi N of Williamson County line
LW-516	San Antonio	Bexar	IH-35	5.3 mi S of LP 1604
LW-522	Pharr	Hidalgo	US 281	9.3 mi N of SH 186

<sup>1</sup> PZ is used to designate piezoelectric sites, while LW designates bending plate sites

### 3.3.1 Aggregate Dataset Background Analysis

The data contained in the aggregate dataset have been evaluated based on three main criteria. These criteria include: 1) temporal and spatial distribution; 2) vehicle classification; and 3) total weight and spacing. Detailed analyses of each of these criteria are provided in the following subsections.

**3.3.1.1 Temporal and Spatial Distribution** As outlined previously, current TxDOT policy and standards indicate that WIM data are to be collected at each of the operational sites for 48 hours during each quarter of the year. In analyzing the 2001 data collected, it became apparent that in addition to the number of operational sites varying each year, the amount of data collected at the operational sites also varied based on the background traffic volumes at each location as well as the total number of days in which data were collected. Of the nine locations where data were available, two locations included data collected during all four quarters of the year (LW-512 and LW-516), two locations included data collected during three quarters of the year (LW-513 and LW-522), while the remaining five locations (PZ-071, PZ-074, PZ-181, PZ-502, and PZ-518) included data from only the fourth quarter. A bar chart summarizing the total vehicle counts for each location is provided in Figure 3.3. It can be seen from this figure that although data were collected during all four quarters of the year at LW-512 (IH-37) and LW-516 (IH-35), the majority of the data for the year were collected at sites LW-513 (IH-35) and LW-516 (IH-35). These two sites account for nearly 57 percent of the dataset. The next two sites in frequency are

sites LW-512 (IH-37) and LW-522 (US 281), which when added to sites LW-513 (IH-35) and LW-516 (IH-35) account for just over 83 percent of the data.

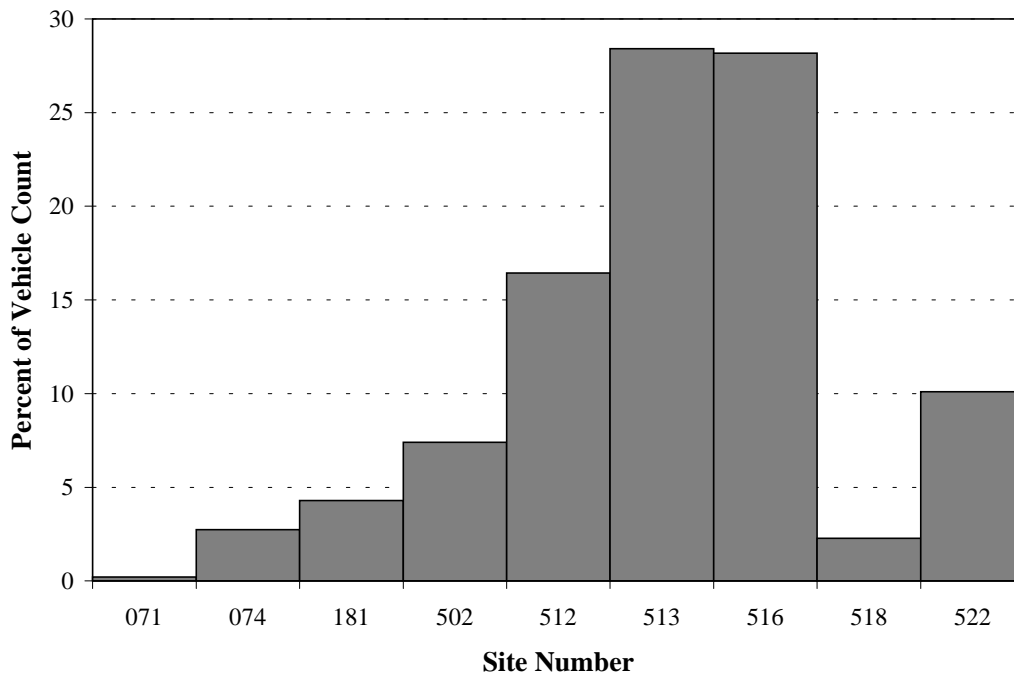


**FIGURE 3.3 2001 aggregate dataset site distribution**

In accordance with TMG recommendations, the data at each site were collected for a minimum 48-hour duration. The data were recorded by hour for the 48-hour time period with the resulting percent of daily traffic by hour-of-day provided in Figure 3.4. It can be seen from this figure that during this 48-hour period, the data indicate that the truck counts peak during the afternoon hours. This trend is somewhat similar to the typical through-truck pattern identified in Section 2.3.2, only with a slightly higher peak in the afternoon hours. It is hypothesized that this is a result of local truck traffic mixed with the through traffic at the data collection sites, thus shifting the peak slightly from a typical through-truck pattern.

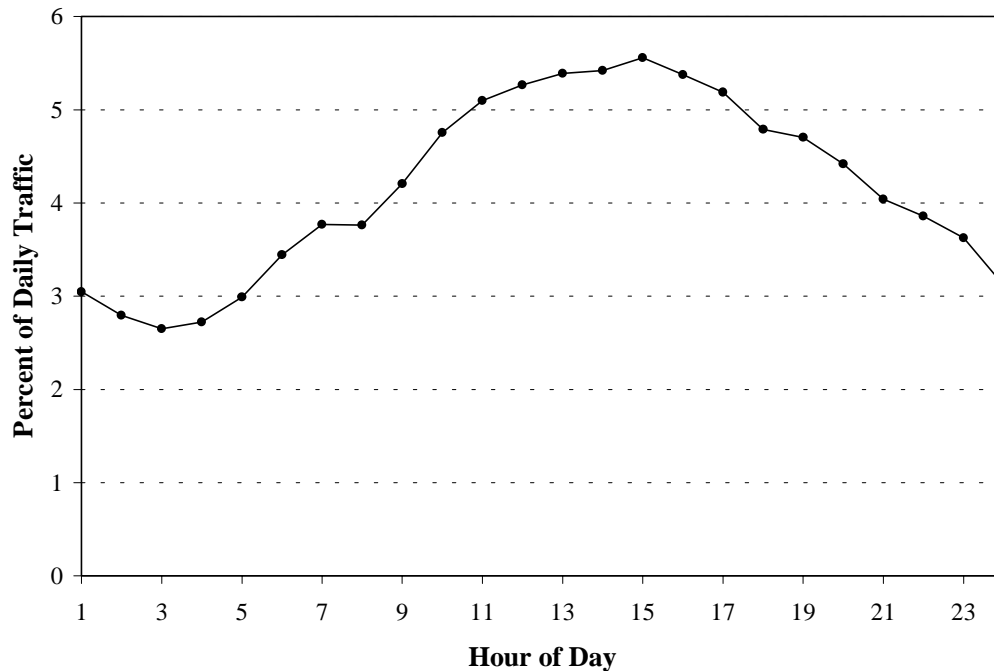


**FIGURE 3.4** 2001 aggregate dataset hourly distribution

**3.3.1.2 Vehicle Classification** The next item for comparison was the relationship between the data observed by vehicle classification. WIM data in the state of Texas are classified according to a six-digit classification scheme that can be converted to the FHWA classification scheme identified in Section 2.3.2, or the Texas 6 classification scheme identified in Section 3.1.3. To identify the trends in the data and to compare the two distribution schemes, a bar chart representation of the truck classes identified in the FHWA classification scheme is provided in Figure 3.5, while a similar representation for the truck classes of the Texas 6 classification scheme is provided in Figure 3.6. Although the majority of the vehicles on the roadway are FHWA Classes 1 through 3 or Texas 6 Classes 1 and 2 (i.e., motorcycle, passenger vehicle), the majority of the trucks classified in the state of Texas, as illustrated in these figures, are FHWA/Texas 6 Class 9 with over 67 percent of the vehicles falling in this category. The second most common truck vehicle classification is FHWA Class 5/Texas 6 Class 4 with nearly 16 percent of the vehicles. Together these two categories (FHWA Classes 5 and 9 or Texas 6 Classes 4 and 9) represent over 80 percent of all trucks on Texas highways.

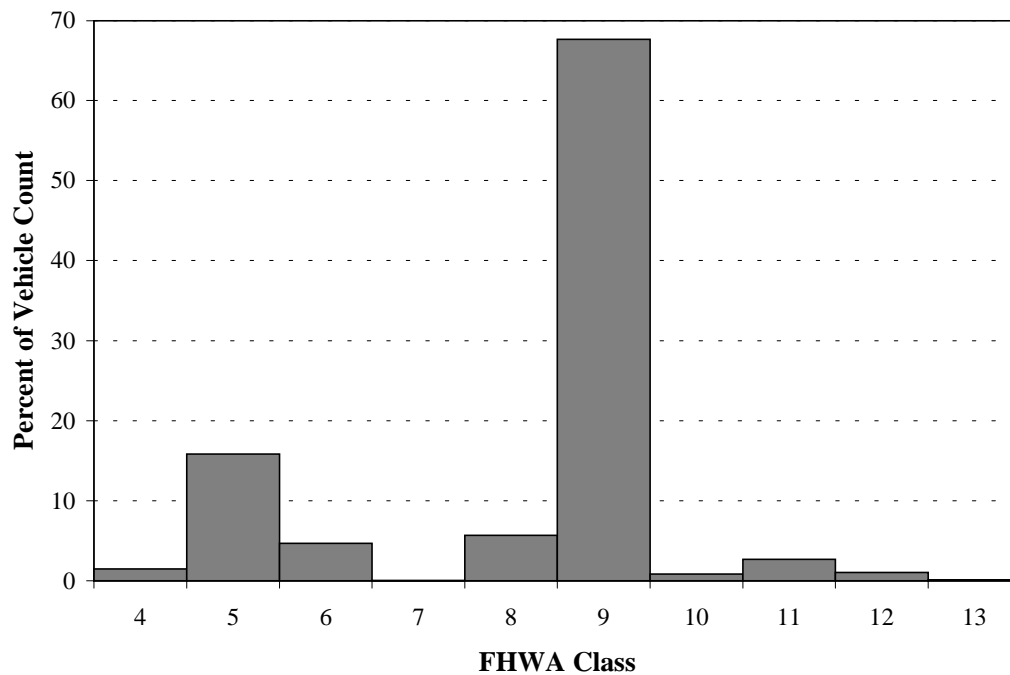


**FIGURE 3.5 FHWA classification count**

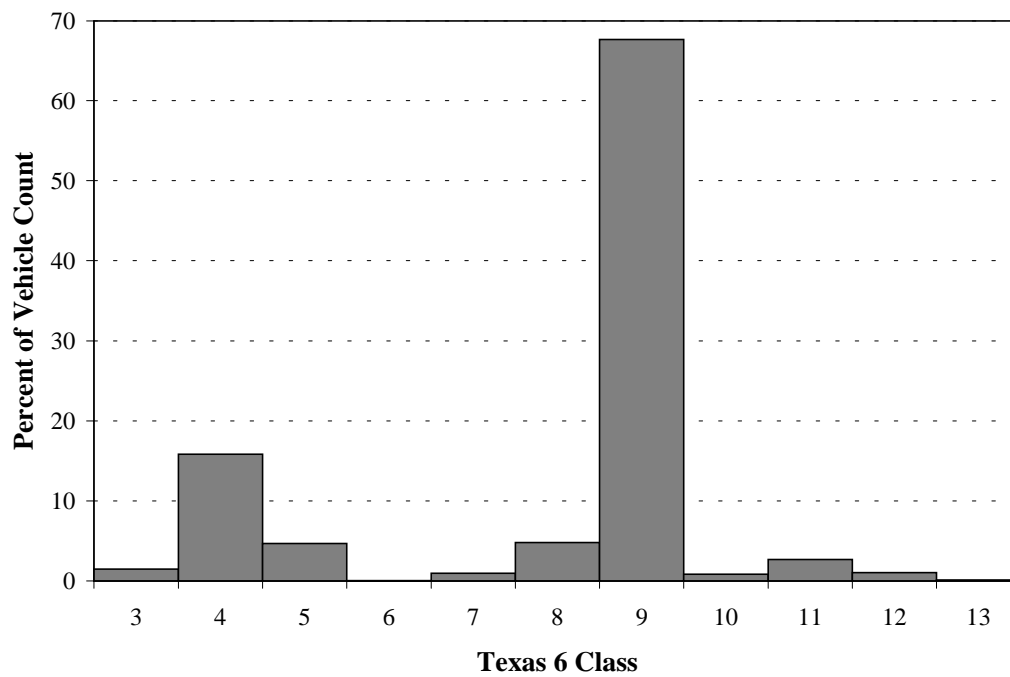


**FIGURE 3.6 Texas 6 classification count**

**3.3.1.3 Weight and Spacing** The final item of comparison for the full dataset was the determination of weight and spacing groups from standard data histograms. The weight data analysis included a histogram of total weight with bin widths of 4,000 pounds covering a range from 6,000 pounds to 102,000 pounds GVW. The results of the full dataset GVW distribution are provided in Figure 3.7. It can be seen from this figure that the total weight across the sites falls into three main categories. The first is light trucks at approximately 6,000 to 10,000 pounds GVW, the second is medium trucks at approximately 30,000 to 34,000 pounds GVW, and the third is heavy trucks at approximately 74,000 to 78,000 pounds GVW. The overall mean total weight for the dataset was 45,273 pounds GVW, with a standard deviation of 23,573 pounds GVW.

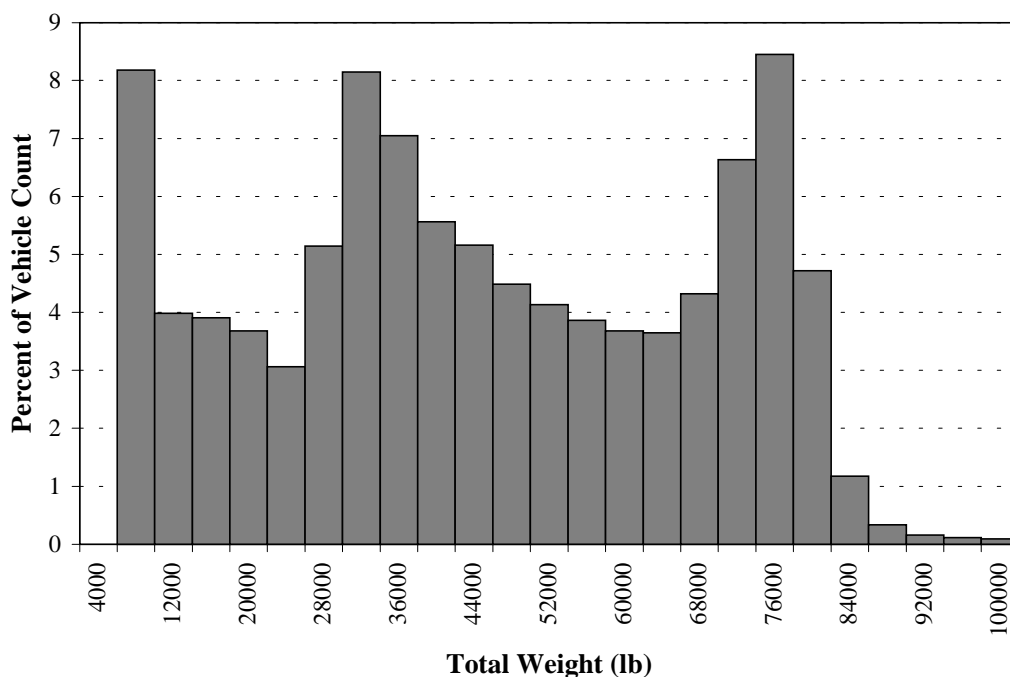


**FIGURE 3.7** Aggregate dataset total weight distribution

The results of this analysis were compared with the WIM “health” monitoring techniques outlined in Section 2.3.5.2 to determine if the results were reasonable. The second criteria in the health monitoring techniques suggests that the total weight histogram for FHWA Class 9 vehicles should include two peaks, the first between 28,000 and 36,000 pounds GVW

and the second between 72,000 and 80,000 pounds GVW. Although the aggregate dataset included more than Class 9 vehicles, the basic monitoring technique holds true, while the additional classifications (particularly FHWA Class 5 and Texas 6 Class 4) would provide justification for the third, lower end peak in the data.

A similar analysis was completed for total spacing with bin widths of 4 feet, covering a range of 10 feet to 80 feet total spacing. The results of this analysis are found in Figure 3.8. The spacing histogram indicates that the total spacing between axles falls into two primary categories. The first is single-unit vehicles with approximately 12- to 16-foot spacing, while the second is longer semi-trailer trucks at approximately 56- to 60-foot spacing. The overall mean total spacing for the dataset was 48 feet, with a standard deviation of 18.1 feet.

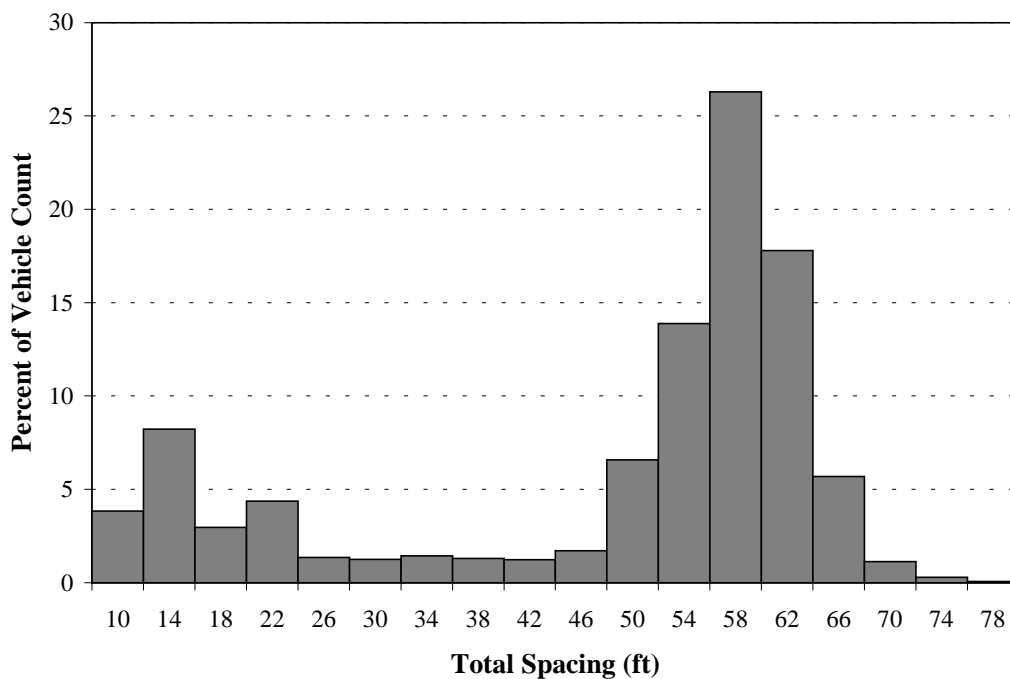


**FIGURE 3.8** Aggregate dataset total spacing distribution

### 3.3.2 *Disaggregate Data Collection Sites*

In addition to providing weight and spacing data comparisons for the aggregate dataset, the overall weight and spacing characteristics for each of the individual sites were examined to identify trends within the data and to develop relationships between sites. The results of this analysis included grouping total weight and total spacing in standard data histograms. As with the aggregate dataset analysis, the weight data analysis includes a histogram of total weight with bin widths of 4,000 pounds covering a range from 6,000 pounds to 102,000 pounds total weight. A similar analysis was completed for total spacing with bin widths of 4 feet, covering a range from 10 feet to 80 feet total spacing, including a summary of mean, standard deviation, and total number of observations for the analysis.

Rather than provide a discussion of each of the nine data collection locations, representative sites from both the piezoelectric data collection sites and the bending plate data collection sites have been evaluated in the following subsections, while summary charts of the results for all nine sites are provided in Appendix B.

**3.3.2.1 Piezoelectric Data Collection Sites** Two piezoelectric data collection sites were chosen for this analysis: 1) PZ-074 (US 77) and 2) PZ-502 (IH-10). The results of the PZ-074 (US 77) total weight distribution analysis are provided in Figure 3.9. It can be seen from this figure that although the total weight for the site does appear to fall into three main categories, the weights of the light truck and heavy truck are shifted slightly from the aggregate data analysis, with a much less pronounced peak for the heavy truck group. For this site, the light trucks exhibit an average weight of approximately 10,000 to 14,000 pounds GVW, the medium trucks approximately 30,000 to 34,000 pounds GVW, and heavy trucks approximately 66,000 to 70,000 pounds GVW. The overall mean total weight for this site was 52,961 pounds GVW, with a standard deviation of 34,328 pounds GVW. Based on the WIM health monitoring techniques discussed previously, the results of this analysis would question the calibration accuracy for this site.

The results of the PZ-074 (US 77) total spacing distribution are provided in Figure 3.10. It can be seen from this figure that the total spacing between axles falls into the same two categories as the aggregate dataset. The first are single-unit vehicles with approximately 12- to 16-foot spacing, while the second are longer semi-trailer trucks at approximately 56- to 60-foot spacing. The overall mean total spacing for the PZ-074 (US 77) sites was 49 feet, with a standard deviation of 15.2 feet.

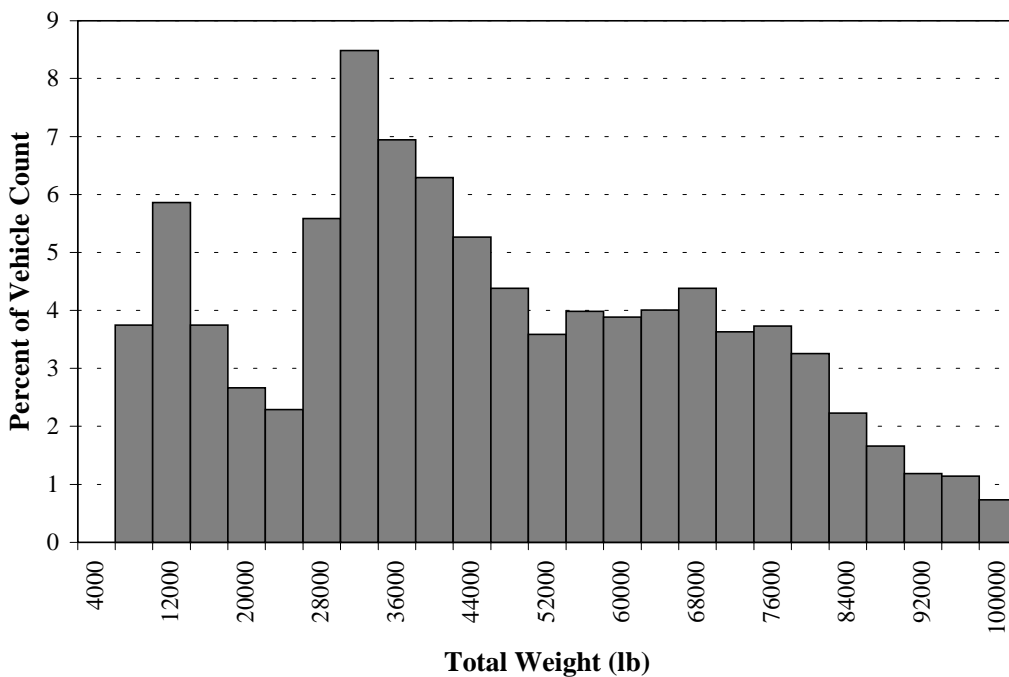


**FIGURE 3.9 PZ-074 (US 77) total weight distribution**

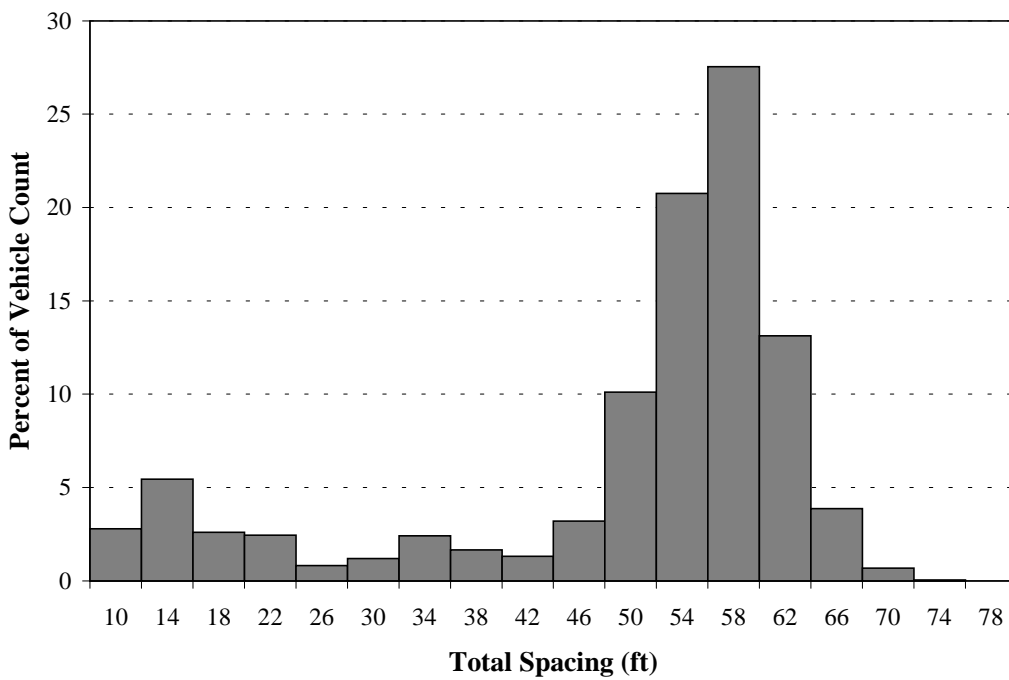


**FIGURE 3.10 PZ-074 (US 77) total spacing distribution**

The results of the PZ-502 (IH-10) total weight distribution analysis are provided in Figure 3.11. At this location the total weight for the site falls into three main categories that very closely resemble the aggregate dataset analysis. Light trucks exhibited an average weight of approximately 6,000 to 10,000 pounds GVW, medium trucks were slightly heavier than the aggregate data results at approximately 34,000 to 38,000 pounds GVW, and heavy trucks were again slightly heavier at approximately 74,000 to 78,000 pounds GVW. The overall mean total weight for this site was 45,866 pounds GVW, with a standard deviation of 23,831 pounds GVW.

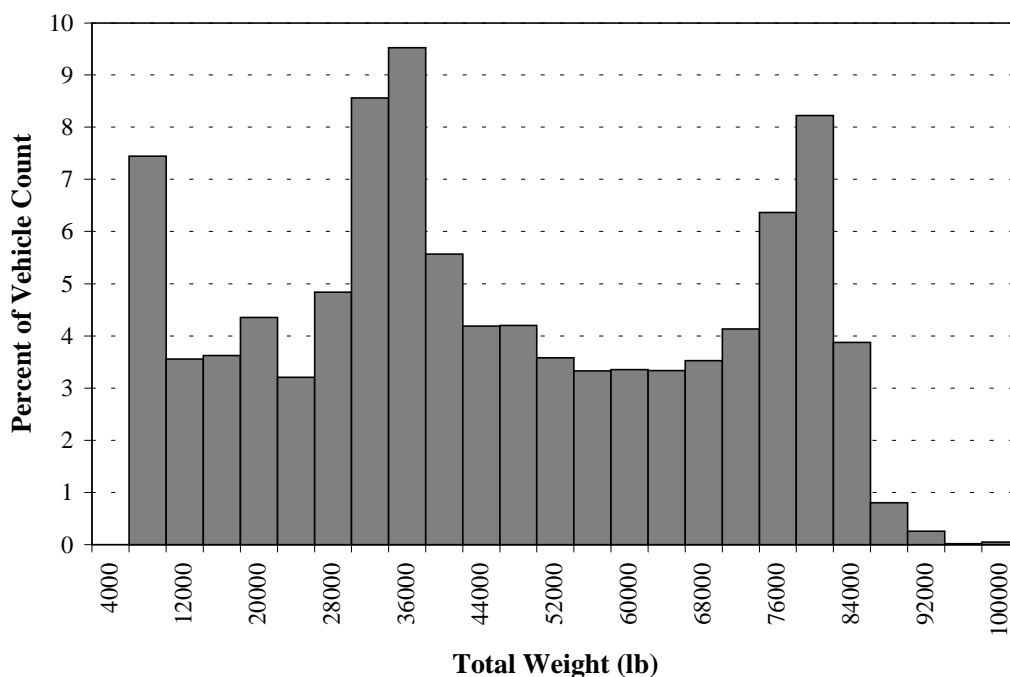


**FIGURE 3.11 PZ-502 (IH-10) total weight distribution**

The results of the PZ-502 (IH-10) total spacing distribution are provided in Figure 3.12. It can be seen from this figure that the total spacing between axles falls into the same two categories as the aggregate dataset, with single-unit vehicles at approximately 12- to 16-foot spacing and semi-trailer trucks at approximately 56- to 60-foot spacing. The overall mean total spacing for the PZ-502 (IH-10) sites was 48 feet, with a standard deviation of 17.0 feet.

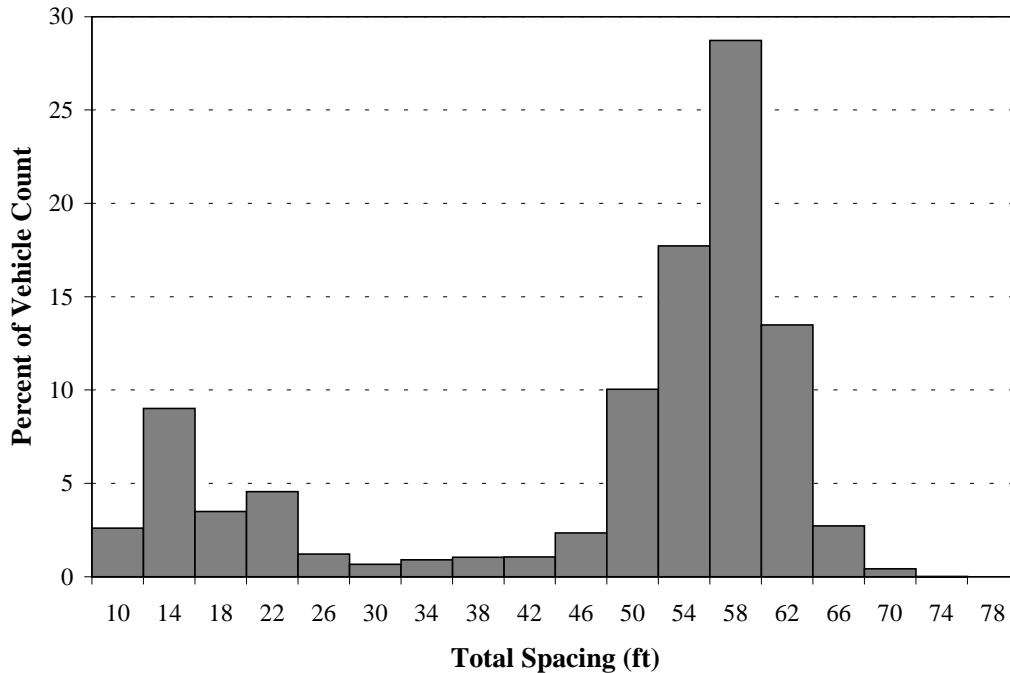


**FIGURE 3.12 PZ-502 (IH-10) total spacing distribution**

**3.3.2.2 Bending Plate Data Collection Sites** Two bending plate data collection sites were also chosen for this analysis: 1) LW-512 (IH-37) and 2) LW-522 (US 281). The results of the LW-512 (IH-37) total weight distribution analysis are provided in Figure 3.13, while the results of the LW-522 (US 281) total weight distribution analysis are provided in Figure 3.14. It can be seen from these figures that these two sites very closely resemble the weight characteristics of the aggregate dataset, with light trucks exhibiting an average weight of approximately 6,000 to 10,000 pounds GVW, medium trucks approximately 30,000 to 34,000 pounds GVW, and heavy trucks approximately 74,000 to 78,000 pounds GVW. This trend is somewhat expected since the bending plate sites account for 83 percent of the total aggregate dataset; thus, the results would be expected to be similar. The trends that exist at the bending plate locations appear to exhibit consistent trends both at each individual location and consistent with the general health monitoring techniques for weight data as outlined in Section 2.3.5.2. The overall mean total weight for LW-512 (IH-37) was 43,978 pounds GVW, with a standard deviation of 23,347 pounds GVW, while the overall mean total weight for LW-522 (US 281) was 44,501 pounds GVW, with a standard deviation of 24,177 pounds GVW.

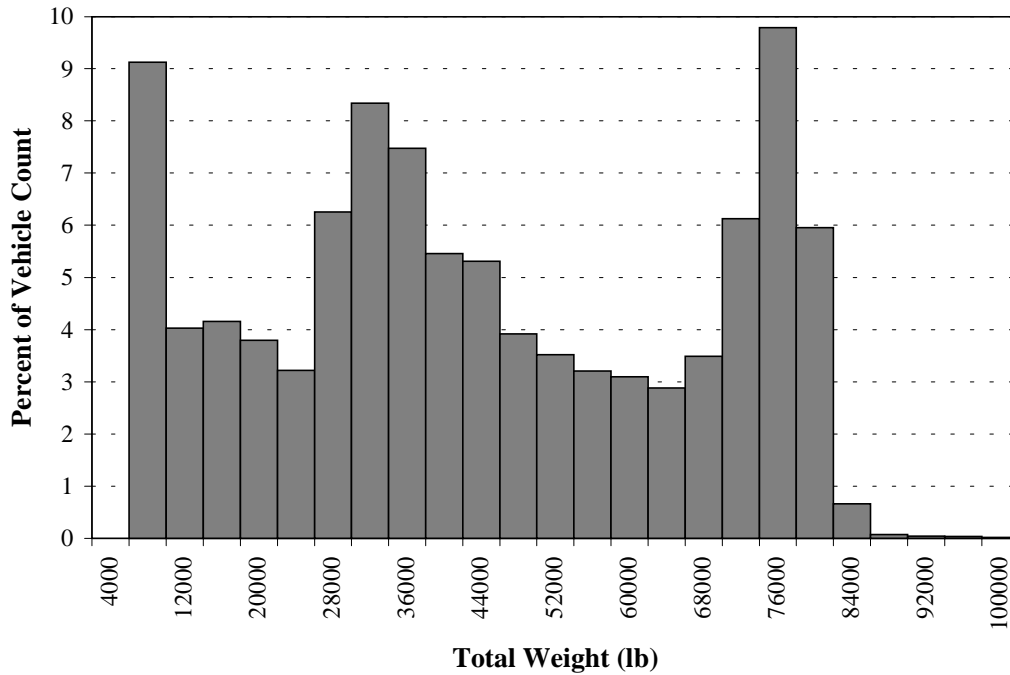


**FIGURE 3.13 LW-512 (IH-37) total weight distribution**

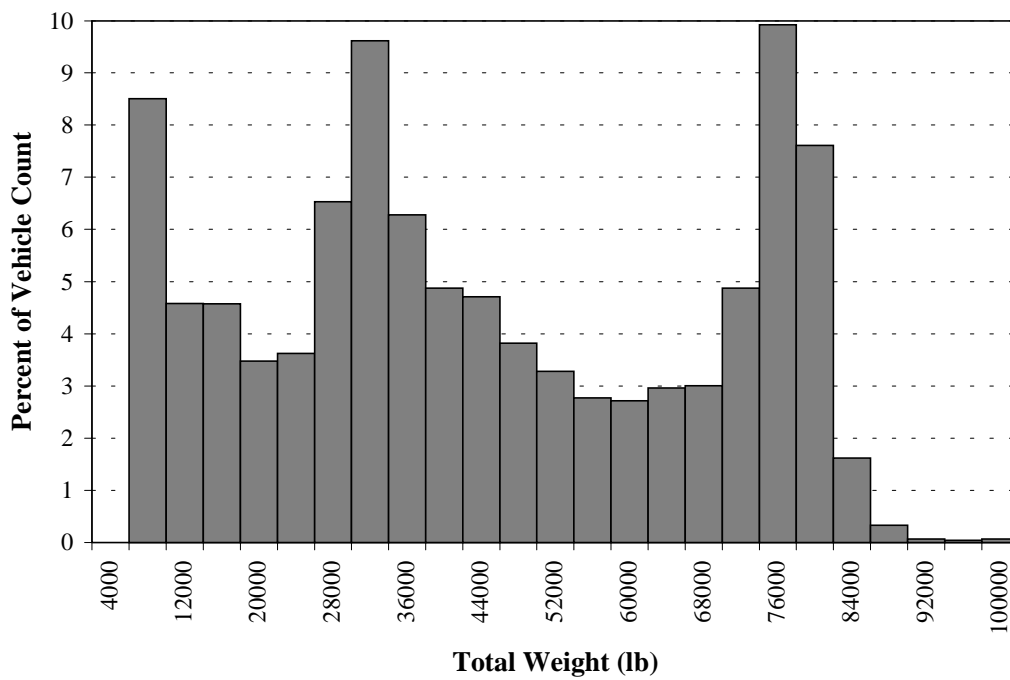


**FIGURE 3.14 LW-522 (US 281) total weight distribution**

The results of the LW-512 (IH-37) total spacing distribution analysis are provided in Figure 3.15, while the results of the LW-522 (US 281) total spacing distribution analysis are provided in Figure 3.16. It can be seen from these figures that, again, the two sites very closely resemble the characteristics of the aggregate dataset, with single-unit vehicles at approximately 12- to 16-foot spacing and longer semi-trailer trucks at approximately 56- to 60-foot spacing observed at both locations. The overall mean total spacing was 47 feet for LW-512 (IH-37) and 48 feet for LW-522 (US 281), with a standard deviation of 18 feet at both locations.

Again, the results of this analysis begin to identify relationships between locations and the general trends that are observed across the state. These relationships as well as detailed statistical methods to analyze the relationships that exist between sites and to develop distributions of vehicles across the state will be examined in greater detail in subsequent sections.

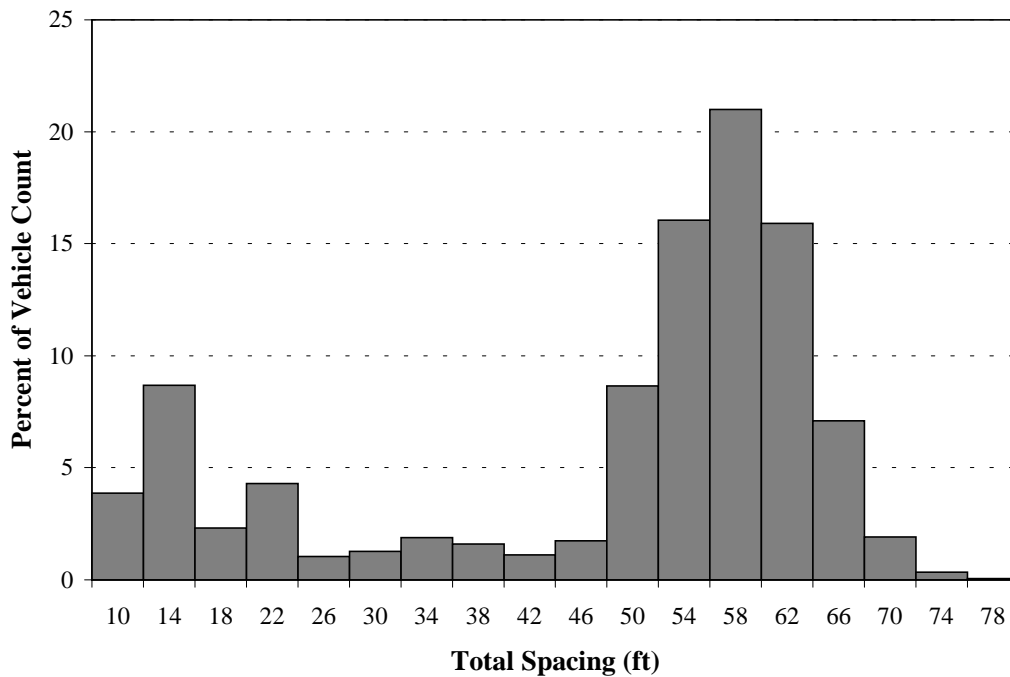


**FIGURE 3.15 LW-512 (IH-37) total spacing distribution**

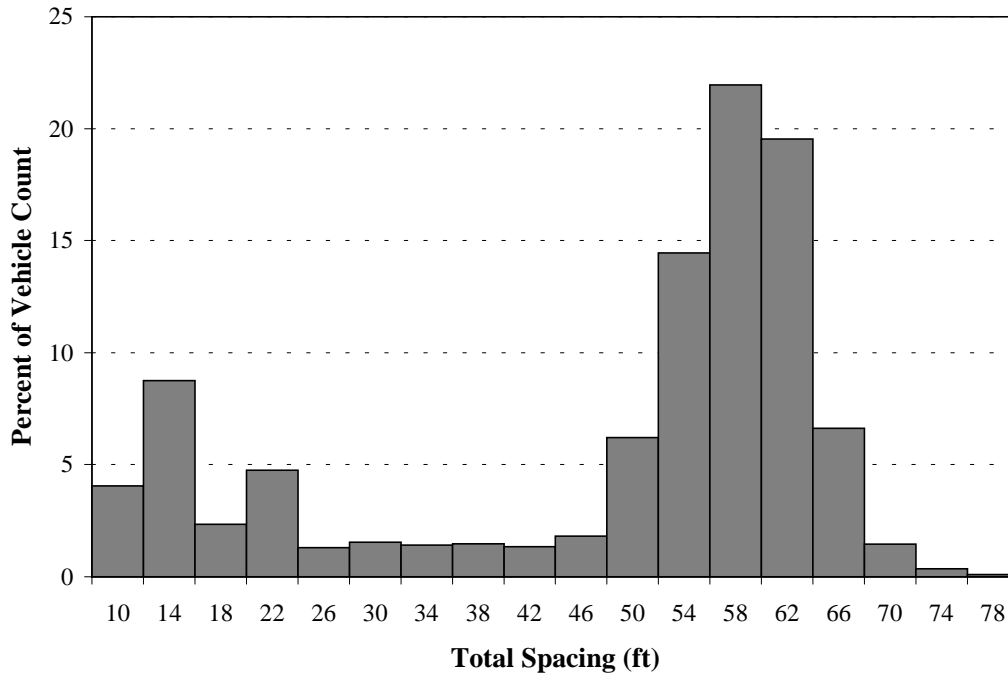


**FIGURE 3.16 LW-522 (US 281) total spacing distribution**

### 3.4 Concluding Remarks

The collection of traffic data is a critical component of traffic and transportation engineering used to establish baseline conditions and to develop relationships that can be used for future traffic analyses. The state of Texas has developed a data collection process that is very valuable for use by planners and engineers as input to both existing and future growth projects within the state. The primary sources of data collection in the state of Texas include: 1) traffic volume data at approximately 160 permanent ATR sites; 2) volume and classification data at approximately 250 AVC sites across the state; and 3) volume, classification, and weight data collected at a maximum of 21 WIM sites across the state. The combination of these three data collection technologies provides volume data at approximately 431 locations (ATR, AVC, and WIM), classification data at approximately 271 locations (AVC and WIM), and weight data collection at a maximum of 21 locations (WIM). Although the combination of the three data collection sources provides coverage across the state, the relationship between the different technologies is not generally known, making it difficult to use the data collected from one source

and apply the information gleaned from this data collection effort as part of a more detailed analysis. The data are available; only the methodology is lacking.

To begin to develop a methodology to better relate the different data collection techniques and to develop methodologies to utilize the limited weight data for application with other data collection methods, a preliminary analysis of the Texas WIM dataset was conducted. The WIM equipment collects traffic volumes by date, time, vehicle classification, aggregate vehicle weight, aggregate vehicle length, disaggregate vehicle length by axle spacing, and disaggregate axle weight. Data are collected at each of the operational sites throughout the state using either piezoelectric Type II or bending plate Type I technology. The Texas WIM dataset was evaluated based on total number of vehicles, vehicle classification, total weight, and total spacing.

WIM data collected in 2001 included nine operational sites, with raw data recorded for over 200,000 vehicles. A preliminary analysis of this dataset began to pinpoint anomalies that required further analysis. These anomalies will be discussed further in the following sections, including detailed statistical analyses to develop a methodology whereby relationships between data collection sites with different detector technologies can be identified, and the data collected at these sites (i.e., WIM sites) used to estimate weight and length distributions at other data collection locations (i.e., AVC sites). In so doing, the total number of sites for which representative weight, length, and vehicle classification data that can be used in critical design tasks will be greatly increased.

## 4. STATISTICAL ANALYSIS OF DATA

In the past, data collection was very difficult to perform, and as a result, data analysis and calibration were performed on a small sample of available data or oftentimes, were not performed at all. More recently the availability of data has increased through the use of ITS data collection methods. The collection of traffic data using ITS methods provides the end user with a wealth of data, some of which can be more useful than others. One of the new challenges with these data is the ability to extract the useful data and to develop relationships within the data to aid in the ease of data analysis.

The purpose of this section is to utilize the statistical analysis tools outlined in Section 2.4 to explore the relationships that exist in the TxDOT WIM dataset identified in Section 3, and to develop a distribution of vehicle weight and length that adequately represents the data. The statistical analysis tools utilized in this section include primarily: 1) PCA and 2) the data-mining tool CART, with additional tools introduced in the analysis as appropriate. To accomplish this purpose, this section has been divided into three subsections. In the first subsection the PCA is conducted, including preliminary, spatial, temporal, and vehicle classification analyses. The second subsection outlines the recursive partitioning analysis results for both FHWA and Texas 6 classification, while the third provides concluding remarks based on the research.

### 4.1 Principal Component Analysis

The first statistical methodology used to analyze the WIM dataset was the PCA methodology outlined in Section 2.4.1. The prime motivation behind utilization of PCA in this analysis was to reduce the dimensionality of the dataset, explore the relationships between the variables, and identify anomalies within the dataset. As was outlined in Section 3.3, the WIM dataset includes data on 24 different parameters for each vehicle that passes over the system. Although the data collection technology is sound, the potential exists for misclassification of the data, leading to potential outliers. PCA provided a means whereby both data reduction and removal of potential outliers in the dataset could be accomplished. The SPSS (96, 134) and Data Desk<sup>®</sup> 6.1 (135) software packages were utilized for the PCA to perform the transformations of the data and to plot the PCs to determine relationships within the dataset.

The PCA was conducted for several iterations and a variety of applications. To summarize the results of these analyses, this section has been divided into five subsections. The first outlines the preliminary analysis performed on the dataset, including a preliminary PCA as well as non-statistical analyses of the data to provide consistency across the dataset. The second provides a spatial analysis of the dataset, including a PCA analysis of the FHWA Class 9 vehicles. The third subsection utilizes the results from the previous analysis to explore temporal relationships within the data, while the fourth summarizes the results and provides a final dataset for analysis. The final subsection explores the classification of vehicles in the final dataset.

#### *4.1.1 Preliminary Analysis of Data*

To begin the PCA, the raw WIM dataset was analyzed to ensure that the data were consistent across all data points. The raw data included 209,551 total vehicles with data on location, time, vehicle classification, total weight, individual axle weight, total spacing, spacing between each consecutive axle pair, and other data as outlined in Section 3.3. As a result of the preliminary analysis, several modifications were made to the raw dataset, including: 1) truncation of the dataset to include only vehicles with GVW of 8,000 pounds or greater to maintain consistency between piezoelectric and bending plate calibration settings; 2) truncation of the dataset to remove vehicles with total length less than 11 feet and/or total spacing between the first two axles less than 10 feet; and 3) removal of all Class 13 data as the preliminary PCA identified Class 13 data as a large contributor to the variation. A discussion of each of these modifications is provided in the following subsections, with a resulting dataset that included 179,175 vehicles carried forward to the spatial analysis of the dataset.

**4.1.1.1 Calibration Consistency** The first step in the preliminary analysis was to understand the properties of each of the data collection sites. The primary difference in the data collection sites was the methodology utilized to collect data. As was outlined in Section 3.1.5, two methodologies for WIM are used in the state of Texas: 1) piezoelectric and 2) bending plate. Although the methodologies are both utilized to collect weight, classification, and volume information, they do not collect the data in exactly the same way. One of the first differences apparent in the data collection methodologies is the cut-off values used for total weight in the calibration methodologies. The piezoelectric sites have a minimum total weight of 8,000 pounds in their calibration methodology. The bending plate sites, however, record vehicles weighing

4,900 pounds or more (31). To be consistent with the piezoelectric scale calibration parameters, the lower limit weight threshold was modified for the bending plate sites to include only vehicles greater than 8,000 pounds total weight. This criterion affected 23,793 vehicles, or 11.4 percent of the raw dataset.

**4.1.1.2 Analysis of Vehicle Length** The second step in the preliminary analysis was to compare the dataset with the standard design criteria for vehicles as outlined in the 2001 AASHTO Green Book (15). The results of this analysis identified several data points in which the overall length of the vehicle and/or the length of axles A to B may be less than that of a standard vehicle. The AASHTO Green Book provides standards for design vehicles that indicate the typical length of a vehicle is 11 feet and that the minimum length between the first (axle A) and second (axle B) axles of any given vehicle type is approximately 10.1 feet (15). For unknown reasons, some of the vehicles in the analysis exhibit characteristics for total length and spacing between axles A and B that are less than these design guidelines, with total spacing recorded as low as 1.9 feet in some instances. The most probable cause for these readings is hypothesized to be incorrect classification, primarily due to equipment failure, calibration failure, and/or other instrument error.

Although all errors in instrumentation cannot be identified, it was determined that the dataset would be truncated based on axle and vehicle spacing. Based on the AASHTO standards outlined, vehicles with spacing between axles A and B of less than 10 feet and vehicles with total length less than 11 feet were eliminated from the dataset. This criterion affected 11,339 vehicles, or approximately 5.4 percent of the raw dataset.

**4.1.1.3 Preliminary PCA** The preliminary PCA included an analysis of the total weight, weight of each individual axle, total spacing, and spacing of each axle pair in the dataset, for a total of 19 parameters. A summary of the resulting eigenvalues and the percent variance for each of these eigenvalues is provided in Table 4.1. The results of the preliminary PCA identified five eigenvalues with a numeric value greater than one, which were subsequently chosen as the PCs (shown in bold in the table). These five PCs accounted for more than 75 percent of the total variance in the variables and were, therefore, considered sufficient for analysis (91).

**TABLE 4.1 Preliminary Dataset Total Variance Explained**

Component	Initial Eigenvalues		
	Total	% of Variance	Cumulative %
1	<b>6.971</b>	<b>36.688</b>	<b>36.688</b>
2	<b>3.432</b>	<b>18.062</b>	<b>54.750</b>
3	<b>1.642</b>	<b>8.642</b>	<b>63.391</b>
4	<b>1.211</b>	<b>6.375</b>	<b>69.766</b>
5	<b>1.161</b>	<b>6.110</b>	<b>75.876</b>
6	0.933	4.909	80.785
7	0.771	4.060	84.845
8	0.698	3.672	88.517
9	0.451	2.373	90.890
10	0.442	2.325	93.214
11	0.378	1.992	95.206
12	0.373	1.963	97.169
13	0.161	0.848	98.017
14	0.134	0.703	98.720
15	0.124	0.653	99.373
16	0.083	0.434	99.808
17	0.035	0.186	99.994
18	0.001	0.005	99.998
19	0.000	0.002	100.000

In addition to the summary of eigenvalues and variances, a data component matrix was generated for the preliminary analysis. The results of the component matrix are provided in Table 4.2 for each of the five chosen PCs. According to the full data component matrix, the first PC places more of an emphasis on the total weight and the weight of axles A through E as well as total spacing and spacing of axles A through E, which represent the axles of an FHWA Class 9 vehicle. The preliminary analysis in Section 3.3.1.2 identified FHWA Class 9 as the most common truck classification, representing over 67 percent of the truck population. Alternately, the second PC places more emphasis on the weight and spacing of axles F through I, with only minor weight on those emphasized in the first PC. PCs three through five provide more of a mixed relationship, with emphasis placed throughout the variables.

**TABLE 4.2 Preliminary PCA Data Component Matrix**

	Component				
	1	2	3	4	5
Total Weight (lb)	0.972	0.009	-0.014	-0.084	-0.035
Axle A Weight (lb)	0.810	-0.052	-0.069	-0.110	0.049
Axle B Weight (lb)	0.812	-0.055	-0.095	-0.055	-0.058
Axle C Weight (lb)	0.941	-0.043	-0.055	-0.033	-0.043
Axle D Weight (lb)	0.923	-0.029	0.005	-0.033	-0.041
Axle E Weight (lb)	0.911	-0.038	-0.020	-0.127	-0.014
Axle F Weight (lb)	0.115	0.523	0.764	-0.156	0.066
Axle G Weight (lb)	0.068	0.825	-0.079	-0.102	-0.374
Axle H Weight (lb)	0.062	0.817	-0.132	-0.080	-0.321
Axle I Weight (lb)	0.036	0.604	-0.298	0.157	0.516
Axles A to B Spacing (ft)	0.464	-0.110	-0.183	-0.290	0.182
Axles B to C Spacing (ft)	0.255	-0.005	0.092	0.837	-0.207
Axles C to D Spacing (ft)	0.821	-0.086	-0.047	-0.127	0.090
Axles D to E Spacing (ft)	0.605	0.033	0.213	0.472	-0.060
Axles E to F Spacing (ft)	0.085	0.350	0.835	-0.077	0.286
Axles F to G Spacing (ft)	0.047	0.705	-0.156	0.000	-0.103
Axles G to H Spacing (ft)	0.046	0.750	-0.178	-0.005	-0.127
Axles H to I Spacing (ft)	0.025	0.483	-0.283	0.207	0.661
Total Spacing (ft)	0.888	-0.017	0.080	0.178	0.057

The next step in the PCA was the analysis of the scores for each of the PCs for each data point analyzed. The scores were computed by multiplying the component eigenvalues for each variable by the actual value in the dataset for that variable. This allowed PC plots to be developed for each of the scores and to compare the values to find anomalies in the data. Once the PCs and the component score coefficient matrix were developed, the relationship between each of the PCs was analyzed by generating scatter plots for each of the different factor score groupings. The results of the component score coefficient matrix, as well as plots of the relationships between each of the combinations of the component scores, are provided in Appendix C. A representative plot of the relationship between PC one and PC two is provided in Figure 4.1. It can be seen from this figure that when a scatter plot of the corresponding scores for each of the PCs is generated, the variation in the data is apparent based on the spread in the PC scores along each of the axes, particularly the x-axis.

The next step in the analysis, therefore, was to analyze the different score values and determine the characteristics of the outliers to better understand the data. This analysis was performed by generating scatter plots of the scores, with histograms of the vehicle classification

(FHWA class) and data collection sites (CSN). Although these data were not included in the PCA, the relationship between these variables and the PCs was retained. When the Class 13 data were selected for analysis, all plots showed Class 13 data outside of the major groupings, quickly pinpointing FHWA Class 13 as a major source of the variation in the data. This was interesting because Class 13 data made up only a small portion (0.11 percent) of the data, but this was also somewhat expected due to the irregularity and variability of Class 13 vehicles identified in the preliminary analysis.

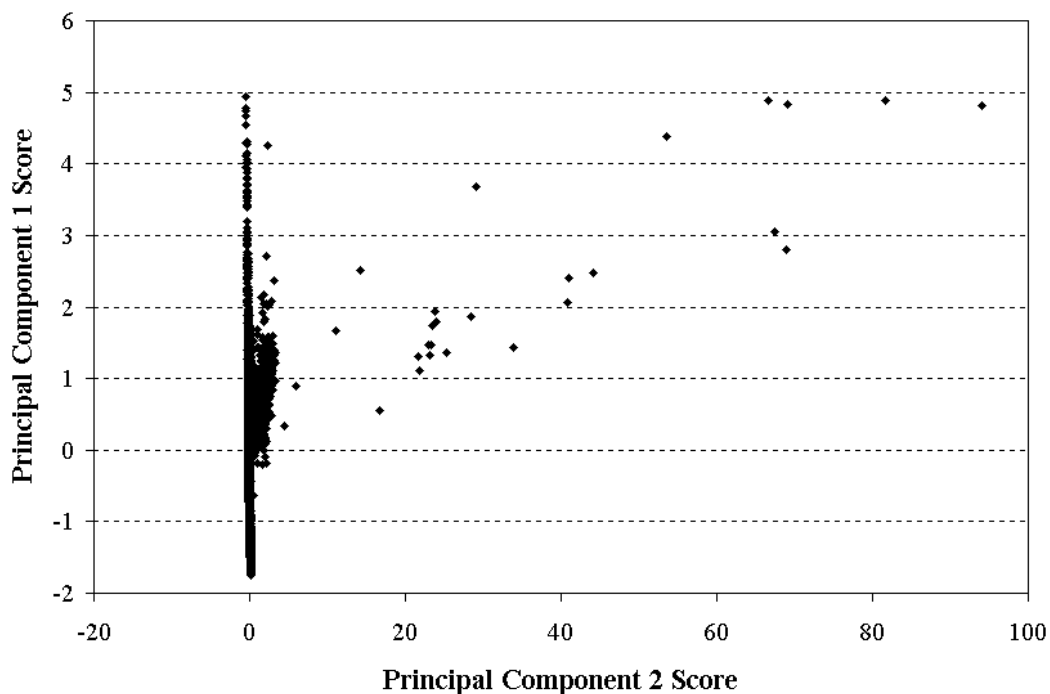


**FIGURE 4.1 Preliminary analysis PC one score versus PC two score**

As a result of this analysis, the final modification made in the preliminary PCA analysis was the removal of all Class 13 data. This was done based on: 1) the results of the PCA and 2) calibration inconsistency. The piezoelectric sites did not collect any Class 13 data, while the bending plate sites did. Because the bending plate sites contained the majority of the data as outlined in Section 3.3.1.1, this was not taken into consideration in the initial calibration consistency step. Based on the calibration inconsistency combined with the variability of the

Class 13 data identified in the PCA, however, all Class 13 data were removed from further analysis. This criterion affected 225 vehicles, or approximately 0.11 percent of the raw dataset.

#### *4.1.2 Spatial Analysis of Data*

Following the preliminary analysis of data, the next step in the PCA was a detailed analysis of the data both spatially and temporally. The first, spatial analysis of the data was accomplished with the primary motivation of determining the relationships that exist between the data collection sites. As was identified in Section 3.1.5, the Texas collects WIM data utilizing two different technologies. Based on the analysis in Section 3.3.2, these two technologies provide somewhat different trends, primarily in the total weight of trucks passing the site. As a result of the preliminary analysis, it was determined that a more detailed analysis of the spatial relationships between the data would be performed.

The results of the preliminary PCA analysis provided a base dataset for use in the spatial data analysis. One trend in the dataset that was identified in this preliminary PCA analysis was the high number of “missing data” locations in the dataset where axles were not present. To illustrate the concept of the “missing data” locations, consider an FHWA Class 9 vehicle. This vehicle type is comprised of five axles with a single trailer, which produces a WIM data entry that includes the parameters illustrated in Table 4.3. It can be seen from this table that there is no information provided for weight of axles F through I, as well as spacing of these same axles since they do not exist for this vehicle type. The analysis that was completed for the preliminary dataset included zero values for each of the locations where data did not exist. By including zero values, a large number of zero value PCs existed in the data, as was identified in the results of the preliminary PCA analysis.

In the spatial analysis of data, therefore, the first modification to the dataset was the reduction of the number of parameters included in the data from an analysis of all axles and axle spacing to a reduced analysis that included only data for axles A through E. The motivation behind this reduction was the limited number of data points where information for these axles existed, and the resulting influx of zero data points that occurs when these “missing data” points remain in the dataset. This reduction does not, however, eliminate all “missing data” in the analysis. Vehicle classes lower than Class 9 include anywhere from two axles to four axles, thus including additional “missing data” points. Therefore, a sensitivity analysis of two additional scenarios was performed. The first scenario utilized the reduced dataset with zero values

included in the remaining missing data locations, while the second dataset included blank values in these locations. By leaving the values blank, the dataset further reduced the PCA to FHWA Class 9 through FHWA Class 12, which included 134,091 vehicles, or approximately 64 percent of the initial raw dataset. The sensitivity analysis produced similar results between the two scenarios, with the second scenario (i.e., FHWA Class 9 through 12) chosen for further analysis.

**TABLE 4.3 Example Class 9 Row Entry**

						<b>Classification</b>			
<b>CSN</b>	<b>Dir.</b>	<b>Date</b>	<b>Quarter</b>	<b>Hour</b>	<b>Peak</b>	<b>6 Digit</b>	<b>FHWA</b>	<b>TxDOT</b>	
181	3	11/19/01	4	8	1	332000	9	9	
<b>Weight Data (lb)</b>									
<b>Total</b>	<b>A</b>	<b>B</b>	<b>C</b>	<b>D</b>	<b>E</b>	<b>F</b>	<b>G</b>	<b>H</b>	<b>I</b>
44200	11000	10500	8500	7100	7100	-	-	-	-
<b>Spacing Data (ft)</b>									
<b>Total</b>	<b>A-B</b>	<b>B-C</b>	<b>C-D</b>	<b>D-E</b>	<b>E-F</b>	<b>F-G</b>	<b>G-H</b>	<b>H-I</b>	
42.4	16.2	4.2	18.0	4.0	-	-	-	-	

'-' denotes missing data (i.e., axles do not exist)

The PCA of the reduced dataset included an analysis of the total weight, weight of axle A through E, total spacing, and spacing of each axle pair from axles A through E, for a total of 11 parameters. A summary of the resulting eigenvalues and the percent variance for each of these eigenvalues is provided in Table 4.4. As shown in this table, the results of the PCA identified three eigenvalues with numeric value greater than one, which were subsequently chosen as the PCs (shown in bold in the table). Again, these three PCs accounted for more than 75 percent of the total variance in the variables and were, therefore, considered sufficient for analysis (91).

In addition to the summary of eigenvalues and variances, a data component matrix was generated for the spatial data analysis. The results of the component matrix are provided in Table 4.5 for each of the three PCs. From the PC matrix it is apparent that the first PC places a heavy emphasis on the weight variables, including total weight and the weight of each individual axle. The second PC shifts this emphasis to the spacing of the individual axles (not total spacing), rather than to the weight of each axle. The third and final PC for this analysis puts the highest emphasis on total spacing, with a mixed emphasis on the remaining variables.

**TABLE 4.4 Spatial Data Analysis Total Variance Explained**

Component	Initial Eigenvalues		
	Total	% of Variance	Cumulative %
<b>1</b>	<b>4.849</b>	<b>44.085</b>	<b>44.085</b>
<b>2</b>	<b>2.661</b>	<b>24.193</b>	<b>68.278</b>
<b>3</b>	<b>1.576</b>	<b>14.327</b>	<b>82.604</b>
4	0.772	7.015	89.619
5	0.552	5.055	94.674
6	0.246	2.240	96.913
7	0.179	1.628	98.542
8	0.065	0.892	99.134
9	0.055	0.500	99.634
10	0.038	0.343	99.977
11	0.003	0.023	100.000

**TABLE 4.5 Spatial Data Analysis Component Matrix**

	Component		
	1	2	3
Total Weight (lb)	0.995	0.053	-0.053
Axle A Weight (lb)	0.454	-0.233	0.236
Axle B Weight (lb)	0.944	0.160	-0.031
Axle C Weight (lb)	0.961	0.042	-0.039
Axle D Weight (lb)	0.947	0.055	-0.098
Axle E Weight (lb)	0.944	0.011	-0.120
Axles A to B Spacing (ft)	0.139	-0.364	0.730
Axles B to C Spacing (ft)	-0.077	0.922	0.103
Axles C to D Spacing (ft)	0.106	-0.869	0.203
Axles D to E Spacing (ft)	-0.007	0.897	0.291
Total Spacing (ft)	0.116	0.173	0.907

As with the preliminary PCA, the next step in the analysis was to compute the scores for each of the PCs for each data point analyzed as the product of the component eigenvalues for each variable and the observed value in the dataset for that same variable. Once the PCs and the component score coefficient matrix were developed, the relationship between each of the PCs was analyzed by generating scatter plots for each of the different PC score groupings. The results of the component score coefficient matrix, as well as plots of the relationships between each of the combinations of the component scores, are provided in Appendix C.

In this analysis, a three-dimensional (3D) scatter plot of the scores was again generated along with histograms of the vehicle classification (FHWA class) and data collection sites (CSN). The first relationship identified within the data was the relationship between the FHWA Class 9 vehicles and the remaining vehicles in the analysis. It became apparent that Class 9 dominated the dataset, which can be expected particularly since these vehicles make up over 67 percent of the entire dataset. In this analysis, however, the percentage is greatly increased since the Class 13 data are removed, and this particular analysis (with missing data) also removes Classes 4, 5, 6, and 8, as well as well as the majority of the Class 7 data. In this dataset, Class 9 vehicles account for approximately 94 percent of the entire dataset.

Based on the analysis, the Class 9 data appeared to be clustered in two defined groups (Cluster A and Cluster B), as illustrated in Figure 4.2. Further analysis determined that the two groups were spatially related, where the first group (Cluster A) included some data points from all sites, with the most pronounced influence in the cluster primarily from sites LW-512 (IH-37) and LW-513 (IH-35). The second cluster (Cluster B) also included some data points from all sites, while this cluster identified that the Class 9 vehicles at PZ-518 (IH-10) displayed characteristics that were different than the same class of vehicles at other sites. The remaining vehicle classifications were also analyzed and did not appear to pose any special problems. The FHWA Class 10 data appeared to provide a boundary for the FHWA Class 9 vehicles, while the FHWA Class 11 and Class 12 vehicles were scattered throughout the cluster of data points.

The results of this analysis identified a need to further analyze the FHWA Class 9 vehicles and to examine the relationships between the average total weight of these vehicles spatially across the state. This was done using three primary statistical tools: 1) box-plots to identify where the differences lie within the data; 2) one-way ANOVA to check for statistical significance between sites; and 3) pairwise comparisons to pinpoint sites that exhibit similar weight characteristics. Each of these topics is discussed in the following subsections, with a fourth subsection to identify the final results of this analysis.

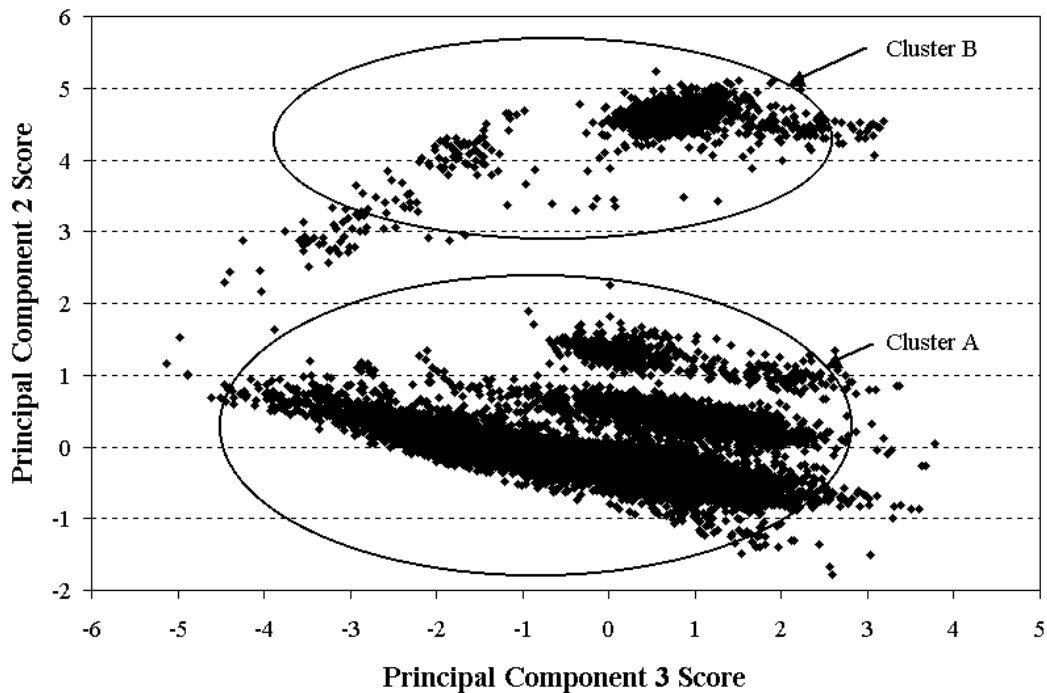


**FIGURE 4.2** Spatial data analysis PC two score versus PC three score

**4.1.2.1 Box-Plot Analysis** The box-plot analysis is a graphical method to display the descriptive statistics of a dataset, including the center (median) and spread (interquartile ranges) of the data, departure from symmetry, and identification of observations that lie outside of the bulk of the data (i.e., outliers). As the name would suggest, a box-plot is a box that encloses the interquartile range, with the lower edge of the box at the first quartile (25<sup>th</sup> percentile) and the upper edge of the box at the third quartile (75<sup>th</sup> percentile) of the data. A line is then drawn through the box at the second quartile, or the median (50<sup>th</sup> percentile). In addition, a line, or whisker, extends from each end of the box to the smallest data point within 1.5 interquartile ranges from the first quartile (lower end) and to a point 1.5 interquartile ranges from the third quartile (upper end). One interquartile range is defined as the difference between the third quartile and the first quartile, thus representing the range of data that lies between the 25<sup>th</sup> percentile and the 75<sup>th</sup> percentile. Any point that lies beyond a whisker but less than three interquartile ranges from the box edge is also identified (by an open circle) as an outlier of the data. Data that are more than three interquartile ranges from the box edge are also identified (using an asterisk) as an extreme outlier (134, 136).

The results of the box-plot analysis for FHWA Class 9 vehicles in the dataset are shown in Figure 4.3. It can be seen from this figure that the median total weights for each of the locations are relatively constant and that the majority of the sites do not contain a large number of outliers. The exception to this statement, however, is site PZ-074 (US 77), a site that includes a high number of both regular outliers as well as extreme outliers. The next step, therefore, was to analyze this location independent of the others to identify trends in the data, particularly for the outliers. This was accomplished by separating the data for site PZ-074 (US 77), rank ordering the data, and comparing the higher weight trucks based on quarter of the year and time-of-day to see if there were noticeable trends in the data. In addition, the total weight of each vehicle was plotted against weights of each individual axle, as well as the spacing for each individual axle to identify any trends in these relationships. The results of this analysis did not identify any abnormal trends in the data, and it was concluded, therefore, that the difference in the average weights at the data collection locations was random with no identified anomalies in the data.

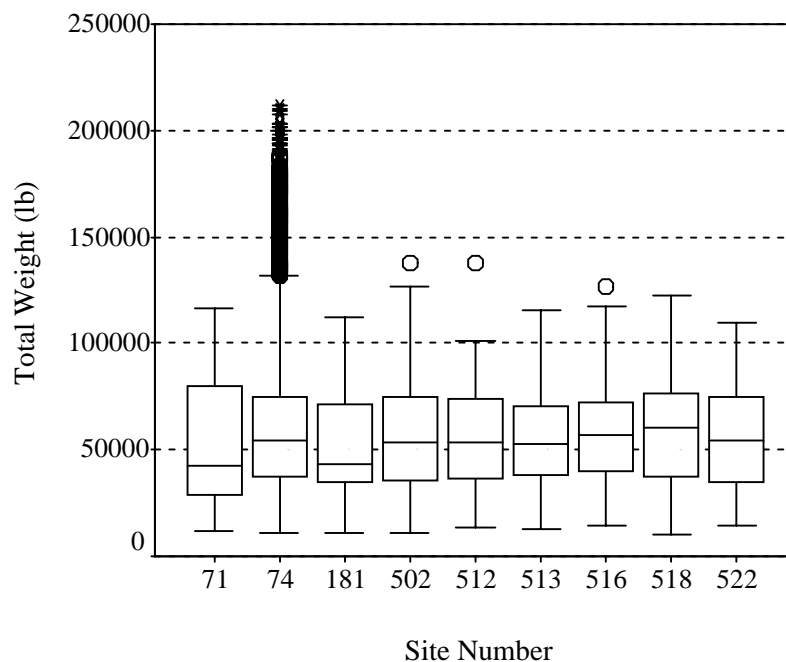


**FIGURE 4.3** Spatial data analysis box-plot results

**4.1.2.2 One-Way ANOVA** The next level of analysis was the one-way analysis of variance (one-way ANOVA), also referred to as the test for equality of factor-level means. The purpose of the one-way ANOVA is to test the hypothesis that a difference between means of more than two factors comes from populations with equal means (134, 137). In other words, the test is set up to determine whether or not the mean values (i.e., mean total weight) at more than two data collection sites (i.e., CSN) are in fact equal. The null hypothesis for this test is identified in Equation 4.1, while the alternative hypothesis ( $H_a$ ) would indicate that not all mean values are equal.

$$H_0 : \mu_i = \dots = \mu_k \quad \forall i = 1, k \quad (4.1)$$

where:  $H_0$  = null hypothesis;  
 $\mu_i$  = mean of group  $i$ ; and  
 $k$  = number of groups.

The  $F$  statistic constructed for testing this hypothesis is outlined in Equation 4.2. From this statistic, it can be determined whether or not the mean values are statistically equal. If the means are far apart relative to the variation within each group, the size of the  $F$  statistic will be large and the null hypothesis will be rejected. Small values of the  $F$  statistic will support  $H_0$  since both the between-groups sum of squares and the within-groups sum of squares have the same expected value when the null hypothesis holds true (134, 137).

$$F = \frac{\text{variation among the sample means}}{\text{variation within the samples}} \quad \text{or} \quad \frac{\text{Between groups sum of squares} / (k - 1)}{\text{Within groups sum of squares} / (N - k)} \quad (4.2)$$

where:  $N$  = total sample size.

One characteristic of the one-way ANOVA that was considered was the relationship between the variances and the sample size. When both the variances and the sample sizes differ for each of the groupings, the standard  $F$  statistic can lack power to analyze the relationships correctly and is thus prone to provide incorrect results. Several additional tests are available to help overcome this shortcoming of the  $F$  statistic (96, 134, 137), including the Brown-Forsythe and Welch methodologies (138, 139), which were included in the analysis. The results of the one-way ANOVA and robust tests of equality of means for the reduced dataset are provided in Table 4.6 and Table 4.7, respectively. The  $F$  statistic and corresponding significance values for

the additional robust test of equalities of variance indicate that the null hypothesis is rejected at a high significance level, and it would therefore be concluded that at least one of the means is not equal.

**TABLE 4.6 Spatial Data Analysis One-Way ANOVA Results**

	<b>Sum of Squares</b>	<b>Degrees of freedom (df)</b>	<b>Mean Square</b>	<b>F</b>	<b>Sig.</b>
Between Groups	3.09 E+11	8	3.86 E+10	109.44	0.000
Within Groups	4.43 E+13	125,716	3.52 E+08		
Total	4.46 E+13	125,724			

**TABLE 4.7 Spatial Data Analysis Robust Tests of Equality of Variance**

	<b>Statistic</b>	<b>df1</b>	<b>df2</b>	<b>Sig.</b>
Welch	69.17	8	4,981.68	0.000
Brown-Forsythe	74.84	8	5,355.45	0.000

In addition to the one-way ANOVA results, error bar charts were also developed for the analysis to graphically identify the differences in the means. Error bars are centered on the mean of the data and include a bar on each side of the mean that represents a confidence interval or specified number of standard errors (*140*). Error bar charts are an effective method utilized to illustrate the variability of the measurement displayed. The results of the error bar chart are provided in Figure 4.4, clearly identifying the locations where the mean values may not be equal as sites PZ-071 (SH 16), PZ-074 (US 77), PZ-181 (SH 48), and PZ-518 (IH-10). These four sites provide the most pronounced differences according to the error bar chart results.

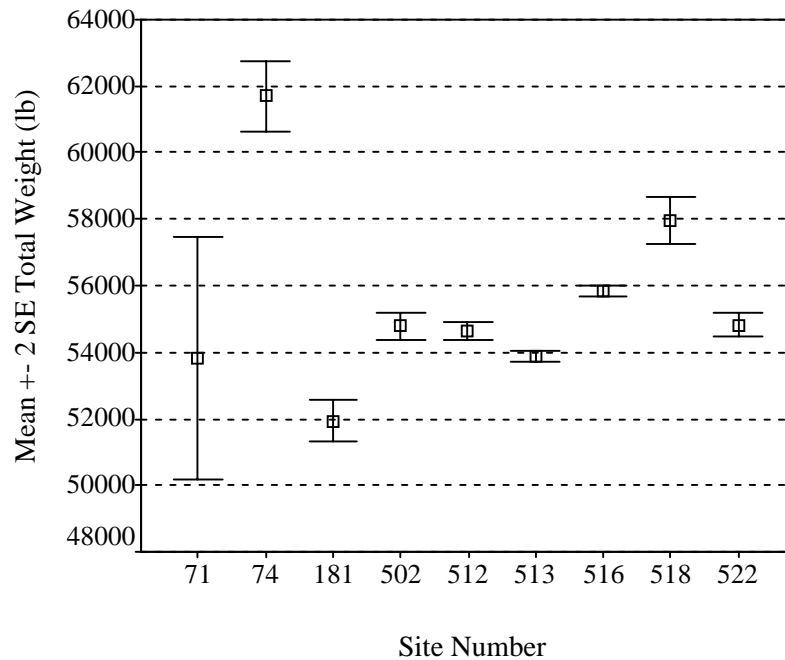


**FIGURE 4.4** Spatial data analysis error bar chart

**4.1.2.3 Pairwise Comparisons** The next question to be answered, therefore, was which of the means are statistically different. In addition to the regular one-way ANOVA and other equality of means testing procedures, *post hoc* tests are also very useful for pairwise comparisons of data to make inferences on the difference between two factor-level means. There are several different *post hoc* tests that can be performed to determine which of the different locations have similar and different mean values. Two of the more common tests are the Tukey and Bonferroni methods (134, 137). The purpose of these tests is to compare the difference in the means for all pairwise datasets and to develop confidence intervals based on the difference in means. The null hypotheses tested for the pairwise comparisons are outlined in Equation 4.3 and Equation 4.4, where all pairs ( $D = \mu_i - \mu_{i'}$ ) are analyzed (137).

$$H_0 : \mu_i - \mu_{i'} = 0 \quad \text{or} \quad \mu_i = \mu_{i'} \quad (4.3)$$

$$H_a : \mu_i - \mu_{i'} \neq 0 \quad \text{or} \quad \mu_i \neq \mu_{i'} \quad (4.4)$$

where:  $\mu_{i'}$  = mean of group  $i'$ .

To provide an analysis of the weight data at each of the locations analyzed, the Tukey and Bonferroni tests were conducted for each of the locations. The results of the two analyses provided consistent results with the complete results of the Bonferroni test tabulated in Appendix C. This table identifies the difference in the mean total weight between the two sites, the standard error of the difference, the resulting significance level, and the 95 percent confidence interval upper and lower bounds. The results of the Bonferroni analysis indicate that several of the mean differences are significant at the 95 percent (0.05) level. The cases where the mean difference is significant are those in which zero (0) is not included in the confidence interval, suggesting that the mean total weights are not the same.

A summary of the pairwise analysis results is provided in Table 4.8. In this table a shaded block identifies the data collection sites where the difference between the mean average weight is not significant, thus indicating the potential to group locations together. These are those sites where a zero is included in the confidence interval for the mean difference, suggesting with 95 percent confidence that the difference in the means is zero, and that the average total weight between the two sites may be the same.

**TABLE 4.8 Spatial Data Analysis Pairwise Comparison Results**

		Site Number (CSN)								
		071	074	181	502	518	512	513	516	522
Site Number (CSN)	071									
	074									
	181									
	502									
	518									
	512									
	513									
	516									
	522									

Note: Shaded squares denote differences between mean average weights are not significant

It is apparent from the results of the pairwise comparison that although a number of sites do exhibit characteristics that would suggest the mean total weights of the trucks crossing the site are the same, the number of locations where this is the case is somewhat limited. The site that provides a relationship with the majority of the sites is PZ-071 (SH 16), most likely due to

the small sample size in relation to the remaining sites. Of those sites that have a relatively large sample size, sites PZ-502 (IH-10), LW-512 (IH-37), and LW-522 (US 281) show the strongest relationships. This is somewhat surprising as these sites represent samples from the piezoelectric sites and the bending plate sites, as well as samples from both interstate and non-interstate routes. One thing that these three sites do share in common, however, is that they all provide access to trucks traveling between San Antonio and the Brownsville and McAllen Mexican border crossing sites. The origin and destination of these vehicles may be comparable, thus providing a possible explanation for the equality in mean total weight.

Based on the results of this analysis two additional groupings of the data were also examined to develop relationships between the data collection sites. The first grouping was to sort the data according to functional classification of the data collection site, namely interstate versus non-interstate locations. The data were further broken down by data collection methodology for interstate and non-interstate sites. The results of all analyses indicated that, regardless of the groupings, the mean values of the total weight for each scenario are not equal at the 95 percent (0.05) significance level. The best estimate of grouping by data, therefore, was to utilize the results of the pairwise comparison analysis to form spatial relationships based on the analysis of total vehicle weight performed.

**4.1.2.4 Spatial Data Analysis Results** Although the results indicated that site PZ-071 (SH 16) showed a significant relationship based on the difference in mean total weight with the majority of the sites, it was determined that this site should be removed from the dataset due to the rural nature of the site, the small number of observations, and the variability of the data identified in the PCA. The obscure nature of the site combined with its insignificant size was sufficient to justify its removal from the dataset. In addition, it was determined that site PZ-074 (US 77) should also be removed from the dataset due to the high number of outliers identified in the box-plot analysis, as well as the lack of relationship between this site and any others as identified in the PCA and one-way ANOVA results. Sites PZ-181 (SH 48) and PZ-518 (IH-10) were also identified for removal from the dataset based on the results of the PCA and box-plot analyses, which identified relatively low and high mean GVW recorded at each of the sites, respectively. This analysis removed 17,279 vehicles or 9.6 percent of the dataset from the preliminary analysis.

The remaining five sites (PZ-502 [IH-10], LW-512 [IH-37], LW-513 [IH-35], LW-516 [IH-35], and LW-522 [US 281]) were selected to remain in the dataset and have been broken into two groups. Group one includes a subset of the sites (PZ-502 [IH-10], LW-512 [IH-37], and LW-522 [US 281]) that were identified in the previous section to exhibit statistically significant characteristics based on the PCA and one-way ANOVA. Group two includes all five locations. Sites LW-513 (IH-35) and LW-516 (IH-35) have been maintained in the analysis due to the large sample size for each of these sites and the consistency of the data as illustrated in the box-plot results and the overall mean values. The box-plot for group one is provided in Figure 4.5, while the box-plot for group two is provided in Figure 4.6. The five sites comprise just over 90 percent of the data in the FHWA Class 9 analysis, or 114,269 vehicles. As evidenced in the analysis and from these figure, the five sites exhibit similar characteristics, including very comparable mean total weights, first and third quartile ranges, and relatively few outliers. These two groups of data will be carried forward in the temporal analysis to determine if specific relationships exist between the two groups on a temporal basis.

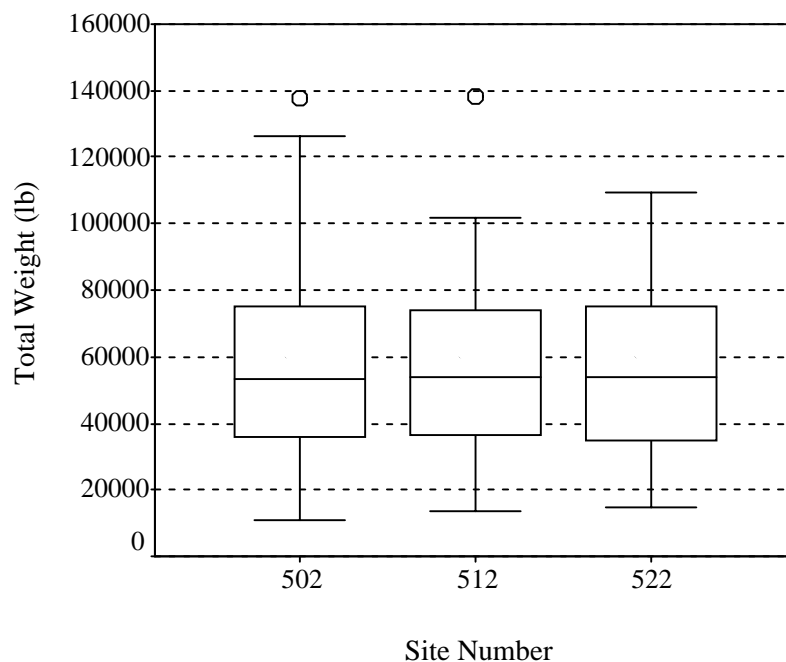


**FIGURE 4.5** Group one box-plot results

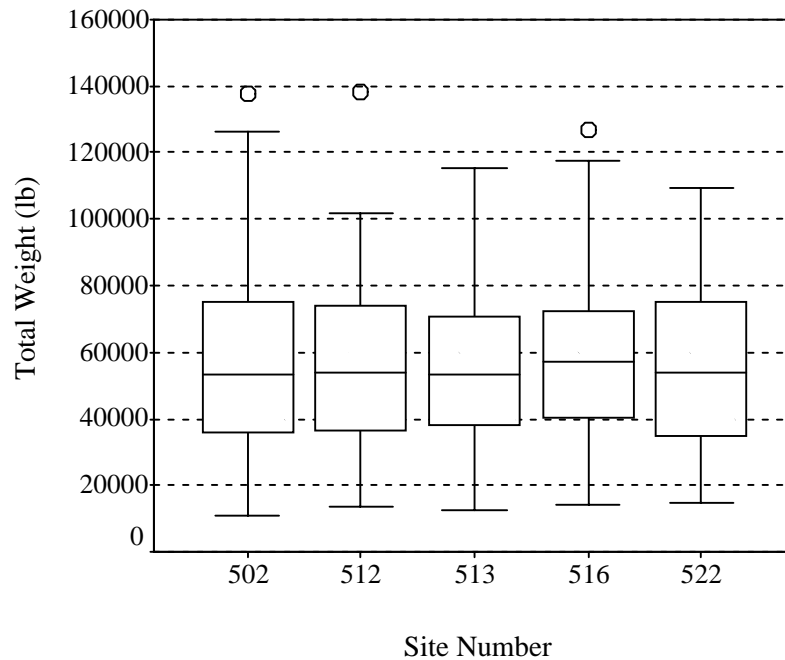


**FIGURE 4.6** Group two box-plot results

#### 4.1.3 Temporal Analysis of Data

The next step in the PCA and data reduction was to explore different characteristics of the data and to develop a method to analyze temporal differences in the data. To accomplish this task, the data were grouped both seasonally and by peak period. The first, seasonal variation, was accomplished by adding a new variable to the dataset for season, or, in this case, quarter of the year. The data were originally collected quarterly; thus a quarterly breakdown presented itself as a logical grouping. Data were therefore grouped according to data collection in the first quarter (January through March), second quarter (April through June), third quarter (July through September), and fourth quarter (October through December). As was outlined in the preliminary analysis of the dataset in Section 3.3.1.1, data were collected for all four quarters of the year at only two sites (LW-512 [IH-37] and LW-516 [IH-35]). Two additional sites (LW-513 [IH-35] and LW-522 [US 281]) collected data for three quarters of the year, while the remaining five sites collected data for only one quarter. As a result of the lack of seasonal data at all sites, a detailed analysis by quarter was not considered.

The second grouping of the data to account for temporal data analysis was according to peak period. This was accomplished by breaking out the data collection times according to six different categories of peaking characteristics. The determination of peak periods was made based on standard peaking characteristics of traffic and the resulting off-peak periods that remain around these traditional peaks (a representation of these typical peaks was provided in Section 2.3.2). The first traditional peak occurs in the morning, generally between 6:00 a.m. and 9:00 a.m., while the second is the midday or lunch peak and occurs between 11:00 a.m. and 1:00 p.m. The third traditional peak is the PM peak, or evening commute, that generally occurs between 4:00 p.m. and 7:00 p.m. Combining the traditional peaks with the time that occurs between peaks, six categories emerge: 1) morning peak; 2) morning off-peak; 3) midday peak; 4) afternoon off-peak; 5) evening peak; and 6) evening/morning off-peak. A summary of the different groupings is provided in Table 4.9.

**TABLE 4.9 Peak Period Categories**

<b>Group Number</b>	<b>Description</b>	<b>Time Period</b>
1	Morning peak	6:00 a.m.–8:59 a.m.
2	Morning off-peak	9:00 a.m.–10:59 a.m.
3	Midday peak	11:00 a.m.–12:59 p.m.
4	Afternoon off-peak	1:00 p.m.–3:59 p.m.
5	Evening peak	4:00 p.m.–6:59 p.m.
6	Evening/morning off-peak	7:00 p.m.–5:59 a.m.

Utilizing the relationships identified in the spatial data analysis section, the peak period analysis was performed based on the two groups of data and was expanded to include all vehicle classifications. As with the spatial analysis of data, the temporal analysis was performed using three primary statistical tools: 1) box-plots; 2) one-way ANOVA; and 3) pairwise comparisons. Each of these topics will be discussed in the following subsections.

**4.1.3.1 Box-Plot Analysis** The box-plot was used as a statistical tool in the peak hour analysis to display the relationships between total weight and peak period. The same methodology outlined previously was utilized to develop box-plots for this analysis (134, 136). The results of the box-plot analysis for all vehicles in the group one dataset are shown in Figure 4.7, while the results of the box-plot analysis for the group two dataset are shown in Figure 4.8.

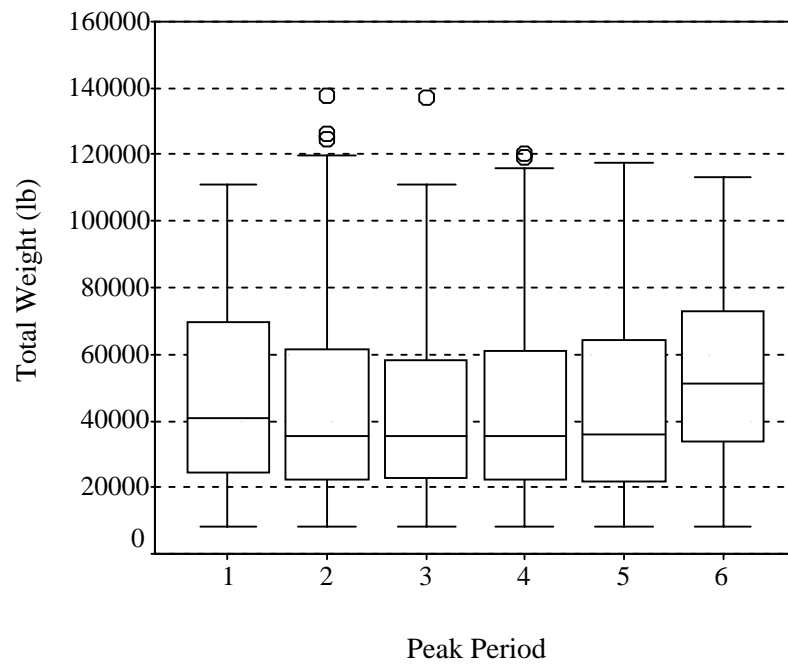


**FIGURE 4.7** Group one temporal data analysis box-plot results

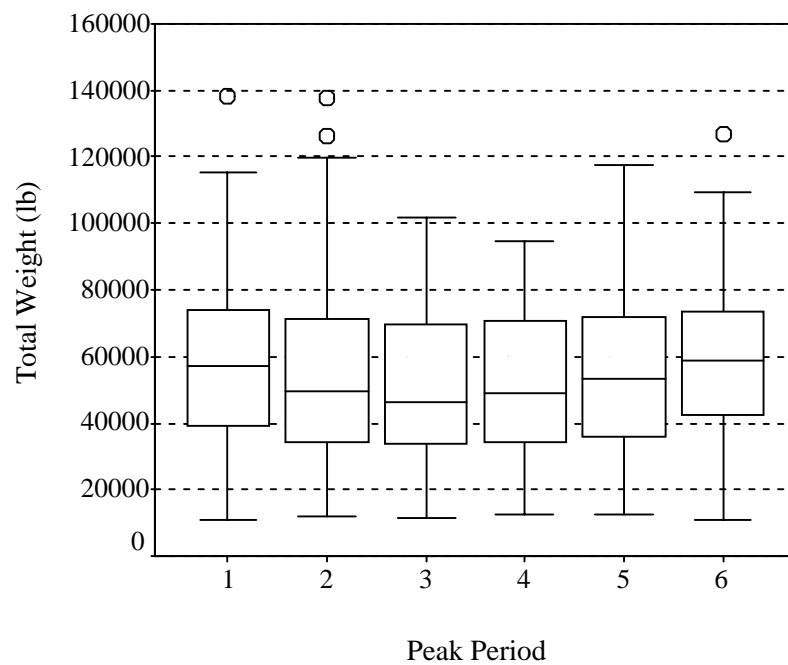


**FIGURE 4.8** Group two temporal data analysis box-plot results

It can be seen from the group one analysis that the median of the data for peak periods two through five are very consistent, while peak periods one and six exhibit slightly higher median results. The group two data identify somewhat of a similar trend, although in this figure peak period five also exhibits slightly higher median total weight results than peak periods two through four. To further identify and classify these trends, error bar chart and one-way ANOVA analyses were completed for the two groups and are included in the next subsection.

**4.1.3.2 One-Way ANOVA** As was identified previously, the purpose of the one-way ANOVA is to test the hypothesis that a difference between means of more than two factors comes from populations with equal means (134, 137). In this analysis, the test is set up to determine whether or not the mean values for total weight during more than two different peak periods are in fact equal. The null hypothesis ( $H_0$ ) for this test was identified previously and assumes that all mean values are equal, while the alternative hypothesis ( $H_a$ ) would indicate that at least one of the mean values is not equal.

The results of the one-way ANOVA for the reduced dataset are provided in Table 4.10 for group one and Table 4.11 for group two. The analysis results for both group one and group two show that when all peak periods are included in the analysis, the  $F$  statistic and corresponding significance value indicates that the null hypothesis is rejected at a high significance level. It would be concluded, therefore, that at least one of the means is not equal.

**TABLE 4.10 Group One Temporal Data Analysis One-Way ANOVA Results**

	<b>Sum of Squares</b>	<b>Degrees of freedom (df)</b>	<b>Mean Square</b>	<b>F</b>	<b>Sig.</b>
Between Groups	1.46 E+12	5	2.91 E+11	541.97	0.000
Within Groups	3.38 E+13	62,939	5.36 E+08		
Total	3.52 E+13	62,944			

**TABLE 4.11 Group Two Temporal Data Analysis One-Way ANOVA Results**

	<b>Sum of Squares</b>	<b>Degrees of freedom (df)</b>	<b>Mean Square</b>	<b>F</b>	<b>Sig.</b>
Between Groups	8.23 E+11	5	1.65 E+11	520.90	0.000
Within Groups	3.61 E+13	114,263	3.16 E+08		
Total	3.69 E+13	114,268			

In addition to the one-way ANOVA results, an error bar chart was also developed for the analysis to graphically identify the difference in the means. The result of an error bar chart for group one is provided in Figure 4.9, while the results for group two is illustrated in Figure 4.10. The results of the one-way ANOVA analysis are verified by the error bar chart for both group one and group two, clearly identifying the locations where the mean values may not be equal. For the group one analysis, the mean total weight is clearly different for peak period one and peak period six, while the group two error bar chart clearly identifies peak period one, peak period five, and peak period six as locations to consider as having different total weight characteristics.

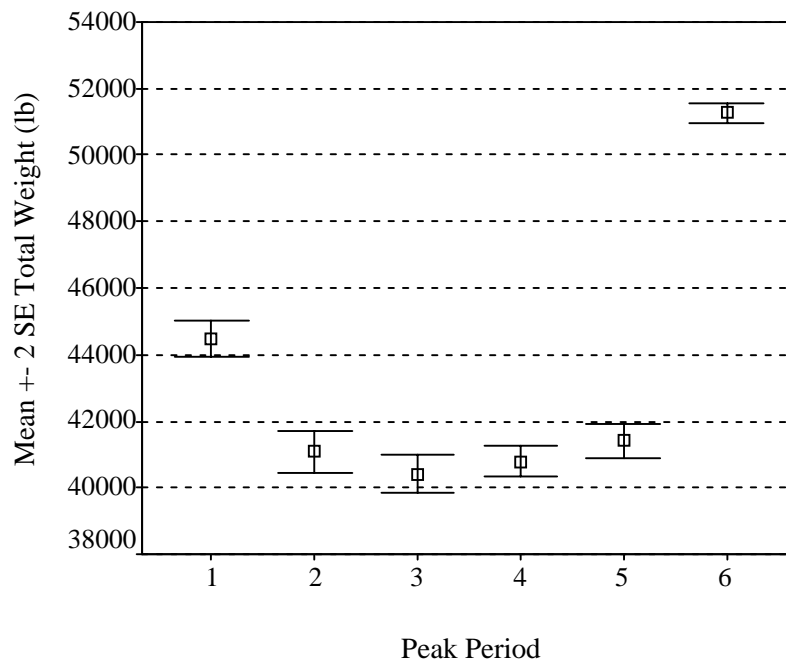


**FIGURE 4.9** Group one temporal data analysis error bar chart

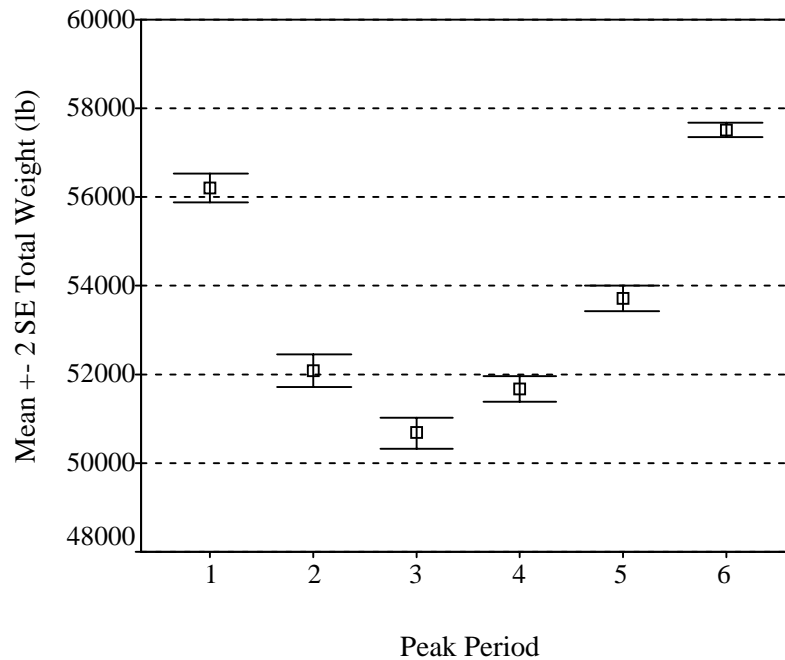


**FIGURE 4.10** Group two temporal data analysis error bar chart

**4.1.3.3 Pairwise Comparison** This result led to the need to determine which of the means is different and to the results of the Bonferroni pairwise comparison test. As was outlined in more detail previously, the purpose of this test is to compare the difference in the means for all pairwise comparisons and to develop confidence intervals based on these differences. The results of this analysis are summarized in Table 4.12 for group one and Table 4.13 for group two. In both of these tables, a shaded block identifies the peak period where the difference between the mean average weight is not significant, thus indicating the potential to group the peak periods.

It is apparent from the results of the peak period pairwise comparison that a significant relationship exists between peak period two and peak period four for both group one and group two. This is somewhat expected as these two periods are off-peak periods, one in the morning and one in the afternoon. In the group one analysis, peak period three and peak period five also exhibit similar characteristics as peak periods two and four. In the group two analysis, however, peak period three does not have as strong of a relationship between two and four; however, when analyzing the box-plot and error bar charts, the relationship does appear to exist. Peak period five, however, does appear to exhibit somewhat differing characteristics for the group two

analysis. For both group one and group two, peak period one and peak period six exhibit very unique characteristics and should be kept separate from the other peak periods. Peak period six is especially unique as it exhibits very high average weight compared to the other time periods.

**TABLE 4.12 Group One Temporal Data Analysis Pairwise Comparison Results**

		Peak Period					
		1	2	3	4	5	6
Peak Period	1						
	2						
	3						
	4						
	5						
	6						

Note: Shaded squares denote differences between mean average weights are not significant

**TABLE 4.13 Group Two Temporal Data Analysis Pairwise Comparison Results**

		Peak Period					
		1	2	3	4	5	6
Peak Period	1						
	2						
	3						
	4						
	5						
	6						

Note: Shaded squares denote differences between mean average weights are not significant

Based on the results of the analysis, it was determined that four different peak periods would be analyzed along with the two location groupings. The peak periods to analyze include AM peak (peak period one), midday peak (peak periods two, three and four), PM peak (peak period five), and night peak (peak period six).

#### 4.1.4 Summary of Principal Component Analysis Dataset

The dataset considered in the analysis to this point is comprised of two groups of spatial data, subdivided into four temporal peak periods. The spatial groupings include data for five sites (PZ-502 [IH-10], LW-512 [IH-37], LW-513 [IH-35], LW-516 [IH-35], and LW-522 [US 281]).

Group one includes a subset of the sites, PZ-502 (IH-10), LW-512 (IH-37), and LW-522 (US 281), those that were identified to exhibit statistically significant characteristics based on the PCA and one-way ANOVA. Group two includes all five locations. These five sites comprise nearly 90 percent of the data in the analysis dataset, or 161,896 CMVs.

As identified in the previous section, four different peak periods were also identified for analysis along with the two location groupings. The peak periods analyzed included AM peak (Peak 1), midday peak (Peak 2), PM peak (Peak 3), and night peak (Peak 4) as defined previously. A summary of the total weight descriptive statistics for each of the two groupings and four peak periods is provided in Table 4.14 for group one and Table 4.15 for group two. This information includes data on total sample size (N), average hourly volume (Avg. Vol.) computed by dividing the sample size by the number of hours in the respective peak period, mean vehicle weight in pounds (Mean), standard deviation of weight in pounds (Std. Dev.), standard error of the mean in pounds (Std. Error), 95 percent confidence intervals (95% C.I.) for the mean in pounds (Lower Bound and Upper Bound) and maximum (Max.) weight recorded for each group in pounds (minimum weight recorded is equal to 8,000 pounds for all datasets).

**TABLE 4.14 Group One Descriptive Statistics**

Peak	N	Avg. Vol.	Mean	Std. Dev.	Std. Error	95% C. I. Bounds		Max.
						Lower	Upper	
1	7,644	2,548	44,467.9	24,409.0	279.2	43,920.6	45,015.2	110,900
2	22,638	3,234	40,758.6	23,256.6	154.6	40,455.6	41,061.5	137,700
3	8,963	2,988	41,411.5	23,807.9	251.5	40,918.5	41,904.4	117,500
4	21,951	1,996	51,269.4	21,953.8	148.2	50,978.9	51,559.8	113,300
<b>Total</b>	<b>61,196</b>	<b>2,550</b>	<b>45,087.8</b>	<b>23,516.9</b>	<b>95.1</b>	<b>44,901.4</b>	<b>45,274.1</b>	<b>137,700</b>

**TABLE 4.15 Group Two Descriptive Statistics**

Peak	N	Avg. Vol.	Mean	Std. Dev.	Std. Error	95% C. I. Bounds		Max.
						Lower	Upper	
1	18,968	6,323	44,238.5	23,806.2	172.9	43,899.7	44,577.3	139,600
2	57,711	8,244	41,367.7	22,531.9	93.8	41,183.9	41,551.5	137,700
3	23,259	7,753	42,484.4	23,395.0	153.4	42,183.8	42,785.1	117,500
4	61,958	5,633	51,502.6	20,791.6	83.5	51,338.9	51,666.3	126,700
<b>Total</b>	<b>161,896</b>	<b>6,746</b>	<b>45,743.1</b>	<b>22,643.9</b>	<b>56.3</b>	<b>45,632.8</b>	<b>45,853.5</b>	<b>139,600</b>

It can be seen from these tables that the overall descriptive statistics between group one and group two are very similar. In the mean total weight, for instance, the mean weights for each of the peak periods vary by as little as 229.4 pounds for AM peak (Peak 1) to a high of 1,072.9 pounds for PM peak (Peak 3). The average hourly volume also provides interesting results with the midday peak (Peak 2) providing the highest average hourly volumes for both group one and group two, followed closely by the PM peak (Peak 3) and then the AM peak (Peak 1). The night peak (Peak 4) volumes are considerably less (38.3 percent less for group one and 31.7 percent less for group two).

To determine whether or not both groups should be considered for analysis, a  $t$ -test was conducted on the means to determine if the difference in means of the two alternatives is significant. This analysis was considered for two different alternatives. The first alternative assumes that the variances are equal, while the second alternative assumes that the variances are not necessarily equal. The data collected and being analyzed for this analysis were considered to be a small sample of the data for all vehicles on the highway during the year. As a result, the population variances are not known and are not necessarily equal. As a result, the analysis in which the variances are unknown and not necessarily equal was conducted to determine if the means are, in fact, different. The null hypothesis tested in this analysis is outlined in Equation 4.5, while the alternative hypothesis is outlined in Equation 4.6 (136).

$$H_0 : \mu_1 - \mu_2 = 0 \quad \text{or} \quad \mu_1 = \mu_2 \quad (4.5)$$

$$H_a : \mu_1 - \mu_2 \neq 0 \quad \text{or} \quad \mu_1 \neq \mu_2 \quad (4.6)$$

The test statistic utilized for this analysis is provided in Equation 4.7 and is distributed approximately as a  $t$ -distribution with degrees of freedom calculated according to Equation 4.8 (136).

$$t_0^* = \frac{\bar{x}_1 - \bar{x}_2 - 0}{\sqrt{\frac{s_1^2}{n_1} + \frac{s_2^2}{n_2}}} \quad (4.7)$$

$$v = \frac{\left( \frac{s_1^2}{n_1} + \frac{s_2^2}{n_2} \right)^2}{\frac{(s_1^2/n_1)^2}{n_1 + 1} + \frac{(s_2^2/n_2)^2}{n_2 + 1}} - 2 \quad (4.8)$$

where:  $t_0^*$  = *t*-test statistic;  
 $\bar{x}_i$  = sample mean;  
 $s_i^2$  = sample variance;  
 $n_i$  = sample size; and  
 $v$  = degrees of freedom.

The results of this analysis are summarized in Table 4.16 for each of the peak periods individually, as well as the combination of all peak periods of data. The analysis compares the difference in the means for the two groups for the peak periods identified. As is apparent from this table, the results are somewhat mixed when determining whether or not the means between the two groups are equal. There are some combinations that, even with the very large sample size, show that the mean differences are not significant (accept  $H_0$ ), indicating that the means are the same.

**TABLE 4.16 Group One versus Group Two *t*-test Equality of Means**

Peak	$v$	$t_0^*$	Significance	Test Result <sup>1</sup>
1	13,808	0.699	0.485	Accept $H_0 (\mu_1 = \mu_2)$
2	40,236	-3.369	0.001	Reject $H_0 (\mu_1 \neq \mu_2)$
3	16,018	-3.643	0.000	Reject $H_0 (\mu_1 \neq \mu_2)$
4	36,800	-1.371	0.170	Accept $H_0 (\mu_1 = \mu_2)$
<b>Combined</b>	<b>106,651</b>	<b>-5.933</b>	<b>0.000</b>	<b>Reject <math>H_0 (\mu_1 \neq \mu_2)</math></b>

<sup>1</sup>Analysis was conducted at the 0.05 (95 percent) confidence level

Considering these results and the extremely large sample size that is tested in this analysis, the final step in determining whether to include both groups fell into a comparison of numbers. As outlined previously, the mean GVW between the two groups is very similar. The mean GVW of group one, as outlined previously in Table 4.14, is approximately 45,100 pounds.

The mean GVW of group two, as outlined previously in Table 4.15, is 45,750 pounds. These two values, although shown to be statistically significant, are within 650 pounds (1.4 percent). When considering the measurement technique used to collect these data, the acceptable error associated with this technique, and the physical implications of an additional 650 pounds on a CMV, it was determined that the two groups may, in fact, be comparable from a practical perspective. As a result, the data for group two were considered for utilization in the analysis since the results are expected to be very similar for either group one or group two analyses. These data (group two) will be utilized as the final dataset for developing classification groups and distributions of the vehicle size and weight.

#### *4.1.5 Analysis of Vehicle Classification*

The final step in the PCA analysis of the data was an analysis of CMV weight and spacing distributions based on FHWA classifications. The purpose for grouping the data according to FHWA classification was to reduce the complexity of the data in one further step for ease in analysis of data. The final dataset outlined in the previous section includes data from FHWA Classes 3 through 12. These classifications are fixed in their descriptions and analysis; therefore, the actual classification scheme itself has not been considered for revision. Instead, the classifications have been considered for grouping to ease in analysis. Following the trends developed and the analysis that has been performed to group the data, three primary statistical tools were utilized for this analysis: 1) box-plots; 2) one-way ANOVA; and 3) pairwise comparisons. More detail on each of these topics will be provided in the following subsections.

**4.1.5.1 Box-Plot Analysis** The box-plot was used in previous analyses to display the relationships between total weight and peak period, as well as to illustrate relationships between groups one and two. The same methodology has been utilized to develop box-plots for FHWA classification analysis (134, 136). The results of the box-plot analysis for all vehicles in the final dataset are shown in Figure 4.11. A comparison of the aggregate and disaggregate peak period analyses indicated that the results for each of the disaggregate peak periods were very consistent with the aggregate dataset. As a result, the relationships outlined in this figure were considered sufficient to represent all peak period alternatives.

It can be seen from this figure that the median of the data is rather inconsistent for several of the FHWA classifications, particularly when comparing the lower classifications

(FHWA Classes 4 through 8) with the higher classifications (FHWA Classes 9 through 12). To further identify and classify these trends, an error bar chart and one-way ANOVA analysis were completed for the full dataset, as well as each individual peak period, to determine the potential relationships that exist within the data.

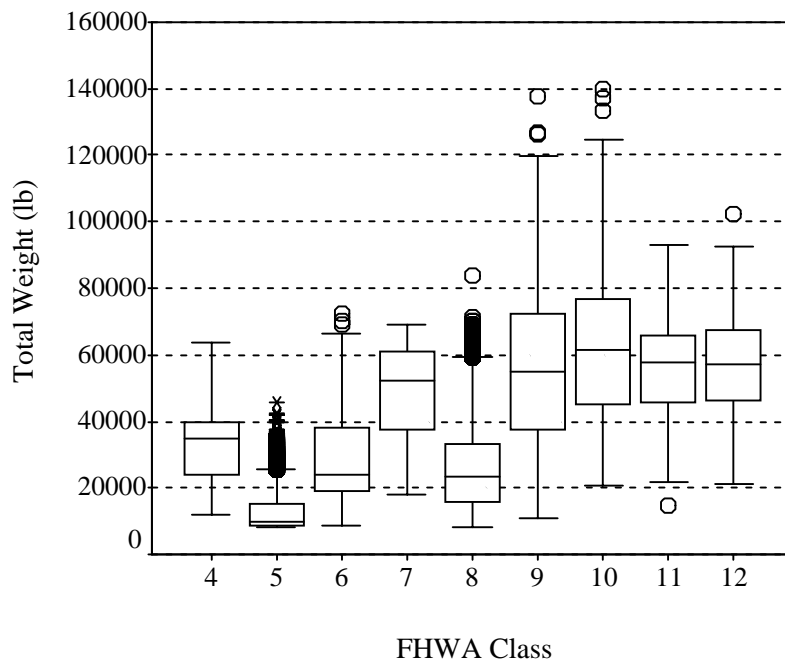


**FIGURE 4.11** Vehicle classification analysis box-plot results

**4.1.5.2 One-Way ANOVA** As previously discussed, the purpose of one-way ANOVA is to test the hypothesis that a difference between means of more than two factors comes from populations with equal means (134, 137). In this analysis, the test is set up to determine whether or not the mean values for total weight for more than two different FHWA classifications are in fact equal. The null hypothesis ( $H_0$ ) for this test was identified previously and assumes that all mean values are equal, while the alternative hypothesis ( $H_a$ ) indicates that not all mean values are equal.

The results of the one-way ANOVA for each of the alternatives clearly indicated that the mean total weight is not equal across all groups. The one-way ANOVA  $F$  statistic for the analysis ranged from 3,089 to 20,507, indicating a very large difference in the mean values and a subsequent rejection of the null hypothesis at high significance levels.

In addition to the one-way ANOVA results, an error bar chart was also developed for the analysis to graphically identify the difference in the means. The result of an error bar chart for the final dataset is provided in Figure 4.12, clearly identifying the differences in the means. Based on the results of the error bar chart, the mean values appear to fall into three main groups: 1) FHWA Class 5; 2) FHWA Classes 4, 6, and 8; and 3) FHWA Classes 7, 9, 10, 11, and 12.

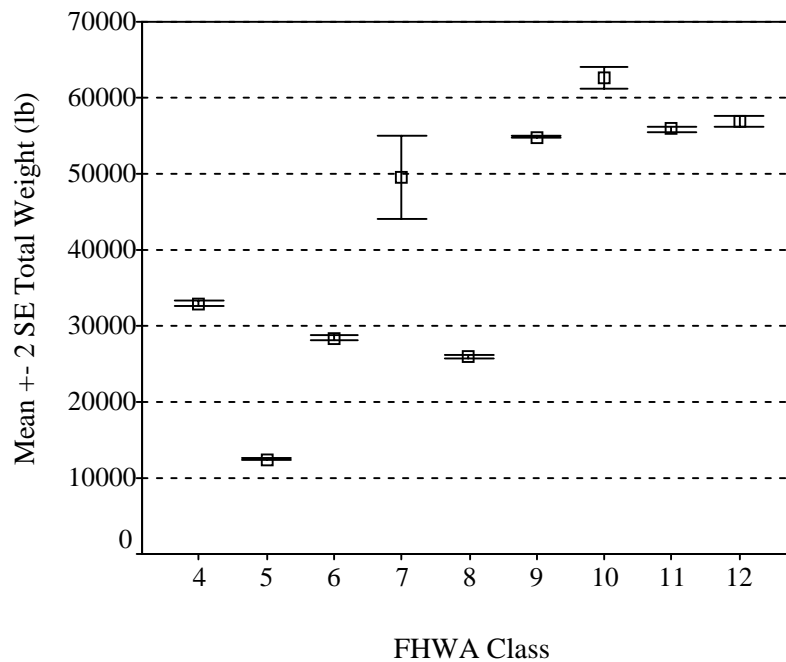


**FIGURE 4.12 Vehicle classification analysis error bar chart**

**4.1.5.3 Pairwise Comparison** As with previous analyses, the next step was to determine statistically which of the means was different. This was again determined based on the results of the Bonferroni pairwise comparison test. The results of this analysis are summarized in Table 4.17 for the full final dataset, in Table 4.18 for the AM peak, Table 4.19 for the midday peak, Table 4.20 for PM peak, and Table 4.21 for the night peak analysis. As with previous group comparison tables, a shaded block identifies the peak period where the difference between the mean average weight is not significant, thus indicating the potential to group the two classifications together.

**TABLE 4.17 Vehicle Classification Analysis Pairwise Comparison—Full Final Dataset**

		FHWA Classification								
		4	5	6	7	8	9	10	11	12
FHWA Classification	4									
	5									
	6									
	7									
	8									
	9									
	10									
	11									
	12									

Note: Shaded squares denote differences between mean average weights are not significant

**TABLE 4.18 Vehicle Classification Analysis Pairwise Comparison—AM Peak**

		FHWA Classification								
		4	5	6	7	8	9	10	11	12
FHWA Classification	4									
	5									
	6									
	7									
	8									
	9									
	10									
	11									
	12									

Note: Shaded squares denote differences between mean average weights are not significant

**TABLE 4.19 Vehicle Classification Analysis Pairwise Comparison—Midday Peak**

		FHWA Classification								
		4	5	6	7	8	9	10	11	12
FHWA Classification	4									
	5									
	6									
	7									
	8									
	9									
	10									
	11									
	12									

Note: Shaded squares denote differences between mean average weights are not significant

**TABLE 4.20 Vehicle Classification Analysis Pairwise Comparison—PM Peak**

		FHWA Classification								
		4	5	6	7	8	9	10	11	12
FHWA Classification	4									
	5									
	6									
	7									
	8									
	9									
	10									
	11									
	12									

Note: Shaded squares denote differences between mean average weights are not significant

**TABLE 4.21 Vehicle Classification Analysis Pairwise Comparison—Night Peak**

		FHWA Classification <sup>1</sup>							
		4	5	6	8	9	10	11	12
FHWA Classification <sup>1</sup>	4								
	5								
	6								
	8								
	9								
	10								
	11								
	12								

<sup>1</sup> Only one case exists for FHWA Class 7; therefore it was not included in the pairwise analysis  
 Note: Shaded squares denote differences between mean average weights are not significant

It can be seen from these tables that although there are several vehicle classification pairwise comparisons in which significance relationships do exist, the results are somewhat inconsistent, particularly across the different peak periods and when compared to the error bar chart results. For the full final dataset analysis, relationships are limited to FHWA Classes 7, 11, and 12, as well as between FHWA Classes 7 and 9. Relationships also exist in the full final dataset for FHWA Classes 4, 6, and 8, but not necessarily between FHWA Classes 6 and 8. For the AM peak analysis, relationships exist between FHWA Classes 4, 6, and 8, as well as FHWA Classes 7, 10, and 12. Relationships also exist between FHWA Classes 7, 9, 10, 11, and 12, but

not necessarily between FHWA Classes 9 and 10, or FHWA Classes 10 and 11. Similar relationships can be found in any of the peak period analyses.

The relationships developed as a result of the box-plot, one-way ANOVA, and pairwise comparisons provide a strong base to begin to develop CMV weight and length distributions as a function of vehicle classification. These results can be built upon, however, using a more advanced statistical tool known as recursive partitioning. The results of this analysis will be presented in the next subsection of this report.

## **4.2 Recursive Partitioning**

The recursive partitioning analysis of the WIM data application included an exhaustive search to identify relationships between each of the variables within the dataset and the classification of the vehicles. This search included an analysis of FHWA classification and TxDOT classification as the predictor variables, with different analyses conducted on the target variables. The following variables were considered as target variables in the analysis:

- total weight (lb),
- axle A weight (lb),
- axle B weight (lb),
- axle C weight (lb),
- axle D weight (lb),
- axle E weight (lb),
- axle F weight (lb),
- axle G weight (lb),
- axle H weight (lb),
- total spacing (ft),
- axles A to B spacing (ft),
- axles B to C spacing (ft),
- axles C to D spacing (ft),
- axles D to E spacing (ft),
- axles E to F spacing (ft),
- axles F to G spacing (ft), and
- axles G to H spacing (ft).

The results of this search produced similar results with the variable “total weight (lb)” providing what was determined to be the most representative results for all scenarios. Consequently, this variable was utilized to determine the final classification groupings. The primary goal of this analysis was to determine the relationship that exists between the FHWA (or Texas 6) classification and the weight distribution of the vehicles. The final product of this section is a distribution of CMVs that can be utilized to estimate weight and length distributions at AVC sites with representative weight, length, and vehicle classification information that can be used in critical design tasks, TMG truck weight groupings, and in microscopic traffic simulation analyses of CMVs. To accomplish this task, this section has been divided into three subsections. The first subsection provides an analysis of the final dataset from the previous section using the recursive partitioning tool CART, while the second and third subsections provides a summary of the results for the FHWA and Texas 6 classifications, respectively.

#### *4.2.1 Dataset Analysis*

The recursive partitioning dataset analysis built upon the final dataset results of the PCA analysis presented in the previous section for the full dataset and for each of the peak periods (AM peak, midday peak, PM peak, and night peak). For the first analysis iteration, the default CART setting was used to determine the best tree, where the default setting is the minimum cost tree regardless of tree size, or the tree that is most accurate given the specified testing method (141). The results of this analysis indicated that anywhere from five trees (AM peak) to nine trees (full data) were necessary to accommodate the data. When analyzing the relative errors of these trees, however, the change in relative error from a three node tree to a full tree was very insignificant, as illustrated in Figure 4.13 for the full dataset alternative. It can be seen from this figure that the relative error is nearly flat from a three terminal node tree to a nine terminal node tree, and that the absolute difference from a two terminal node tree to a nine terminal node tree is also very insignificant, changing by only 6 percent from the two terminal node to the nine terminal node tree.

Consequently, the analysis was modified such that the final tree would be selected to be within one standard error of the minimum cost tree. This analysis identified final trees that ranged between three, four, and five terminal nodes, with relative error (RE) as outlined in Table 4.22.

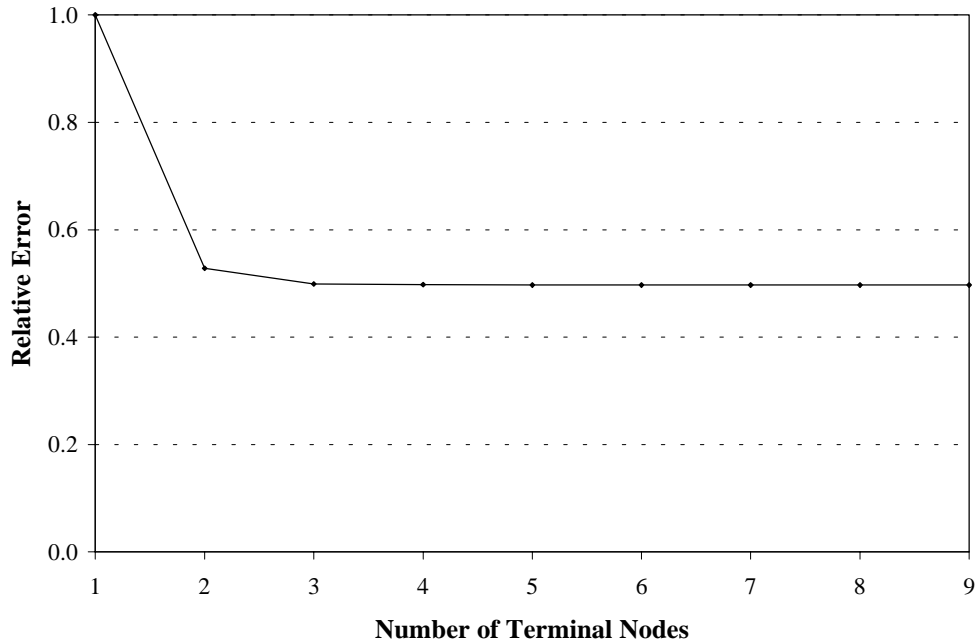


**FIGURE 4.13** Full dataset relative error results

**TABLE 4.22** CART Analysis Results—1 S.E. of Minimum Cost Tree

Dataset	# Terminal Nodes	Relative Error
Full	4	0.498
AM Peak	3	0.435
Midday Peak	5	0.505
PM Peak	3	0.448
Night Peak	3	0.569

Based on the results of the analysis for the different datasets; three, four, and five terminal node alternatives were analyzed to determine which should be used in the final distribution. This process included comparison of the mean and standard deviation for the different terminal node alternatives as well as a comparison of the box-plots for each alternative to easily identify the relationships between the data and to determine the need for additional groupings. A summary of the results of the full dataset tree analysis for the three, four, and five terminal node alternatives is provided in Figure 4.14, Figure 4.15, and Figure 4.16, respectively. Similar results were also identified for each of the peak period datasets and subsequently have not been included in this section of the analysis but will be referenced in the next subsection.

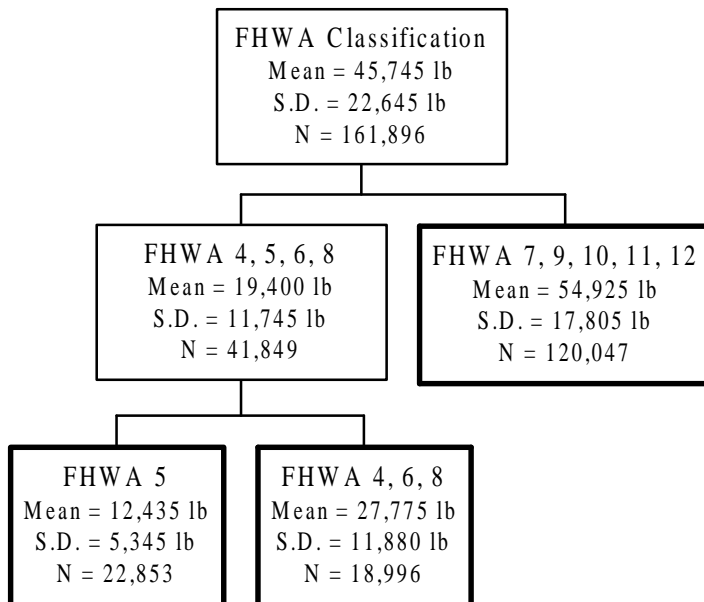


**FIGURE 4.14 Full dataset three terminal node tree results**

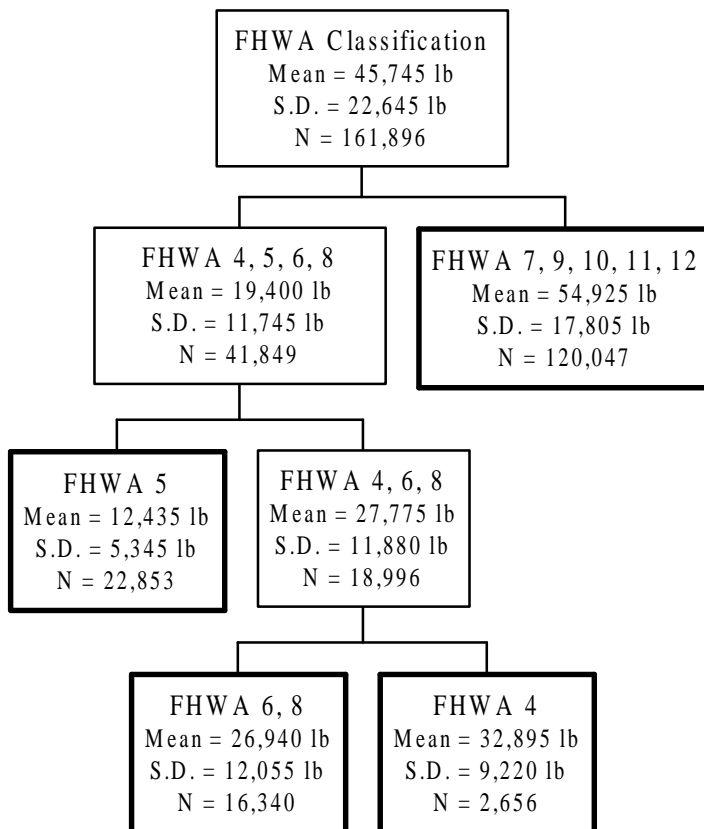


**FIGURE 4.15 Full dataset four terminal node tree results**

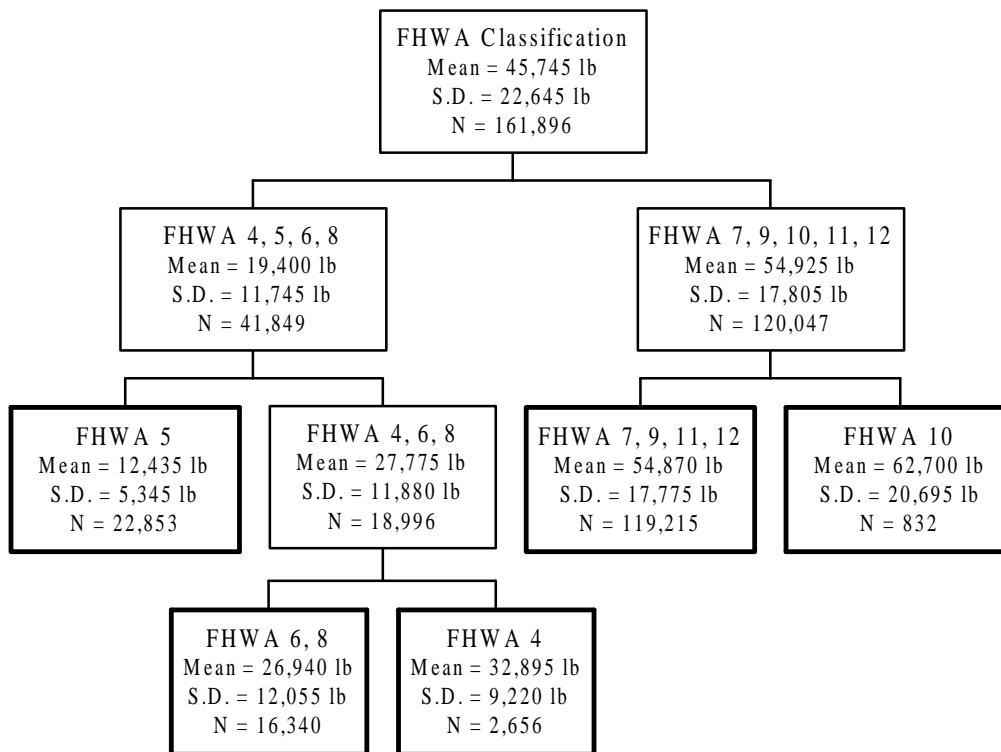


**FIGURE 4.16 Full dataset five terminal node tree results**

The statistics outlined in the tree results do not show a large fluctuation in the mean and standard deviation of the groupings beyond the three terminal node results. In the four terminal node results, for example, FHWA Classes 4, 6, and 8 are split to create a category for FHWA Class 4 and a separate category for FHWA Classes 6 and 8. The mean total weight for the initial category is 27,775 pounds, and the two new categories have mean total weights of 32,895 pounds (18 percent increase) and 26,940 pounds (3 percent decrease). In the five terminal node tree, FHWA Classes 7, 9, 10, 11, and 12 are split to form two new categories. The first splits out FHWA Classes 7, 9, 11, and 12 with a 0.1 percent decrease in mean total weight, and FHWA Class 10 with a 14 percent increase in total weight.

In addition to the actual number analysis, box-plots for each of the different terminal node alternatives (three, four and five) for the full dataset are provided in Figure 4.17, Figure 4.18, and Figure 4.19. The box-plots show very consistent breaks between the groups in the three terminal node alternative, while the four and five terminal node box-plot results show overlap between nodes, indicating the potential to combine categories in an effort to eliminate the overlap between alternatives.

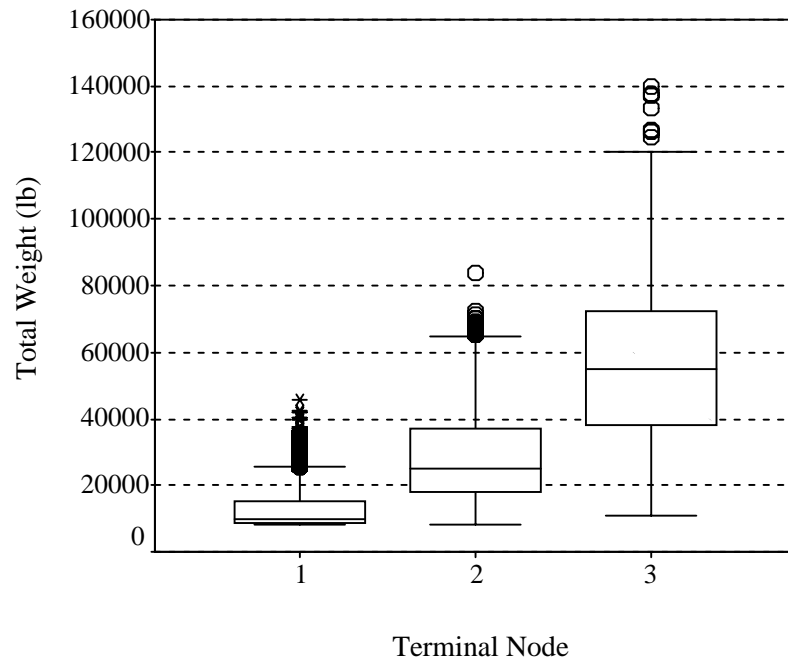


**FIGURE 4.17** Full dataset three terminal node box-plot results

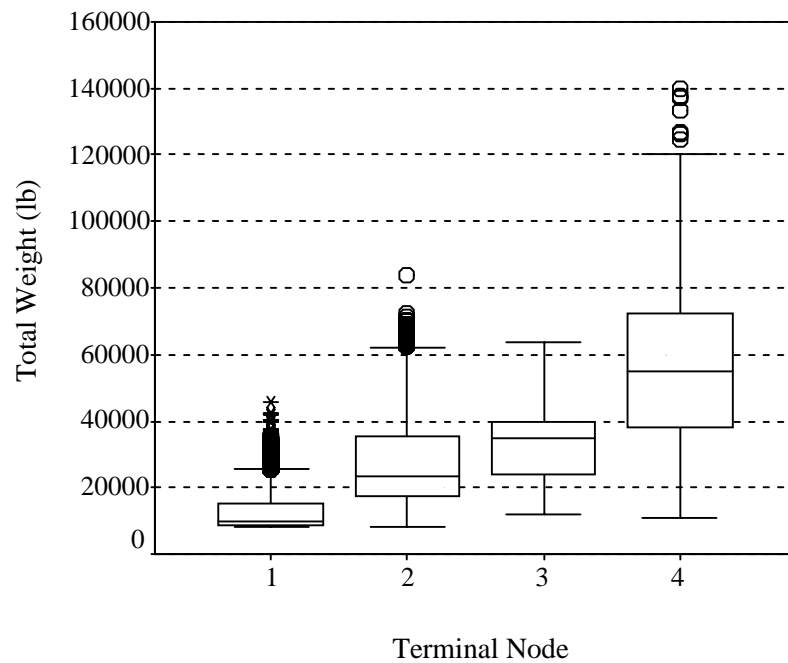


**FIGURE 4.18** Full dataset four terminal node box-plot results

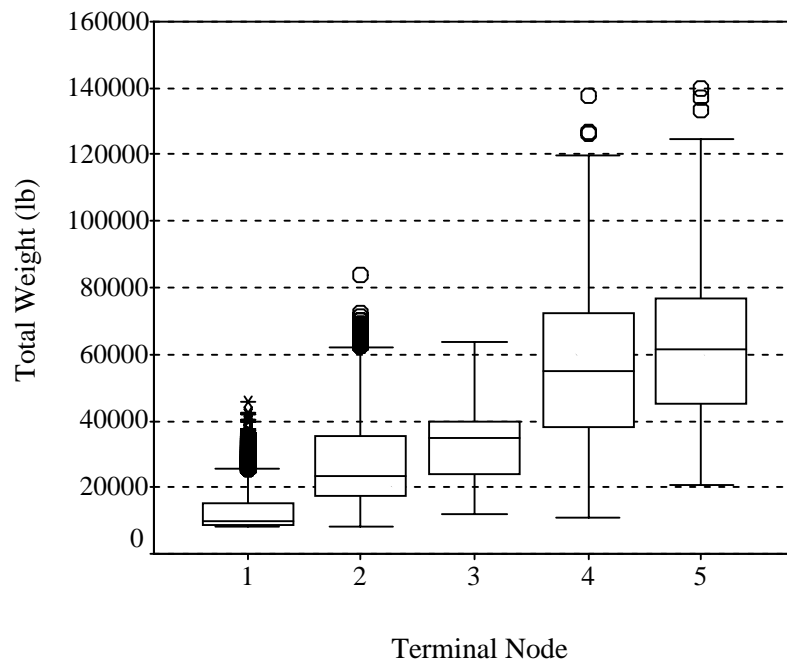


**FIGURE 4.19 Full dataset five terminal node box-plot results**

The final metric used to compare the three alternatives, therefore, was to compare the relative error of the alternatives, where relative error is defined in CART as a “measure of accuracy” (85), in the prediction of the groups. Table 4.23 compares the relative error results for the three terminal node alternative and a full tree. As can be seen clearly from these results, the accuracy that existed in the three terminal node tree was very comparable to a full nine terminal node tree, which would break out each of the FHWA classifications separately. This table also identifies the percent difference between the three terminal node relative error and the nine terminal node relative error as less than 1 percent for all scenarios.

**TABLE 4.23 Relative Error Comparison—Three Node versus Full Tree**

Dataset	Relative Error Results		% Difference
	Three Node Tree	Full Tree	
Full	0.498	0.497	0.20
AM Peak	0.435	0.434	0.23
Midday Peak	0.509	0.504	0.98
PM Peak	0.448	0.445	0.67
Night Peak	0.569	0.568	0.18

#### 4.2.2 Final Results—FHWA Classification

It is clear from the analysis presented in the previous section that a three terminal node tree is sufficient to accommodate the variability of the data and to account for the accuracy of the data based on box-plots, mean of the data, standard deviation of the data, and the relative error metric. The final distribution, therefore, is a distribution that includes data for the full dataset (entire day), for the four different time periods (AM peak, midday peak, PM peak, and night peak), and for three different classification groups, as summarized in Table 4.24 for the FHWA classification groupings. In addition to summarizing the FHWA classifications included in each of the three groups, this table includes the percentage of vehicles that fall within each of these groups for the full day as well as each of the four different time periods. As is apparent from this table, this percentage varies only slightly from peak period to peak period, with the exception of the night peak where Group C clearly dominates.

**TABLE 4.24 FHWA Classification Groupings**

Group	FHWA Classification	% of Total Volume by Peak Period				
		Full Day	AM	Midday	PM	Night
A	5	14%	19%	17%	19%	8%
B	4, 6, 8	12%	13%	14%	12%	9%
C	7, 9, 10, 11, 12	74%	68%	69%	69%	83%

The results of the full analysis (all peak periods) final distributions for each axle weight and spacing are summarized in Table 4.25 for the full analysis, Table 4.26 for Group A, Table 4.27 for Group B, and Table 4.28 for Group C. It was found in analyzing the data that the results were similar for all peak periods; therefore, only the full analysis results are presented in this section, while the aggregate results for all peak periods are provided in Appendix C. A summary of the results are as follows: 1) Group A (light trucks) had an average total weight of approximately 12,500 pounds for all scenarios; 2) Group B (medium trucks) had an average total weight of approximately 28,000 pounds for all scenarios; and 3) Group C (heavy trucks) had an average total weight of approximately 55,000 pounds for all scenarios.

**TABLE 4.25 Full Analysis Final Distributions**

	<b>N</b>	<b>Minimum</b>	<b>Maximum</b>	<b>Mean</b>	<b>Std. Dev.</b>
Total Weight (lb)	161,896	8,000	139,600	45,743.14	22,643.88
Axle A Weight (lb)	161,896	1,600	27,700	9,582.06	2,441.76
Axle B Weight (lb)	161,896	1,100	32,800	10,793.33	4,569.60
Axle C Weight (lb)	138,341	600	29,100	10,679.35	4,378.40
Axle D Weight (lb)	128,233	700	30,500	10,334.35	4,879.68
Axle E Weight (lb)	120,022	800	36,100	10,679.56	4,905.82
Axle F Weight (lb)	2,526	700	25,300	8,668.45	3,996.17
Axle G Weight (lb)	3	13,300	17,000	14,833.33	1,929.59
Axle H Weight (lb)	3	12,600	16,700	15,033.33	2,154.84
Total Spacing (ft)	161,896	11.0	98.5	49.25	17.21
Axles A to B Spacing (ft)	161,896	10.0	38.3	16.26	2.91
Axles B to C Spacing (ft)	138,341	2.3	45.0	6.18	6.04
Axles C to D Spacing (ft)	128,233	2.1	45.8	29.66	8.35
Axles D to E Spacing (ft)	120,022	2.0	41.0	5.33	3.80
Axles E to F Spacing (ft)	2,526	3.4	25.5	16.32	8.29
Axles F to G Spacing (ft)	3	14.5	30.9	19.97	9.47
Axles G to H Spacing (ft)	3	4.0	4.7	4.47	0.40

**TABLE 4.26 Group A Final Distributions—Full Analysis**

	<b>N</b>	<b>Minimum</b>	<b>Maximum</b>	<b>Mean</b>	<b>Std. Dev.</b>
Total Weight (lb)	22,853	8,000	45,800	12,435.47	5,345.00
Axle A Weight (lb)	22,853	2,500	17,400	5,467.63	1,823.80
Axle B Weight (lb)	22,853	1,400	32,800	6,967.83	3,882.59
Total Spacing (ft)	22,853	11.0	23.6	14.78	3.10
Axles A to B Spacing (ft)	22,853	11.0	23.6	14.78	3.10

**TABLE 4.27 Group B Final Distributions—Full Analysis**

	<b>N</b>	<b>Minimum</b>	<b>Maximum</b>	<b>Mean</b>	<b>Std. Dev.</b>
Total Weight (lb)	18,996	8,000	83,900	27,774.32	11,879.96
Axle A Weight (lb)	18,996	2,000	24,800	8,705.91	3,162.53
Axle B Weight (lb)	18,996	1,300	31,900	9,874.43	5,300.55
Axle C Weight (lb)	18,294	600	29,100	7,010.42	4,291.24
Axle D Weight (lb)	8,186	800	28,200	5,668.21	3,615.93
Total Spacing (ft)	18,996	13.3	68.2	32.96	11.81
Axles A to B Spacing (ft)	18,996	10.0	38.3	16.57	4.23
Axles B to C Spacing (ft)	18,294	2.3	45.0	13.13	11.34
Axles C to D Spacing (ft)	8,186	2.1	44.1	8.69	10.30

**TABLE 4.28 Group C Final Distributions—Full Analysis**

	<b>N</b>	<b>Minimum</b>	<b>Maximum</b>	<b>Mean</b>	<b>Std. Dev.</b>
Total Weight (lb)	120,047	10,900	139,600	54,927.18	17,806.96
Axle A Weight (lb)	120,047	1,600	27,700	10,503.95	1,277.07
Axle B Weight (lb)	120,047	1,100	32,500	11,666.98	4,142.77
Axle C Weight (lb)	120,047	800	29,100	11,238.45	4,113.60
Axle D Weight (lb)	120,047	700	30,500	10,652.53	4,791.40
Axle E Weight (lb)	120,022	800	36,100	10,679.56	4,905.82
Axle F Weight (lb)	2,526	700	25,300	8,668.45	3,996.17
Axle G Weight (lb)	3	13,300	17,000	14,833.33	1,929.59
Axle H Weight (lb)	3	12,600	16,700	15,033.33	2,154.84
Total Spacing (ft)	120,047	22.1	98.5	58.39	4.86
Axles A to B Spacing (ft)	120,047	10.0	24.9	16.49	2.51
Axles B to C Spacing (ft)	120,047	2.8	39.6	5.13	3.74
Axles C to D Spacing (ft)	120,047	2.3	45.8	31.09	5.94
Axles D to E Spacing (ft)	120,022	2.0	41.0	5.33	3.80
Axles E to F Spacing (ft)	2,526	3.4	25.5	16.32	8.29
Axles F to G Spacing (ft)	3	14.5	30.9	19.97	9.47
Axles G to H Spacing (ft)	3	4.0	4.7	4.47	0.40

#### 4.2.3 Final Results—Texas 6 Classification

The final analysis that was completed was an analysis of the Texas 6 classification using the same process outlined for the FHWA classification. The final classification grouping results for this analysis are summarized in Table 4.29. The results of the distribution analysis for the Texas 6 classification are identical to the FHWA classification results. The three groups of vehicles identified for final distribution are identical (adjusted for the different classification schemes); thus the statistics presented in the previous section are the same as well.

**TABLE 4.29 Texas 6 Classification Groupings**

<b>Group</b>	<b>TxDOT Classification</b>
A	4
B	3, 5, 7, 8
C	6, 9, 10, 11, 12

A final representation of the mean GVW for the full analysis and for each peak period analyzed is presented in Figure 4.20. The results shown here identify the trends in the data by GVW and peak period.

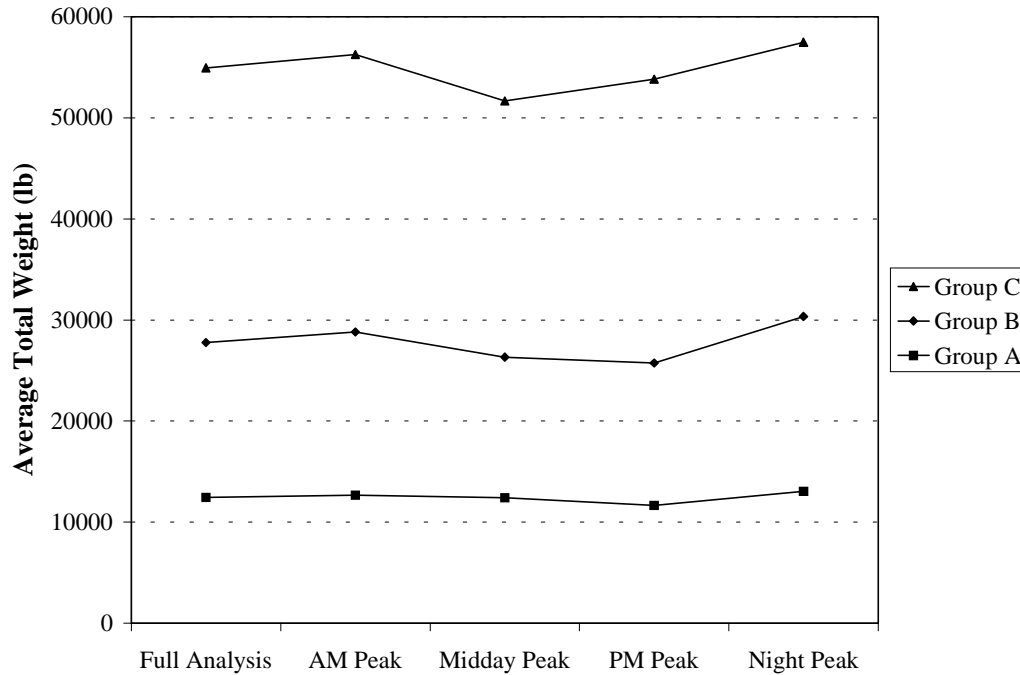


**FIGURE 4.20 Final distribution results**

### 4.3 Concluding Remarks

This section utilized several statistical tools to reduce the dimensionality of the multivariate WIM dataset and to transform this dataset into a distribution of vehicle size and weight that can be utilized for analysis. The tools utilized included primarily PCA and the recursive partitioning tool CART. Additional tools such as one-way ANOVA, box-plots, pairwise comparisons, and *t*-tests were also very useful as relationships between variables were explored. The final results of this section provide a distribution of vehicle weight and length for the FHWA and Texas 6 classification groupings for a full day and are disaggregated by peak period.

The preliminary analysis of the dataset resulted in several modifications to the data, including: 1) truncation of the dataset to include only vehicles with GVW of 8,000 pounds or greater; 2) truncation of the dataset to remove vehicles with a total length less than 11 feet and/or total spacing between the first two axles less than 10 feet; and 3) removal of all Class 13 data. The data were then analyzed to identify additional anomalies in the data, to group the data spatially according to data collection locations, and to group the data temporally by peak travel periods. The results of the spatial analysis provided the basis for elimination of four of the nine

WIM data collection sites based on the results of the statistical analysis of vehicle size and weight characteristics, while the results of the temporal analysis identified four primary peak periods for further analysis including: 1) AM peak; 2) midday peak; 3) PM peak; and 4) night peak. The resulting dataset maintained approximately 77 percent of the raw dataset, eliminating anomalies in the data and providing a dataset of vehicle size and weight for further analysis.

The final step in the analysis was the development of distributions in vehicle size and weight based on FHWA and Texas 6 classifications. The purpose for grouping the data according to classification was to: 1) further reduce the complexity of the multivariate dataset for ease in analysis of the data; 2) provide an alternative for weight groupings identified in the TMG; 3) accommodate further analysis in microscopic traffic simulation models such as CORSIM; and 4) identify the relationships between vehicle classification and weight data to use in estimating weight and length distributions at AVC sites.

Two primary methodologies were utilized to group the data according to classifications. The first utilized methods from the previous analysis (i.e., one-way ANOVA, box-plots, pairwise comparisons) to provide a base for comparison. In addition, a more robust data mining methodology was utilized to expand these relationships. CART was used to group the data according to the minimum variance between the data groupings. The CART analysis identified three primary groupings of the data according to total weight, as well as weight of individual axles, and vehicle length (weight and length). The groupings of the vehicles were completed for each of the four peak periods, with vehicle size and weight distributions developed for each of these alternatives. The final weight groupings can be summarized as follows: 1) light trucks (average total weight approximately 12,500 pounds); 2) medium trucks (average total weight approximately 28,000 pounds); and 3) heavy trucks (average total weight approximately 55,000 pounds).

It can be concluded from this section that statistical tools are readily available to reduce the dimensionality of multivariate datasets to aid in a variety of applications. The application utilized in this analysis was the reduction of vehicle size and weight characteristics into classifications that can be utilized for further analyses, such as in TMG truck weight groupings and in microscopic traffic simulation analyses of CMVs. The methodology outlined in this section has proven to be successful in reducing the dataset and can be applied to similar applications for ease in analysis of large multivariate datasets.

## 5. CMV MICROSCOPIC TRAFFIC SIMULATION

Microscopic traffic simulation research has begun to capitalize on the maturation of digital computing technology, particularly during the last decade. Substantial progress has been made to improve the models, while methods to simulate accurately and precisely individual elements of the transportation system have also improved. Several concepts still remain to be explored to more accurately and precisely model existing transportation systems, including: 1) parameter calibration; 2) analysis of vehicle operating characteristics (i.e., acceleration, deceleration); and 3) calibration and analysis of fleet distribution.

The purpose of this section is to discuss the parameters available in microscopic traffic simulation models to address the needs of both passenger cars and CMVs. To accomplish this purpose, this section has been divided into four main subsections. The first subsection provides a discussion of the calibration of microscopic traffic simulation models, including a proposed calibration methodology. The second outlines an application of the methodology using the microscopic traffic simulation model CORSIM applied to two specific test networks in Houston, Texas. The third identifies the calibration parameters available within the microscopic traffic simulation model, including a methodology to calibrate the parameters based on observed conditions, while the final subsection provides concluding remarks for the analysis.

### 5.1 Calibration of Microscopic Traffic Simulation Models

Sections 1.1.3 and 2.5.4 identified model calibration as a key component in developing a successful microscopic traffic simulation model. Model calibration was defined in this discussion as the process in which the model parameters are adjusted, such that the model accurately reflects specific components of the system being modeled. Model calibration is essential to accurately portray existing conditions through the proper replication of both supply and demand characteristics, as well as their interactions.

One aspect of microscopic traffic simulation model calibration that has not historically been included in calibration methodologies is the vehicular composition of the traffic stream and the ability of the model to accurately represent the characteristics of each vehicle type. This can be particularly critical in areas where a high percentage of truck traffic exists on a given interstate or arterial roadway (i.e., NAFTA corridors). Research efforts to date appear to have focused primarily on the calibration and subsequent simulation of automobile traffic, rather than

attempting to focus on a mixture of vehicle types. Particularly in the area of calibration of microscopic traffic simulation models, researchers and analysts have generally treated all vehicles equally and with equal distributions or, more common yet, have relied on default parameters in the model, rather than calibrating the operating characteristics and distributions based on actual conditions.

It has been theorized that one of the reasons for the tendency to exclude calibration by vehicle type could be related to the paucity of available data necessary to perform this calibration. These data includes: 1) an OD estimate for the CMVs that is generally assumed to be different than that of automobile traffic, although it is rarely treated this way; 2) reliable information on the operating characteristics of the CMV (i.e., acceleration, deceleration, power) because of their effect on capacity, speed, and other operating criteria; and 3) data on the weight characteristics of the CMVs in the traffic stream. The weight characteristics are related to the operating characteristics (i.e., heavier vehicles have slower acceleration), yet they are separate in terms of infrastructure impacts, including primarily the impacts to bridges and pavements as a result of the load factors and their respective equivalent single-axle load (ESAL) characteristics (24, 25).

A conceptualization of a proposed calibration methodology adapted from research performed by Rilett and Kim (142) to include the effects of CMVs in microscopic traffic simulation models is outlined in Figure 5.1. This figure outlines seven specific steps for calibration. First, the methodology identifies the input to the calibration process as two primary steps: 1) supply input (step 1) and 2) demand input (step 2). The supply input includes the links, nodes, and traffic control systems that will be explained in more detail in later sections, while the demand input includes the point-to-point trip movements as represented by an OD trip matrix and corresponding network volumes. In addition, a vehicle-specific OD trip matrix, as well as vehicle characteristics such as length, weight, classification, and operating characteristics, should also be included as part of both the supply and demand input. These characteristics are critical to accurately model an existing or proposed facility.

Although the demand input is one of the most critical aspects of the microscopic traffic simulation model, these data are often difficult and costly to obtain. With the increase in ITS technology, however, these data have become more readily accessible for model input. As a result, the OD demands are generally estimated from ITS data (step 5), and are based on traffic information collected from the network. The ITS data would be, from among other sources,

WIM detectors, video imaging detection (VID) systems, AVC data, and AVI detector data for the network under consideration. These data are also utilized as input to step 6, optimization, in the proposed methodology. As a result, this estimation is endogenous to the simulation model because it is utilized in both the optimization step to compare model output and in the demand input step of the model.

The modeling of the interaction of the supply and demand for the model occurs in step 3, simulation. Some of the critical components to consider in the simulation model are the vehicle characteristics and the subsequent parameters associated with these characteristics, as outlined previously.

The results of the simulation model are generated in step 4, model output. The characteristics of the model that are output with the simulation include both spatial and temporal characteristics. The defining characteristics of the advanced simulation model are that while supply and demand are on the surface exogenous to the model, in reality these values are estimated within the model itself. For example, the capacity of any given link is a function of the physical infrastructure, the system operational characteristics, and the travel demand. The new models attempt to capture this reality by modeling the capacity as emergent from the model rather than estimating it *a priori*, which has often been the norm in the past.

Based on the results of a comparison between the simulation model output and the ITS data identified earlier, step 6, optimization, is conducted. In this step, new simulation parameters are chosen and used as input to the model to improve output. This calibration process continues in a loop as illustrated until the difference between the empirical and simulated results are within an “acceptable” range. More detailed information on an automated calibration methodology will be provided in Section 6. Once the optimization criterion has been satisfied, step 7, stopping criteria, is met and the model has been calibrated.

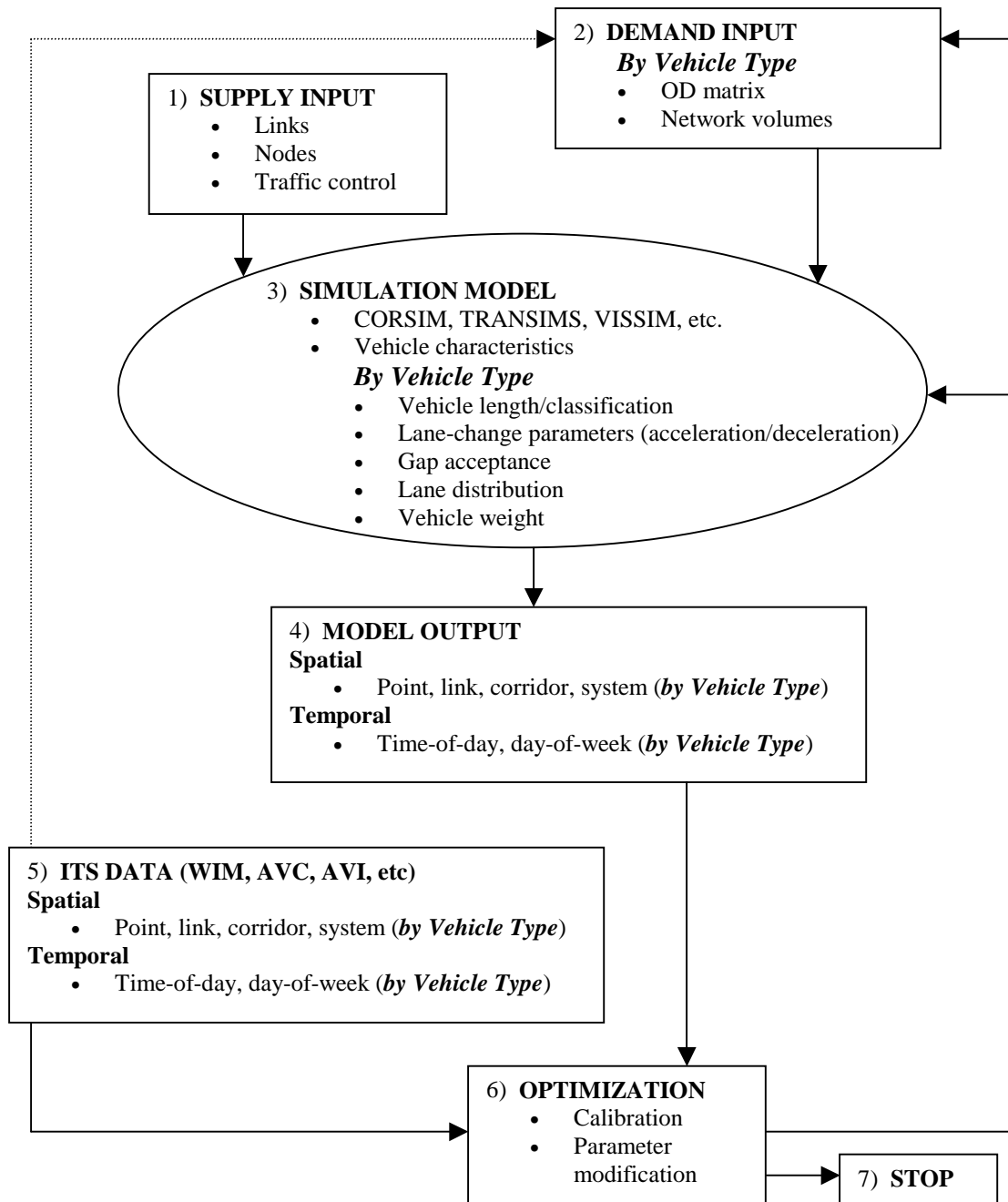


**FIGURE 5.1** Proposed calibration methodology

## 5.2 CORSIM Application of Proposed Methodology

To apply the concepts outlined in the previous section, an application of the proposed methodology is presented. CORSIM has been identified as the state of the practice microscopic traffic simulation model for modeling vehicles on both freeway and arterial networks. CORSIM simulates traffic utilizing some of the most commonly accepted vehicle and driver behavior models and combines two of the most widely used traffic simulation models, NETSIM for surface streets and FRESIM for freeway operations. The traffic simulation characteristics and analysis of CORSIM have been applied by thousands of practitioners and researchers worldwide over the past 30 years.

CORSIM has been identified as a medium scale, high fidelity model because it is designed primarily for analysis of freeway and arterial networks and is designed to represent the spatial interactions of drivers on a continuous, rather than a discrete, basis (26). CORSIM applies time-step simulation to describe traffic operations, where one time-step represents one second. Each vehicle is modeled as a distinct object that is moved every second, while each variable control device in the network is also updated every second for drivers to react. CORSIM is a stochastic model where random numbers are assigned to driver and vehicle characteristics as well as the decision-making processes. The stochastic and dynamic nature of the model allows more accurate representation of actual conditions for both freeway and arterial performance. The CORSIM model is operated in a Windows<sup>®</sup> environment through the use of the TSIS package (102). TSIS version 5.0 was utilized for the analysis in this dissertation. While the results of this application are specific to the CORSIM model, the methodologies applied are applicable to any microscopic traffic simulation model.

To provide background information on the CORSIM network, this section has been divided into two subsections. The first identifies the test network location and data sources, while the second outlines the supply and demand network coding information.

### 5.2.1 Test Network

Two freeway test networks were utilized in this analysis to analyze the effects of CMVs using microscopic traffic simulation models. Both networks are located to the west of downtown Houston, Texas, one on IH-10 and the second test bed on US 290, as illustrated in Figure 5.2. Both networks are grade-separated divided freeway facilities, with high occupancy vehicle

(HOV) facilities in the median, on- and off-ramps connected to the main lanes, and AVI readers on the main freeway lanes.

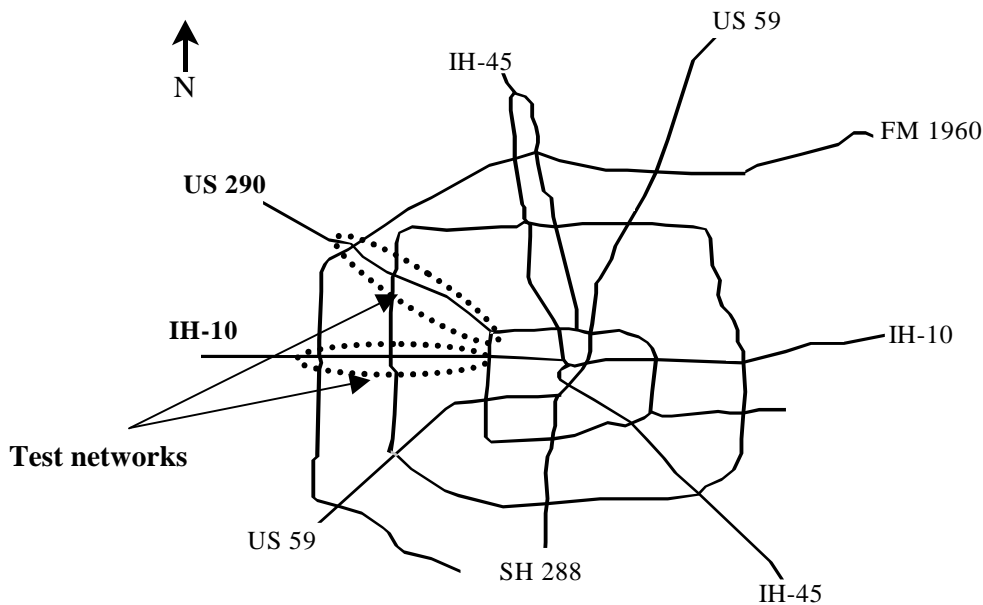


**FIGURE 5.2 Test network locations**

**5.2.1.1 IH-10 Houston, Texas** The first test network utilized in the analysis was a 13.9-mile section of Interstate Highway 10 (IH-10) Katy Freeway eastbound in Houston, Texas. The IH-10 network extended from just west of Barker Cypress Road to a point just east of Silber (west of the IH-610 West Loop). The IH-10 network includes 14 on-ramps and 13 off-ramps, with five AVI stations that divide the facility into four links, as illustrated in Figure 5.3. The IH-10 network is monitored as part of the Houston TranStar advanced traffic management system (ATMS), providing real-time traffic information for motorists along the corridor.

Traffic volume data were collected along the entire length of the corridor using ILD and pneumatic tubes during the months of May and June 1996 as part of an AADT data collection effort. These counts were supplemented by additional data collected in July and August 1996 from which a database of traffic counts was developed. This database was used to summarize Wednesday and Thursday counts that were then aggregated into hourly volumes. The data were analyzed and traffic counts adjusted to ensure consistency and to account for all vehicles from node to node along the network. AVI data were also collected during this time and used to

calculate the average space mean travel time for each AVI link by time-of-day during the data collection time periods. These time periods included AM peak period (7:00 a.m. to 8:00 a.m.), off peak period (2:00 p.m. to 3:00 p.m.), and PM peak period (5:00 p.m. to 6:00 p.m.). The detailed link and node diagram as well as the observed traffic volume data is provided in Appendix D.

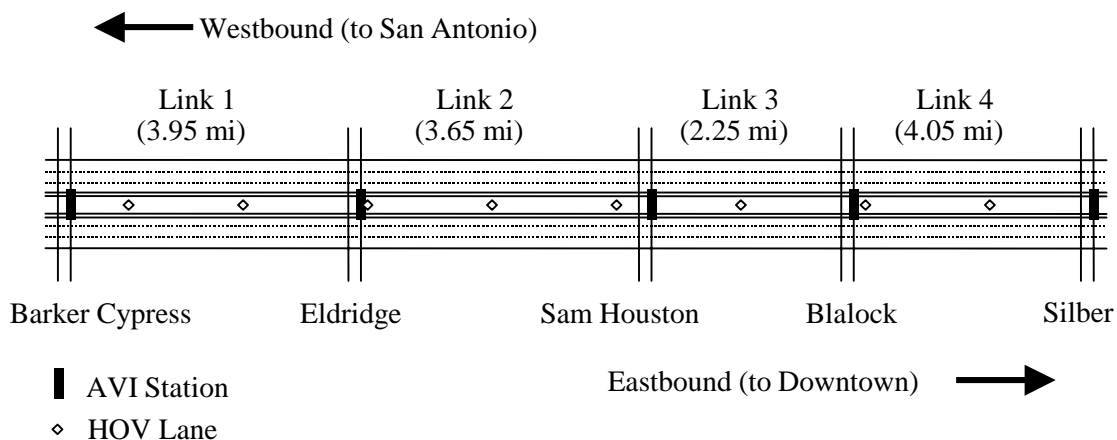


**FIGURE 5.3 IH-10 Houston, Texas, test network**

**5.2.1.2 US 290 Houston, Texas** The second test network for this analysis was a 14.3-mile section of US 290 eastbound in Houston, Texas. The network begins east of FM 1960 and extends to the west, west of IH-610, and includes 12 on- and off-ramps as well as six AVI stations that were in operation at the time of data collection. The six AVI stations divide the facility into five links, as illustrated in Figure 5.4. This network is also monitored as part of the Houston TranStar ATMS, providing real-time traffic information to motorists who utilize the corridor.

Traffic volume data were collected for this section of US 290 using ILD and pneumatic tube counters in May and June of 1996 as part of an AADT estimation count in the same manner as the data collected on IH-10. The data obtained were aggregated into hourly volumes and adjusted to ensure consistency across the network. Data for this network were collected during the AM peak period (7:00 a.m. to 8:00 a.m.) only. The detailed link and node diagram, as well as the observed traffic volume data, is provided in Appendix D.

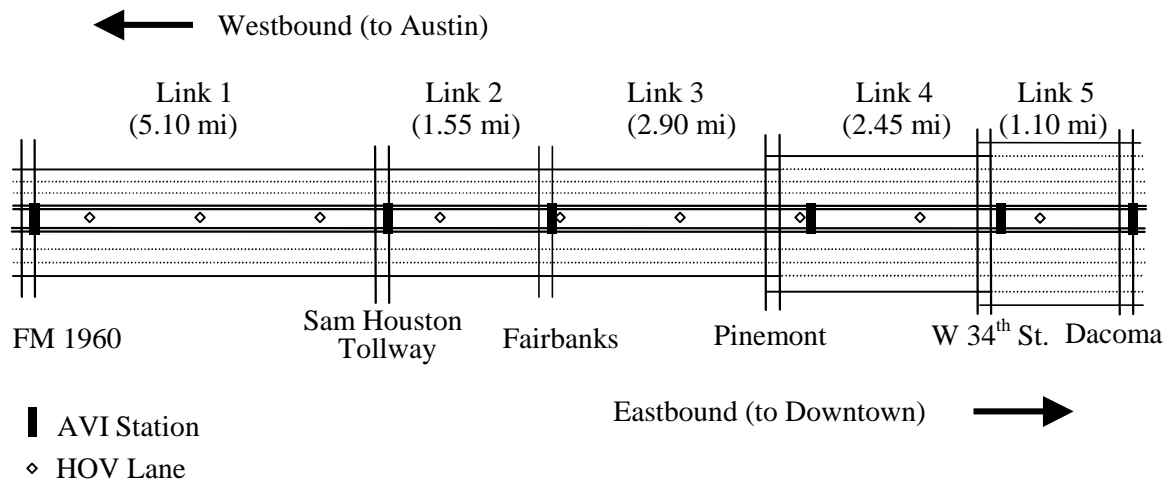


**FIGURE 5.4 US 290 Houston, Texas, test network**

In the years since these data were collected, AADT estimates have been recorded along both the IH-10 and US 290 networks. These estimates have been generated using pneumatic tube and ILD volume counts and adjusted based on ATR traffic volume data in the Houston metropolitan area according to the methodology outlined in Section 3.1.1. A detailed corridor count as extensive as the one undertaken in 1996, however, has not been conducted in more recent years. As a result, the 1996 data are utilized in this analysis due to the consistency of the data and the data collection methodology. These volumes can be updated using a combination of the traffic volume counts and detector data available today; however, this task was not undertaken as part of this dissertation.

### 5.2.2 Network Coding

As indicated in previous sections, the basic architecture of microscopic traffic simulation models includes input on the supply and demand of the transportation network. The supply input includes the links, nodes, and traffic control system. Link attributes include length, grade, and any other distinguishing features of the link (i.e., number of driveways, bus stop locations). Node attributes include number of lanes, lane widths, total approaches to the link, and so forth. The traffic control system includes, first, type of intersection control (i.e., signal control, stop sign control, uncontrolled) and the appropriate attributes of each control type (i.e., signal location, signal timing, actuated control, four-way stop control). The demand input includes

point-to-point trip movements as represented by an OD trip matrix, as well as the base traffic volume information at the entry nodes.

Various aspects of the traffic simulation model input vary over time and space across the network. The characteristics that vary over time are generally the demand input characteristics, including the point-to-point trip movements and OD information, as well as supply input, particularly traffic control (signal timing and traffic regulations). The characteristics that vary over space include the link and node attributes of the supply input, primarily the traffic geometry and link type (i.e., freeway or arterial street). More detailed information on both the supply and demand input coding in the CORSIM networks is provided in the following subsections.

**5.2.2.1 Supply Input Coding** The primary supply input for the test networks included the freeway link geometry, node attributes, and traffic control information. The major inputs in the CORSIM model included the following:

- node numbers and x,y coordinates;
- link numbers and node-to-node configuration;
- type and length of acceleration and deceleration lanes;
- lane geometry including number of lanes, lane width, etc.;
- AVI station location (coded as a node);
- traffic control at each node; and
- connectivity data between nodes and between links.

The majority of the supply input data was obtained from previous studies performed at the Texas Transportation Institute (TTI) TransLink<sup>®</sup> research center and verified based on network diagrams and engineering drawings. On- and off-ramps were coded as links and connected to freeway mainline links, while AVI stations were also identified in the model and coded as nodes connecting freeway links.

**5.2.2.2 Demand Input Coding** As previously identified, demand input includes point-to-point trip movements as represented by an OD trip matrix, as well as the base traffic volume information at the entry nodes. Demand input can generally be entered in CORSIM for a freeway network in two ways. The first method includes the identification of traffic volumes at

entrance nodes (CORSIM record type 50) with turning movement percentages (i.e., exit volumes) identified at each ramp exit (CORSIM record type 25). From this information, CORSIM utilizes a gravity model to calibrate the turning percentages to an OD table in percentages (102).

The second methodology used to generate demand input in CORSIM is a synthetic OD estimation in which the user specifies an OD pair in percentage from an origin node to a destination node. In this alternative, the user is responsible to ensure that the traffic volumes for all destination nodes agree with the traffic volume calibrated in the previous alternative using the volumes and turn percentages of record types 25 and 50 (102). The analysis in this dissertation compares both demand input alternatives by including traffic volumes and turning percentages, as well as a synthetic OD estimate obtained using a technique developed by Dixon and Rilett, based on the data collected at the AVI stations located along each network (143, 144). It is important to point out here that neither approach differentiates between vehicle type, but an estimate of OD for CMVs obtained from ITS traffic data or survey methods is important in providing a more accurate representation of existing conditions. The majority of research that has been performed on both calibration and OD estimation, however, has not generally included CMV OD estimation.

For both the CORSIM gravity model alternative and the synthetic OD demand input alternative, traffic volumes must be generated at each entry node in the network. CORSIM can generate vehicle entry headway either non-stochastically or stochastically using a normal or an Erlang distribution. The default arrival pattern for entry node generation is the uniform distribution. The Erlang distribution follows the form outlined in Equation 5.1 (102).

$$f(t) = \frac{(qa)^a}{(a-1)!} t^{a-1} e^{-aqt} \quad 0 < t < \infty \quad (5.1)$$

where:  $f(t)$  = probability density function for vehicle headways;  
 $q$  = average traffic volume per lane (vph);  
 $a$  = level of randomness of the distribution ranging from  $a = 1$  (most random) to  $a = \infty$  (complete uniformity); and  
 $t$  = headway (sec).

One special case of the Erlang distribution occurs when  $a = 1$ . In this alternative, the Erlang distribution is known as the negative exponential distribution outlined in Equation 5.2. In

this alternative, the result is actually a shifted negative exponential distribution because vehicle separation is prohibited from falling below a specific minimum value. This allows the program to closely replicate random, Poisson vehicle arrivals on external links (145). This distribution was utilized in the analyses.

$$f(t) = qe^{-qt} \quad (5.2)$$

### 5.3 CORSIM Calibration Parameters

CORSIM includes a variety of inputs commonly referred to as calibration parameters. These parameters allow the user to fine-tune CORSIM to match existing traffic conditions. The CORSIM calibration parameters can be summarized into two general categories: 1) driver behavior parameters and 2) vehicle performance parameters. The driver behavior parameters include factors such as mean start-up delay at ramp meters, distribution of free flow speed by driver type, incident rubbernecking factor, car-following sensitivity factor, lane-change gap acceptance parameters, and parameters that affect the number of discretionary lane changes. Vehicle performance parameters include speed and acceleration characteristics, fleet distribution, passenger occupancy, and maximum deceleration rates (102).

Calibration parameters in CORSIM include several general calibration parameters that are universal across the network as well as specific vehicle type calibration parameters. Each of these parameter types is discussed in the following subsections.

#### 5.3.1 General Calibration Parameters

The base calibration parameters for CORSIM that have been considered in this analysis are outlined in Table 5.1 (102). The first column of this table identifies the parameter number ( $P_1$  through  $P_{19}$ ), the second column provides the description of the parameter based on the CORSIM user's manual, the third column lists the units for the parameter, while the fourth column identifies the default CORSIM value. The fifth and sixth columns identify the minimum and maximum allowable values, respectively, utilized in this analysis. It is important to note here that the majority of these latter values (minimum and maximum allowable) are not defined in the program but were based on reasonableness criteria that will be discussed in later sections.

The calibration parameters can be classified into three general categories: 1) car-following sensitivity factors ( $P_1$  through  $P_{11}$ ); 2) acceleration/deceleration factors ( $P_{12}$  and  $P_{13}$ );

and 3) lane-change factors ( $P_{14}$  through  $P_{19}$ ), each of which will be discussed in the following subsections.

**TABLE 5.1**    **CORSIM General Calibration Parameters**

<b>Parameter (<math>P_i</math>)</b>	<b>Description</b>	<b>Unit</b>	<b>Default Value</b>	<b>Min. Value</b>	<b>Max. Value</b>
$P_1$ - $P_{10}$	Car-following sensitivity factor for driver type 1 through 10	1/100 sec	35-125	30	150
$P_{11}$	PITT car-following constant	ft	10	3	10
$P_{12}$	Lag time to accelerate	1/10 sec	3	1	10
$P_{13}$	Lag time to decelerate	1/10 sec	3	1	10
$P_{14}$	Time to complete a lane-change maneuver	1/10 sec	20	10	60
$P_{15}$	Minimum separation for generation of vehicles	1/10 sec	16	10	30
$P_{16}$	Mandatory lane-change gap acceptance parameter	N/A	3	1	6
$P_{17}$	Percent of drivers desiring to yield right-of-way to lane-changing vehicles	%	20	5	40
$P_{18}$	Multiplier for desire to make a discretionary lane-change	tenths of units	5	1	10
$P_{19}$	Advantage threshold for discretionary lane-change	tenths of units	4	1	10

**5.3.1.1 Car-Following Sensitivity Factors** The car-following sensitivity factors are based on the idea that the desire of an individual driver to follow the car in front of them varies from driver to driver according to a specified level of sensitivity. To account for the variability of driver types, 10 different car-following sensitivity factors ( $P_1$  through  $P_{10}$ ) are identified in CORSIM. The sensitivity factors are input in the model in units of hundredths of a second, such that a sensitivity factor of 1.05 seconds would be entered as a value of 105. The distribution of these factors is stored in an array that is used to determine the desired car-following distance according to the PITT car-following model (102, 146). The default car-following sensitivity factor distribution has varied over the years, ranging from values between 1.5 and 0.6 seconds

(147, 148, 149) to the current range summarized in Table 5.2, where each driver type corresponds to  $P_1$  through  $P_{10}$  in the calibration parameter descriptions (102).

**TABLE 5.2 Default Distribution of Car-Following Sensitivity Factors**

Parameter ( $P_j$ )	$P_1$	$P_2$	$P_3$	$P_4$	$P_5$	$P_6$	$P_7$	$P_8$	$P_9$	$P_{10}$
Driver Type	1	2	3	4	5	6	7	8	9	10
Factor (sec.)	1.25	1.15	1.05	0.95	0.85	0.75	0.65	0.55	0.45	0.35

The basic car-following methodology is based on the PITT car-following model identified in the original INTeGrated TRAffic Simulation (INTRAS) microscopic freeway simulation model. The PITT car-following model follows the base assumption that a vehicle will try to maintain space headway, according to Equation 5.3 (146, 147, 150, 151, 152) and illustrated graphically in Figure 5.5.

$$H = L + P_j v_t + P_{11} + b P_j (u_t - v_t)^2 \quad \forall j = 1, N \quad (5.3)$$

where:

- $H$  = space headway (ft);
- $L$  = length of the leading vehicle (ft);
- $P_j$  = driver sensitivity factor for the follower (sec);
- $P_{11}$  = PITT car-following constant (ft);
- $u_t$  = speed of leading vehicle at time  $t$  (ft/sec);
- $v_t$  = speed of the following vehicle at time  $t$  (ft/sec);
- $j$  = calibration parameter;
- $N$  = number of vehicle types (i.e., in TSIS 5.0,  $N = 10$ ); and

$$b = \begin{cases} 0.1 & u_t < v_t \\ 0 & u_t \geq v_t \end{cases}$$

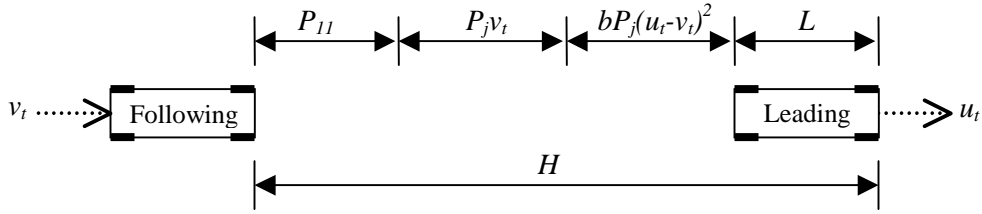


**FIGURE 5.5** CORSIM car-following headway

The first three terms in the equation ( $L + P_j v_t + P_{11}$ ) are necessary to maintain the minimum space headway between vehicles. The first term accounts for the length of the leading vehicle, while the second term is used to represent the variability in driver headway through the use of driver sensitivity factors defined previously. The third term, the PITT car-following constant ( $P_{11}$ ), is used to determine the minimum absolute vehicle headway and can be calibrated to any integer value in the range between 3 feet and 10 feet. The final term in the equation, ( $b P_j (u_t - v_t)^2$ ), was introduced to allow for high relative closing speed behavior based on empirical studies and inclusion of a calibration constant  $b$  that is assigned a value of 0.1 or 0 depending on the relationship between the speed of the leading and following vehicles. The value of  $b$  is documented two ways, the first of which was outlined previously, the second of which assigns a value of 0.1 to  $b$  for  $u_t - v_t \leq 10$  and a value of  $b = 0$  otherwise. This scenario is outlined in the original INTRAS documentation (146) but has been modified in more recent documentation (147). The new requirement provides a slightly larger headway for all vehicles where the speed of the leading vehicle ( $u_t$ ) is less than the speed of the following vehicle ( $v_t$ ).

Based on this relationship, the acceleration of the following vehicle for any interval can be derived as a function of the vehicle length, minimum spacing, and the relationships between speed and location of the leading and following vehicles. The resulting relationship is summarized in Equation 5.4, while the associated derivations for this equation can be found in the literature (146, 150).

$$a_f = \frac{2(x_{t+T} - y_t - L - P_{11} - v_t(P_j + T) - b P_j (u_{t+T} - v_t)^2)}{T^2 + 2P_j T} \quad \forall j = 1, N \quad (5.4)$$

where:  $a_f$  = acceleration of the follower in the interval  $t$  to  $t+T$  (ft/sec<sup>2</sup>);  
 $y_t$  = position of follower at time  $t$  (ft);  
 $T$  = time scanning interval (sec);  
 $x_{t+T}$  = position of leader at time  $t+T$  (ft); and  
 $u_{t+T}$  = speed of leader at time  $t+T$  (ft/sec).

Several limitations are placed on the vehicle acceleration computed from this relationship (147):

1. The lower bound for the computed acceleration is equal to the maximum non-emergency deceleration rate, where the default maximum non-emergency deceleration rate is equal to 8 feet per second squared.
2. The maximum change in acceleration between successive scanning intervals is equal to the jerk value (third derivative of position), where the default jerk value is equal to 7 feet per second cubed.
3. The acceleration is applied to the vehicle after the driver's response lag time has elapsed unless there is no change in sign from the previous scanning interval. The default value for the response lag time is 0.3 seconds.

The time headway between vehicles is directly proportional to the driver sensitivity factor,  $P_j$ . As a result of the proportional relationship between headway and sensitivity factor, a high value of the sensitivity factor results in higher headway and subsequently a lower capacity of the roadway being simulated. To examine the car-following sensitivity values, a sensitivity analysis for both time and space headway for a range of speeds and car-following sensitivity values was conducted. The results of this analysis are provided in Figures 5.6 and 5.7 for space and time headway sensitivity analyses, respectively. The headways outlined in these figures are upper and lower car-following sensitivity ( $P_j$ ) ranges ( $P_1 = 1.50$ ,  $P_{10} = 0.30$ ) calculated for three different speed differential ranges (0, 5, and 10 miles per hour). In addition to providing a representation of the calculated time and space headway curves, "approximate" field results were also plotted based on research documented in the 1950 *Highway Capacity Manual* (153) and referenced in several more recent publications (109, 154, 155). The "approximate" field results indicate that the average driver increases following distance with increased speed and that the higher the facility type (i.e., freeway), the smaller the space headway recorded.

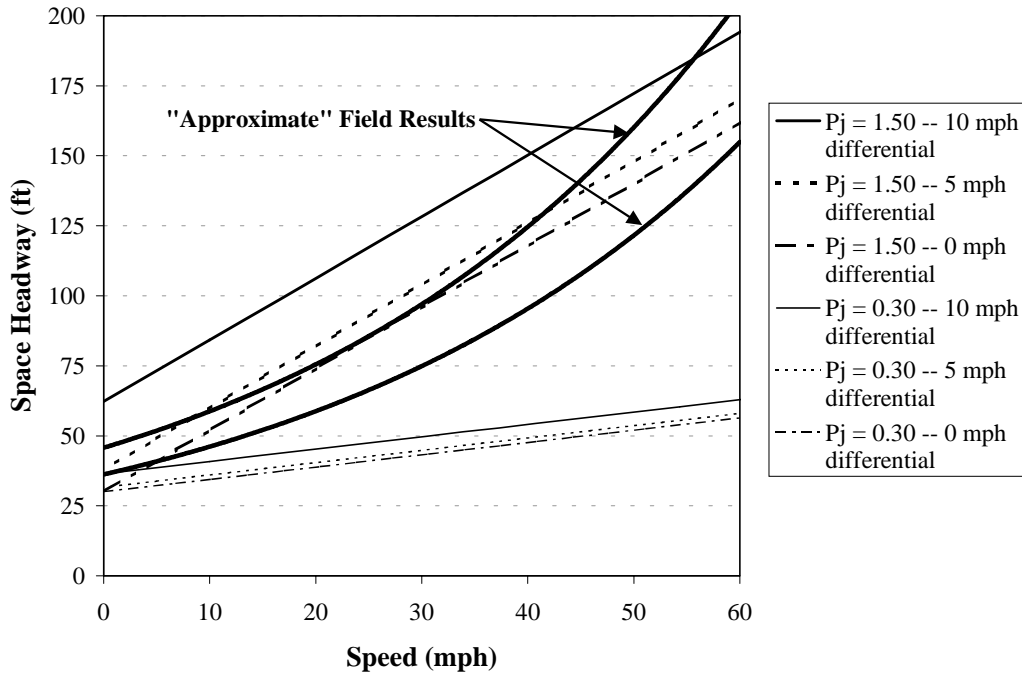


FIGURE 5.6 Space headway sensitivity analysis

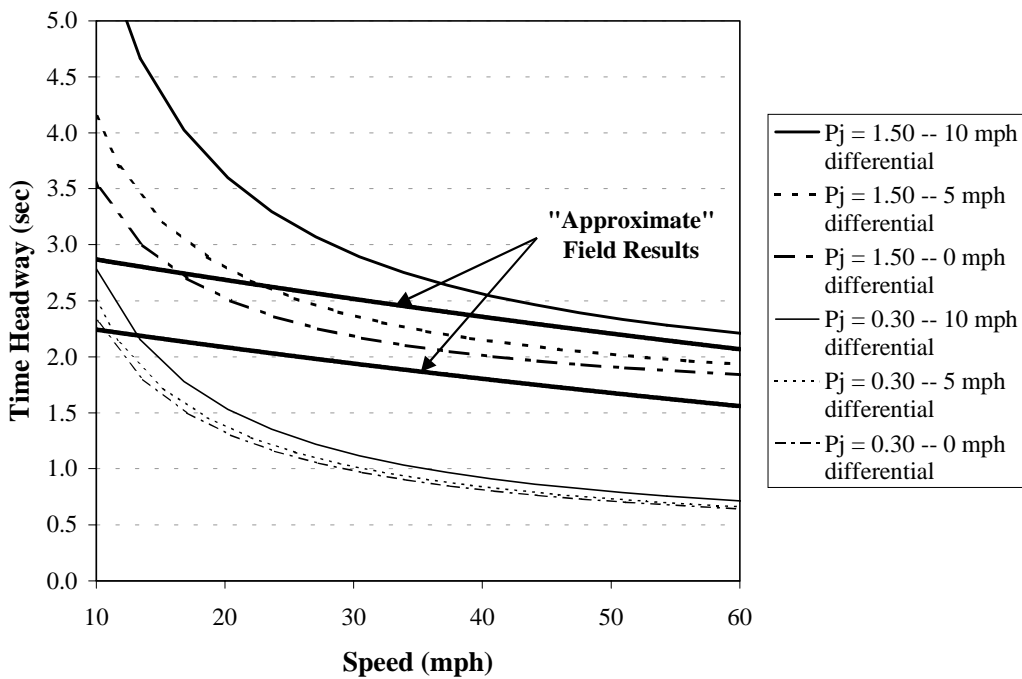


FIGURE 5.7 Time headway sensitivity analysis

The results presented in the space and time headway sensitivity analyses clearly indicate that the range of car-following sensitivity factors from 1.50 seconds to 0.30 seconds provide an alternative to include all possible average field results. One may argue based on this analysis that the range is too broad and that the lower limit should be increased. Recent research performed by Khan et al. utilized a range of car-following sensitivity factors from 1.70 seconds to 0.60 seconds, indicating that the upper range (1.70 seconds) overestimated headways, while the lower range (0.60 seconds) underestimated the headway results (148). In a 1993 publication on the distribution of high traffic flows, observed headways were recorded on IH-279 near downtown Pittsburgh during morning rush hour. The results of this analysis indicated that average observed time headways ranged from 1.24 seconds to 1.75 seconds, while the standard deviation of these headways ranged from 0.52 seconds to 0.94 seconds (156). Separate research performed in Israel on minimum and comfortable driving headways concluded that average time headways, where headway is defined in this research as the distance between the “front bumper of the vehicle you are driving and the rear bumper of the lead vehicle,” remained relatively constant across a range of speeds at approximately 0.64 to 0.69 seconds (157). If a vehicle length of 20 feet were assumed in this calculation, the equivalent time headway would range from approximately 0.90 seconds to 1.10 seconds. These values were compared with recent and early headway research, indicating that the recent research has consistently shown shorter time headways when compared with the early research (157). These results are also consistent with the changes that have been made in recent versions of the CORSIM software, where the default car-following sensitivity factors have been reduced from an earlier range of 1.50 to 0.60 seconds to the current range of 1.25 seconds to 0.35 seconds. Based on the results of this recent research, it is hypothesized that the “approximate” field results illustrated previously would be shifted if measured in today’s freeway traffic, rather than the traffic of the 1950s, the source of these data.

Based on the actual calculated headways for the car-following sensitivity factors and the recent trends identified in time and space headway research, the range of car-following sensitivity factors to include in the analysis has been set to provide a wide range of values, with the intent of maintaining average headways within an acceptable range. The calibration process presented in Section 6 will allow the distribution of these values to be calibrated based on site-specific conditions. The range of values, as indicated previously for this parameter, has been set between 0.3 seconds (input as a value of 30) for aggressive drivers to 1.50 seconds (input as a value of 150) for passive drivers. The motivation for this range of values is based on both

previous research on CORSIM car-following sensitivity factors as well as an analysis of the calculated time and space headways that result from these values.

Although the analysis presented in this dissertation is designed to calibrate the car-following sensitivity factors based on the calibration procedure presented in Section 6, these values could also be calibrated based on a sensitivity analysis of observed headway conditions. By rearranging the car-following sensitivity equation identified previously, the car-following sensitivity factor ( $P_j$ ) can be calculated according to Equation 5.5. Using a measured headway distribution for observed speeds, the car-following sensitivity factors could be calculated and used as input to the simulation model.

$$P_j = \frac{H - L - P_{11}}{v_t + b(u_t - v_t)^2} \quad \forall j = 1, N \quad (5.5)$$

**5.3.1.2 Acceleration/Deceleration Factors** The acceleration/deceleration factors are used in the model to identify the lag to accelerate and lag to decelerate, where the lags are time delays that motorists experience when making required maneuvers. These factors are introduced into the car-following equations, after the acceleration of the follower has been calculated and when the new speed and position are defined, as outlined in Equations 5.6 and 5.7 (146).

$$v_{t+T} = v_t + a_f(T - P_j) \quad (5.6)$$

$$y_{t+T} = y_t + v_t T + \frac{1}{2} a_f (T - P_j)^2 \quad (5.7)$$

where:  $v_{t+T}$  = speed of leader at time  $t+T$  (ft/sec);  
 $y_{t+T}$  = position of follower at time  $t+T$  (ft);  
 $P_j$  = reaction lag time (sec) ( $P_j < T$ ); and  
 $j$  = calibration parameter ( $j = 12$  for acceleration and  $j = 13$  for deceleration).

The value of the acceleration/deceleration parameter was initially calculated based on empirical data to be 0.2 seconds for acceleration and 0.3 seconds for deceleration (146). The current defaults for this parameter are 0.3 seconds for both lag to accelerate and lag to decelerate ( $P_{12}$  and  $P_{13}$ ) (102). A range of values, as indicated previously for this value, has been set between 0.1 seconds (entered as 1) and 1 second (entered as 10), based on the empirical analysis

done previously, to coincide with 1 second time scanning intervals in an attempt to ensure  $P_j < T$ , and based on stopping sight distance research performed previously (50).

**5.3.1.3 Lane-Change Factors** The FRESIM component of the CORSIM model utilizes a multi-faceted lane-change algorithm that includes both the supply (gap evaluation) and demand (gap acceptance) side of the lane-changing decision. The algorithm also includes behavioral traits related to the lane-change decision by providing a variety of input values used to determine an individual driver's desire to improve his/her current situation through the lane-change maneuver.

The various parameters associated with the lane-changing process and the decisions that must be made are illustrated in Figure 5.8 (147). This illustration identifies the position of the putative leader and follower vehicles in relation to the vehicle determining to make a lane-change. The primary inputs to consider in the lane-change maneuver are identified as the leading gap and trailing gap in the target lane. The decision whether or not to make a lane-change is determined through an evaluation of the lead gap and trailing gap size. The lead gap is evaluated based on the required deceleration during the lane-changing period, by the ability of the lane changer to maintain a safe position relative to the putative leader and putative follower, as well as by the advantage gained by the lane-change. A series of equations have been developed that identify the required deceleration by the lane changer to maintain a safe position relative to the putative leader and follower and can be found in the literature (147).

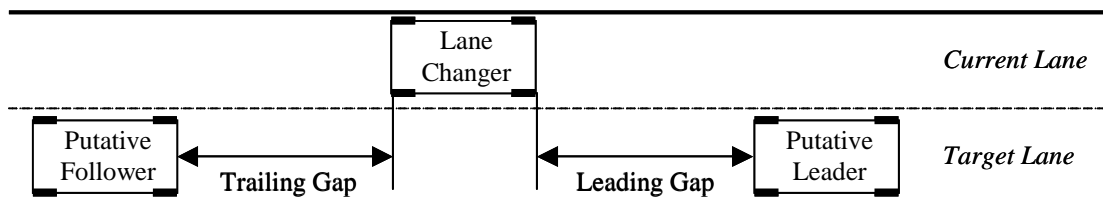


**FIGURE 5.8** Lane-change parameters (adapted from 147)

Several parameters in the lane-changing algorithm can be adjusted as outlined in the parameter identification set. The first of these parameters is the lane-change period or hiatus period, which represents the duration of time to complete the lane-change. This parameter ( $P_{14}$ )

is an input value in the lane-change acceleration equations and has a default value of 2 seconds (entered as 20 in the model). This value was determined based on early research on lane-changing that showed that the time to change lanes was a function of speed but that the relationship was not very strong. The background analysis concluded, therefore, that a constant changing time to complete a lane-change maneuver was a reasonable assumption (146). As a result, a constant value within a range from 1 second (entered as 10) to 6 seconds (entered as 60) was identified for the model.

The second parameter identified under the lane-changing parameter heading is the minimum separation for generation of vehicles. This parameter is utilized to govern the maximum rate at which vehicles can be emitted onto the network in a given lane (102). The default value for this parameter ( $P_{15}$ ) is 1.6 seconds (entered as 16), with a range identified for evaluation of 1.0 seconds (entered as 10) and 3.0 seconds (entered as 30) for evaluation.

The premise of the basic lane-changing equation is based on the gap acceptance and the process of determining whether the lead and trailing gaps are acceptable to the lane changer. For these gaps to be acceptable, the required deceleration to accommodate the lane-change should not exceed the acceptable level of risk by the lane-changer and the putative follower. The acceptable level of risk for both of these vehicles is identified as the maximum acceptable deceleration rate necessary to perform the lane-change. An additional behavioral trait is also included in this analysis, that of the level of cooperation of the putative follower to allow the lane changer to make the change. The maximum acceptable deceleration rate for a cooperative driver has been set at 10 feet per second squared, while the maximum acceptable deceleration rate for a non-cooperative driver has been set at 8 feet per second squared. The default parameter in the model ( $P_{17}$ ) assumes that 20 percent of the drivers will cooperate with the lane changer, while the remaining 80 percent will not (102, 147).

Lane-changing is modeled in CORSIM using three distinct categories: 1) mandatory lane-change; 2) discretionary lane-change; and 3) anticipatory lane-change. The details for each of these categories are described briefly in the following subsections.

*5.3.1.3.1 Mandatory Lane-Changing* Mandatory lane-changing is the most stringent of the lane-change categories, with the driver accepting the largest level of risk in performing mandatory lane changes. The following situations are treated as mandatory lane changes (147):

- merging traffic entering from the on-ramp;
- lane-changing by traffic to reach the proper lane to exit the freeway;
- vacating a lane blocked by an incident; and
- vacating a lane that is dropped further downstream.

The acceptable risk in performing a mandatory lane-change for traffic on an auxiliary lane attempting to merge with mainline traffic is determined according to Equation 5.8 (147).

$$a = a_{\min} + (e - a_{\min}) \sqrt{\frac{d}{l}} \quad (5.8)$$

where:  $a$  = acceptable deceleration rate (ft/sec<sup>2</sup>);  
 $a_{\min}$  = minimum acceptable deceleration rate (ft/sec<sup>2</sup>);  
 $e$  = emergency deceleration rate (ft/sec<sup>2</sup>);  
 $d$  = distance between the vehicle and the on-ramp gore (ft); and  
 $l$  = length of the acceleration auxiliary lane (ft).

For vehicles that are attempting to reach the proper lane to exit the freeway network, the acceptable deceleration is computed according to Equation 5.9 (147).

$$a = \begin{cases} e & d > 200 \\ a_{\min} + (e - a_{\min}) \sqrt{\frac{d}{l}} & d \leq 200 \end{cases} \quad (5.9)$$

CORSIM allows the user to determine the acceptable gap for mandatory lane changes through the calibration parameters ( $P_{16}$ ). The mandatory lane-change gap acceptance parameter is utilized to determine the acceptable gap for lane changes and to choose the most aggressive (1) to least aggressive (6) lane-changing for all drivers. The default value for this parameter is 3, with an overall range of values from 1 to 6 (102).

**5.3.1.3.2 Discretionary Lane-Changing** Discretionary lane-changing refers to those performed to bypass slow-moving vehicles, to obtain a more favorable position on the network, and to attain higher speeds. Discretionary lane-change logic is based on behavioral factors of the driver to make the lane-change. These factors include: 1) motivation; 2) advantage; and 3) urgency.

Motivational lane-changing is performed in the model through the assignment of an intolerable speed below which the driver is highly motivated to perform the lane-change. The intolerable speed is computed according to Equation 5.10 (147).

$$v_i = v_{ff} \frac{50 + 2c}{100} \quad (5.10)$$

where:  $v_i$  = intolerable speed (ft/sec);  
 $v_{ff}$  = desired free-flow speed (ft/sec); and  
 $c$  = driver type factor.

In the motivational lane-change equation, the driver type factor is a randomly assigned number from 1 to 10, where 10 represents the most aggressive driver and 1 represents the most passive driver. These factors are assumed constant for each individual driver throughout the simulation. Once the intolerable speed is calculated, the desire to perform a discretionary lane-change is then modeled based on Equation 5.11 (147).

$$D = \begin{cases} 100 & v \leq v_i \\ 100 \left[ 1 - \frac{(v - v_i)}{(v_{ff} - v_i)} \right] & v_i < v < v_{ff} \\ 0 & v \geq v_{ff} \end{cases} \quad (5.11)$$

where:  $D$  = desire to perform a discretionary lane-change and  
 $v$  = speed of the lane changer (ft/sec).

Discretionary lane-change by advantage provides drivers an opportunity to improve their current situation and is modeled in terms of a lead factor ( $F_l$ ) and a putative factor ( $F_p$ ). The lead factor represents the disadvantage of remaining in the current lane, while the putative factor represents the gain in moving to a new lane. The lead factor is computed according to Equation 5.12, while the existing headway in the current lane (input to Equation 5.12) is calculated according to Equation 5.13 (147).

$$F_l = \begin{cases} 1 & h \leq h_{\min} \\ 1 - \frac{h - h_{\min}}{h_{\max} - h_{\min}} & h_{\min} < h < h_{\max} \\ 0 & h \geq h_{\max} \end{cases} \quad (5.12)$$

$$h = \frac{s - F_s v_d}{v_{ff}} \quad (5.13)$$

where:  $F_l$  = lead factor;  
 $h$  = existing headway in the current lane;  
 $h_{\min}$  = minimum headway (sec);  
 $h_{\max}$  = maximum headway (sec);  
 $s$  = separation distance between the vehicle and its leader in the current lane (ft);  
 $F_s$  = speed threshold factor (sec); and  
 $v_d$  = speed differential between the vehicle and its leader (ft/sec).

The putative factor represents the perceived gain in performing a lane-change and is calculated for both lanes adjacent to the current lane, with the target lane selected as the lane with the largest putative factor. The algorithm for calculating the putative factor is identical to the one just outlined for the lead factor with one exception. In the putative factor calculation, the headway computation is performed with respect to the putative leader in the target lane, as illustrated previously in Figure 5.8. The overall advantage and determination of a discretionary lane-change is then computed as the difference between the putative factor and the lead factor, with the lane-change permitted if it exceeds the advantage threshold ( $P_{19}$ ), which has a default value of 0.4 and ranges from 0.1 to 1.0 (102, 147). A range of values as indicated previously for this parameter has been set to range between 0.1 (input as 1) to 1 second (input as 10).

The final discretionary lane-change type is that of urgency for lane-change. Urgency is based on the assumption that the driver who has a desire to make a lane-change but cannot, will gradually become impatient and will accept a higher level of risk to make the lane-change. The basic methodology behind this decision centers on the urgency factor (U) computed according to Equation 5.14 and the impatience factor (IMP) in Equation 5.15 (147).

$$U = (1 - F_l)IMP(t) \quad (5.14)$$

$$IMP(t) = IMP(t - \Delta t) + \frac{c+1}{20} X(t) \quad (5.15)$$

where:  $IMP(t)$  = impatience factor;  
 $t$  = current time;  
 $\Delta t$  = simulation time-step duration; and  
 $X(t)$  = 0 if the vehicle does not want to make a lane-change, or 1 if the vehicle desires to make a lane-change.

The acceptable deceleration by the lane changer to perform a discretionary lane-change based on the urgency factor is then computed according to Equation 5.16, where the default minimum acceptable deceleration for discretionary lane-change is set to be 5 feet per second squared and the default maximum acceptable deceleration for discretionary lane-change is 10 feet per second squared (147).

$$a = \begin{cases} a_{\min} & U < 1 - 0.05c \\ a_{\min} + (a_{\max} - a_{\min}) \frac{U + 0.05c - 1}{0.05c} & U \geq 1 - 0.05c \end{cases} \quad (5.16)$$

where:  $a_{\min}$  = minimum acceptable deceleration rate for discretionary lane-change (ft/sec<sup>2</sup>);  
 $a_{\max}$  = maximum acceptable deceleration rate for discretionary lane-change (ft/sec<sup>2</sup>); and  
 $U$  = urgency factor.

None of the default values and functional relationships used in the discretionary lane-change algorithm outlined in the previous sections can be altered by the user. However, the multiplier for desire to make a discretionary lane-change ( $P_{18}$ ) and the advantage threshold for discretionary lane-change ( $P_{19}$ ) can be adjusted.

**5.3.1.3.3 Anticipatory Lane-Changing** The final type of lane-changing used in the CORSIM model is anticipatory lane-changing which refers to lane changes performed upstream of on-ramps in anticipation of downstream congestion. The primary difference between anticipatory lane-changing and discretionary lane-changing is the method of computation of the advantage in performing the lane-change, which is based on the volume and prevailing average speed in the vicinity of the on-ramp gore, and the desire to perform the lane-change, which is set to 1 for anticipatory lane-changing, indicating a high level of desire to change lanes.

### 5.3.2 Vehicle Type Calibration Parameters

To aid in the analysis of CMVs, each vehicle in CORSIM is identified by fleet (auto, carpool, truck, or bus) and by vehicle type. CORSIM allows the user to identify up to nine different vehicle types to define the four vehicle fleets, as outlined in Table 5.3. Each of the nine vehicle types can be assigned different operating and performance specifications, thus aiding in the process of simulation of real-world conditions (102).

**TABLE 5.3 Default CORSIM Fleet and Vehicle Types**

Fleet Component	Vehicle Type	Vehicle Description
Passenger Car	1	Low performance vehicle
	2	High performance vehicle
Truck	3	Single-unit truck
	4	Semi-trailer truck with medium load
	5	Semi-trailer truck with full load
	6	Double-bottom trailer truck
Bus	7	Conventional bus
Carpool	8	Low performance vehicle
	9	High performance vehicle

While the general calibration parameters outlined in the previous section primarily affect driver behavior, the vehicle type calibration parameters provide an opportunity to calibrate operation and fleet characteristics. The vehicle type calibration parameters are classified according to three general categories: 1) maximum non-emergency deceleration by vehicle type; 2) speed and acceleration characteristics; and 3) fleet distribution. Each of these parameters will be discussed in the following subsections.

**5.3.2.1 Maximum Non-Emergency Deceleration** The maximum non-emergency deceleration value ( $P_{20}$  through  $P_{28}$ ) is the largest value of deceleration that is allowed in the car-following methodology outlined in the previous section. This parameter includes a separate value for each of the nine different vehicle types, with a default value of 8 feet per second squared (entered as 80 based on the units of tenths of a foot per second squared), as indicated in Table 5.4 (102). As with the previous analyses, the minimum and maximum values identified in this table are those utilized in this analysis. In general, vehicle types 1 and 2 represent automobiles, vehicle types 3

through 6 represent trucks, vehicle type 7 represents a bus, while types 8 and 9 are used for HOV traffic.

**TABLE 5.4**    **CORSIM Vehicle Type Calibration Parameters**

<b>Parameter (<math>P_i</math>)</b>	<b>Description</b>	<b>Unit</b>	<b>Default Value</b>	<b>Min. Value</b>	<b>Max. Value</b>
$P_{20}$	Maximum non-emergency freeway deceleration for vehicle type 1	1/10 ft/s <sup>2</sup>	80	70	120
$P_{21}$	Maximum non-emergency freeway deceleration for vehicle type 2	1/10 ft/s <sup>2</sup>	80	70	120
$P_{22}$	Maximum non-emergency freeway deceleration for vehicle type 3	1/10 ft/s <sup>2</sup>	80	40	100
$P_{23}$	Maximum non-emergency freeway deceleration for vehicle type 4	1/10 ft/s <sup>2</sup>	80	40	100
$P_{24}$	Maximum non-emergency freeway deceleration for vehicle type 5	1/10 ft/s <sup>2</sup>	80	40	100
$P_{25}$	Maximum non-emergency freeway deceleration for vehicle type 6	1/10 ft/s <sup>2</sup>	80	40	100
$P_{26}$	Maximum non-emergency freeway deceleration for vehicle type 7	1/10 ft/s <sup>2</sup>	80	40	100
$P_{27}$	Maximum non-emergency freeway deceleration for vehicle type 8	1/10 ft/s <sup>2</sup>	80	70	120
$P_{28}$	Maximum non-emergency freeway deceleration for vehicle type 9	1/10 ft/s <sup>2</sup>	80	70	120

Note: A description for each vehicle type can be found in Table 5.3

The deceleration rates applied in the freeway logic of CORSIM are utilized by the car-following logic explained in the previous section. The basic parameters for calibration of deceleration in CORSIM are maximum non-emergency freeway deceleration and maximum deceleration by vehicle type on level grade and dry pavement (102, 146).

In the original INTRAS version of CORSIM, a friction coefficient of 0.65 was assumed, resulting in a deceleration rate of 0.65g (21.0 feet per second squared). This value was initially utilized as a default value in the INTRAS model for all vehicle types except trailer trucks. The maximum deceleration rates for trailer trucks was set at 0.50g (16.0 feet per second squared), based on early research in this area (146, 154). In addition to providing maximum deceleration rates, the original INTRAS model also provided default values for coasting decelerations that

occur when the driver releases the gas pedal but does not apply the brakes. A coasting deceleration rate of 0.03g (1 foot per second squared) was utilized in the early model (146).

Several research projects have been completed both prior to and following the initial development of the INTRAS model that have evaluated the maximum deceleration rates for both non-emergency and emergency situations. The majority of this research has focused on stopping sight distance, primarily at signalized intersections. A summary of this research was provided in Section 2.2.4. Based on the results of this research, the ranges outlined previously in Table 5.4 for maximum non-emergency deceleration rates were utilized in this analysis. For emergency deceleration rates, a conservative range was utilized in the analysis, with 0.47g (15.0 feet per second squared) utilized for passenger cars and all categories of trucks.

**5.3.2.2 Speed and Acceleration Characteristics** The original INTRAS model was developed to represent five different vehicle types. This has been expanded with recent advancements in the model to represent a total of nine vehicle types, although the operating characteristics of types 1 and 2 overlap with that of types 8 and 9, thus providing for distinct operating characteristics for seven different vehicle types. Early research on INTRAS identified several sources for vehicle performance characteristics (18, 37, 154, 158, 159) and a variety of descriptive characteristics for vehicle performance standards that are utilized in CORSIM (146).

The majority of the vehicle performance background for the CORSIM model was derived from a procedure outlined by St. John and Kobett in 1978 based on the weight to horsepower ratios of each vehicle type (37). Vehicle acceleration profiles in the original INTRAS model were based on the assumption that typical vehicle acceleration is influenced by speed as well as by grade and vehicle characteristics. As a result, speed categories of 20 feet per second were defined, within which acceleration was assumed constant. Normal mean acceleration for passenger car vehicles were based on tests performed by the Highway Traffic Safety Center of Michigan State University in the late 1950s and recorded in the ITE *Traffic Engineering Handbook* (146, 154). Vehicle accelerations were developed based on two performance categories: 1) low and 2) high. The resulting acceleration rates were then adjusted based on the effect of grade and resulting acceleration profiles generated. Truck and bus accelerations were also generated based on early research to produce acceleration for each vehicle type, by grade and speed category. The results of the initial acceleration rates for freeway and non-freeway conditions at grade are provided in Table 5.5 (146).

**TABLE 5.5 INTRAS Calibration Normal Acceleration Rates,  $g$  (ft/sec<sup>2</sup>) by Vehicle Type**

Vehicle Type	Roadway	Speed (ft/sec)				
		0 to 20	20 to 40	40 to 60	60 to 80	80+
Low Performance Car	Freeway	0.19 (6)	0.19 (6)	0.19 (6)	0.09 (3)	0.06 (2)
	Non-freeway	0.12 (4)	0.09 (3)	0.06 (2)	0.06 (2)	0.06 (2)
High Performance Car	Freeway	0.34 (11)	0.34 (11)	0.31 (10)	0.16 (5)	0.09 (3)
	Non-freeway	0.22 (7)	0.16 (5)	0.09 (3)	0.09 (3)	0.09 (3)
Single-Unit Trucks	All	0.09 (3)	0.06 (2)	0.03 (1)	0.03 (1)	0.03 (1)
Trailer Trucks	All	0.03 (1)	0.03 (1)	0.03 (1)	0.03 (1)	0.03 (1)

As the number of distinct vehicle types available in the INTRAS, FRESIM, and CORSIM models has increased, acceleration values have also been adjusted to account for these improvements. The current maximum acceleration table for the CORSIM model is provided in Table 5.6. This table illustrates some of the changes that have taken place with respect to the vehicle acceleration profiles, as well as the current profiles for each vehicle performance index, where the performance index is defined in Table 5.7. The rates outlined in the maximum acceleration table appear to be representative of current acceptable acceleration characteristics and as such will be utilized in the analysis.

**TABLE 5.6 CORSIM Maximum Acceleration Rate,  $g$  (ft/sec<sup>2</sup>) by Performance Index**

		Performance Index						
		1	2	3	4	5	6	7
Speed (ft/sec)	0	0.25 (8.0)	0.19 (6.0)	0.15 (4.7)	0.09 (2.8)	0.09 (2.8)	0.08 (2.5)	0.23 (7.5)
	10	0.28 (9.0)	0.37 (12.0)	0.17 (5.4)	0.07 (2.4)	0.07 (2.4)	0.07 (2.1)	0.16 (5.3)
	20	0.19 (6.0)	0.31 (10.0)	0.15 (4.9)	0.07 (2.2)	0.06 (1.8)	0.04 (1.4)	0.10 (3.2)
	30	0.16 (5.0)	0.25 (8.0)	0.11 (3.5)	0.06 (2.0)	0.05 (1.6)	0.03 (1.1)	0.08 (2.7)
	40	0.16 (5.0)	0.22 (7.0)	0.10 (3.1)	0.05 (1.7)	0.04 (1.3)	0.03 (0.9)	0.07 (2.3)
	50	0.16 (5.0)	0.19 (6.0)	0.08 (2.6)	0.04 (1.4)	0.03 (1.0)	0.02 (0.6)	0.05 (1.7)
	60	0.12 (4.0)	0.12 (4.0)	0.07 (2.1)	0.03 (1.1)	0.02 (0.7)	0.01 (0.4)	0.04 (1.4)
	70	0.09 (3.0)	0.12 (4.0)	0.05 (1.7)	0.02 (0.8)	0.02 (0.5)	0.01 (0.3)	0.03 (1.0)
	80	0.06 (2.0)	0.12 (4.0)	0.04 (1.3)	0.02 (0.6)	0.01 (0.3)	0.00 (0.1)	0.02 (0.8)
	90	0.06 (2.0)	0.06 (2.0)	0.03 (0.9)	0.01 (0.3)	0.00 (0.1)	0.00 (0.0)	0.02 (0.5)
	100	0.03 (1.0)	0.06 (2.0)	0.02 (0.5)	0.00 (0.1)	0.00 (0.0)	0.00 (0.0)	0.00 (0.0)
	110	0.03 (1.0)	0.06 (2.0)	0.00 (0.1)	0.00 (0.0)	0.00 (0.0)	0.00 (0.0)	0.00 (0.0)

**TABLE 5.7**    **CORSIM Performance Index Definitions**

<b>Performance Index</b>	<b>Performance Description</b>
1	Low performance passenger car
2	High performance passenger car
3	Single-unit truck
4	Semi-trailer truck with medium load
5	Semi-trailer truck with full load
6	Double-bottom trailer truck
7	Conventional bus

One additional acceleration characteristic utilized in the CORSIM model to account for vehicle operations is the jerk value, or rate of change of acceleration. The jerk value is utilized to govern the maximum change allowed in the value of acceleration from one time-step to the next. The units for the jerk value are feet per second cubed since this value represents a rate of change for the acceleration value (i.e., third derivative of position). Very little information is available in the literature on the jerk value and how this parameter affects the performance of vehicles both within the simulation and in real-world application. A handful of literature is available on jerk value threshold rates for use in transit application and fixed guideway design. An early study by Botzow on the development of a level of service concept for evaluating public transportation provided information on acceptable jerk values based on passenger comfort. Botzow's research indicated that jerk rates about 0.19g per second (6.0 feet per second cubed) were undesirable for passengers (160). In a study by Frankel et al. on intelligent vehicle highway system (IVHS) technology, a jerk rate of 0.25g per second (8.2 feet per second cubed) was recommended for merge simulations on IVHS vehicle analysis (161). This study indicates further that the literature currently suggests jerk values that range between 0.20g per second and 0.25g per second (6.6 to 8.2 feet per second cubed) as comfortable for design.

To understand the effects of this parameter and to make a determination on the impacts that this value had on the simulation, a sensitivity analysis was conducted on the two test networks outlined previously. The purpose of the sensitivity analysis was to determine the magnitude of impact for variations in the jerk value. The sensitivity analysis was conducted on both the IH-10 and the US 290 CORSIM networks. The default value of 0.22g per second (7.0 feet per second cubed) was utilized in the initial analysis and was then adjusted within a range of acceptable limits of 0.03g per second and 0.31g per second (1 to 10 feet per second

cubed, respectively). No change was recorded in any of the network statistics for the model between the default value and the upper limit of 0.31g per second (10 feet per second cubed), while the lower limit of 0.03g per second (1 foot per second cubed) showed no change in overall travel time (minutes per vehicle mile) or delay time (minutes per vehicle mile), and less than 1 percent variation in total delay (vehicle minutes) on the network. These results suggested that the sensitivity of the jerk value for this network and level of congestion was low and that the default value of 0.22g (7 feet per second cubed) was acceptable and was, therefore, retained in the analysis.

**5.3.2.3 Fleet Distribution** The final parameters for calibration in the CORSIM model are the fleet distribution parameters identified in record type 71 of the CORSIM model. This record allows the user to modify fleet component and vehicle type characteristics according to actual vehicle distributions (102). Section 4 outlined a methodology to develop a distribution of vehicle types based on ITS data. The distribution generated provided an opportunity to calibrate the simulation model based on actual vehicle distributions. The distribution yielded three distinct heavy vehicle classifications that were used in conjunction with AVC data within the study network to develop network-specific vehicle characteristics for use in analysis. The primary vehicle characteristics of interest include: 1) bumper-to-bumper vehicle length; 2) vehicle performance index; and 3) vehicle distribution. Each of these topics will be addressed in the following subsections.

*5.3.2.3.1 Bumper-to-Bumper Vehicle Length* The methodology identified in Section 4.2.2 produced distributions of both weight and spacing for each of the three groups identified. These distributions provided data for the full analysis of vehicles, as well as disaggregate data by peak period. The spacing distributions provided data that were relatively consistent for both the aggregate and disaggregate analysis; therefore, the full analysis results were utilized in developing bumper-to-bumper lengths for each of the three distributions. A summary of the results of the total spacing distribution is provided in Table 5.8.

The results of this table illustrate the variability that exists in the total spacing for each individual vehicle as a function of the group. Based on this variability, rather than develop vehicle design spacing based on the mean value as has been commonly used throughout the analyses in this dissertation, it was determined that a comparison of 85<sup>th</sup> percentile design

spacing would be considered, along with a comparison of the data histograms to those of a normal distribution, and to then compare the resulting vehicle spacing with standard AASHTO design vehicle configurations.

**TABLE 5.8 Summary of Total Spacing Distributions for Full Analysis**

<b>Group</b>	<b>Minimum</b>	<b>Maximum</b>	<b>Mean</b>	<b>Std. Dev.</b>
A	11.0	23.6	14.8	3.1
B	13.3	68.2	33.0	11.8
C	22.1	98.5	58.4	4.9

To accomplish this objective, histograms of total spacing for each group were generated based on the standards identified previously. In addition to the generation of the histograms, the normal distribution of the data was also plotted to determine the approximate properties of the distribution of the data. The results of the total spacing histogram with normal distribution plot for Group A is provided in Figure 5.9, for Group B in Figure 5.10, and for Group C in Figure 5.11. Figures 5.9 and 5.11 clearly show that the total spacing for Group A and Group C follow very closely that of a normal distribution. Figure 5.10 shows that the distribution for Group B, however, may not actually follow a normal distribution since it appears to include two peaks. An alternative analysis to provide a distribution that more closely follows a normal distribution would be to disaggregate the data to provide two groups of spacing data for this group. This was considered in the analysis but, given that the majority of the data fall below the mean spacing value, utilizing a normal distribution with one peak was determined to be a conservative estimate and was used in the analysis.

The first step in generating the distributions was to determine where the 85<sup>th</sup> percentile of the distribution would occur based on standard normal distribution procedures. Utilizing a standard normal distribution table, the probability that a given value was less than or equal to the 85<sup>th</sup> percentile of a normal distribution was calculated. The resulting standard normal random variable  $Z$ , was calculated to be 1.04 based on the cumulative standard normal distribution table (136). The 85<sup>th</sup> percentile spacing was then calculated according to Equation 5.17 by rearranging terms and substituting the mean and standard deviation for each group.

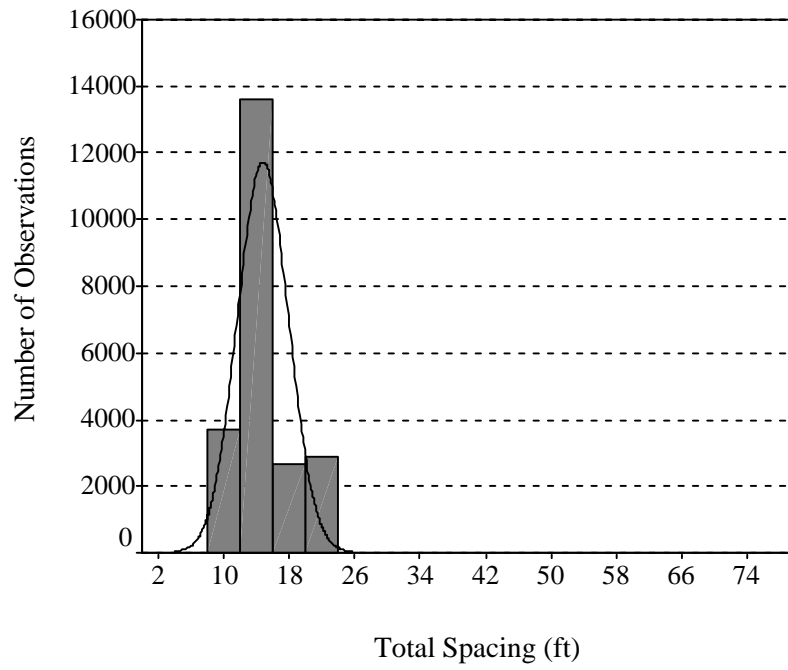


**FIGURE 5.9 Group A total spacing histogram with normal distribution displayed**

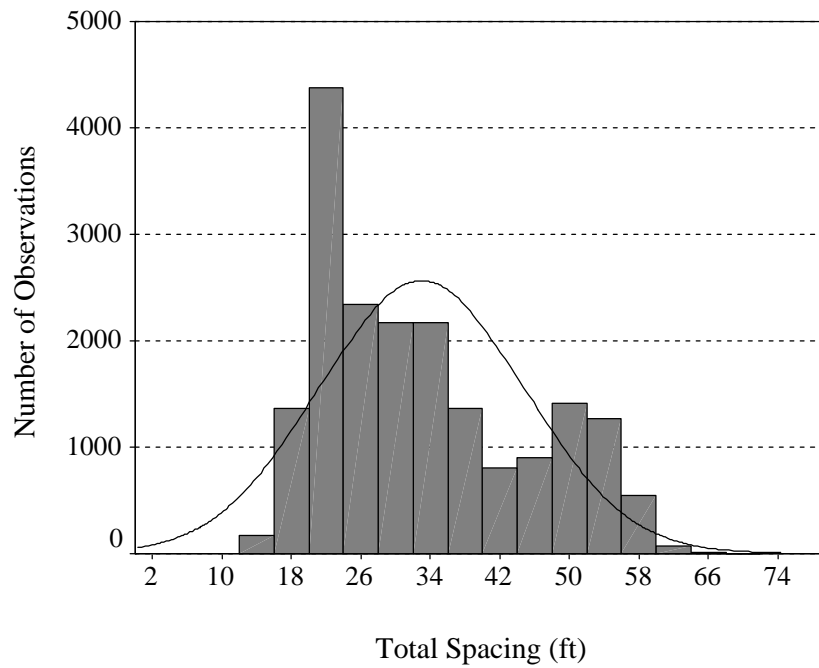


**FIGURE 5.10 Group B total spacing histogram with normal distribution displayed**

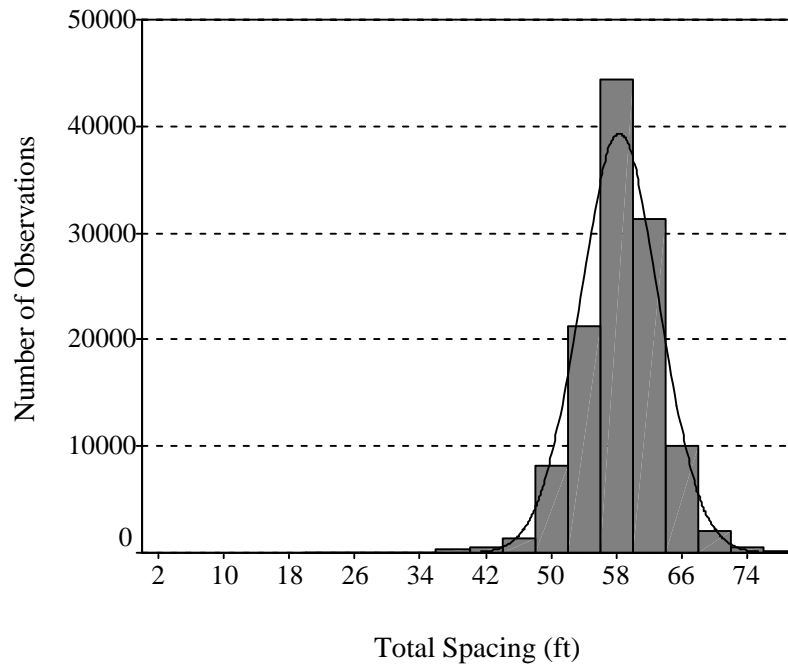


**FIGURE 5.11 Group C total spacing histogram with normal distribution displayed**

$$Z = \frac{X - \mu}{\sigma} \quad (5.17)$$

where:  $Z$  = standard normal random variable;  
 $X$  = normal random variable;  
 $\mu$  = mean value of the normal random variable; and  
 $\sigma$  = standard deviation of the normal random variable.

The normal random variable to calculate based on this equation was the design spacing for each of the vehicle groups. The resulting equation to calculate the design spacing, therefore, was as outlined in Equation 5.18.

$$S = 1.04\sigma + \mu \quad (5.18)$$

where:  $S$  = design spacing (ft).

To calculate the required parameter for bumper-to-bumper spacing, however, additional length must be added to the design spacing to accommodate overhang on the front and rear of

each vehicle. The standard overhang for each of the design vehicles can be calculated using Exhibit 2-1 of the 2001 AASHTO Green Book (15), based on the general vehicle type for each of the three groups. Group A, for example, includes only FHWA Class 5 vehicles, which are categorized as two-axle, six-tire, single-unit trucks. The standard overhang for this vehicle type was determined to be 6 feet for the rear and 4 feet for the front, for a total of 10 feet of overhang. Group B and C include more diversity in their design but can generally be classified as intermediate or interstate semi-trailers. This design vehicle includes standard overhang values between 2.5 feet and 4.5 feet for the rear, and 3 feet to 4 feet in the front, for a total overhang of 5.5 to 8.5 feet. The total bumper-to-bumper vehicle length, therefore, can be calculated according to Equation 5.19.

$$B = S + O \quad (5.19)$$

where:  $B$  = total bumper-to-bumper spacing (ft) and  
 $O$  = overhang (ft).

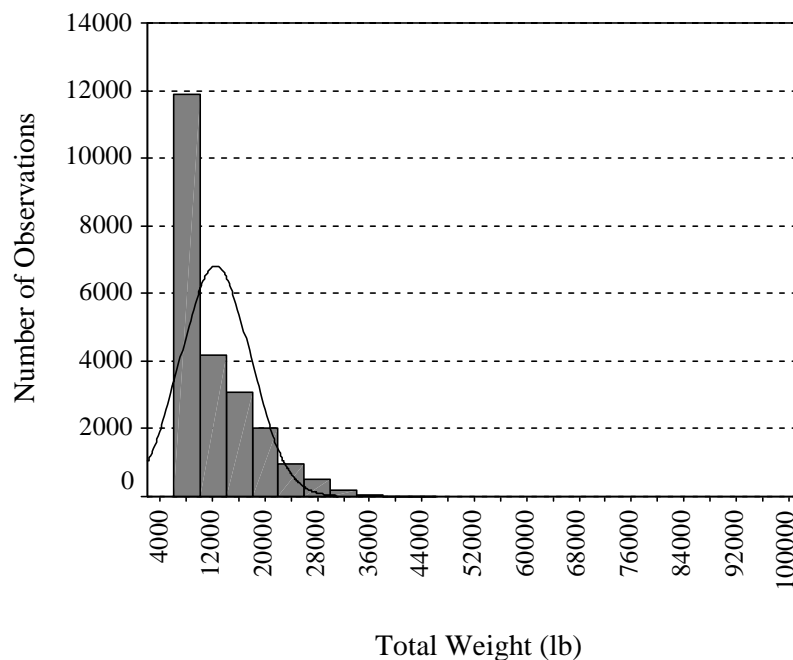
The results of the analysis as well as the recommended spacing for each group are summarized in Table 5.9. The recommended spacing of 30 feet for Group A corresponds to the design bumper-to-bumper length of an AASHTO single-unit (SU) vehicle. The recommended spacing of 55 feet for Group B corresponds to the bumper-to-bumper length for an AASHTO WB-50 design vehicle, while the recommended spacing of 73 feet for Group C corresponds to the bumper-to-bumper length for an AASHTO WB-65/WB-67 design vehicle (15). Because the design spacing distributions provided results that closely match those of standard AASHTO design vehicles, it was determined that these values would be used in the analysis.

**TABLE 5.9 Summary of Total Spacing Distributions**

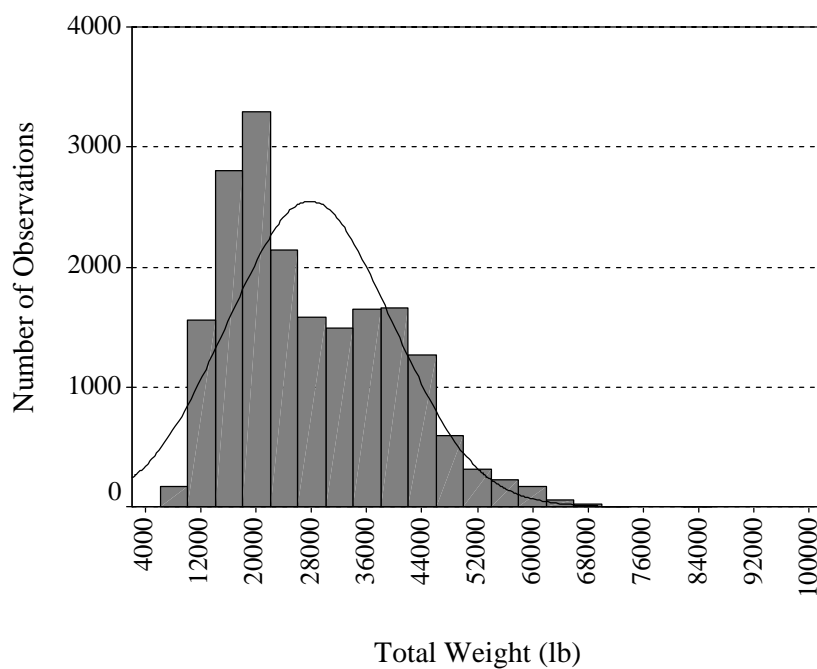
Group	Mean $\mu$ , (ft)	Std. Dev. $\sigma$ , (ft)	Design Spacing $S$ , (ft)	Overhang $O$ , (ft)	Total Spacing $B$ , (ft)	Recommended Spacing (ft)
A	14.8	3.1	18.0	10.0	28.0	30
B	33.0	11.8	45.3	8.5	53.8	55
C	58.4	4.9	63.5	8.5	72.0	73

*5.3.2.3.2 Vehicle Performance Index* The next step in the calibration of the fleet distribution was the determination of the vehicle performance index for each of the vehicle types. The standard performance indexes were identified previously in Table 5.7, while the standard maximum acceleration values were outlined in Table 5.6. Given the variability in the vehicle fleet and the range of operating characteristics possible for each of these vehicles, it was determined that this analysis would utilize the standard maximum acceleration values based on the standard performance index. An alternative approach would be to pull a representative distribution of vehicles from the traffic stream and develop a distribution for acceleration and deceleration characteristics. This was not, however, completed as part of the analysis.

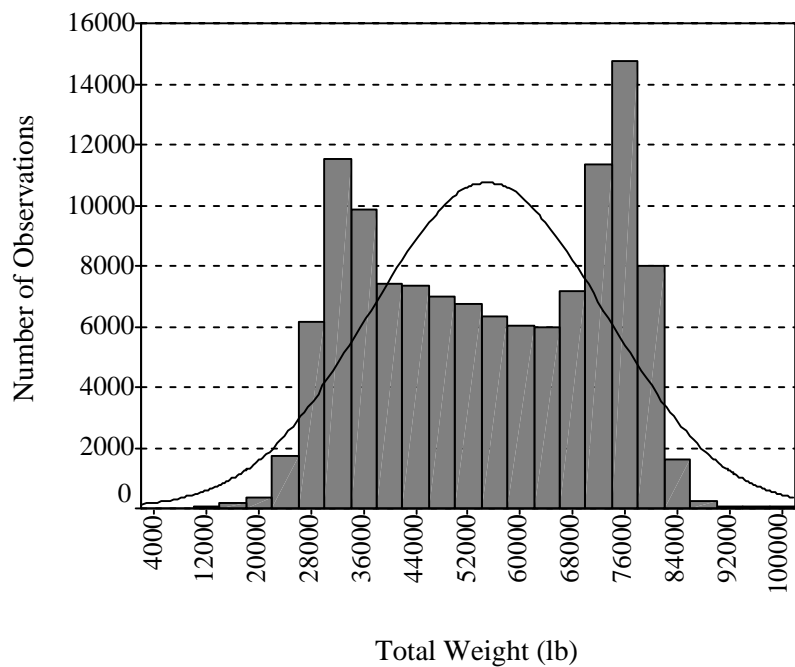
The opportunity still existed, however, to select specific a performance index for each of the CMV truck distributions based on actual conditions. To accomplish this task, specific weight characteristics for each of the groups were analyzed using histograms of the weight data following the same guidelines outlined in the previous sections. Again, the normal distribution plots were added to aid in the analysis and representation of the data. The results of this histogram for Group A are provided in Figure 5.12, for Group B in Figure 5.13, and for Group C in Figure 5.14.



**FIGURE 5.12 Group A total weight histogram with normal distribution displayed**



**FIGURE 5.13** Group B total weight histogram with normal distribution displayed



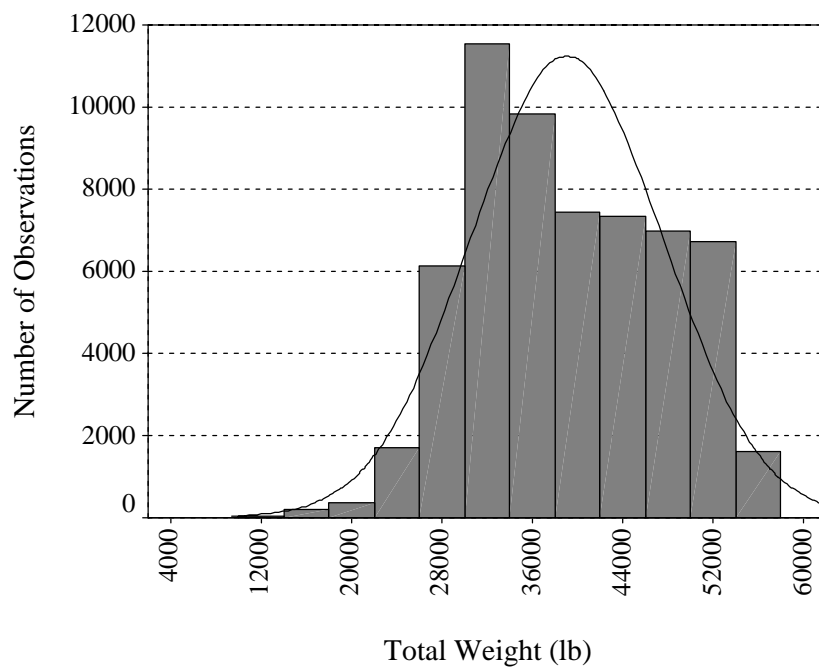
**FIGURE 5.14** Group C total weight histogram with normal distribution displayed

Figure 5.12 (Group A) shows a weight distribution that is somewhat skewed to the left, but that appears to generally follow a normal or lognormal distribution with one primary peak in total weight. Figure 5.13 (Group B) shows somewhat differing results, with one primary peak at approximately 20,000 pounds GVW and a smaller, less pronounced peak at approximately 40,000 pounds GVW. Figure 5.14 (Group C) shows two pronounced peaks at approximately 32,000 pounds and 76,000 pounds GVW. The results for both Group B and Group C would point toward the need to break each distribution into two separate groups, one to accommodate lighter empty trucks and the second to accommodate heavier, loaded vehicles. The distribution outlined in the Group B results, however, is slightly skewed to the left, indicating that the majority of the vehicles have lighter weight characteristics, indicating that the current distribution may, in fact, be somewhat conservative since the overall weight distribution would be slightly heavy. The results for Group C, however, show that the majority of the data are actually heavier, thus establishing the need to disaggregate the data into two distributions of vehicles, one for empty trucks and one for loaded trucks.

To generate the two distributions, the data were disaggregated according to the mean total weight, or mean GVW of the vehicles. The first group included vehicles with a GVW less than the mean of 55,000 pounds, while the second group included vehicles with GVW greater than or equal to 55,000 pounds. The descriptive statistics for the original Group C results, along with each subgroup, are provided in Table 5.10. The resulting histograms and normal distribution for subgroup C1 and subgroup C2 are subsequently provided in Figures 5.15 and 5.16, respectively. These figures clearly show an improvement in the relationship between total weight and the resulting distribution of this weight. Figure 5.15 provides a distribution for empty vehicles, while Figure 5.16 provides the distribution for loaded trucks. These distributions can be used in the simulation to better accommodate the effects of CMV in the simulation model.

**TABLE 5.10 Group C Final Distribution Disaggregate Analysis Results**

	Total Weight (lb)				
	N	Minimum	Maximum	Mean	Std. Dev.
Group C	120,047	10,900	139,600	54,927.18	17,806.96
Subgroup C1 (GVW < 55,000 lb)	59,903	10,900	54,900	39,050.58	8,487.15
Subgroup C2 (GVW ≥ 55,000 lb)	60,144	55,000	139,600	70,740.16	7,749.34



**FIGURE 5.15 Subgroup C1 total weight histogram with normal distribution displayed**

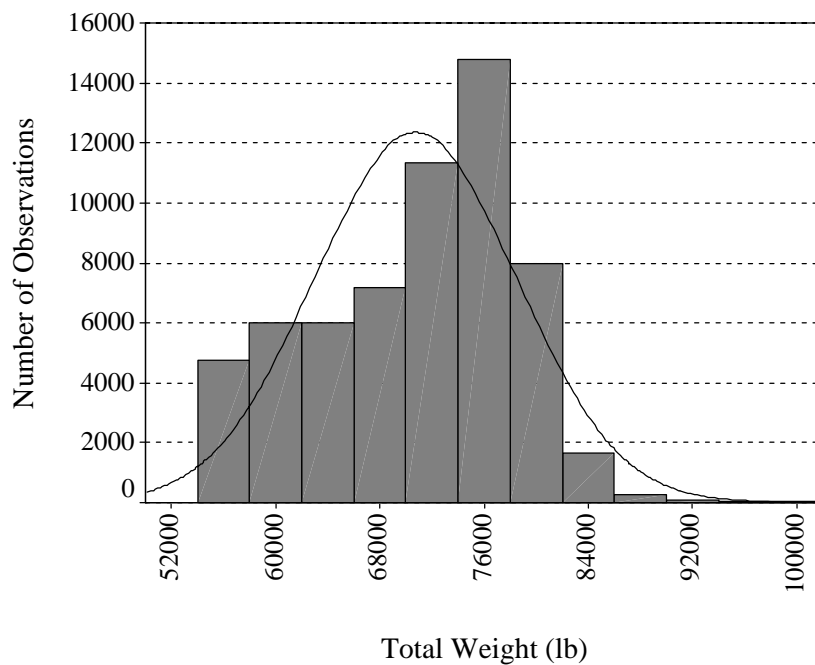


**FIGURE 5.16 Subgroup C2 total weight histogram with normal distribution displayed**

To account for the spacing and weight distributions outlined in the previous section using CORSIM, four specific categories of trucks were modeled. These categories included spacing characteristics for the original three distributions, with the third distribution (Group C) disaggregated to account for both empty and loaded trucks. Based on average weight for each category, the corresponding performance index in CORSIM was assigned to the distribution. The results of this assignment and the corresponding distribution are provided in Table 5.11.

**TABLE 5.11 Final Distribution for CORSIM Analysis**

	<b>Bumper-to-Bumper Spacing (ft)</b>	<b>Mean Total Weight (lb)</b>	<b>Performance Index<sup>1</sup></b>
Group A	30	12,435	3
Group B	55	27,774	4
Group C1	73	39,051	4
Group C2	73	70,740	5

<sup>1</sup> Refer to Table 5.7 for a definition of each performance index

*5.3.2.3.3 Vehicle Distribution* The final step in the calibration of parameters was the distribution of the vehicle types on the roadway network. The distribution of vehicles was calculated using AVC data on both the IH-10 and US 290 corridors. The distributions generated in Section 4.2.2 included data from across the state of Texas due to the limited availability of WIM data in all areas of the state. AVC data, however, is much more readily available and is utilized to generate both total truck percentages for use in the model, as well as distribution of trucks based on the distribution outlined. The data sites utilized for the analysis included HP-850 on IH-10 and MS-3 on US 290. These data were collected in 2001 for 24 hours at each of the locations outlined as part of the TxDOT data collection program.

Using the data from the AVC sites, the total vehicle fleet distribution based on FHWA class was calculated according to Equations 5.20 and 5.21. The resulting truck distribution by group was subsequently calculated using Equations 5.22 and 5.23. The results of the analysis are summarized in Table 5.12 for total truck percentage at each location and time period analyzed, and in Table 5.13 for truck distribution by group for each location and time period analyzed. It is important to recall that the truck percentage distribution for Group C has been disaggregated based on the results presented in the previous section to include distributions for subgroups C1 and C2.

The results of Table 5.13 identify a distribution of CMVs that is different from the original WIM distribution identified in Section 4.2.2. This can be expected because the majority of the WIM sites utilized to generate the distribution were of a rural interstate nature, while the data collected on IH-10 and US 290 for this analysis are from an urban interstate setting. As a result, a higher percentage of single-unit trucks have been observed in the test network. In addition, the data utilized to generate the vehicle distributions included a cut-off value for trucks at 8,000 pounds. The AVC data, however, do not include such a calibration parameter, thus increasing the total number of vehicles that could be observed, particularly in the Group A (FHWA Class 5) category. Even with the different vehicle mix in the test network, the weight characteristics are assumed to be the same.

The final CORSIM input file for the AM peak period IH-10 test network based on the discussion in this section can be found in Appendix D.

$$\% Trucks = 100 \left( \frac{1}{N} \sum_{f=4}^{13} T_f \right) \quad (5.20)$$

$$\% Autos = 100 - \% Trucks \quad (5.21)$$

where:  $N$  = total number of observed vehicles;  
 $T_f$  = number of trucks by classification  $f$ ; and  
 $f$  = FHWA classification.

$$T_g = \sum_{f \in g} T_f \quad \forall g = 1, G \quad (5.22)$$

$$\% Trucks_g = 100 \left( \frac{T_g}{T} \right) \quad (5.23)$$

where:  $G$  = total number of truck distribution groups;  
 $T_g$  = number of trucks by group  $g$ ;  
 $T$  = total number of trucks; and  
 $g$  = classification group.

**TABLE 5.12 Total Truck Percentage 2001**

Location	Time Period	Auto (%)	Truck (%)
IH-10	AM peak (7:00 a.m. to 8:00 a.m.)	97	3
	Off peak (2:00 p.m. to 3:00 p.m.)	91	9
	PM peak (5:00 p.m. to 6:00 p.m.)	94	6
US 290	AM peak (7:00 a.m. to 8:00 a.m.)	94	6

**TABLE 5.13 Truck Percentage by Distribution**

Location	Time Period	Group A (%)	Group B (%)	Group C (%)	
				Subgroup C1 (%)	Subgroup C2 (%)
IH-10	AM peak (7:00 a.m. to 8:00 a.m.)	39	32	15	14
	Off peak (2:00 p.m. to 3:00 p.m.)	50	10	20	20
	PM peak (5:00 p.m. to 6:00 p.m.)	44	23	17	16
US 290	AM peak (7:00 a.m. to 8:00 a.m.)	57	11	16	16

#### 5.4 Concluding Remarks

To adequately model traffic conditions using microscopic traffic simulation models, these models must be calibrated. Calibration is defined in this application as the process in which the model parameters are adjusted such that the model accurately reflects specific components of the system being modeled. Model calibration is essential to accurately portray existing conditions and to adequately analyze future traffic. One aspect of the calibration process that has not historically been included is the calibration of vehicle composition, including an analysis of the effects of vehicle composition on the traffic stream. A conceptualization of a proposed calibration methodology is presented in this section to include the effects of CMVs in microscopic traffic simulation models. This methodology includes primarily the standard supply and demand input for the model, supplemented with a vehicle-specific trip (OD) matrix, as well as vehicle-specific characteristics such as length, weight, classification, and operating characteristics.

To apply the concepts outlined in the calibration methodology, an application using the CORSIM model was introduced. CORSIM was identified for this analysis, since it is arguably the most commonly used microscopic traffic analysis tool in the United States. Two freeway test networks were identified for the analysis, both of which are located west of downtown Houston,

Texas. The first network includes analysis of a 13.9-mile segment of the IH-10 Katy Freeway. The second test network is located on US 290 and includes a 14.3-mile section of this network. Both test networks include both volume and travel time data to be utilized in the analysis.

The final section outlines the calibration parameters available in CORSIM that allow the user to calibrate, or fine-tune the model to match existing conditions. The calibration parameters are discussed in terms of both general calibration parameters and vehicle-specific calibration parameters. One of the most critical general calibration parameters identified in the analysis were the car-following sensitivity parameters. These parameters have been analyzed in several different research projects and have been shown to have an effect on the results of the simulation. In addition to the car-following sensitivity factors, acceleration, deceleration, and lane-change factors were also considered to be important in the general calibration parameter analysis.

The vehicle-specific calibration parameters were identified to be composed of three primary categories: 1) maximum non-emergency deceleration by vehicle type; 2) speed and acceleration characteristics; and 3) fleet distribution. The non-emergency deceleration characteristics, as well as the speed and acceleration characteristics, were analyzed according to general vehicle characteristics, with ranges identified for use in calibration analyses. The fleet distribution characteristics were calibrated based on the results of Section 4, where a methodology to generate a distribution of vehicle types based on ITS data was developed. These classifications were used in conjunction with AVC data available within the study network to generate network-specific vehicle characteristics for use in analysis.

The vehicle characteristics developed based on this methodology included: 1) bumper-to-bumper vehicle length; 2) vehicle performance characteristics (based on vehicle weight); and 3) overall distribution of vehicles within the traffic stream. The results of this analysis identified four distributions of CMVs, in addition to the standard automobile distributions. The four distributions can be summarized as follows: 1) 30-foot-long single-unit truck, average total weight 12,500 pounds; 2) 55-foot-long semi-trailer truck, average total weight 28,000 pounds (medium load); 3) 73-foot-long semi-trailer truck, average total weight 40,000 pounds (medium load); and 4) 73-foot-long semi-trailer truck, average total weight 71,000 pounds (full load).

The resulting CMV distribution and calibration parameters provided an opportunity to analyze the traffic stream and to provide a more accurate calibration of the test network, a topic that will be discussed in more detail in the next section of this dissertation.

## 6. AUTOMATED CALIBRATION METHODOLOGY

Section 2.6 identified the GA automatic calibration methodology as the method of calibration selected for this dissertation to accommodate CMVs using microscopic traffic simulation models. The purpose of this section is not to develop the GA but to utilize previous GA calibration research, build upon this research, and provide an automated calibration methodology to accommodate CMV calibration utilizing microscopic traffic simulation models.

The contents of this section have been organized to discuss the basis of the GA and its application in this dissertation, outline the alternatives utilized for comparison within the GA, and finally calibrate the test networks for utilization in the remainder of the analysis. To accomplish this objective, this section has been divided into seven subsections. The first three provide a discussion of the GA calibration code, parameter distribution alternatives, and evaluation criteria. Following this discussion, the fourth subsection provides an application of the GA methodology, followed in the fifth subsection by a sensitivity analysis of the GA model calibration parameters. The sixth subsection provides the final model selection and network calibration results, while seventh provides concluding remarks on the analysis.

### 6.1 Genetic Algorithm Calibration Code

The GA calibration code utilized for this dissertation was written in the Perl language and was originally developed at the TTI TransLink<sup>®</sup> Research Center (9, 123). This code was modified to meet the needs of this dissertation, including adjustment of the minimum and maximum values for several of the calibration parameters identified in Section 5.3, development of two new car-following parameter distribution algorithms discussed later in this section, and inclusion of maximum non-emergency deceleration rates outlined in Section 5.3.2.1 as part of the automated calibration process, as well as modifications to some of the calibration logic included in the original model to meet the needs of CMV simulation and to improve calibration success.

Each of the 28 parameters identified in Section 5.3 have been coded for binary representation in preparation for utilization in the automatic calibration methodology. The default parameters as well as the minimum value, maximum value, required chromosome length, and location of the parameter in the chromosome are summarized in Table 6.1. Each of the binary string lengths were calculated based on a precision value of 1 (binary), with a total bit length to represent all parameters of 163 bits. This yields a search space for the CORSIM

analysis of  $2^{163}$ , illustrating the importance of a robust analysis technique for optimization to find a suitable parameter set.

**TABLE 6.1 Calibration Parameter Set**

Description	Default Value	Min. Value	Max. Value	Bit Length	$x_{ij}$
Car-Following Sensitivity Factor for Driver Type 1 through 10 (1/100 sec)	35-125	30	150	7 x 10	$x_{i1}$ - $x_{i70}$
PITT Car-Following Constant (ft)	10	3	10	3	$x_{i71}$ - $x_{i73}$
Lag to Accelerate (1/10 sec)	3	1	10	4	$x_{i74}$ - $x_{i77}$
Lag to Decelerate (1/10 sec)	3	1	10	4	$x_{i78}$ - $x_{i81}$
Time to Complete a Lane-Change Maneuver (1/10 sec)	20	10	60	6	$x_{i82}$ - $x_{i87}$
Minimum separation for generation of vehicles (1/10 sec)	16	10	30	5	$x_{i88}$ - $x_{i92}$
Mandatory Lane-Change Gap Acceptance Parameter	3	1	6	3	$x_{i93}$ - $x_{i95}$
Percent of Drivers Desiring to Yield Right-of-Way to Lane-Changing Vehicles	20	5	40	7	$x_{i96}$ - $x_{i101}$
Multiplier for Desire to Make a Discretionary Lane-Change	5	1	10	4	$x_{i102}$ - $x_{i105}$
Advantage Threshold for Discretionary Lane-Change	4	1	10	4	$x_{i106}$ - $x_{i109}$
Maximum Non-Emergency Freeway Deceleration for Vehicle Type 1 (1/10 ft/sec <sup>2</sup> )	80	70	120	6	$x_{i110}$ - $x_{i115}$
Maximum Non-Emergency Freeway Deceleration for Vehicle Type 2 (1/10 ft/sec <sup>2</sup> )	80	70	120	6	$x_{i116}$ - $x_{i121}$
Maximum Non-Emergency Freeway Deceleration for Vehicle Type 3 (1/10 ft/sec <sup>2</sup> )	80	40	100	6	$x_{i122}$ - $x_{i127}$
Maximum Non-Emergency Freeway Deceleration for Vehicle Type 4 (1/10 ft/sec <sup>2</sup> )	80	40	100	6	$x_{i128}$ - $x_{i133}$
Maximum Non-Emergency Freeway Deceleration for Vehicle Type 5 (1/10 ft/sec <sup>2</sup> )	80	40	100	6	$x_{i134}$ - $x_{i139}$
Maximum Non-Emergency Freeway Deceleration for Vehicle Type 6 (1/10 ft/sec <sup>2</sup> )	80	40	100	6	$x_{i140}$ - $x_{i145}$
Maximum Non-Emergency Freeway Deceleration for Vehicle Type 7 (1/10 ft/sec <sup>2</sup> )	80	40	100	6	$x_{i146}$ - $x_{i151}$
Maximum Non-Emergency Freeway Deceleration for Vehicle Type 8 (1/10 ft/sec <sup>2</sup> )	80	70	120	6	$x_{i152}$ - $x_{i157}$
Maximum Non-Emergency Freeway Deceleration for Vehicle Type 9 (1/10 ft/sec <sup>2</sup> )	80	70	120	6	$x_{i158}$ - $x_{i163}$

## 6.2 Parameter Distribution Alternatives

The discussion in Section 5.3 outlined the calibration parameters for the CORSIM model. Similar calibration parameters can be found in any representative microscopic traffic simulation model. The first 11 calibration parameters are utilized in the model to replicate driver performance variability. As was explained in detail in Section 5.3.1, the first 10 parameters are car-following sensitivity factors that are utilized to represent the car-following characteristics of drivers within a population. One of the challenges in replicating these car-following sensitivity factors is determining the methodology to utilize in developing the different factors for a range of driver types. As was identified in Section 5.3.1, the default car-following sensitivity factors for CORSIM range from 1.35 seconds to 0.35 seconds, with a linear relationship utilized to identify the sensitivity factors for the remaining driver types. This section further identified the range of values to be utilized in this analysis as a range from 1.50 seconds to 0.30 seconds.

Two alternatives have been considered to represent the distribution of the car-following sensitivity parameters. The first alternative is to treat each parameter as an independent random value and to model the parameters individually. The second alternative is to model the car-following sensitivity factors utilizing statistical distributions based on the mean and standard deviation of the distribution. The disadvantage to the first approach is the inability to replicate the distribution using simply the standard statistical measures of mean and variance. Although the measures of central tendency and dispersion (i.e., mean, variance) can be calculated for the matrix of sensitivity factors, the distribution of these factors cannot be duplicated from these measures. In the second alternative, rather than model each parameter individually, values for the mean and standard deviation of the distribution of driver types would be determined, with the sensitivity factors developed according to this distribution. This alternative has three primary advantages: 1) a statistical distribution of individual driver characteristics can be generated from the mean and variance; 2) redundancy in the calibration parameters can be reduced since the alternative would require only two parameters (mean and standard deviation) rather than 10; and 3) the process is simpler.

To determine the distributions to consider in modeling car-following behavior, headway analysis was considered due to the direct relationship between car-following sensitivity and vehicle headway. Early research indicates that headway distributions generally follow a normal distribution (57). Research performed by Daou in the early 1960s, however, analyzed the nature of driver behavior within platoons and concluded that when vehicles are classified according to

speed, the logarithms of their headways are normally distributed, and thus the headways are distributed according to a lognormal distribution (162). During this same time period, Greenberg utilized a stochastic process to describe vehicular traffic that led to the same conclusion (163). Subsequent studies have confirmed this assumption, with researchers demonstrating that the lognormal distribution may be superior to the normal distribution, particularly at high traffic flows (164, 165).

As a result of the results outlined in the literature, two distributions were considered for analysis of car-following sensitivity: 1) lognormal and 2) normal. The purpose for including both the normal and the lognormal distribution was to compare the two distributions and to determine which distribution is best suited for the simulation model. A discussion of each of these distributions will be discussed in the following subsections.

### 6.2.1 Lognormal Distribution

A random variable  $X$  whose natural logarithm ( $\ln X$ ) is normally distributed (i.e.,  $\ln X \sim N[\mu, \sigma^2]$ ) is said to have a logarithmic normal, or lognormal distribution. In the case of the lognormal distribution, the probability density function (pdf) of  $X$  can be obtained by the transformation of the normal pdf (166). The pdf of the lognormal distribution is positively skewed and can be obtained utilizing the formula outlined in Equation 6.1 (167). The cumulative distribution function (cdf) can then be obtained from the pdf utilizing Equation 6.2.

$$f_X(x) = \frac{1}{\sqrt{2\pi} \zeta x} e^{-\frac{1}{2} \left( \frac{\ln x - \lambda}{\zeta} \right)^2} \quad 0 \leq x \leq \infty, -\infty \leq \lambda \leq \infty, \zeta > 0 \quad (6.1)$$

where:  $f_X(x)$  = lognormal probability density function;

$X$  = random variable;

$\lambda$  = mean of  $\ln X$ ; and

$\zeta$  = standard deviation of  $\ln X$ .

$$F_X(x) = P\{X \leq x\} = \int_{-\infty}^x f_X(u) du \quad (6.2)$$

where:  $F_X(x)$  = cumulative distribution function.

In the application of the lognormal distribution, the random variable  $X$  represents the distribution of car-following sensitivity factors ( $P_j$ ). To implement the lognormal distribution in the automatic calibration methodology, an algorithm was developed consisting of three primary steps: 1) determination of values for the mean and standard deviation of  $\ln X$ ; 2) transformation of the mean and standard deviation to a pdf and subsequent cdf for a range of  $X$  values; and 3) mapping of the cdf values to obtain the  $X$  values that best represent the full distribution within an acceptable range. More detailed information on each of these steps will be discussed in the following paragraphs.

The first step in developing the lognormal distribution of car-following sensitivity parameters is to determine sample values for the mean and standard deviation of  $\ln X$ , which can be accomplished in one of two ways. The first is through the use of an automated calibration process, while the second would involve actual field measurements of vehicle headway distributions. The automated calibration alternative was used in this dissertation; however, field measurements could also be used to generate the input values.

A modified GA automated calibration program originally developed at the TTI TransLink<sup>®</sup> Research Center (9, 123) in the Perl language was utilized to sample values of the mean of  $\ln X$  ( $\lambda$ ) and the standard deviation of  $\ln X$  ( $\zeta$ ) from a specified range of values. In the original calibration methodology, car-following sensitivity parameters within the specified range are selected at random as the first 10 parameters of the binary string. In the lognormal distribution alternative, these first 10 parameters are replaced with two parameters, one to represent the mean of  $\ln X$  and the second to represent the standard deviation of  $\ln X$ . The range outlined for the mean ( $\lambda$ ) corresponds to the natural log of the upper and lower limits of the car-following sensitivity factors (30 to 150), or a range of 3.4 ( $\ln 30$ ) to 5.0 ( $\ln 150$ ). This range allows the majority of the mean values to fall within the variable range of 30 to 150. Those values that may extend beyond this range are then truncated to the upper and lower limits, as will be explained later. The range for the standard deviation ( $\zeta$ ) was calculated based on the standard ranges that occur between the mean ( $\mu$ ) and standard deviation ( $\sigma$ ) of a normal distribution. In a standard normal distribution, approximately 99 percent of all values fall within a range between plus or minus three standard deviations. Given the range of 30 to 150 outlined for the upper and lower limits of the random variable,  $X$ , a minimum standard deviation range was calculated to be approximately 20. This normal range was then converted to lognormal values for a corresponding range of 0.1 to 3.0 ( $\ln 20$ ) for the lognormal distribution. The length of the binary

string is subsequently reduced from the original model for 10 parameters with a precision level of 1 (70 bits) to the new model with only two parameters with a precision level of 0.01 (17 bits).

The two parameters ( $\lambda$  and  $\zeta$ ) are utilized in Equations 6.1 and 6.2 to generate the pdf and subsequent cdf for a range of variables corresponding to the range identified previously for the car-following sensitivity factors ( $P_1$  through  $P_{10}$ ). The cumulative probability is calculated for each variable within the range and can then be utilized to generate the discrete distribution of car-following sensitivity factors. An example of the cumulative probability that is generated for a range of random variables is provided in Figure 6.1. In this representation, three different values of mean ( $\lambda$ ) are illustrated for one value of the standard deviation ( $\zeta$ ) to show how the cdf varies depending on the mean and standard deviation calculated with the automated calibration procedure.

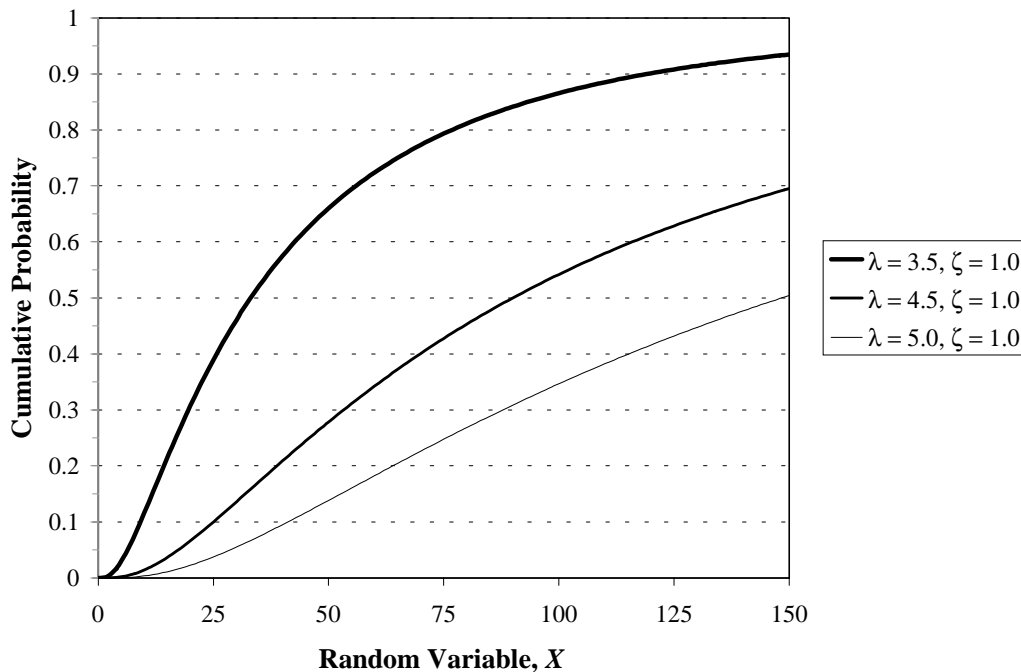


**FIGURE 6.1** Lognormal cumulative distribution function

The final step in generating the car-following sensitivity factors based on the lognormal distribution algorithm is mapping of the cdf values to obtain the parameters for use in the model. Two mapping functions are utilized in this step: 1) generate the random variable that

corresponds to the chosen cumulative probability and 2) “truncate” the values based on the minimum and maximum values identified previously. The first mapping rule finds the  $X$  value that corresponds to a predetermined range within the cdf. To generate a representative population from the cdf,  $X$  values are generated at the midpoint of each of the 10 percentiles within the distribution, based on the mapping rule identified in Equation 6.3. To ensure that the  $X$  values fall within the specified range, a second mapping rule is then utilized, as identified in Equation 6.4. This truncation limits the upper and lower limits of the parameter and thus modifies the lognormal distribution to that of a “truncated lognormal distribution.”

$$P_j = \bar{X}_j \in [l_j < F_X(x|\lambda, \zeta) \leq u_j] \quad \forall j = 1, n \quad (6.3)$$

where:  $P_j$  = car-following factor for parameter  $j$ ;

$\bar{X}_j$  = average  $X$  for parameter  $j$ ;

$l_j$  = lower bound of  $F_X(x/\lambda, \zeta)$  for parameter  $j$  (0.0, 0.1, ..., 0.9);

$u_j$  = upper bound of  $F_X(x/\lambda, \zeta)$  for parameter  $j$  (0.1, 0.2, ..., 1.0);

$F_X(x/\lambda, \zeta)$  = cumulative distribution function of  $x$ , given  $\lambda$  and  $\zeta$ ; and

$n$  = number of car-following parameters ( $n = 10$  in this application).

$$P'_j = \begin{cases} 30, & \text{if } P_j \leq 30; \\ P_j, & \text{if } 30 < P_j \leq 150; \\ 150, & \text{if } P_j > 150. \end{cases} \quad (6.4)$$

where:  $P'_j$  = final car-following sensitivity factor corresponding to parameter  $j$ .

### 6.2.2 Normal Distribution

The normal distribution assumes that the variable  $X$  is normally distributed with mean  $\mu$  and variance  $\sigma^2$ ,  $N(\mu, \sigma^2)$ . In the normal distribution, the mean is utilized to determine the center of the distribution, while the variance determines the width. The normal distribution takes on the shape of a bell curve and is symmetrical about the mean. The pdf of the normal distribution for a random variable  $X$  can be calculated according to Equation 6.5, with the cdf obtained using Equation 6.6 (136).

$$f(x) = \frac{1}{\sqrt{2\pi}\sigma} e^{-\frac{1}{2}\left(\frac{x-\mu}{\sigma}\right)^2} \quad 0 \leq x \leq \infty, -\infty \leq \mu \leq \infty, \sigma > 0 \quad (6.5)$$

where:  $f(x)$  = normal probability density function;

$\mu$  = mean of  $X$ ; and

$\sigma$  = standard deviation of  $X$ .

$$\Phi(z) = P(Z \leq z) = \int_{-\infty}^z f(u) du \quad (6.6)$$

where:  $\Phi(z)$  = cumulative distribution function and

$Z$  = standard normal random variable ( $\mu = 0, \sigma^2 = 1$ ).

The implementation of the normal distribution follows the same basic steps as the lognormal distribution: 1) determination of sample values for the mean and standard deviation of  $X$ ; 2) transformation of the mean and standard deviation to normal random variables; and 3) mapping of the normal random variables within the range of car-following sensitivity factor values. More details on each of these steps are outlined in the following paragraphs.

The first step in the normal distribution alternative is the utilization of the Perl automated calibration program to sample values of the mean ( $\mu$ ) and the standard deviation ( $\sigma$ ) from a range of values. This was accomplished utilizing the same methodology as outlined in the lognormal distribution algorithm; however, rather than set the limits for the minimum and maximum values of the variables to be at the natural log of  $X$ , in this case, the minimum and maximum values were set at the corresponding  $X$  values. Based on the lognormal analysis, the range for the mean ( $\mu$ ) was set between 30 and 150, while the standard deviation ( $\sigma$ ) was initially set between 0.1 and 20. A sensitivity analysis was conducted to ensure that the resulting parameter sets provided a suitable range of values. It was noted in the sensitivity analysis that the parameter values did not consistently provide a distribution over the entire car-following sensitivity factor range, possibly due to the truncation of the dataset. To provide a more conservative range and to allow more flexibility in the optimization program, a range of 0.1 to 50 was utilized. The length of the binary string was again reduced from the original model for 10 parameters with a precision level of 1 (80 bits) to the new model for only two parameters with a precision level of 0.1 (20 bits).

The second step in the calculation of the car-following parameter set from the normal distribution involves calculation of the parameters as normal random variables based on the cumulative standard normal distribution. In this analysis, the values of the standard normal random variable are set to correspond to percentiles that will generate an even distribution amongst the car-following values. These values are determined based on the values of the cdf corresponding to 0.05, 0.15, 0.25, ..., 0.95, as summarized in Table 6.2. These values are then utilized in Equation 6.7, with the mean ( $\mu$ ) and standard deviation ( $\sigma$ ) selected from the automated calibration procedure to calculate the corresponding normal random variables.

**TABLE 6.2 Standard Normal Random Variables**

Parameter ( $j$ )	Cumulative Distribution Function, $\Phi(z)$	Standard Normal Random Variable ( $Z_j$ )
1	0.05	-1.64
2	0.15	-1.04
3	0.25	-0.68
4	0.35	-0.38
5	0.45	-0.13
6	0.55	0.13
7	0.65	0.38
8	0.75	0.68
9	0.85	1.04
10	0.95	1.64

$$P_j = Z_j \sigma + \mu \quad \forall j = 1, n \quad (6.7)$$

where:  $P_j$  = car-following factor for parameter  $j$  and  
 $Z_j$  = standard normal random variable for parameter  $j$ .

The final step in generating the car-following sensitivity factors based on the normal distribution is the mapping of the car-following factors to fall within the range of variable  $X$ . As with the lognormal distribution, this modifies the normal distribution to a “truncated normal distribution” using the same mapping function as the lognormal distribution outlined previously in Equation 6.4. This truncation limits the upper and lower car-following sensitivity factors of the random variable  $X$  to ensure that they fall within the range of 30 and 150.

### 6.3 Evaluation Criteria

Several alternatives for evaluation criteria were considered in the development of an automated calibration methodology, with the primary focus on two main concepts: 1) the source of data utilized in the calibration methodology to compare actual conditions with simulated conditions and 2) the representation of the fitness function generated in the comparison of simulated and actual conditions. Each of these topics will be discussed in detail in the following subsections.

#### 6.3.1 Calibration Data Sources

The implementation of ITS data sources in recent years has increased the availability of traffic data for use in calibration procedures. The primary sources of ITS data were discussed in Section 2.3 and include traffic volume counts, vehicle classification counts, and truck weight monitoring. Two data sources have been utilized for calibration of the simulation model: 1) traffic volume data and 2) travel time ITS data.

**6.3.1.1 Traffic Volume Data** As outlined in Section 5.2.1, traffic volume data were collected along the entire length of both the IH-10 and US 290 corridors using ILD and pneumatic tubes during the months of May and June 1996 as part of an AADT data collection effort. These counts were supplemented by additional data collected in July and August 1996, from which a database of traffic counts was developed. This database was used to summarize Wednesday and Thursday counts that were then aggregated into hourly volumes. The data were analyzed and traffic counts adjusted to ensure consistency across the network and to account for all vehicles from node to node along the network. The time periods analyzed included the AM peak period (7:00 a.m. to 8:00 a.m.) for the IH-10 and US 290 test networks, as well as the off peak (2:00 p.m. to 3:00 p.m.) and PM peak (5:00 p.m. to 6:00 p.m.) periods for the IH-10 test network. More detailed information on the traffic volume counts and the test networks can be found in Section 5.2.1.

**6.3.1.2 Travel Time ITS Data** Section 5.2.1 indicated that AVI data were collected on the IH-10 corridor during the same time period that the traffic volumes were being collected. The AVI data were used to calculate the average space mean travel time for each AVI link by time-of-day during the data collection time periods. The AVI data collected during that time did not include data for US 290; rather it included only data for the IH-10 corridor. As a result of the

availability of data collected during the same time period as the traffic counts on IH-10, these data were utilized in calibration analyses. Because the US 290 data were not available during this same time period, historic travel time data were obtained from the TTI Mobility Monitoring Program for this corridor. The data obtained from TTI included raw AVI speed and travel time data for 2001 on each link along the network, along with historic data from 1997 through 2001 for each of these links for extended peak periods (i.e., 6:30 a.m. to 8:30 a.m. and 4:30 p.m. to 6:30 p.m.). The historic data for travel times along each of the two corridors show that the average speed and travel time have remained relatively constant in the period from 1997 to 2001. As a result of the consistency along the corridor and the availability of raw data for 2001, travel times were extracted from the raw data and utilized to obtain travel time data during the specific peak period (7:00 a.m. to 8:00 a.m.) analyzed. The travel times extracted from the 2001 data were adjusted based on the historic travel time data according to the relationship identified in Equation 6.8 and used in the analysis.

$$TT = TT_T \left( \frac{TT_{h1} - TT_{h2}}{TT_{h2}} \right) \quad (6.8)$$

where:  $TT$  = desired travel time for analysis (US 290 AM peak);  
 $TT_T$  = specific target period travel time data (2001 AM peak);  
 $TT_{h1}$  = historic peak period travel time for desired year (1997); and  
 $TT_{h2}$  = historic peak period travel time for target year (2001).

The peak periods considered in the analysis included AM peak (7:00 a.m. to 8:00 a.m.) for the IH-10 and US 290 test networks, as well as off peak (2:00 p.m. to 3:00 p.m.) and PM peak (5:00 p.m. to 6:00 p.m.) periods for the IH-10 corridor. A summary of the travel times by link for the US 290 corridor by peak period are provided in Table 6.3, while a summary of the travel times by link for the IH-10 corridor are provided in Table 6.4.

The availability of both volume and travel time data provides an alternative to calibrating the simulation model based on either of the two performance metrics, or based on a combination of both travel time and volume. The performance metrics considered in this analysis include volume independent of travel time and a combination of both volume and travel time. These performance alternatives will be discussed in the next section.

**TABLE 6.3 US 290 Link Travel Time and Speed Data**

<b>Peak Period</b>	<b>Link Description</b>	<b>Length (mi)</b>	<b>Travel Time (sec)</b>	<b>Speed (mph)</b>
<b>AM Peak</b>	FM 1960 to Sam Houston Tollway	5.10	417	44
	Sam Houston to Fairbanks	1.55	222	25
	Fairbanks to Pinemont	2.90	377	28
	Pinemont to W. 34 <sup>th</sup>	2.45	312	28
	W. 34 <sup>th</sup> to Dacoma (IH-610)	1.10	227	17

**TABLE 6.4 IH-10 Eastbound Link Travel Time and Speed Data**

<b>Peak Period</b>	<b>Link Description</b>	<b>Length (mi)</b>	<b>Travel Time (sec)</b>	<b>Speed (mph)</b>
<b>AM Peak</b>	Barker Cypress to Eldridge	3.95	413	34
	Eldridge to Sam Houston Tollway	3.65	346	38
	Sam Houston to Blalock	2.25	399	20
	Blalock to Silber (IH-610)	4.05	408	36
<b>Off Peak</b>	Barker Cypress to Eldridge	3.95	217	66
	Eldridge to Sam Houston Tollway	3.65	211	62
	Sam Houston to Blalock	2.25	168	48
	Blalock to Silber (IH-610)	4.05	318	46
<b>PM Peak</b>	Barker Cypress to Eldridge	3.95	238	60
	Eldridge to Sam Houston Tollway	3.65	401	33
	Sam Houston to Blalock	2.25	289	28
	Blalock to Silber (IH-610)	4.05	328	44

### 6.3.2 Identification of Fitness Function

One of the most critical aspects of the GA is the identification of the fitness function. The fitness function value is utilized in the GA to identify how well each chromosome meets the overall objective of the algorithm and to determine subsequent generations. In the case of a minimization problem, the most “fit” individuals are identified from the fitness function value as those with the lowest numerical value of the associated function. Alternatively, in a maximization problem, the most “fit” individual is identified from those with the highest numerical value associated to the function. A variety of functions are available to identify the level of fitness associated with the application, including exponential functions, power functions, linear functions, etc. The basic fitness function is normally used to transform the objective function value into a measure of relative fitness (127). To adequately generate the required

fitness function, the two performance metrics (volume and travel time) must be considered. These performance metrics, along with a discussion of the combination of the two will be discussed in this section.

**6.3.2.1 Traffic Volume Data Fitness Function** The objective function value utilized for traffic volume data in this dissertation is the MAER identified in Equation 6.9. The MAER is commonly used in transportation analyses and is a measure of the relationship between observed and simulated data in this application. Because the MAER returns a value related to the absolute value of the difference between observed and simulated data, the MAER is a minimization function that is difficult to solve mathematically, due to the absolute value criteria. As a result of the difficulty in solving this relationship mathematically, a robust non-gradient technique such as GA is ideal for this situation.

$$g(X_i^t) = MAER(X_i^t) = \frac{1}{M} \sum_{l=1}^M \left( \frac{|V_l^O - V_{il}^E|}{V_l^O} \right) \quad (6.9)$$

where:  $g(X_i^t)$  = traffic volume data objective function (MAER);

$X_i^t$  = parameter set for chromosome  $i$ , generation  $t$ ;

$V_l^O$  = observed volume on link  $l$ ;

$V_{il}^E$  = estimated volume on link  $l$  for simulation of chromosome  $i$ ;

$M$  = number of comparison links in network;

$i$  = chromosome; and

$t$  = generation number.

The fitness function utilized to transform the traffic volume data objective function value into a measure of relative fitness was chosen as an exponential function that would convert the MAER minimization function into an exponential maximization function. The purpose for this conversion from minimization to an exponential maximization function was to provide a better measure of the overall effectiveness of each alternative and to provide a more robust mathematical representation of the results. The basic fitness function chosen for analysis is based on research performed at TTI and is outlined in Equation 6.10. Prior research on the constants in this equation indicated that the value of  $C$  did not seem to affect the convergence

rate of the fitness function, but the value of  $\beta_1$  was critical to convergence (9). These constants will be discussed in more detail in Section 6.5.4.

$$F_V(X_i^t) = f(g(X_i^t)) = C e^{(-\beta_1 g(X_i^t))} \quad (6.10)$$

where:  $F_V(X_i^t)$  = traffic volume data fitness function value and

$C, \beta_1$  = constants.

**6.3.2.2 Travel Time ITS Data Fitness Function** The objective function value utilized for travel time ITS data is the same MAER metric as used in the traffic volume data fitness function. In the development of the travel time MAER value, however, average travel time over a series of nodes is necessary to match the link data for which observed AVI travel time data are available. The base equation to develop the objective MAER is identified in Equation 6.11.

$$g'(X_i^t) = MAER'(X_i^t) = \frac{1}{N} \sum_{n=1}^N \left( \frac{|T_n^O - \sum_{l=1}^M t_{inl}^E|}{T_n^O} \right) \quad (6.11)$$

where:  $g'(X_i^t)$  = travel time objective function (MAER);

$T_n^O$  = mean observed travel time on AVI link  $n$ ;

$t_{inl}^E$  = estimated average travel time on link  $l$  within AVI link  $n$  for simulation of chromosome  $i$ ;

$N$  = number of AVI links in the network; and

$M$  = number of comparison links within the AVI link.

The fitness function utilized to transform the travel time objective function value into a measure of relative fitness was again chosen as an exponential function that would convert the MAER minimization function into an exponential maximization function. The basic fitness function chosen for analysis is outlined in Equation 6.12. In this equation the constant  $\beta_2$  is critical in the convergence and fitness calculation and will be discussed in more detail in Section 6.5.4.

$$F_T(X_i^t) = f(g'(X_i^t)) = C e^{(-\beta_2 g'(X_i^t))} \quad (6.12)$$

where:  $F_T(X_i^t)$  = travel time fitness function value and  
 $C, \beta_2$  = constants.

**6.3.2.3 Volume and Travel Time Fitness Function** When both traffic volume data and travel time ITS data are available for a selected network, both sources of data can be utilized in developing the appropriate fitness function. In this alternative, a combination of volume and travel time fitness values is utilized to determine the best overall fitness function through the use of a control factor to determine the weight to place on either travel time or volume MAER (9). The relationship between the fitness functions and the control factor for comparing volume and travel time metrics is identified in Equation 6.13.

$$F = \alpha F_T + (1 - \alpha) F_V \quad (6.13)$$

where:  $F$  = total fitness function value;  
 $F_V$  = traffic volume data fitness function value;  
 $F_T$  = travel time fitness function value; and  
 $\alpha$  = control factor.

**6.3.2.4 Fitness Function and Probability** The value of the fitness function is utilized in the reproduction of the next generation by increasing the probability of being chosen for reproduction. The  $P$  chromosomes that have the highest fitness values based on volume, travel time, or both are chosen to form the new set of parent chromosomes, where  $P$  is the population size chosen for analysis. The remaining chromosomes are discarded from future use, while the “best” chromosomes are utilized to generate the parent chromosomes of the next generation. At the beginning of each generation, the total fitness value is calculated for the new parent population, according to Equation 6.14. A subsequent probability is then assigned to each of the chromosomes based on the fitness value relative to the total fitness value, as outlined in Equation 6.15. The fitness values and probabilities are utilized in the crossover and mutation steps of the algorithm, concepts that will be discussed in the next sections.

$$F^t = \sum_{i=1}^P F(X_i^t) \quad \forall t = 1, T \quad (6.14)$$

$$p_i = \frac{F(X_i^t)}{F^t} \quad \forall i = 1, N \quad \forall t = 1, T \quad (6.15)$$

where:  $F^t$  = fitness function value for generation  $t$ ;  
 $F(X_i^t)$  = fitness function value for chromosome  $i$ , generation  $t$ ;  
 $P$  = size of the population; and  
 $p_i$  = probability that chromosome  $i$  is selected in the crossover operation.

## 6.4 Genetic Algorithm Application Methodology

As explained in Section 2.6, the GA is an iterative process in which a parent set of chromosomes is developed, analyzed, and then utilized to generate offspring chromosomes that are subsequently analyzed to generate a new population for analysis. This process is continued until the stopping criteria have been attained. There are five basic steps in the GA process, illustrated graphically in Figure 6.2 and outlined briefly in the following subsections.

### 6.4.1 Step 1: Initialization of the GA Parameters and Selection of Parent Population

The first step in the GA algorithm is the initialization of the GA parameters and the selection of the parent chromosomes. As explained in Section 2.6.2.2, the primary operators for the GA include the population size ( $P$ ), the maximum number of iterations or generations ( $T$ ), the crossover probability ( $P_c$ ), and the probability of mutation ( $P_m$ ). In addition, the number of microscopic traffic simulation parameters ( $M$ ) to be calibrated is identified along with a scheme to represent each of the parameters. In this step an initial population of parent chromosomes ( $P$ ) is generated utilizing a random process in which each of the chromosomes is randomly assigned a value of zero or one, with equal probability provided for each alternative.

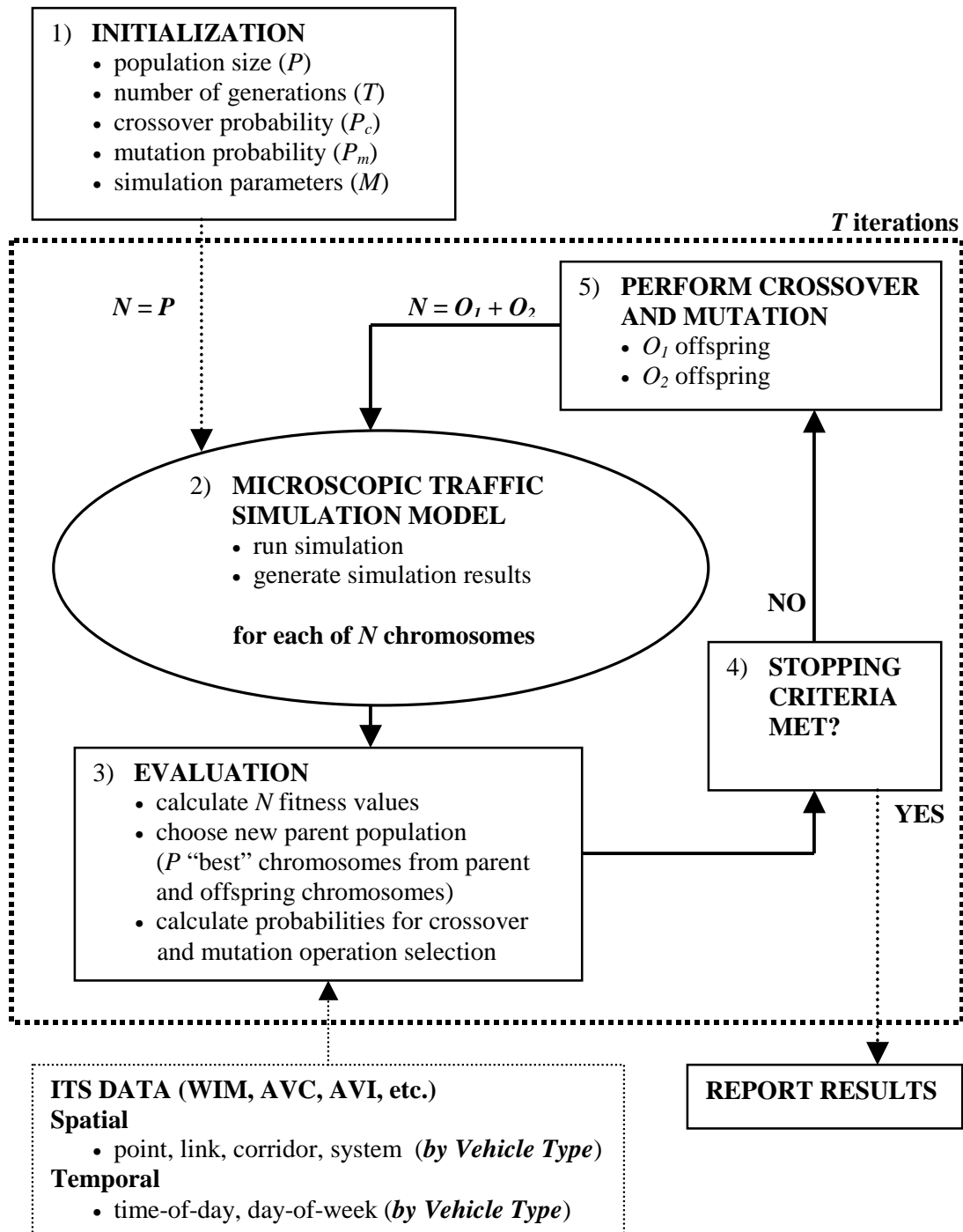


FIGURE 6.2 Genetic algorithm calibration methodology

#### 6.4.2 Step 2: Microscopic Traffic Simulation Model

The next step in the analysis is the operation of the microscopic traffic simulation model. The GA calibration process can easily accommodate a variety of simulation models, the selection of which will affect the format of the parameter set and the simulation output. Regardless of the model chosen for analysis, the simulation is repeated for each of the  $N$  chromosomes in each iteration. It is not possible to set the total number of simulation runs for each iteration prior to the simulation because the number of chromosomes in each iteration, with the exception of the first iteration, is constantly changing based on the results of the crossover and mutation steps outlined in detail in Section 2.6.3.

#### 6.4.3 Step 3: Evaluate Model Output and Select “New” Parameter Set

The evaluation of the model output and selection of the “new” parameter set are some of the most critical components of the GA methodology. The method for reproducing chromosomes for each iteration determines the potential optimization of the parameter set. A variety of reproduction methods are available to pass chromosomes from one generation to another, the easiest of which is to create a biased roulette wheel selection where each current chromosome in the population has a roulette wheel slot sized in proportion to its fitness (110). This roulette wheel selection mechanism was utilized in the evaluation phase and is based upon the fitness function and probability selection explained.

#### 6.4.4 Step 4: Check Stopping Rules

Following the evaluation of the parent or offspring chromosomes, the stopping rules established for the analysis are checked. If stopping rules are met, the algorithm is ended and the results reported. If stopping rules are not met, the algorithm proceeds to step 5 to generate offspring chromosomes and proceed with analysis.

#### 6.4.5 Step 5: Perform Crossover and Mutation Operations

Based on the fitness function and probability of selection, crossover and mutation operations are performed to generate offspring chromosomes. The total number of offspring chromosomes generated from this step is equal to  $O_1 + O_2$  defined previously. Once the offspring chromosomes have been selected, the algorithm proceeds to step 2 to simulate and evaluate the offspring chromosomes, and the process continues.

## 6.5 Model Sensitivity Analysis

As identified in the previous sections, several parameters must be identified *a priori* as input to the GA model. These parameters include maximum generation, population size, probability of crossover, probability of mutation, fitness function coefficients, CORSIM OD, and distribution of car-following sensitivity parameter selection. To perform a sensitivity analysis to determine appropriate values for these parameters, base values for each of these parameters were assigned to the model for use in comparison of parameter ranges. The base values of the parameters were set as follows:

- Maximum generation = 30 iterations;
- Population size = 40 chromosomes;
- Probability of crossover ( $P_c$ ) = 0.5;
- Probability of mutation ( $P_m$ ) = 0.3;
- Fitness function coefficient ( $C$ ) = 100;
- Volume fitness function coefficient ( $\beta_1$ ) = 5;
- Travel time fitness function coefficient ( $\beta_2$ ) = 0.5;
- Base model for use in sensitivity analysis = lognormal volume only; and
- OD model for use in sensitivity analysis = synthetic (A\_OD) model.

Model sensitivity analysis was performed utilizing a calibration process in which the parameters were evaluated using the IH-10 AM peak period test network, with calibration performed on parameters  $P_1$  through  $P_{19}$ . Using the lognormal distribution volume only calibration model, sensitivity analyses were first conducted for maximum generation and population size, probability of crossover, and probability of mutation. A sensitivity analysis was then conducted for the fitness function coefficient using the lognormal distribution model calibrated for both volume and travel time to determine the best travel time coefficient. The OD model selection sensitivity analysis was conducted next using all three car-following distribution alternatives for the AM peak period volume only calibration models. The final sensitivity analysis then compared the AM peak period for all car-following distribution alternatives, with calibration performed based on both volume only and a combination of volume and travel time to determine the distribution model to use in the final model selected. The results of each of the sensitivity analyses are presented in the following subsections.

### 6.5.1 Maximum Generation and Population Size

To determine the best combination of both maximum generation and population size (number of chromosomes), a sensitivity analysis was conducted for 30 generations using population sizes of 10 chromosomes, 20 chromosomes, 30 chromosomes, and 40 chromosomes. The results of the minimum MAER for each of the four alternatives are provided in Figure 6.3. This graph shows the difference in convergence rates for each of the population sizes, with the 30 and 40 chromosome alternatives providing the best overall results (lowest MAER) in the least number of generations. The 40 chromosome alternative provides optimal results in less than five generations, while the 30 chromosome alternative provides optimal results within approximately 10 generations. Based on this analysis, it is recommended that the population size be set to a minimum of 30 chromosomes, with a minimum of 20 generations to ensure that optimal values can be reached.

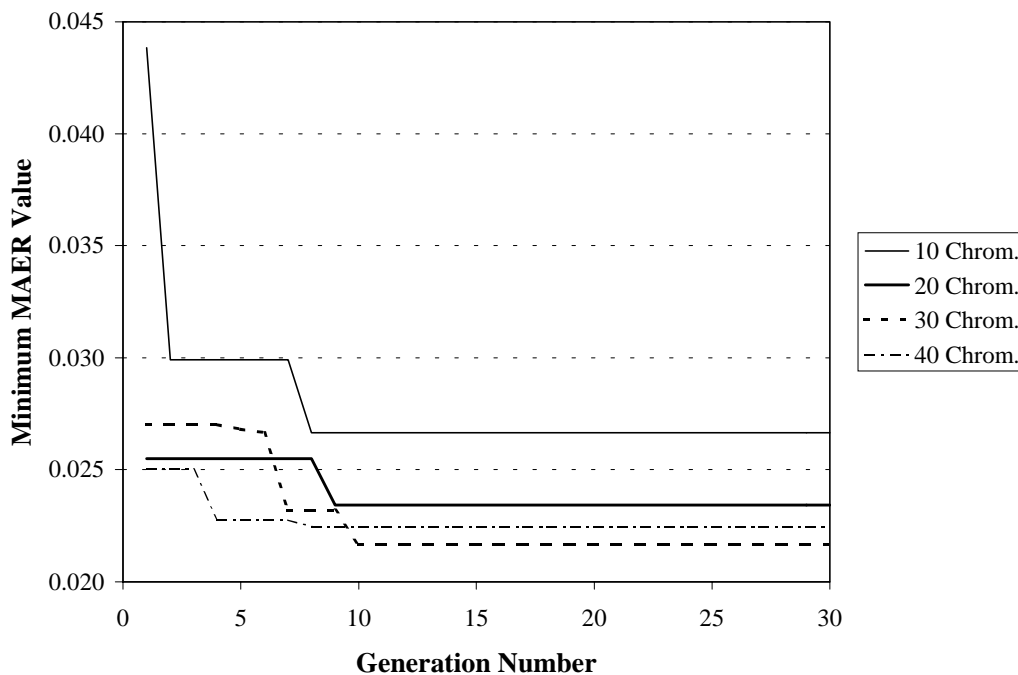


**FIGURE 6.3** GA maximum generation and population size sensitivity analysis

### 6.5.2 Probability of Crossover

To determine the best combination of probability of crossover ( $P_c$ ), a sensitivity analysis was conducted for  $P_c$  values of 0.3, 0.4, 0.5, and 0.6. The results of the minimum MAER for each of the four alternatives is provided in Figure 6.4. This graph shows the difference in convergence rates for each of the crossover probabilities analyzed, with similar results recorded for all four alternatives. The  $P_c = 0.5$  and  $P_c = 0.6$  alternatives produced the best overall results (lowest MAER) in the least number of generations, while  $P_c = 0.3$  produced the lowest MAER after 15 generations. Based on this analysis, it can be seen that the crossover probability is not a major determinant in the overall calibration results. It is recommended that the  $P_c$  be maintained at the base value of 0.5 for future analyses.

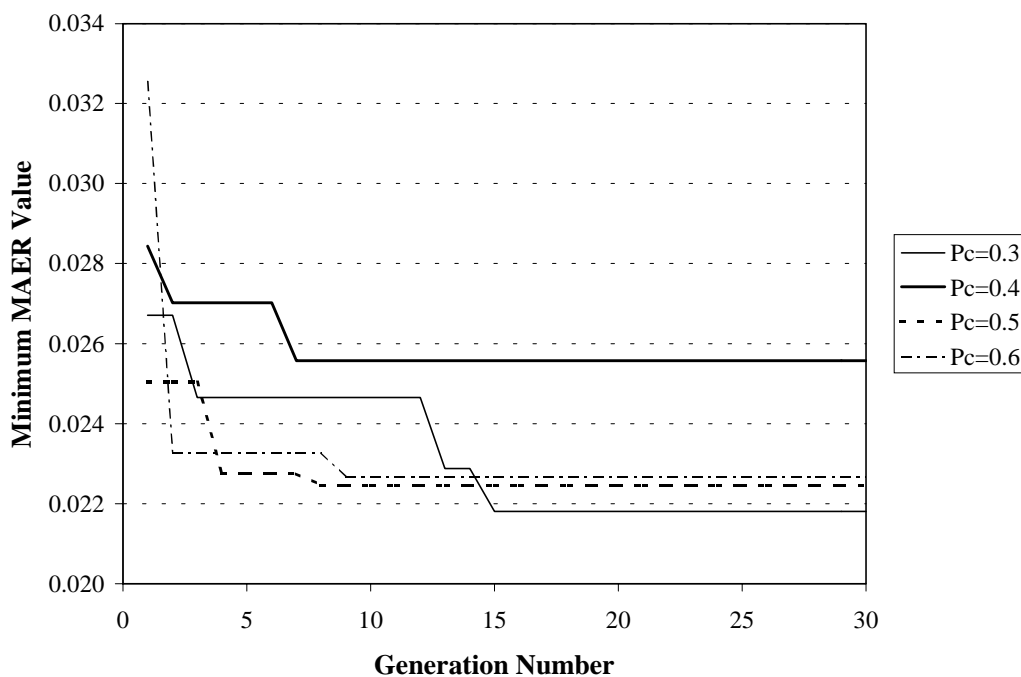


**FIGURE 6.4** GA probability of crossover ( $P_c$ ) sensitivity analysis

### 6.5.3 Probability of Mutation

To determine the best combination of probability of mutation ( $P_m$ ), a sensitivity analysis was conducted for  $P_m$  values of 0.1, 0.2, 0.3, and 0.4. The results of the minimum MAER for each of

these four alternatives are provided in Figure 6.5. This graph shows the difference in convergence rates for each of the probability of mutation alternatives analyzed, and as with the probability of crossover analysis, each of the probability of mutation alternatives produces similar results for all four alternatives. The  $P_m = 0.1$  and  $P_m = 0.3$  alternatives produced the best overall results (lowest MAER) in the least number of generations, with  $P_m = 0.3$  producing the lowest MAER overall. As with the  $P_c$  analysis, the  $P_m$  analysis clearly indicates that the probability of mutation is not a major determinant in the overall calibration results. It is recommended that the  $P_m$  be maintained at the base value of 0.3 for future analyses.

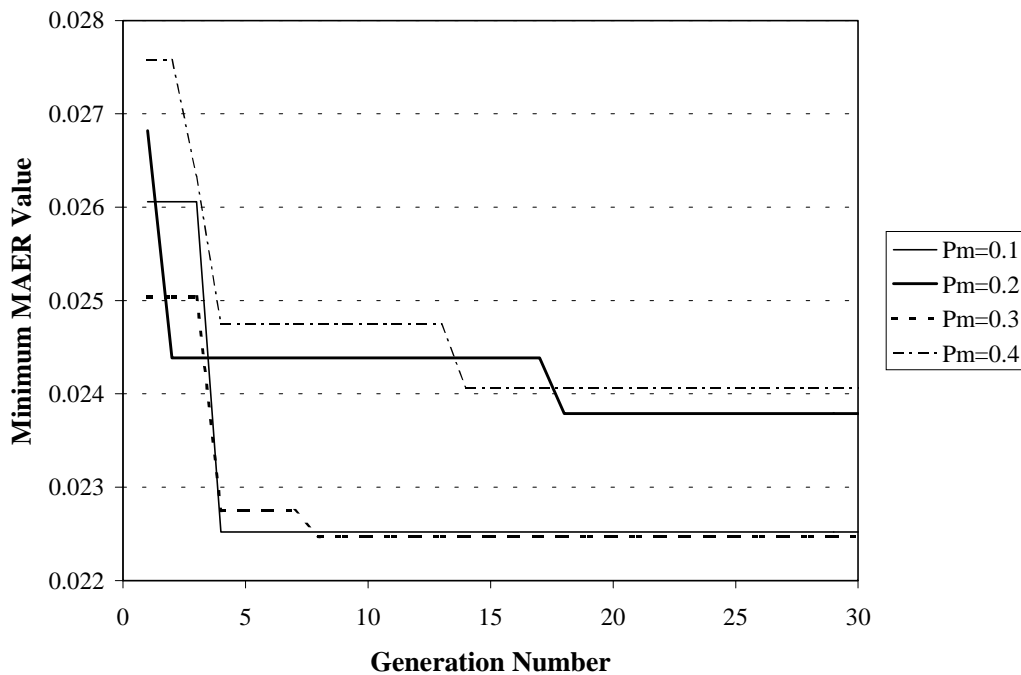


**FIGURE 6.5** GA probability of mutation ( $P_m$ ) sensitivity analysis

#### 6.5.4 Fitness Function Coefficients

In the identification of the fitness function, four coefficients were introduced for use in the sensitivity analysis. These coefficients are  $C$ ,  $\beta_1$ ,  $\beta_2$ , and  $\alpha$ , identified previously in Equations 6.10, 6.12, and 6.13. The coefficients  $C$  and  $\beta_1$  were selected based on a sensitivity analysis in which it was determined that the value of  $C$  did not have a substantial impact on the convergence

rate for calibration; the value of  $\beta_1$ , however, did have an impact (9). The values determined for  $C$  and  $\beta_1$  for use in this analysis based on the sensitivity analysis performed were 100 and 5, respectively.

As with the value of  $\beta_1$ , the value of  $\beta_2$  and  $\alpha$  are critical in the analysis of both volume and travel time since these parameters place emphasis on one criterion over the other in determining the overall fitness function. It was determined that the value of  $\alpha$  would be set at 0.5 to provide an equal weighting on the volume fitness value and the travel time fitness value, but a sensitivity analysis of  $\beta_2$  would be performed during the AM peak period for values 0.5, 1.25, 2.5, and 5.0. The results of the MAER and resulting final fitness function for each of these alternatives are provided in Table 6.5.

**TABLE 6.5 Travel Time Fitness Function Sensitivity Analysis Results**

	Defaults	Lognormal Distribution Volume and Travel Time			
		$\beta_2 = 0.5$	$\beta_2 = 1.25$	$\beta_2 = 2.5$	$\beta_2 = 5.0$
<b>Volume MAER</b>	<b>0.115</b>	0.031	0.044	0.079	0.075
<b>Travel Time MAER</b>	<b>0.227</b>	0.335	0.271	0.175	0.175
<b>FITNESS VALUE</b>		85.0	75.8	66.0	55.2

As would be expected, as the value of  $\beta_2$  is increased, the travel time MAER is decreased and the volume MAER increases. At a  $\beta_2$  of 0.5, for instance, the volume MAER indicates excellent replication with an MAER of 0.031 (3.1 percent), but the travel time is not very consistent with an MAER of 0.335 (33.5 percent). These results indicate that the volume can be replicated within 3 percent of actual volumes; however, the travel time is only replicated to be within 33 percent of actual values. On the other end of the sensitivity analysis, at a  $\beta_2$  of 5.0, the volume MAER results show a value of 0.075 (7.5 percent), indicating that volume MAER has increased over 100 percent and is now only replicated to be within 7.5 percent of observed, while the travel time MAER has been reduced by nearly 50 percent to a value of 0.175 (17.5 percent), indicating much better calibration results when comparing the travel time MAER.

It is much more difficult to compare the absolute results of the fitness value because the scale for this value changes with each subsequent increase of the  $\beta_2$  parameter. To better illustrate the overall results, therefore, the volumes and travel times were plotted along the

corridor outlining the ability of the different travel time fitness functions to adequately replicate the actual conditions. The results of the volume analysis are provided in Figure 6.6, while the travel time results are provided in Figure 6.7.

It is apparent from these plots that the calibration of the model using both volume and travel time is essential in attempting to duplicate actual conditions. It is also apparent that for congestion conditions (i.e., AM peak period), the replication of both volume and travel time is difficult. Sensitivity analyses of less congested conditions (i.e., off peak and PM peak periods) show much better duplication of both volume and travel time results. It is important to note that the relationships between the average travel time and the variability of travel time during these same time periods are not represented in these figures. The AVI data indicate that the standard deviation of travel time varies by as much as 75 seconds on Link 1, 80 seconds on Link 2, 132 seconds on Link 3, and 63 seconds on Link 4, where the individual links were identified in Section 5.2.1. When these variability factors are included for both travel time and volume, it is apparent that the results of the analysis are within the range of values expected on the roadway.

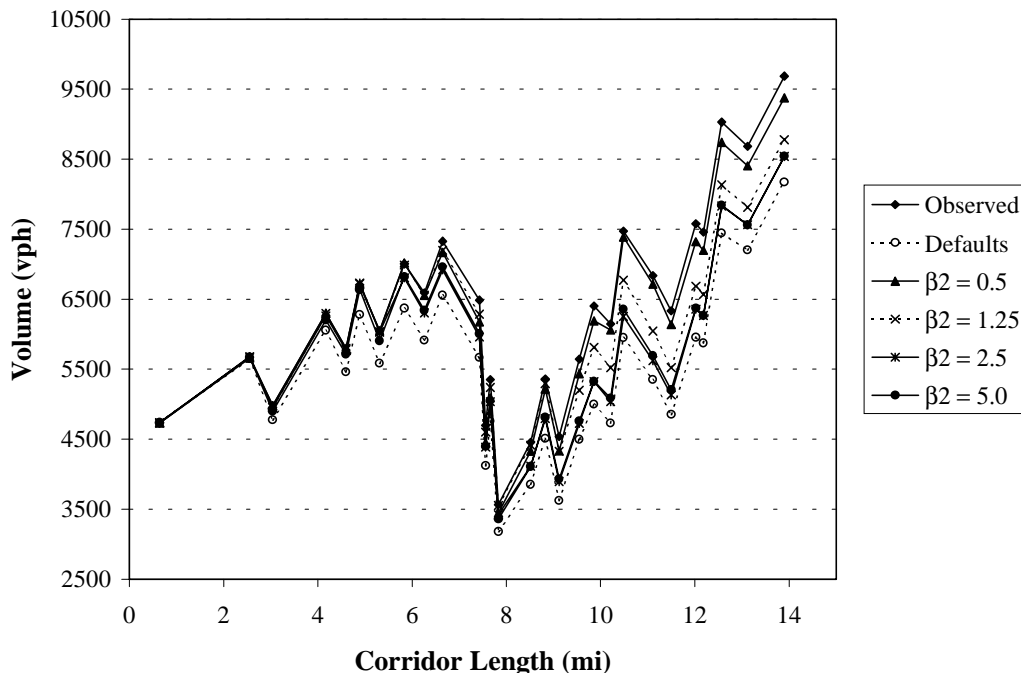
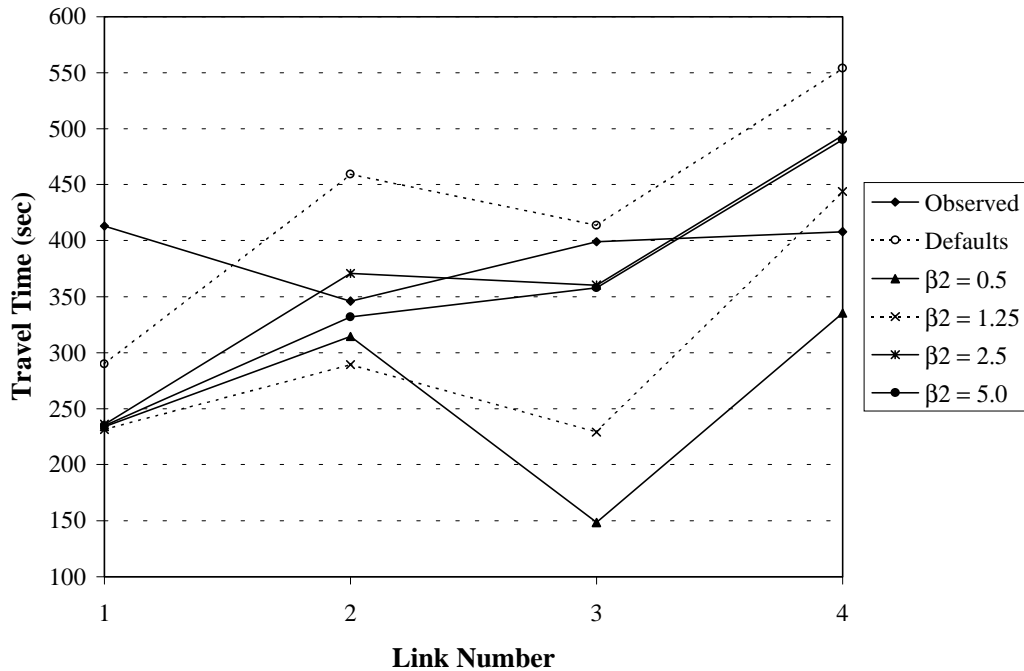


FIGURE 6.6 AM peak period  $\beta_2$  traffic volume sensitivity analysis



**FIGURE 6.7** AM peak period  $\beta_2$  travel time sensitivity analysis

Based on the sensitivity analysis performed, a  $\beta_2$  value of 2.50 was selected for use in all further analyses. Although this parameter does not provide exact replication of both volume and travel time, the trade-off between these values and the duplication during less congested periods warrant the use of this value for this analysis. It is recommended that a sensitivity analysis of this value be conducted for analysis on alternate networks since the value used in the fitness function is critical in providing acceptable calibration results and should be independently evaluated for all analyses.

#### 6.5.5 Origin-Destination Model Selection

One of the more critical components of any microscopic traffic simulation model is the representation of the OD matrix to accurately replicate traffic through the network. In this dissertation, two different OD methodologies were compared for analysis. The first technique utilized CORSIM OD estimates generated directly from the CORSIM model. In this alternative, a gravity model internal to the CORSIM logic uses traffic volumes at entrance nodes (CORSIM record type 50) and turning movement percentages at ramp exits (CORSIM record type 25) to generate a calibrated OD table in percentages that represents the input volumes. The second

technique available to generate OD estimation in the model is to manually specify OD pairs in percentages from origin nodes to destination nodes. In this alternative, the user must ensure that the traffic volumes for all destination nodes agree with the traffic volumes calibrated in the previous alternative using the volumes and turn percentages of record types 25 and 50 (102). To accurately provide OD information between nodes, a synthetic OD estimate was obtained using a technique developed by Dixon and Rilett, based on travel time and location data collected at AVI stations located along both the IH-10 and US 290 test networks (143, 144). It is important to point out here that neither approach differentiates between vehicle type since the CORSIM model does not provide the user an opportunity to input more than one OD table.

The results of the analysis for both the CORSIM OD alternative (C\_OD) and the synthetic AVI OD alternative (A\_OD) are provided in Table 6.6. For this analysis, the IH-10 test network was modeled using both OD alternatives, and the results for the lognormal distribution, normal distribution, and random distribution volume only calibration results were compared between the different OD alternatives and with the default calibration parameters.

**TABLE 6.6 Origin-Destination Sensitivity Analysis Results**

	Defaults		Random Distribution		Lognormal Distribution		Normal Distribution	
	C_OD	A_OD	C_OD	A_OD	C_OD	A_OD	C_OD	A_OD
<b>MAER Value</b>	<b>0.111</b>	<b>0.115</b>	0.077	0.024	0.075	0.024	0.078	0.025
<b>Fitness Value</b>	<b>57.3</b>	<b>56.4</b>	68.2	88.5	68.8	88.6	67.8	88.5

The results clearly identify the synthetic A\_OD alternative as a better method for calibration of the test network. The A\_OD MAER results consistently fall within approximately 2.5 percent of observed conditions (2.4 percent, 2.4 percent, and 2.5 percent for random, lognormal, and normal distributions, respectively), while the C\_OD results consistently fall within approximately 7.5 percent of observed conditions (7.7 percent, 7.5 percent, and 7.8 percent for random, lognormal, and normal distributions, respectively). Although the A\_OD and C\_OD calibrated models perform better than the default parameters (11.1 percent and 11.5 percent of observed conditions for C\_OD and A\_OD, respectively), the A\_OD models provide MAER results approximately 240 percent lower for the A\_OD models when compared

to the C\_OD models. It is recommended, therefore, that the synthetic A\_OD models be utilized for all further analyses.

#### 6.5.6 Car-Following Sensitivity Distribution Model Selection

The distribution alternatives outlined previously identified the need to evaluate car-following sensitivity distribution alternatives in microscopic traffic simulation models compared to default parameter results. Three models were identified in this discussion and are summarized as follows:

- random car-following sensitivity analysis;
- lognormal car-following sensitivity analysis; and
- normal car-following sensitivity analysis.

Each of the three alternatives was calibrated for the AM peak period using a control factor ( $\alpha$ ) of 0 (volume only calibration) and 0.5 (volume and travel time calibration). For the volume and travel time calibration ( $\alpha = 0.5$ ), the constants  $\beta_1$  and  $\beta_2$  were set at 5.0 and 2.5, respectively, with a constant  $C$  of 100 used in the analysis. The results of the objective function and fitness value results for each alternative are provided in Table 6.7, with analysis results summarized for each of the distributions for volume only and volume and travel time (TT).

**TABLE 6.7 Car-Following Sensitivity Analysis Results**

	Defaults	Random Distribution		Lognormal Distribution		Normal Distribution	
		Volume Only ( $\alpha = 0$ )	Volume + TT ( $\alpha = 0.5$ )	Volume Only ( $\alpha = 0$ )	Volume + TT ( $\alpha = 0.5$ )	Volume Only ( $\alpha = 0$ )	Volume + TT ( $\alpha = 0.5$ )
<b>Volume MAER</b>	<b>0.115</b>	0.024	0.094	0.024	0.079	0.025	0.080
<b>TT MAER</b>	<b>0.227</b>	0.438	0.149	0.436	0.175	0.434	0.182
<b>Fitness Value</b>	<b>56.5</b>	88.5	65.8	88.6	66.0	88.5	65.2

It is apparent from the table that all three of the models (random, lognormal, and normal) replicate the observed traffic volumes with MAER results less than 0.025 (2.5 percent) and corresponding fitness value results near 90. The calibrated models also replicate observed

volumes better than default parameters, where default parameters provide volume MAER results of 0.115 (11.5 percent). The lognormal distribution provides the best overall performance for the volume only analysis, with an MAER of 0.024 (2.4 percent) and corresponding fitness value of 88.6. With the inclusion of travel time in the objective function, the volume MAER increases but remains within 10 percent of observed (9.4 percent, 7.9 percent, and 8.0 percent for random, lognormal, and normal distributions, respectively), with travel time simulations within 20 percent of observed (14.9 percent, 17.5 percent, and 18.2 percent for random, lognormal, and normal distributions, respectively). When considering the overall fitness value, it is again apparent that all three models provide similar calibration results, with maximization fitness function values ranging from a low of 65.2 for the normal distribution to 66.0 for the lognormal distribution.

In addition to the fitness function analysis, a graphical representation of the simulated traffic volumes versus the observed traffic volumes along the corridor is provided in Figures 6.8 and 6.9 for the volume only calibration ( $\alpha = 0$ ) and the volume and travel time calibration ( $\alpha = 0.5$ ), respectively. These figures illustrate the ability of the models to replicate the observed traffic volumes, as well as the differences between the calibrated models and the default parameter set, indicating that any of the three distribution alternatives provide traffic volumes closer to observed conditions than default parameters for both fitness functions.

Finally, a graphical representation of the discrete distributions of the car-following headway parameters for each alternative is also provided in Figures 6.10 and 6.11 for the volume only ( $\alpha = 0$ ) and the volume and travel time ( $\alpha = 0.5$ ) calibrations, respectively. These representations provide a visual understanding of the variability that exists in the discrete distributions of the car-following headway parameters that produce similar calibration results.

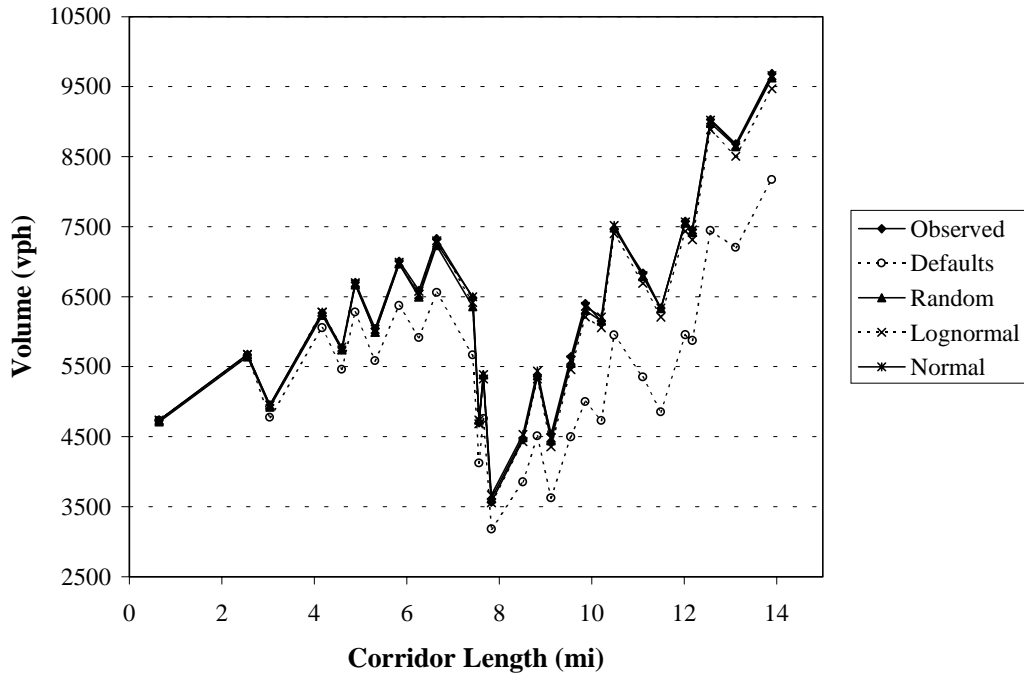


FIGURE 6.8 Traffic volume analysis—volume only calibration

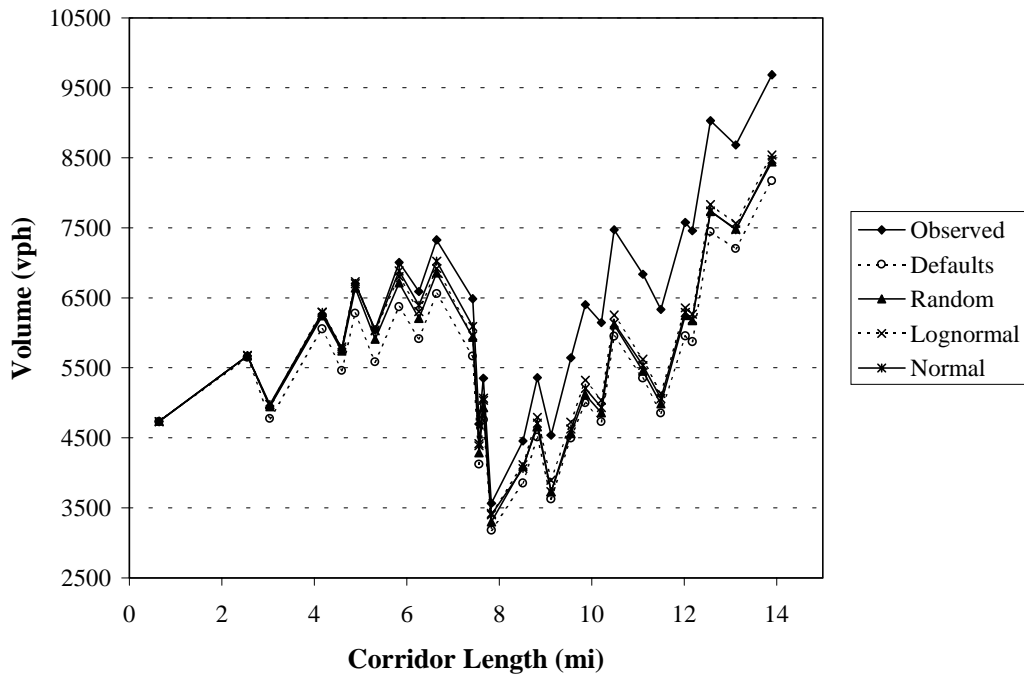


FIGURE 6.9 Traffic volume analysis—volume and travel time calibration

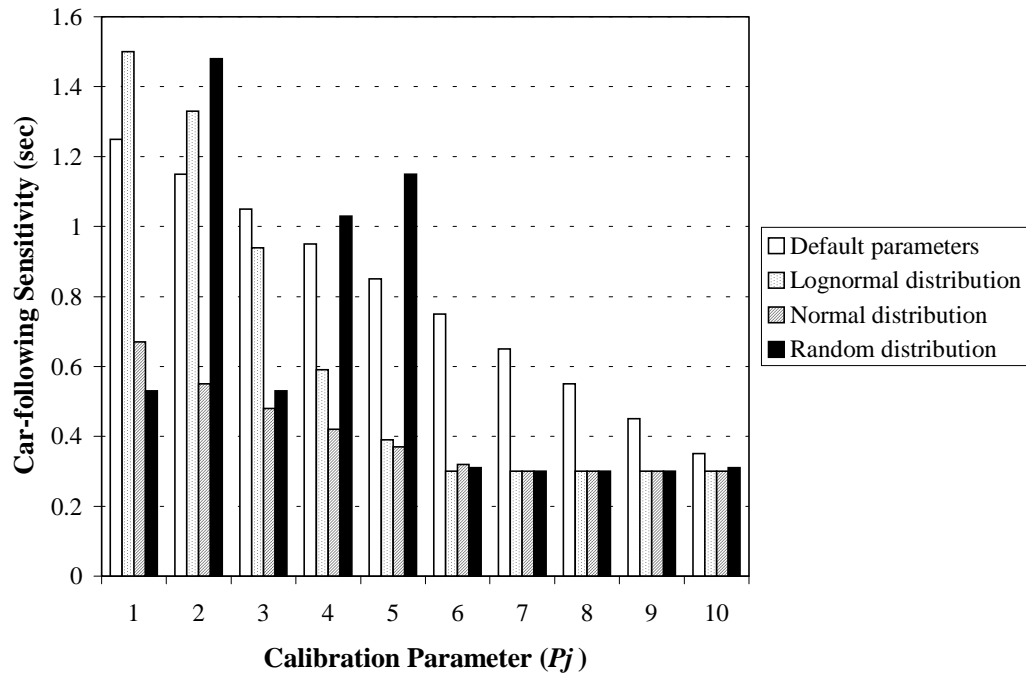


FIGURE 6.10 Discrete distribution analysis results—volume only calibration

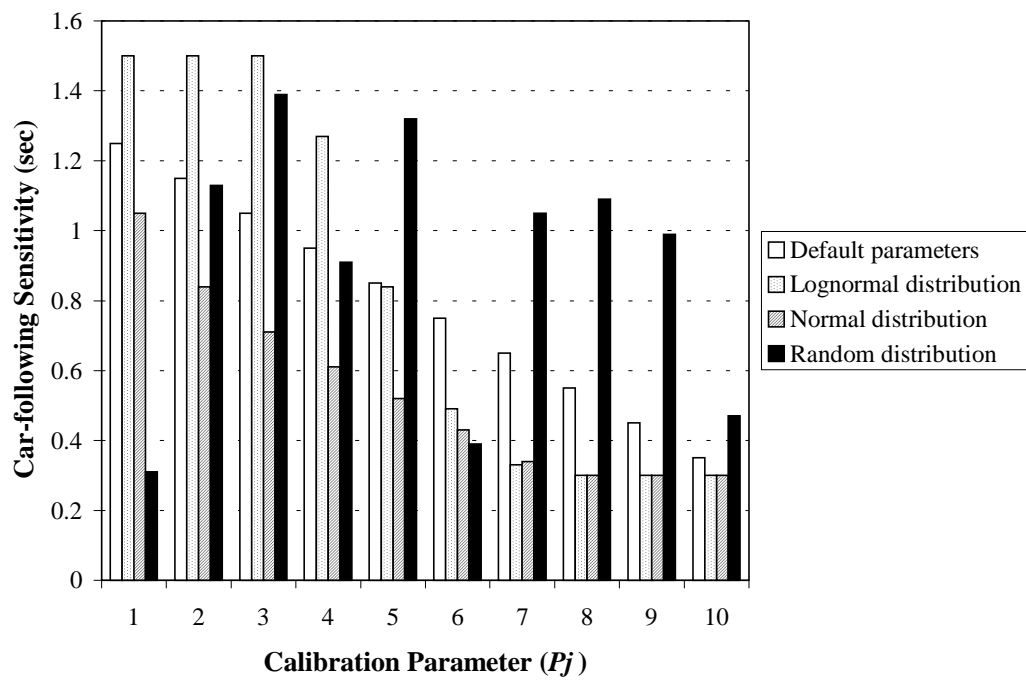


FIGURE 6.11 Discrete distribution analysis results—volume and travel time calibration

The analysis indicates that all three alternatives are effective at modeling the observed conditions; however, the lognormal and normal distributions provide advantages over the random assignment that are not necessarily apparent from these results. These advantages include the following: 1) a statistical distribution of individual driver characteristics can be generated from the mean and variance; 2) redundancy in the calibration parameters can be reduced since the alternative would require only two parameters (mean and standard deviation), rather than 10; and 3) the process is simpler. The lognormal and normal distributions have been identified in the literature as representations of headway distributions and, based on the analysis presented in this dissertation, can be used to represent car-following sensitivity parameters as well. As a result of the analysis and the background behind the alternatives, it is recommended that the lognormal distribution model be utilized for future calibration analyses.

## 6.6 Network Calibration

Combining the results of all sensitivity analyses, the final model selection to be used in generating the model calibration alternatives includes the following characteristics:

- maximum generation = 30 iterations;
- population size = 30 chromosomes;
- probability of crossover ( $P_c$ ) = 0.5;
- probability of mutation ( $P_m$ ) = 0.3;
- fitness function coefficient ( $C$ ) = 100;
- volume fitness function coefficient ( $\beta_1$ ) = 5;
- travel time fitness function coefficient ( $\beta_2$ ) = 2.5;
- control factor ( $\alpha$ ) = 0.5;
- the OD model utilized will be the synthetic AVI OD model; and
- the base model for use in the analysis will be the lognormal volume plus travel time model.

Based on the results of the model selection, final calibration runs were completed to select the calibrated parameters for use in all further analyses. This included final calibration of the IH-10 test network for AM, off, and PM peak periods, as well as a final calibration set for the US 290 test network during the AM peak period. Two scenarios were calibrated for the networks, including calibration of the base 19 parameters in the CORSIM parameter set, as well

as calibration of the base 19 parameters, plus the nine maximum non-emergency deceleration parameters for each vehicle type outlined in Section 5.3. The final calibration parameter set and resulting MAER and fitness values are provided in Table 6.8 for the base calibration model analysis results (19 parameters) and in Table 6.9 for the full calibration model analysis results (28 parameters). Each of these tables includes a summary of the parameter set as well as the volume MAER, travel time MAER, and corresponding fitness value based on calibration according to both volume and travel time. In addition, the corresponding mean and standard deviation of the discrete parameter set has been included in the results, as well as the mean and standard deviation of the natural log of the parameter set utilized in the lognormal distribution analysis. To provide a comparison with default values, the corresponding analysis results using default calibration parameters for each network and peak period are outlined in Table 6.10.

The analysis results outlined in these tables indicates that the calibration of the models provides considerable improvement in the ability of the model to replicate observed conditions. During the AM peak period on the IH-10 test network, for instance, the fitness function is increased from 56.5 using the default parameters to a value of 66.0 when calibrating for base calibration model conditions and to 65.8 when calibrating to full calibration model conditions. The results also indicate that both the volume and travel time MAER are improved in this instance, and that this trend holds true for nearly all scenarios, with the exception of the IH-10 PM peak period volume MAER and the US 290 AM peak period travel time MAER. In the IH-10 PM peak period model, the overall fitness value (maximization function) is increased for both of the calibrated models; however, in the full calibration model analysis, the volume MAER (minimization function) is also increased from 0.05 (5 percent) to 0.06 (6 percent). In the US 290 AM peak period, the fitness value is also increased from default conditions for both calibrated models; however, in this model the travel time MAER increases in the base calibration model analysis from a value of 0.326 (32.6 percent) in the default scenario to 0.356 (35.6 percent) in the base calibration model. In both of these instances, however, as well as in all other cases, the calibrated model provides better overall results than the default conditions, thus justifying the calibration procedure and providing a model that better represents the combination of both travel time and volume.

**TABLE 6.8 Base Calibration Model Analysis Results**

Parameter	Default	IH-10			US 290
		AM Peak	Off Peak	PM Peak	AM Peak
<b>Mean</b>	<b>80.0</b>	83.3	78.0	76.4	90.6
<b>Std. Dev.</b>	<b>30.3</b>	55.3	55.9	55.8	55.9
<b>Mean ln(X)</b>	<b>N/A</b>	4.13	3.75	3.60	4.44
<b>Std. Dev. ln(X)</b>	<b>N/A</b>	2.07	2.39	2.64	2.00
<i>P</i> <sub>1</sub>	<b>125</b>	150	150	150	150
<i>P</i> <sub>2</sub>	<b>115</b>	150	150	150	150
<i>P</i> <sub>3</sub>	<b>105</b>	150	150	148	150
<i>P</i> <sub>4</sub>	<b>95</b>	127	114	109	145
<i>P</i> <sub>5</sub>	<b>85</b>	84	60	54	113
<i>P</i> <sub>6</sub>	<b>75</b>	49	36	33	68
<i>P</i> <sub>7</sub>	<b>65</b>	33	30	30	40
<i>P</i> <sub>8</sub>	<b>55</b>	30	30	30	30
<i>P</i> <sub>9</sub>	<b>45</b>	30	30	30	30
<i>P</i> <sub>10</sub>	<b>35</b>	30	30	30	30
<i>P</i> <sub>11</sub>	<b>10</b>	9	3	5	9
<i>P</i> <sub>12</sub>	<b>3</b>	2	2	5	3
<i>P</i> <sub>13</sub>	<b>3</b>	1	5	3	4
<i>P</i> <sub>14</sub>	<b>20</b>	33	12	52	49
<i>P</i> <sub>15</sub>	<b>16</b>	20	13	19	19
<i>P</i> <sub>16</sub>	<b>3</b>	5	2	1	2
<i>P</i> <sub>17</sub>	<b>20</b>	36	10	15	18
<i>P</i> <sub>18</sub>	<b>5</b>	10	3	5	3
<i>P</i> <sub>19</sub>	<b>4</b>	5	5	6	3
<b>Volume MAER</b>		<b>0.079</b>	<b>0.025</b>	<b>0.046</b>	<b>0.024</b>
<b>Travel Time MAER</b>		<b>0.175</b>	<b>0.065</b>	<b>0.050</b>	<b>0.356</b>
<b>Fitness Value</b>		<b>66.0</b>	<b>86.7</b>	<b>83.8</b>	<b>64.8</b>

**TABLE 6.9 Full Calibration Model Analysis Results**

Parameter	Default	IH-10			US 290
		AM Peak	Off Peak	PM Peak	AM Peak
<b>Mean</b>	<b>80.0</b>	66.8	81.0	73.3	72.5
<b>Std. Dev.</b>	<b>30.3</b>	42.5	55.1	51.2	54.1
<b>Mean ln(X)</b>	<b>N/A</b>	3.95	4.03	3.86	3.43
<b>Std. Dev. ln(X)</b>	<b>N/A</b>	0.82	1.91	1.53	2.68
<i>P</i> <sub>1</sub>	<b>125</b>	149	150	150	150
<i>P</i> <sub>2</sub>	<b>115</b>	126	150	150	150
<i>P</i> <sub>3</sub>	<b>105</b>	91	150	127	137
<i>P</i> <sub>4</sub>	<b>95</b>	71	120	87	93
<i>P</i> <sub>5</sub>	<b>85</b>	57	73	58	45
<i>P</i> <sub>6</sub>	<b>75</b>	46	45	40	30
<i>P</i> <sub>7</sub>	<b>65</b>	37	32	31	30
<i>P</i> <sub>8</sub>	<b>55</b>	31	30	30	30
<i>P</i> <sub>9</sub>	<b>45</b>	30	30	30	30
<i>P</i> <sub>10</sub>	<b>35</b>	30	30	30	30
<i>P</i> <sub>11</sub>	<b>10</b>	5	6	5	8
<i>P</i> <sub>12</sub>	<b>3</b>	5	6	5	5
<i>P</i> <sub>13</sub>	<b>3</b>	4	7	9	1
<i>P</i> <sub>14</sub>	<b>20</b>	23	22	17	57
<i>P</i> <sub>15</sub>	<b>16</b>	13	22	17	13
<i>P</i> <sub>16</sub>	<b>3</b>	3	2	3	1
<i>P</i> <sub>17</sub>	<b>20</b>	20	27	40	13
<i>P</i> <sub>18</sub>	<b>5</b>	8	10	10	1
<i>P</i> <sub>19</sub>	<b>4</b>	2	1	5	1
<i>P</i> <sub>20</sub>	<b>80</b>	74	96	87	76
<i>P</i> <sub>21</sub>	<b>80</b>	91	81	111	75
<i>P</i> <sub>22</sub>	<b>80</b>	88	85	84	69
<i>P</i> <sub>23</sub>	<b>80</b>	74	86	56	81
<i>P</i> <sub>24</sub>	<b>80</b>	48	97	55	92
<i>P</i> <sub>25</sub>	<b>80</b>	79	80	77	55
<i>P</i> <sub>26</sub>	<b>80</b>	54	40	56	40
<i>P</i> <sub>27</sub>	<b>80</b>	116	112	92	74
<i>P</i> <sub>28</sub>	<b>80</b>	105	81	80	86
<b>Volume MAER</b>		<b>0.086</b>	<b>0.043</b>	<b>0.061</b>	<b>0.037</b>
<b>Travel Time MAER</b>		<b>0.163</b>	<b>0.044</b>	<b>0.053</b>	<b>0.255</b>
<b>Fitness Value</b>		<b>65.8</b>	<b>85.1</b>	<b>80.7</b>	<b>68.0</b>

**TABLE 6.10 Default Calibration Parameter Analysis Results**

	IH-10			US 290
	AM Peak	Off Peak	PM Peak	AM Peak
<b>Volume MAER</b>	0.115	0.045	0.050	0.058
<b>Travel Time MAER</b>	0.227	0.217	0.107	0.326
<b>Fitness Value</b>	56.5	69.0	77.2	59.5

Another finding from the calibration analysis is the difficulty that was experienced in calibrating both the IH-10 and the US 290 test networks based on both volume and travel time under congested conditions (i.e., AM peak period). Previous analysis results indicate that when calibrating both networks to volume only, the results that are obtained using the GA calibration methodology are excellent, with volume calibrated to within 2 percent or less of observed conditions. When the travel time is added to the fitness function, however, the results are not as good. It is theorized that this is the case due to an inability of the model to adequately shift from congested to non-congested conditions, thus moving to the lower half of a standard speed flow relationship. The additional calibration parameters do not appear to aid in making this shift; thus the final calibrated results for the congested periods may not adequately represent actual conditions.

Finally, when comparing the base calibration model analysis results to the full calibration model analysis results, it does not appear as though inclusion of the maximum non-emergency deceleration rates has a profound effect on the calibration results. This will be analyzed along with other aspects of the CMV calibration procedure in Section 7.

## **6.7 Concluding Remarks**

This section has outlined an automated calibration methodology based on the principles of natural selection and genetics using an automated GA calibration code. Two distribution alternatives were also developed to represent car-following sensitivity factors and were subsequently coded as part of the automated calibration methodology. The first distribution utilized a truncated lognormal distribution, while the second distribution utilized a truncated normal distribution. In addition, a third random distribution was also analyzed, where car-following sensitivity parameters were randomly assigned to the 10 car-following parameters.

The evaluation criterion for the automated calibration methodology included criteria to evaluate the calibration results based on traffic volumes and travel time ITS data. Objective

function criteria were developed for each evaluation alternative based on the MAER of the criteria. A fitness function was then developed to transform the traffic volume and/or travel time data minimization objective function (i.e., MAER) to an exponential maximization function (i.e., fitness value). The final fitness value was then calculated based on a linear relationship between the traffic volume data fitness function value and the travel time fitness function value and utilized in the reproduction processes of the algorithm.

Five basic steps in the GA process were identified to calibrate the two test networks. Prior to the final calibration process, a sensitivity analysis was performed on the critical parameters of the model, with calibration parameters chosen for maximum generation, population size, probability of crossover and mutation, fitness function coefficients, OD model, and base car-following sensitivity model for use in the analysis. The results of the sensitivity analysis identified several major findings, three of which are summarized here. First, the analysis of the distribution alternatives identified all three alternatives (lognormal, normal, and random) as effective in modeling observed traffic volumes, producing volume only MAER results less than 0.025 (2.5 percent) for all three models. This represented a 78 percent reduction from default conditions (0.115 to 0.025). The second finding from the distribution analysis was the relationship between volume only calibration versus volume and travel time calibration. The analysis found that with the inclusion of travel time in the objective function, the volume MAER increased from 2.4 percent to 7.9 percent for the lognormal distribution, while the travel time MAER decreased from 43.6 percent to 17.5 percent for this same distribution. Although the results did not show both volume and travel time within 10 percent of observed conditions, the volume and travel time analysis did provide better representation of the overall network conditions. Finally, the lognormal distribution was recommended for this analysis based on the sensitivity analysis results, as well as the advantages outlined in the parameter distribution alternative development.

Based on the results of the model selection sensitivity analysis, final calibration runs were completed to select the calibrated parameters for use in all further analysis in this dissertation. The results of the calibration runs indicated that by calibrating the simulation models, the representation of observed conditions improved based on the objective and fitness functions identified. The models calibrated in this section will be utilized in Section 7 to determine the ability of the model to represent CMV parameters.

## 7. SENSITIVITY OF SIMULATION RESULTS

The preceding sections have developed a methodology to calibrate CMVs within microscopic traffic simulation models, specifically the CORSIM model. The purpose of this section is to examine and verify the output from this process in comparison with different calibration parameters and vehicle distributions, and to perform sensitivity analyses on the objective functions (i.e., MAER, fitness value), the operational characteristics (i.e., volume, travel time, delay), and the emissions output for each alternative. The focus of this analysis is the IH-10 Katy Freeway test network during the AM peak period. As was outlined previously in Section 5.2.1, the IH-10 test network was used in this analysis in the eastbound (inbound) direction representing worst case (i.e., congested) conditions and as such has been utilized throughout this analysis. Finally a sensitivity analysis based on traffic volumes and vehicle distribution growth will be conducted to examine the impacts of calibration on constant growth scenarios.

To accomplish this purpose, this section has been divided into six subsections. The first subsection provides a summary of the sensitivity analysis alternatives considered for the analysis. The second subsection provides a verification of the CMV distribution for these alternatives and includes a methodology to generate a full vehicle distribution from the model output. The third provides the results of the objective function and operational characteristics sensitivity analysis, while the fourth subsection provides a sensitivity analysis of the different alternatives based on the emissions impacts. The fifth subsection explores the constant growth of both traffic volume and vehicle distribution, and the implications of model calibration on this process. The sixth subsection provides concluding remarks on the analyses.

### 7.1 Sensitivity Analysis Alternatives

The data structure of CORSIM and other microscopic traffic simulation models provides the user with an opportunity to adjust various parameters to represent actual operating conditions. This calibration process as it has been referred to throughout this dissertation is somewhat complex, involving interaction between several input parameters. The input parameters that have been analyzed include the specific calibration parameter set included in record types 68, 69, and 70 of the CORSIM input code, as well as the distribution of vehicle types included in record type 50 (overall vehicle composition) and in record type 71 (vehicle distribution) (102). Previous

sections in this dissertation have explained these parameters in detail and have outlined a methodology to account for CMVs through the calibration of these parameters.

The structure of the input file format provides the user with an opportunity for a number of coding combinations, the extent of which would be difficult to quantify in a succinct manner. In an attempt, however, to evaluate the usefulness of the calibration process, several alternatives have been evaluated and compared with the calibrated parameter set identified in Section 6.6. These alternatives include combinations of default versus calibrated parameter sets, default versus calibrated vehicle type specifications (vehicle distribution), and variations of the vehicle distribution input. A detailed description of the base model and the five specific alternatives evaluated are summarized in the following subsections.

#### *7.1.1 Calibrated Model (Base)*

The first model is the base model consisting of the parameter set calibrated in Section 6.6, as well as the calibrated vehicle distribution calculated in Section 5.3. The calibrated model provides the baseline for comparison of all other models in the sensitivity analysis. This model is assumed to represent observed conditions, to the extent that these conditions can be duplicated using the microscopic traffic simulation model.

#### *7.1.2 Default Parameter Set No Trucks (Alternative 1)*

The first alternative model (Alt. 1) is included in the sensitivity analysis to provide baseline conditions for the microscopic traffic simulation model. This alternative utilizes the default calibration parameter set identified in Section 5.3, as well as baseline vehicle distribution excluding all trucks from the network. This model represents the base conditions of the CORSIM model for the test network analyzed.

#### *7.1.3 Default Parameter Set Calibrated Distribution (Alternative 2)*

The second alternative (Alt. 2) is comprised of the default calibration parameter set and the calibrated vehicle distribution, both of which are identified in Section 5.3. The purpose for this model in the sensitivity analysis is to evaluate the inclusion of the calibrated parameter set in the model, while still including the calibrated vehicle distribution identified to represent the network.

#### *7.1.4 Calibrated Parameter Set Default Distribution (Alternative 3)*

The third alternative (Alt. 3) is comprised of the calibrated parameter set identified in Section 5.3 with the default CORSIM vehicle distribution. This distribution utilizes the vehicle fleet identified in Section 5.3.2 with a truck distribution that includes 31 percent vehicle type 3, 36 percent vehicle type 4, 24 percent vehicle type 5, and 9 percent vehicle type 6, where an explanation of the fleet and vehicle types was provided previously in Table 5.3. The purpose of this model in the sensitivity analysis is to evaluate the inclusion of the calibrated vehicle distribution in the model based on the calibrated parameter set identified previously.

#### *7.1.5 Calibrated Parameter Set Semi-Trailer Truck with Medium Load (Alternative 4)*

The fourth alternative (Alt. 4) is included in the sensitivity analysis to evaluate a vehicle distribution alternative different from the default or calibrated distribution alternatives while maintaining the calibrated parameter set. This alternative is comprised of the calibrated parameter set with 100 percent of the truck distribution as vehicle type 5, performance index 4. An explanation of the vehicle type and performance index distributions was provided previously in Section 5.3.2.2, with performance index 4 representing a semi-trailer truck with a medium load.

#### *7.1.6 Calibrated Parameter Set Semi-Trailer Truck with Full Load (Alternative 5)*

The fifth and final alternative (Alt. 5) used in this analysis is again included to evaluate a vehicle distribution alternative different than the default or calibrated distribution alternatives while maintaining the calibrated parameter set. This alternative is comprised of the calibrated parameter set with 100 percent of the truck distribution as vehicle type 6, performance index 5, with performance index 5 representing a semi-trailer truck with a full load.

## **7.2 Verification of Simulated Vehicle Distribution**

One of the first steps in the sensitivity analysis was the verification of the microscopic traffic simulation model output compared to the input, primarily related to the vehicle distribution. To evaluate this distribution and to verify the results of the output file, this section has been broken into three subsections. The first subsection will provide background on the distribution verification process utilized in this analysis. The second subsection provides the distribution

verification results, while the third subsection will identify a methodology to generate a full vehicle distribution from the simulation model output.

### *7.2.1 Background on Verification Process*

The verification of simulation vehicle distribution was accomplished by analyzing the TRAFVU output (168) generated during the CORSIM simulation run. TRAFVU was designed by the Systems Division of ITT Industries, Inc., and is designed to display and animate the results of traffic simulation models, primarily the CORSIM simulation model. The TRAFVU model provides an interface where the output from the CORSIM model is passed into a self-contained binary data file that outputs the results of the simulation. The time-step file that is created in the TRAFVU output describes the state of each individual vehicle within the simulation model at each one-second time-step in the simulation. These data are stored for each link and time-step within the model and are specially designed to provide quick access to data within each individual time-step data (.tsd) file. A second file contains indexes, or pointers, that allow the animation to jump from time-step to time-step (168).

A conversion program written in C++ was used to convert the binary TRAFVU time-step data file to an ASCII file that could be utilized to analyze the output results. The conversion program was applied to each of the five alternatives for the AM peak period, analyzing the vehicle distribution on one link of the test network. The link analyzed was from node 19 to node 20, which includes a bridge segment over Kirkwood Road located in Link 2 of the corridor identified in Section 5.2.1.1. The conversion program extracts vehicle-specific data at one-second time increments between specific nodes of the corridor, including node number, time-step (in one-second increments), global vehicle identification number, vehicle fleet, vehicle type, vehicle length, vehicle acceleration, and vehicle speed. The resultant data file included over 150,000 records at one-second time increments over this segment of roadway. Because the data included one-second time increments, the majority of vehicles on the link were included in multiple time-steps as they traversed the network. To alleviate this duplication of vehicles and to aid in the verification of the vehicle distribution, the data file was aggregated such that only one record would exist for each vehicle on the network. The vehicle operational data for each of these vehicles was then averaged and included in the aggregated data file.

### 7.2.2 Verification of Analysis Results

The results of the distribution verification analysis are included in Table 7.1 for the base simulation model and alternative two, and in Table 7.2 for alternatives one and three. The first table compares the distribution results for the calibrated vehicle distribution models, while the second table compares the simulation results of the default vehicle distribution models. The distribution results of alternatives four and five were also conducted but are not included in these tables since they were not based on default or calibrated alternatives.

**TABLE 7.1 Calibrated Vehicle Distribution Verification Results**

Fleet <sup>1</sup>	Vehicle Distribution	Distribution Results, %		
		Input Value	Base Model	Alt. 2
Auto	1	25	26	24
	2	75	74	76
Truck	3	39	49	40
	4	32	28	30
	5	15	10	17
	6	14	13	13

<sup>1</sup> Auto = 0, Truck = 1

**TABLE 7.2 Default Vehicle Distribution Verification Results**

Fleet <sup>1</sup>	Vehicle Distribution	Distribution Results, %		
		Input Value	Alt. 1	Alt. 3
Auto	1	25	25	25
	2	75	75	75
Truck	3	31	N/A	29
	4	36	N/A	41
	5	24	N/A	25
	6	9	N/A	5

<sup>1</sup> Auto = 0, Truck = 1

The results of this analysis clearly indicate that the distributions generated in the output of the model closely match those in the input file. Alternatives two and three provide nearly identical results between the input and output values, while the base model provides a slightly

higher percentage of vehicle distribution three (49 percent versus 39 percent) and slightly lower distributions on vehicle distributions four, five, and six. It is not expected that the distributions would match exactly due to the stochastic and dynamic nature of the model. Since the results represent only one link in the model, the network-wide statistics may provide a closer match between input and output distributions.

### 7.2.3 Conversion to Full Distribution

The final step in the verification of simulated vehicle distributions was the conversion of the simulated distribution back to a full distribution of FHWA classification identified in Section 2.3.2. This conversion follows the same basic methodology outlined in Section 5.3.2.3.3 to convert FHWA classification to resulting truck distributions by vehicle group, only in this analysis the reverse operation is performed, converting the output of the model as a function of the distribution group to a full FHWA classification. The first step in accomplishing this task was to identify the output of the simulation model as a percentage of all traffic, rather than by vehicle fleet. This analysis was accomplished for the base model, as well as alternatives two and three, utilizing the output of the TRAFVU data file, with the results tabulated in Table 7.3.

**TABLE 7.3 Simulated Distribution Results**

Fleet <sup>1</sup>	Vehicle Distribution	Simulation Results, % (Count)		
		Base Model	Alt. 2	Alt. 3
Auto	1	25.2 (1,611)	22.8 (1,371)	23.9 (1,515)
	2	72.1 (4,607)	74.4 (4,465)	73.3 (4,640)
Truck	3	1.3 (85)	1.1 (67)	0.8 (52)
	4	0.8 (48)	0.8 (50)	1.2 (74)
	5	0.3 (18)	0.5 (29)	0.7 (45)
	6	0.3 (22)	0.4 (21)	0.1 (9)
<b>Total</b>		<b>100 (6,391)</b>	<b>100 (6,003)</b>	<b>100 (6,335)</b>

<sup>1</sup> Auto = 0, Truck = 1

The total number of simulated vehicles for each FHWA class can be calculated based on the simulated distribution results according to the relationships identified in Equations 7.1 and 7.2. The results of these calculations are summarized in Table 7.4.

$$T_{fg} = \frac{T_f}{T_g} \quad \forall f \in g, \quad \forall g = 1, G \quad (7.1)$$

$$T_{f'} = T_{fg} T_{g'} \quad \forall f \in g, \quad \forall g = 1, G \quad (7.2)$$

where:

- $T_{fg}$  = ratio of trucks by FHWA class in group  $g$ ;
- $T_f$  = number of trucks by classification  $f$  in original distribution;
- $T_g$  = number of trucks by group  $g$  in original distribution;
- $f$  = FHWA classification;
- $g$  = classification group;
- $G$  = total number of classification groups;
- $T_{f'}$  = number of trucks by classification  $f$  in simulated distribution; and
- $T_{g'}$  = number of trucks by group  $g$  in simulated distribution.

**TABLE 7.4 Simulated FHWA Distribution Results**

FHWA Truck Class <sup>1</sup>	Simulation Count		
	Base Model	Alt. 2	Alt. 3
4	35	37	54
5	85	67	52
6	13	13	20
7	0	0	0
8	0	0	0
9	36	45	49
10	0	0	0
11	3	4	4
12	1	1	1
13	0	0	0
<b>Total</b>	<b>173</b>	<b>167</b>	<b>180</b>

<sup>1</sup> Refer to Section 2.3.2 for FHWA vehicle classification descriptions

The results of this analysis illustrate the breakdown of different vehicle types from the simulation model for simulation link 19 to 20 as outlined previously. This analysis indicates that on the IH-10 Katy Freeway over Kirkwood Road, the majority of the trucks that cross this bridge for the base model and alternative two are FHWA Class 5, followed by FHWA Class 9, FHWA Class 4, FHWA Class 6, FHWA Class 11, and FHWA Class 12. For alternative three the results

are varied slightly, where the majority is FHWA Class 4, followed by FHWA Class 5, FHWA Class 9, FHWA Class 6, FHWA Class 11, and finally FHWA Class 12. As can be seen from this table, no vehicles from FHWA Classes 7, 8, 10, or 13 are observed on this segment in the original distribution and as such are not included in the simulated distribution results.

### **7.3 CMV Sensitivity Analysis**

With the verification of the simulation results complete, the next step in the analysis was to examine the sensitivity of CMV parameter calibration and distribution. The sensitivity analysis has been broken down into three primary subsections. The first subsection analyzes the objective function for each of the alternatives to determine if the calibrated parameter set and calibrated vehicle distribution have an impact on the objective function results. The second compares the volume and travel time results, as well as the overall network delay, as a function of the different alternatives, while the third subsection summarizes the results of the analysis.

#### *7.3.1 Objective Function Analysis*

The first step in the sensitivity analysis was an evaluation of the objective function results, including an analysis of the volume MAER, travel time MAER, and fitness value. A comparison of the volume and travel time MAER results is provided in Table 7.5, with a graphical representation of the volume and travel time MAER results provided in Figure 7.1, and the fitness value results provided in Figure 7.2. Although the MAER and fitness values appear to be relatively consistent when compared to the base conditions, the volume MAER does vary from 0.086 to 0.115 (33.7 percent increase) for alternative two and from 0.086 to 0.088 (2.3 percent increase) for alternative four. The travel time MAER values vary from 0.163 to 0.227 (39.3 percent increase) for alternative two and from 0.163 to 0.171 (4.91 percent increase) for alternative four. The fitness function values are not as variable as the MAER function, ranging from a 7.8 percent decrease for alternative one, a 14.1 percent decrease for alternative two, a 0.9 percent decrease for alternative three, a 1.5 percent decrease for alternative four, and a 7.3 percent decrease for alternative five.

This analysis shows that alternatives three and four provide the closest results to the base model as a function of overall objective function analyses. These results would tend to indicate that the calibration of the parameter set is more critical than the calibration of the vehicle distribution since alternative three utilizes the calibrated parameter set and the default

distribution, while alternative four utilizes the calibrated parameter set and a truck distribution that is comprised of 100 percent semi-trailer medium load vehicles. It is hypothesized that the calibrated vehicle distribution, the default distribution, and the vehicle distribution identified in alternative four portray similar aggregate operating characteristics for the entire vehicle fleet as demonstrated in their consistency to provide similar results. It is important to note here that the alternative in which no trucks are included in the distribution (alternative one) and the alternative where all trucks are categorized as semi-trailers with full loads (alternative five) do not provide similar results to the base conditions, thus pointing to the necessity of inclusion of the vehicle distribution, with the hypothesis that more than one vehicle distribution can provide similar results, as can more than one parameter set, as illustrated in Section 6.6.

**TABLE 7.5 Objective Function Analysis Results**

<b>Alt.</b>	<b>Description</b>	<b>Volume MAER</b>	<b>TT MAER</b>	<b>Fitness Value</b>
<b>Base</b>	Calibrated parameter set and distribution	0.086	0.163	65.8
<b>1</b>	Default parameter set and distribution—no trucks	0.090	0.220	60.7
<b>2</b>	Default parameter set, calibrated distribution	0.115	0.227	56.5
<b>3</b>	Calibrated parameter set, default distribution	0.082	0.179	65.2
<b>4</b>	Calibrated parameter set, semi-trailer medium load	0.088	0.171	64.8
<b>5</b>	Calibrated parameter set, semi-trailer full load	0.107	0.183	61.0

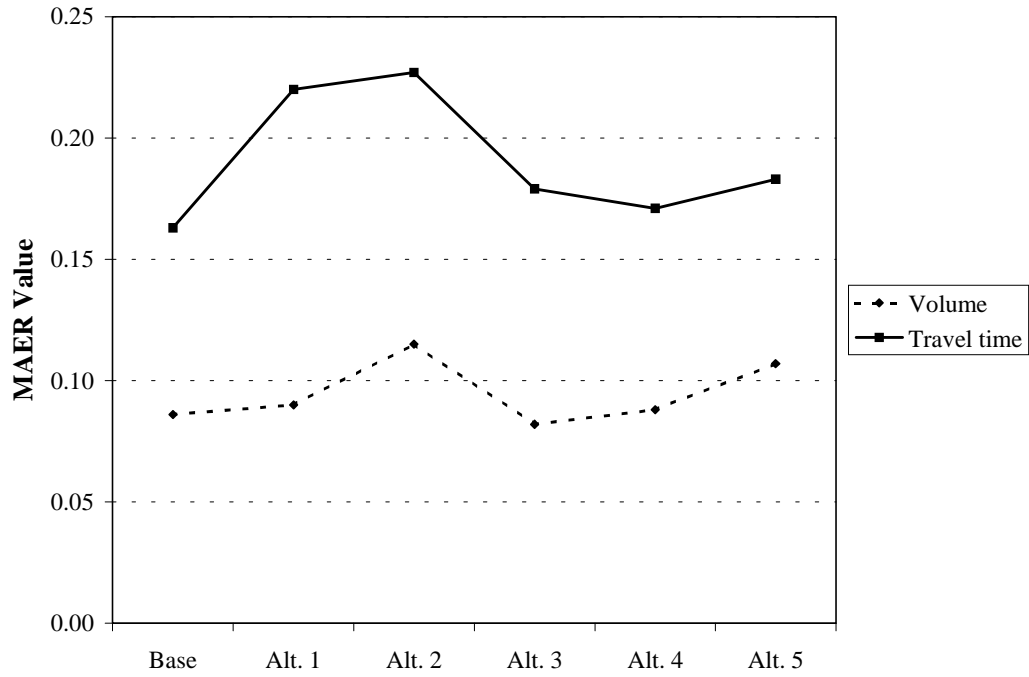


**FIGURE 7.1 MAER sensitivity analysis results**

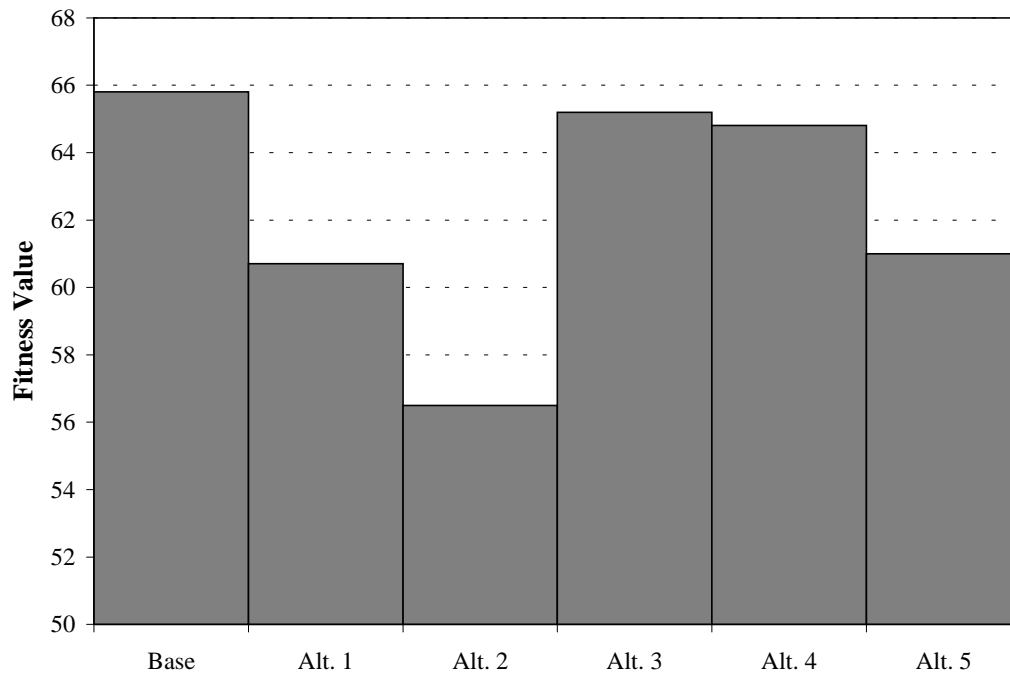


**FIGURE 7.2 Fitness value sensitivity analysis results**

### 7.3.2 Volume, Travel Time, and Delay

The next step in the sensitivity analysis was an evaluation of the simulated volume and travel time results, along with an analysis of the vehicle delay across the network recorded as minutes of delay per vehicle mile of travel. The results of the delay values are provided in Table 7.6, while a graphical representation of the volume and travel time results are provided in Figure 7.3 for the volume analysis and in Figure 7.4 for the travel time results. It is important to point out that in these figures, the y-axis does not cross at zero. This allows the results to be displayed more clearly, but it should be noted when considering the overall scale of these values.

The results of the delay analysis are similar to the MAER and fitness value results, with the largest difference between base conditions and evaluation alternatives occurring in alternative two, where the delay increases from a value of 0.78 minutes of delay per vehicle mile to 1.0 minutes of delay per vehicle mile (28.2 percent increase). The minimum variation occurs for alternative four, where the delay decreases from 0.78 minutes of delay per vehicle mile to 0.75 minutes of delay per vehicle mile (3.85 percent decrease). The results do vary, however, particularly for alternative one, where the fitness value decreased by 7.75 percent, while the delay value differs by only 3.85 percent, equal in value to the variation between the base model and alternative four.

**TABLE 7.6 Network Delay Time Analysis Results**

<b>Alt.</b>	<b>Description</b>	<b>Network Delay (min/veh-mi)</b>
<b>Base</b>	Calibrated parameter set and distribution	0.78
<b>1</b>	Default parameter set and distribution—no trucks	0.81
<b>2</b>	Default parameter set, calibrated distribution	1.00
<b>3</b>	Calibrated parameter set, default distribution	0.69
<b>4</b>	Calibrated parameter set, semi-trailer medium load	0.75
<b>5</b>	Calibrated parameter set, semi-trailer full load	0.86

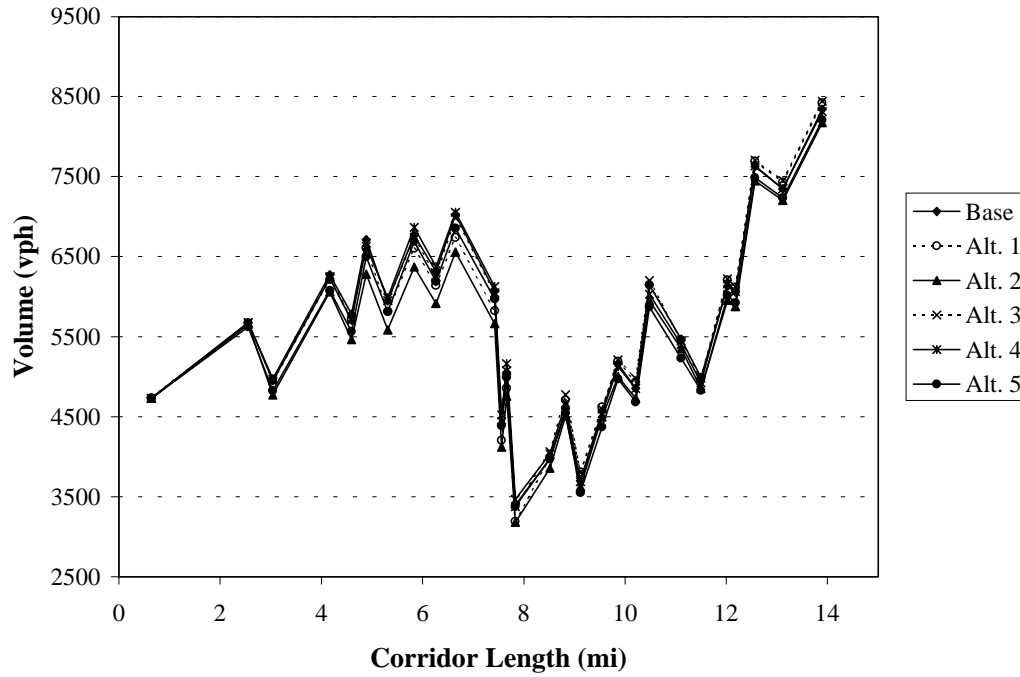


FIGURE 7.3 Volume sensitivity analysis results

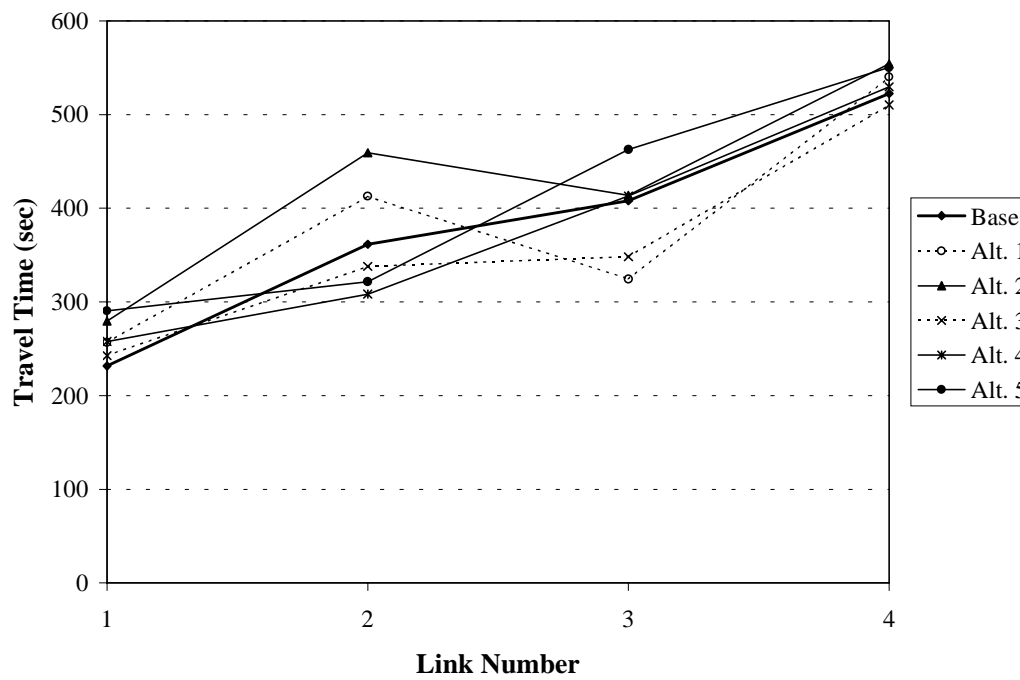


FIGURE 7.4 Travel time sensitivity analysis results

This analysis shows that alternatives one and four provide the closest results to the base model in terms of overall network delay, while alternative two provides the least comparable relationship. The results of the volume analysis indicate that all alternatives follow the same basic pattern; however, the volumes do vary by as much as 10 percent, with alternative two again providing the least comparable results. The travel time analysis results vary on individual links from 346 seconds to 459 seconds (27 percent increase) on link two for alternative two and from 399 seconds to 413 seconds (1.2 percent increase) on link three for alternative four. The total travel time results vary across the network from 1524 seconds to 1707 seconds (12 percent increase) for alternative two, from 1524 seconds to 1534 seconds (0.7 percent increase) for alternative one, and from 1524 seconds to 1509 seconds (1.0 percent decrease) for alternative four. The results shown in this graph do not include the variability of travel time during these same time periods. Although the actual variation in travel time for these alternatives is not known, it is anticipated from the AVI data results identified in Section 6.5.4 that the travel time variability across the network would be greater than 10 percent, making specific recommendations based on the travel time results difficult.

### *7.3.3 CMV Sensitivity Analysis Results*

Overall, the results presented in the previous two sections indicate that the calibration of the parameter set may be more critical in this application than the calibration of the vehicle distribution for this test network. This assumption is based on the results of the objective function sensitivity analysis and the delay analysis, where the calibrated parameter set provides results that most closely resemble the base calibrated model. The alternatives wherein the default calibration parameter set are utilized, particularly in comparing the MAER and fitness value, show results that do not as closely match the base calibration results. The alternatives that utilize the calibrated parameter set with different distributions (particularly the default distribution and the truck distribution that includes 100 percent semi-trailer with a medium load) provide similar results to the base calibrated model. It is hypothesized that these distributions portray similar aggregate operating characteristics for the entire vehicle fleet as demonstrated in their consistency to provide similar results, which may not occur if the calibrated distribution exhibited different characteristics. Overall, the results do indicate a need to calibrate the parameter set to provide results consistent with base conditions, as well as a need to calibrate the vehicle distribution to actual conditions or to a distribution consistent with actual conditions.

## 7.4 Emissions Analysis

The next step in providing an evaluation of the different alternatives was an emissions analysis of the base model and the five alternatives. A handful of models are currently available to evaluate air quality emissions at both an aggregate and disaggregate level. The primary models for modeling emissions output are the MOBILE models developed by the United States Environmental Protection Agency (EPA) (169), the EMFA model developed by the California Air Resources Board (CARB), and the Comprehensive Modal Emissions Model (CMEM) developed at the College of Engineering—Center for Environmental Research and Technology (CE-CERT) at the University of California, Riverside, with support from researchers at the University of Michigan and Lawrence Berkeley National Laboratory (170, 171). In addition to these models, a number of other models have also been developed over the years, as well as emissions models internal to simulation programs. The emissions analysis in this section was completed for each scenario using the CMEM model based on the ability of the model to estimate emissions from disaggregate data, including second-by-second velocity data for each vehicle in the network. This analysis was completed for one link (node 19 to node 20) along the network and included an analysis of the base conditions and each of the five alternatives.

To evaluate the emissions output, this section will be broken into four subsections. The first subsection provides background information on the CMEM model, the second subsection presents the input data process, the third subsection provides the output data from the CMEM model, while the fourth and final subsection outlines the results of the analysis.

### 7.4.1 Comprehensive Modal Emissions Model Background

As indicated previously, CMEM was developed at CE-CERT and was sponsored by the NCHRP (Project 25-11), with the primary objective to develop and verify a modal emissions model that would accurately reflect the emissions produced by light-duty vehicles (LDV) (i.e., cars, small trucks) as a function of the vehicle's operating mode (i.e., velocity, acceleration). CMEM is a comprehensive model because it is able to predict emissions from a variety of LDVs in various conditions (i.e., properly functioning, malfunctioning, deteriorating). The output of the model provides second-by-second tailpipe emissions estimates for hydrocarbons (HC), carbon monoxide (CO), nitrogen oxides (NO<sub>x</sub>), and fuel consumption for a wide range of vehicle categories (170).

Although the initial purpose of the CMEM research project was to develop a modal emissions model that would estimate emissions for LDVs, a later phase of the project determined the need to include additional vehicle and technology categories in the model to better estimate emissions inventories. The additional categories included both diesel- and gasoline-powered heavier trucks (greater than 8,500 pounds gross vehicle weight [ $> 8,500$  GVW]), as well as late model high emitting vehicles and other high mileage vehicles (170). These additional categories provided a means to estimate tailpipe emissions for a wide variety of vehicle types. A detailed description of all vehicle types and the analysis undertaken to develop the base model can be found in the literature (170, 171).

#### 7.4.2 Emissions Input Data Process

The DOS version of the CMEM batch model was utilized in this analysis to estimate emissions output for the base model and each of the alternatives outlined previously. The CMEM batch model allows the user to obtain emissions data for multiple vehicle types with different trajectories specified in the vehicle activity file. The basic input files of the batch model include: 1) a parameter control file; 2) a time-ordered vehicle activity file; and 3) a vehicle definitions file. More detail on each of these files will be discussed in the following subsections.

**7.4.2.1 Parameter Control File** The parameter control file is used in the model to set the model running parameters and to overwrite default parameters in the model. The running parameters are used to specify the input and output data format and include parameters such as input/output units, vehicle category definitions, soak time, secondary loads, specific humidity, vehicle mass, engine specifications, and so forth. A detailed description of each of the parameters included in the parameter control file can be found in the literature (170). The analysis completed in this dissertation utilized default parameters for the control file.

**7.4.2.2 Vehicle Activity File** The second input file for the CMEM analysis is the vehicle activity file used to define the paths of each of the vehicles on the link or network analyzed and includes time-step, vehicle identification number, velocity, and optional parameters for acceleration, grade, and secondary load for every time-step and vehicle in the network. The time-step is entered in seconds corresponding to each second of the simulation, while the vehicle identification number is necessary to provide a means of identifying each individual vehicle in

the simulation. Each vehicle is assigned a unique identification number, allowing the vehicle to be tracked through the system at each time-step. The velocity is entered in units of miles per hour (mph) and corresponds to the instantaneous velocity of each individual vehicle at that specific time-step. Optional parameters can also be identified in this file, including the acceleration, and grade, as well as a secondary load flag identifying additional demands to the vehicle power (170).

The data utilized in this analysis were second-by-second data obtained from the TRAFVU time-step data conversion outlined previously. This conversion process was utilized to identify the actual vehicle distribution from the model and was subsequently used in the emissions analysis to obtain the required second-by-second output data for analysis. As with the distribution verification analysis, the link analyzed for emissions output was from node 19 to node 20, which includes a bridge segment over Kirkwood Road located in Link 2 of the corridor identified in Section 5.2.1.1. These data were time-ordered and then vehicle-ordered to provide a logical sequence of vehicle activity.

**7.4.2.3 Vehicle Definition File** The batch model vehicle definitions file specifies the categories, soak time values, and specific humidity for each of the vehicles in a given run. The data are entered in the file according to the vehicle identification number, corresponding vehicle category, soak time, and specific humidity. The vehicle identification number is a unique number corresponding to the vehicle identification number used in the activity file to identify each individual vehicle in the simulation. The vehicle category is a number ranging from 1 to 69 corresponding to the vehicle category to be assigned to that vehicle identification number. A detailed description of all vehicle categories available in the model can be found in the literature (170), with a summary of the vehicle categories utilized in this analysis based on the CORSIM vehicle type outlined in Table 7.7. It can be seen from this table that the vehicles in the emissions analysis were modeled based on a small subset of the potential CMEM vehicle technology categories. Although the model provides an opportunity to model individual vehicles on a very specific basis, the breakdown of individual vehicle technology characteristics was not readily available for this analysis. As a result of this lack of site-specific technology characteristics, and to provide for common vehicle technologies across each alternative, only one CMEM category was provided for each CORSIM vehicle type. An alternative to this methodology would be to choose a subset of each vehicle at random and assign different CMEM

vehicle technology categories to each of these subsets based on a known distribution of vehicle technology characteristics.

**TABLE 7.7 Vehicle/Technology Modeled Categories**

<b>CORSIM Distribution</b>	<b>CMEM Category No.</b>	<b>CMEM Vehicle Technology Category</b>
1	10	Tier 1, <50,000 miles, low power/weight
2	11	Tier 1, <50,000 miles, high power/weight
3	25	Gasoline-powered, LDT (>8,500 GVW)
4	25	Gasoline-powered, LDT (>8,500 GVW)
5	40	Diesel-powered, LDT (>8,500 GVW)
6	40	Diesel-powered, LDT (>8,500 GVW)

The soak time defines a vehicle's soak time in minutes and can range from a value of zero (corresponding to hot stabilized operation) to a value of 1,440 (representing a cold start). The soak time utilized in this analysis was zero, indicating all vehicles on the link had been in operation long enough to warm their engines to hot stabilized conditions. The final input is the specific humidity input in units of grains of water per pound of dry air. The default specific humidity value is 75 grains of water per pound of dry air, which represents test conditions at 75 degrees Fahrenheit and 40 percent humidity (170). A slightly higher value of 80 was used in the analysis to correspond to higher humidity conditions in the study area.

#### *7.4.3 Emissions Output Data Process*

The output from the CMEM batch model analysis produces two output files: 1) a second-by-second, time-ordered emissions file and 2) a vehicle integrated emissions file (170). Each of these files will be discussed in the following subsections.

**7.4.3.1 Time-Ordered Emissions Output File** The first of the output files generated by the CMEM analysis is a time-ordered emissions output file providing second-by-second emissions output data for the batch run. The data are presented in a time-ordered and vehicle-ordered fashion following the same format as the vehicle activity input file. The data output in this file includes velocity (mph), tailpipe HC emissions (grams per mile), tailpipe CO emissions (grams

per mile), tailpipe NO<sub>x</sub> emissions (grams per mile), and fuel use (grams per liter of fuel) for each time-step and vehicle modeled (170).

**7.4.3.2 Vehicle-Integrated Emissions File** The second output file presents a summary of the processes followed by the model and includes integrated second-by-second emissions data and optional data specified by the user. This file also provides an aggregate summary of the time-ordered emissions output file for each individual vehicle during the simulation run (170).

#### 7.4.4 Emissions Analysis Results

The aggregate emissions summary results for one hour of analysis from node 19 to node 20 are provided in Table 7.8 for each of the pollutants by alternative analyzed. These data represent an aggregate average of the total emissions generated for each individual pollutant, divided by the total number of vehicles in the simulation since the total number of vehicles was not constant for each alternative. More detailed descriptive statistics for each alternative are summarized in Table 7.9, including the total number of vehicles (N), the minimum emissions output value (Min.), the maximum emissions output value (Max.), the mean (Mean), and the standard deviation (Std. Dev.) of the emissions output results.

**TABLE 7.8 One-Hour Aggregate Emissions Summary Data—Node 19 to Node 20**

	Mean Aggregate Emissions Results			
	HC (g/mi)	CO (g/mi)	NO <sub>x</sub> (g/mi)	Fuel (g/L)
<b>Base</b>	0.63	72.3	0.80	222.4
<b>Alt. 1</b>	0.82	95.2	0.94	271.1
<b>Alt. 2</b>	0.62	71.2	0.86	246.5
<b>Alt. 3</b>	0.57	64.9	0.72	206.2
<b>Alt. 4</b>	0.53	60.1	0.69	192.3
<b>Alt. 5</b>	0.64	72.4	0.73	217.0

**TABLE 7.9 One-Hour Emissions Descriptive Statistics—Node 19 to Node 20**

		Emissions Results			
		HC (g/mi)	CO (g/mi)	NO <sub>x</sub> (g/mi)	Fuel (g/L)
<b>Base</b>	<b>N</b>	6,391	6,391	6,391	6,391
	<b>Min.</b>	0.01	0.05	0.01	39.60
	<b>Max.</b>	2.49	283.81	7.20	630.60
	<b>Mean</b>	0.63	72.28	0.80	222.44
	<b>Std. Dev.</b>	0.50	60.17	0.66	103.03
<b>Alt. 1</b>	<b>N</b>	6,245	6,245	6,245	6,245
	<b>Min.</b>	0.01	0.09	0.1	54.90
	<b>Max.</b>	2.70	317.45	2.15	515.60
	<b>Mean</b>	0.82	95.15	0.94	271.12
	<b>Std. Dev.</b>	0.54	64.70	0.42	101.48
<b>Alt. 2</b>	<b>N</b>	6,003	6,003	6,003	6,003
	<b>Min.</b>	0.01	0.09	0.01	41.80
	<b>Max.</b>	2.74	326.25	6.89	563.70
	<b>Mean</b>	0.62	71.22	0.86	246.49
	<b>Std. Dev.</b>	0.50	64.52	0.67	108.49
<b>Alt. 3</b>	<b>N</b>	6,335	6,335	6,335	6,335
	<b>Min.</b>	0.00	0.09	0.01	50.40
	<b>Max.</b>	3.87	465.26	6.84	636.10
	<b>Mean</b>	0.57	64.90	0.72	206.22
	<b>Std. Dev.</b>	0.50	60.16	0.61	104.58
<b>Alt. 4</b>	<b>N</b>	6,457	6,457	6,457	6,457
	<b>Min.</b>	0.00	0.11	0.01	37.80
	<b>Max.</b>	3.71	434.21	4.44	674.70
	<b>Mean</b>	0.53	60.08	0.69	192.34
	<b>Std. Dev.</b>	0.48	58.07	0.58	99.04
<b>Alt. 5</b>	<b>N</b>	6,277	6,277	6,277	6,277
	<b>Min.</b>	0.00	0.08	0.01	39.30
	<b>Max.</b>	3.71	448.50	2.79	650.00
	<b>Mean</b>	0.64	72.39	0.73	216.95
	<b>Std. Dev.</b>	0.48	58.36	0.41	93.98

The mean aggregate emissions values for HC output ranges from a low of 0.53 grams per mile for alternative four to a high of 0.82 grams per mile for alternative one. The mean aggregate emissions values for CO range from a low of 60.1 for alternative four to a high of 95.2 for alternative one. The mean aggregate emissions value for NO<sub>x</sub> range from a low of 0.96 grams per mile to a high of 0.94 grams per mile for alternative one, and the mean aggregate emissions value for fuel emissions range from a low of 192.3 grams per liter for alternative four to a high of 271.1 grams per liter for alternative one. Each of these results is consistent with the

lowest values occurring in each instance for alternative four and the highest emissions rates occurring for alternative one. Alternative four represents a model utilizing the calibrated parameter set and a truck distribution that includes all semi-trailer medium load vehicles with corresponding CMEM category diesel-powered heavy truck, while alternative one is a model in which the default parameter set and distribution with no heavy trucks is modeled. These results would indicate, therefore, that the inclusion of CMVs in the traffic stream tends to reduce the overall emissions rates on the freeway, with the alternative in which no trucks are present in the traffic stream providing the highest aggregate emissions for each pollutant. These results are further summarized in the detailed descriptive statistics for each model as outlined.

To further analyze the comparisons between alternatives and to provide a statistical analysis of the mean pollutant levels for each alternative, Tukey and Bonferroni pairwise comparisons outlined previously in Section 4.1.2.3 were conducted for each of the pollutants analyzed. The purpose of these tests were to compare the difference in the means for all pairs of pollutants and to develop confidence intervals based on the difference in means. The results of this analysis are summarized in Table 7.10 for the HC analysis, Table 7.11 for the CO analysis, Table 7.12 for the NO<sub>x</sub> analysis, and Table 7.13 for the fuel emissions. In these tables, a shaded block identifies the alternatives where the difference between the mean average emission level is not significant, thus indicating that the alternatives may be the same.

The results of the pairwise analyses show different results than an initial analysis of the mean values by indicating that the mean difference for the majority of the alternatives and pollutants are significantly different. For the HC and CO pollutants, the base analysis, alternative two, and alternative five provide mean differences that are not significant, suggesting that there is little correlation between the calibrated parameter set and the vehicle distribution with respect to HC and CO, as alternative two utilizes the default parameter set and alternative five is comprised of a truck distribution that includes only one category of vehicles. For the NO<sub>x</sub> analysis, alternatives three and five exhibit similar characteristics, where alternative three is comprised of a model that includes the calibrated parameter set and default distribution and alternative five is comprised of the calibrated parameter set and a truck distribution that includes only one category of trucks. The fuel emissions results show that none of the alternatives are the same, indicating that there are no similarities between models when considering the fuel emission rates.

**TABLE 7.10 HC Emission Results Pairwise Analysis**

	Base	Alt. 1	Alt. 2	Alt. 3	Alt. 4	Alt. 5
Base						
Alt. 1						
Alt. 2						
Alt. 3						
Alt. 4						
Alt. 5						

Note: Shaded squares denote differences between mean average emissions level are not significant

**TABLE 7.11 CO Emission Results Pairwise Analysis**

	Base	Alt. 1	Alt. 2	Alt. 3	Alt. 4	Alt. 5
Base						
Alt. 1						
Alt. 2						
Alt. 3						
Alt. 4						
Alt. 5						

Note: Shaded squares denote differences between mean average emissions level are not significant

**TABLE 7.12 NO<sub>x</sub> Emission Results Pairwise Analysis**

	Base	Alt. 1	Alt. 2	Alt. 3	Alt. 4	Alt. 5
Base						
Alt. 1						
Alt. 2						
Alt. 3						
Alt. 4						
Alt. 5						

Note: Shaded squares denote differences between mean average emissions level are not significant

**TABLE 7.13 Fuel Emission Results Pairwise Analysis**

	Base	Alt. 1	Alt. 2	Alt. 3	Alt. 4	Alt. 5
Base						
Alt. 1						
Alt. 2						
Alt. 3						
Alt. 4						
Alt. 5						

Note: Shaded squares denote differences between mean average emissions level are not significant

The overall results of the analysis would suggest that there is little correlation between the calibrated parameter set or calibrated distribution when analyzing the emissions results. This is contrary to the results obtained in the previous sections where MAER, fitness function, and delay provided more correlation between calibration parameters and overall results. One result that is conclusive in this analysis is that the emissions analysis alternatives one and four seem to define worst and best emission rates, respectively, indicating that the inclusion of vehicle distribution provides lower overall emissions than including all passenger cars in the analysis.

## **7.5 CMV Growth Sensitivity Analysis**

The final analysis performed to analyze the sensitivity of the calibrated model was a growth analysis, wherein the existing conditions model was analyzed under a constant growth scenario and analyzed for each alternative. The purpose of this analysis was not to forecast expected conditions on the test network; rather the purpose was to analyze the robustness of the calibrated model assuming constant growth on the network. The growth sensitivity analysis included both volume and distribution, with results analyzed based on volume and travel time. To evaluate the growth sensitivity analysis, this section will be presented in three subsections. The first subsection will present the results of traffic volume growth trends, the second subsection will analyze the vehicle composition trends across the network, and the third section will provide the results of the analysis. In keeping with the previous sections of this dissertation, the primary network analyzed in this section is the IH-10 Katy Freeway AM peak period.

### *7.5.1 Traffic Volume Trends*

The traffic volume growth process included an analysis of traffic volume trends in the general vicinity of the test network. The data collection methodologies outlined in Section 3.1 provided the basis for data collection across the state of Texas and included short-term and long-term data collection methods, comprised primarily of continuous count and short-duration count programs. As outlined in Section 3.1, the primary purpose of the continuous count program is to better understand the temporal changes in traffic volumes, including time-of-day, day-of-week, and seasonal variations that can be used to improve the accuracy of traffic estimates and subsequent traffic analyses (55). TxDOT collects data on a continuous basis using a variety of data collection techniques as outlined in Section 3.1. The primary source of data collection utilized for this analysis was that of ATR volume data in and around the study area.

TxDOT has in place a number of ATR sites in the downtown Houston core that collect traffic volumes on a continuous basis. As outlined, the network analyzed in this analysis is the IH-10 Katy Freeway, west of downtown. Unfortunately, there is not an ATR site along this corridor that has consistently collected traffic volume data over the past several years. There are, however, other ATR sites in the general vicinity of the test network where sufficient data have been collected over the years. The primary site where data are available occurs on the IH-610 loop, 0.7 miles west of IH-45 in downtown Houston. Traffic data collected at this site indicate that traffic volume growth has ranged from a low of -4.1 percent from 2000 to 2001 to a high of 5.0 percent between 1988 and 1989, with an average straight-line growth rate from 1988 to 2001 of approximately 1.95 percent (172).

Based on the results of the ATR growth trends, a straight-line growth rate of 2.0 percent was utilized in the forecasting analysis to project traffic volumes from the 1996 base conditions to a “simulated” future analysis year of 2010. The future projections analysis was kept somewhat basic, with the 2.0 percent growth rate applied at all locations along the network to provide an analysis of the ability of the microscopic traffic simulation model to model constant growth scenarios. The background traffic volumes and resulting future traffic volume analysis results are provided in Appendix E.

### 7.5.2 *Vehicle Composition Trends*

The collection of vehicle classification data has also been discussed in some detail in Sections 3.1.3 and 4.2.2 of this dissertation, while the use of existing year AVC data was later introduced in Section 5.3.2.3.3 as a successful methodology to calibrate vehicle composition for analysis in microscopic traffic simulation models and subsequently to generate vehicle distribution data in the base traffic simulation model. In order to examine the future projections of vehicle composition, a similar analysis to the one presented for traffic volumes was undertaken for vehicle composition. In this analysis, vehicle classification data were obtained along the IH-10 corridor for 1997 (173), 1998 (174), 1999 (175), and 2001 (172) to explore the trends in vehicle distribution. The results of this analysis as a percent of total vehicles along the corridor are provided in Table 7.14 for automobiles and Groups A, B, and C as identified in Section 4.2.2, while Table 7.15 provides the distribution of trucks for each of the respective groups.

**TABLE 7.14 IH-10 Katy Freeway Vehicle Composition Trends 1997–2001**

	Vehicle Composition, %			
	2001	1999	1998	1997
<b>Auto</b>	92.2	90.6	92.1	93.5
<b>Group A</b>	2.7	3.4	3.0	1.7
<b>Group B</b>	1.2	1.5	1.2	1.0
<b>Group C</b>	3.9	4.6	3.7	3.8

**TABLE 7.15 IH-10 Katy Freeway Truck Distribution Trends 1997–2001**

	Truck Distribution, %			
	2001	1999	1998	1997
<b>Group A</b>	34.4	35.5	37.3	25.9
<b>Group B</b>	14.9	15.9	15.6	15.5
<b>Group C</b>	50.6	48.6	47.0	58.5

The data in these tables represent aggregate data for traffic volumes across the entire day rather than representing disaggregate design hours as has been presented in previous sections. The analysis results indicate that overall auto percentages have ranged from a low of approximately 91 percent in 1999 to a high of nearly 94 percent in 1997. Group A distributions have ranged from a high of approximately 37 percent in 1998 to a low of approximately 26 percent in 1997, Group B distributions have ranged from a low of approximately 15 percent in 2001 to a high of approximately 16 percent in 1998, and Group C distribution have ranged from a low of 47 percent in 1998 to a high of nearly 59 percent in 1997. Overall, the distributions have remained relatively unchanged in the urban core, even with the overall increases in truck traffic that were identified in Section 2.1. As a result of the relative consistency on this corridor, the distributions have remained unchanged in this analysis.

### 7.5.3 Constant Growth Analysis Results

A graphical representation of the volume and travel time constant growth analysis results are provided in Figure 7.5 for the volume analysis and in Figure 7.6 for the travel time results, while the AM peak period constant growth sensitivity analysis results of the delay values are provided in Table 7.16.

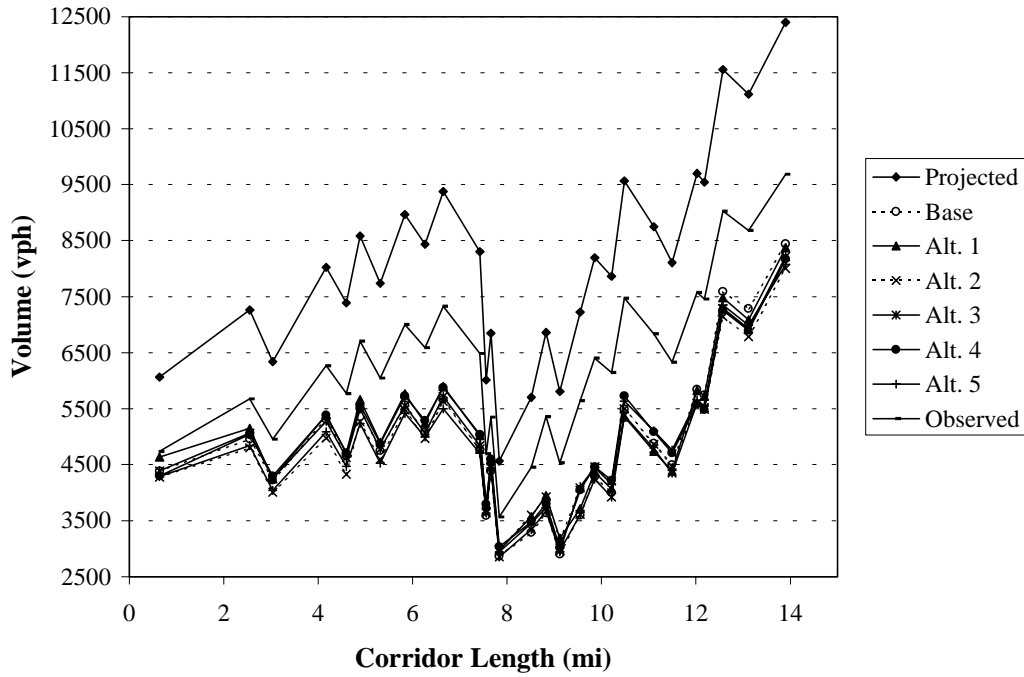


FIGURE 7.5 Constant growth volume sensitivity analysis (AM peak period)

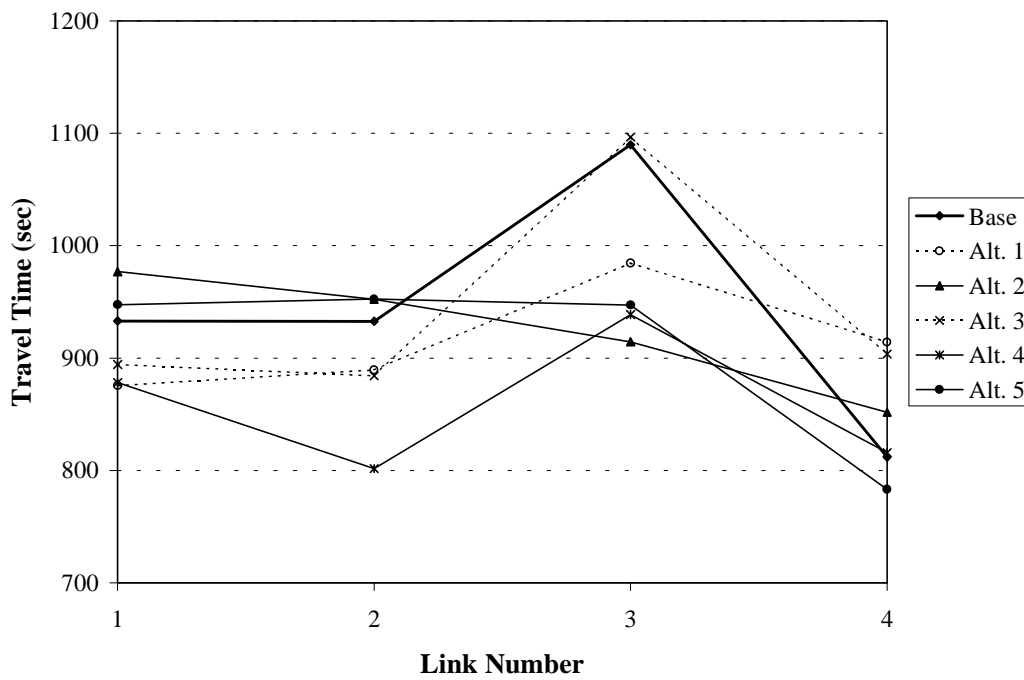


FIGURE 7.6 Constant growth travel time sensitivity analysis (AM peak period)

**TABLE 7.16 Constant Growth Network Delay Results (AM Peak Period)**

<b>Alt.</b>	<b>Description</b>	<b>Network Delay (min/veh-mi)</b>
<b>Base</b>	Calibrated parameter set and distribution	3.12
<b>1</b>	Default parameter set and distribution—no trucks	3.06
<b>2</b>	Default parameter set, calibrated distribution	3.18
<b>3</b>	Calibrated parameter set, default distribution	3.16
<b>4</b>	Calibrated parameter set, semi-trailer medium load	2.86
<b>5</b>	Calibrated parameter set, semi-trailer full load	3.07

The results of the delay analysis clearly show that the overall delay increased substantially from the existing conditions analysis and was relatively consistent for all alternatives. The largest difference between future base conditions and evaluation alternatives occurs in alternative four where the delay decreases from 3.12 minutes of delay per vehicle mile to 2.86 minutes of delay per vehicle mile (8.33 percent decrease). The minimum variation occurs for alternative three, where the delay increases from 3.12 minutes of delay per vehicle mile to 3.16 minutes of delay per vehicle mile (1.28 percent increase). These results are contrary to the results presented in the original model, where alternative four provided the best comparison. It is important to note, however, that the overall variation between each of the alternatives is less than 10 percent, which generally indicates that the results are very similar. It is hypothesized in this case that the delay results have leveled off due to the overly congested conditions displayed by this analysis.

The volume and travel time analysis confirms the assumption from the delay analysis results that the model has reached capacity and is unable to provide for the demand outlined in the constant growth 2010 model. The volume analysis results indicate that all alternatives follow the same basic pattern and that the volumes are well below both future projected and existing observed volume results. The travel time analysis also shows very similar results with variation less than 200 seconds across all alternatives. It is again hypothesized that the traffic demand far exceeds capacity on the network and gridlock conditions now exist, which is consistent with current design plans since this segment of freeway is currently scheduled for major reconstruction work due to capacity constraints.

To provide a more conservative future growth scenario, therefore, an analysis of the off peak period results was conducted based on the same growth rates and vehicle distribution adjustments outlined earlier in this section. The off peak period analysis provides a better

opportunity to analyze the ability of the model to adequately represent projected conditions. The off peak period analysis was conducted for the base and alternative one equivalent conditions only and includes an analysis of delay and volume only. The off peak period constant growth sensitivity analysis results of the delay values are provided in Table 7.17, while a graphical representation of the volume results is provided in Figure 7.7.

**TABLE 7.17 Constant Growth Network Delay Results (Off Peak Period)**

Alt.	Description	Network Delay (min/veh-mi)
<b>Base</b>	Calibrated parameter set and distribution	0.52
<b>1</b>	Default parameter set and distribution—no trucks	1.06

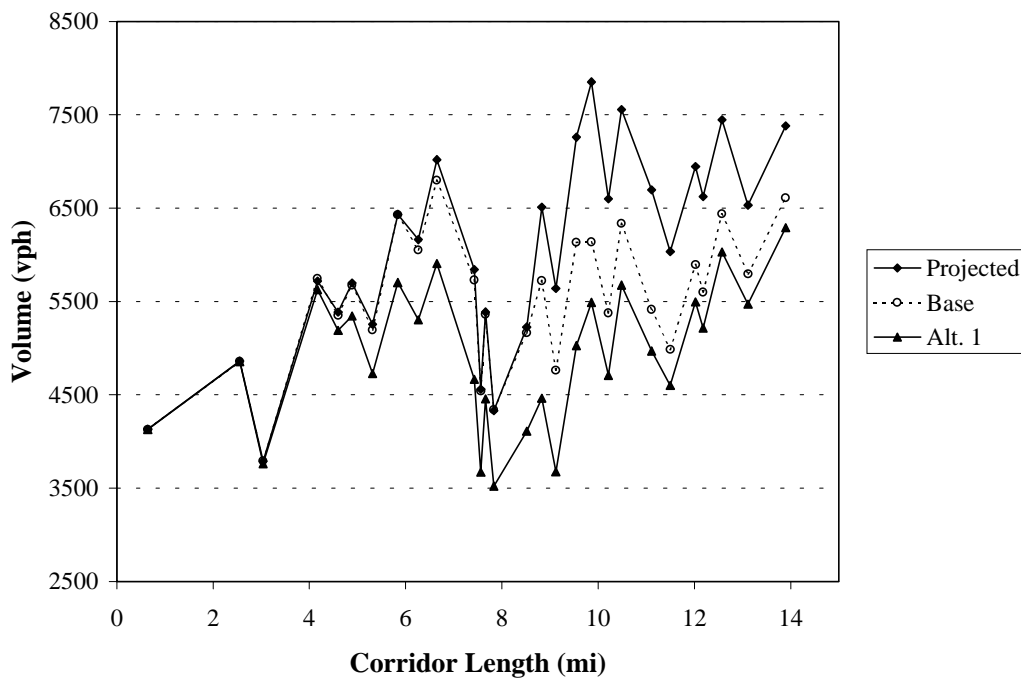


**FIGURE 7.7 Constant growth volume sensitivity analysis (off peak period)**

The results of the delay analysis clearly show that the overall delay increases substantially from the base model analysis to the default conditions analysis. The overall network delay increases over 100 percent from 0.52 minutes of delay per vehicle mile to

1.06 minutes of delay per vehicle mile. The calibrated model provides far better results when compared to default conditions for the constant growth analysis during the off peak period.

The volume analysis presented for the off peak period provides confirmation that the calibrated base model provides better analysis results than the default conditions, particularly in areas where the model has not reached capacity. The volume analysis results indicate that the base model provides results that better represent projected conditions, particularly early in the corridor. Once the midpoint in the corridor is reached, the ability to adequately represent these conditions is diminished, as the corridor begins to approach capacity. The calibrated network, however, would provide an opportunity to implement design changes to the corridor and analyze the impacts that these changes have on the ability of the model to represent projected conditions. The calibrated model provides a better representation of the projected operating conditions, thus improving the accuracy of future conditions analyses.

## **7.6 Concluding Remarks**

This section has provided a sensitivity analysis of the calibrated microscopic traffic simulation model, providing comparisons between the base calibrated model and five alternatives exhibiting different combinations of calibrated and default inputs. The five alternatives included: 1) default parameter set with no trucks; 2) default parameter set with a calibrated truck distribution; 3) calibrated parameter set with default truck distribution; 4) calibrated parameter set with 100 percent of the truck distribution represented by semi-trailer medium load vehicles; and 5) calibrated parameter set with 100 percent of the truck distribution represented by semi-trailer full load vehicles.

The first step in the sensitivity analysis was a verification of the simulated vehicle distributions. This step was necessary to ensure that the models were simulating the distributions as input and to identify the distribution of vehicles output by the model. The results of this analysis indicated that the distributions generated by the model closely match the input. This step is also critical in evaluating possible infrastructure impacts from the model results. By generating model output distributions, infrastructure impacts can be estimated using pavement and/or structural analysis methods (24).

The CMV sensitivity analysis was performed utilizing the objective function, travel time, volume, delay, and emissions output. When comparing the objective function between all alternatives, the base calibrated model appeared to most closely resemble alternatives three and

four, both of which include a calibrated parameter set, with alternative three including the default distribution and alternative four including a truck distribution of all semi-trailer medium load vehicles. It is hypothesized in this case that the calibrated, default, and semi-trailer medium load truck distributions provided similar aggregate operating characteristics and, therefore, similar results. If the calibrated distributions provided more diversity by vehicle types, it is anticipated that this relationship might not hold. The overall result of the objective function analysis, therefore, was that the calibrated parameter set is an important factor in accurately representing both volume and travel time along the corridor. The results of the volume, travel time, and delay analyses were comparable to the objective function analysis, with the calibrated parameter set providing delay results that most closely match the base calibration alternative.

The next sensitivity analysis performed was that of emissions. The results of this analysis indicated that the emissions output from the base alternative most closely matched the emissions output from alternative two (default parameter set and calibrated distribution) and alternative five (calibrated parameter set, semi-trailer full load truck distribution), placing more emphasis on the vehicle distribution than the parameter set. It is apparent from the emissions analysis results that the calibrated distribution results provide lower overall emissions output results and, therefore, the calibration of the distribution is important in maintaining accurate emissions reporting for alternatives.

In analyzing these results, it is clear that the calibration of both the parameter set and the distribution is important in providing comparable analyses for both existing and growth conditions. The constant growth analysis performed in Section 7.5 showed that the calibrated alternatives performed better than the default model, and it is hypothesized that the calibrated model would provide better overall analysis results when analyzing improvement alternatives. Although the results indicate that a calibrated parameter set is necessary to provide a more accurate representation of existing conditions, the results also show that a full calibration may not be necessary. The results of Section 6.6 indicated that the objective function might be satisfied just as well with a calibration of parameters  $P_1$  through  $P_{19}$ , as with  $P_1$  through  $P_{28}$ . A thorough calibration of the primary calibration parameters as well as the distribution of vehicles appeared to provide the “best” alternative for existing and growth analyses.

## 8. CONCLUSIONS AND FUTURE RESEARCH

### 8.1 Summary

The problem statement for this research identified three primary needs: 1) the need to incorporate CMV weight and classification ITS data into microscopic traffic simulation models; 2) the need to develop a methodology to calibrate microscopic traffic simulation models to account for CMVs; and 3) the need to generate accurate disaggregate input data for use in CMV infrastructure, travel time, and emissions analyses. Each of these three needs has been addressed through the research objectives and subsequent work plan. A summary of each of these needs and the resulting research to address these needs is provided in the following subsections.

#### *8.1.1 Incorporating CMV ITS Data into Microscopic Traffic Simulation Models*

The need to incorporate CMV ITS data into microscopic traffic simulation models was established primarily in Section 3 and Section 4. The purpose of Section 3 was to identify the data collection methodologies and techniques in the state of Texas for collection of volume, classification, and weight data, and to subsequently use these data to develop a methodology to incorporate CMV ITS data into microscopic traffic simulation models. The primary sources of data collection in the state of Texas for these metrics included: 1) traffic volume data at approximately 160 permanent ATR sites; 2) volume and classification data at approximately 250 AVC sites across the state; and 3) volume, classification, and weight data collected at a maximum of 21 WIM sites across the state. The most important of these three, and subsequently the focus of Section 3, was the collection of CMV volume, classification, and weight data. These data were determined to be the most critical ITS data source as they provide information that is used as input to some of the most critical tasks in transportation engineering and planning, including: 1) pavement and bridge design, maintenance, and loading restrictions; 2) economic analyses, including the development of equitable tax structures; 3) CMV weight enforcement actions; 4) geometric design considerations; and 5) safety improvement analyses (55). It is important to note that although the data collected for this analysis focused on the state of Texas, the process can be applied to any state.

To accomplish the purpose outlined in Section 3, WIM data were obtained for the nine operational sites in Texas during 2001, providing data on over 200,000 CMVs with traffic data recorded by date, time, vehicle classification, aggregate vehicle weight, aggregate vehicle length,

disaggregate vehicle length by axle spacing, and disaggregate axle weight. A preliminary analysis of the dataset was conducted and evaluated based on: 1) temporal and spatial distribution; 2) vehicle classification; and 3) total weight and spacing. The results of this analysis began to pinpoint anomalies in the dataset that required further analysis.

In Section 4 statistical analysis tools were used to provide a more detailed analysis of the dataset generated in Section 3, including a distribution of vehicle weight and length that adequately represented the data. The statistical analysis tools used included primarily: 1) PCA and 2) the recursive partitioning tool, CART. First, a preliminary analysis of the dataset was conducted, resulting in the following modifications: 1) truncation of the dataset to include only vehicles with GVW of 8,000 pounds or greater; 2) truncation of the dataset to remove vehicles with a total length less than 11 feet and/or total spacing between the first two axles less than 10 feet; and 3) removal of all Class 13 data based on the initial PCA results. The resulting dataset was carried forth through the analysis.

Secondary analyses were conducted using the preliminary analysis dataset, including spatial and temporal analyses of the data, as well as an analysis of the distribution and the relationship between total weight and vehicle classification. The final dataset from this analysis included approximately 77 percent of the original raw dataset, with weight and spacing characteristics consistent across the state. This dataset was then used as input to the data mining tool CART to develop a distribution of CMV weight and length that could be used in microscopic traffic simulation models. The results of this analysis identified three primary groupings of the vehicles summarized as: 1) light trucks (average total weight approximately 12,500 pounds); 2) medium trucks (average total weight approximately 28,000 pounds); and 3) heavy trucks (average total weight approximately 55,000 pounds). In addition to providing a distribution of vehicle types for use in microscopic traffic simulation models, this analysis also provided an opportunity to: 1) further reduce the complexity of the multivariate dataset for ease in analysis of the data; 2) provide an alternative for weight groupings identified in the TMG; and 3) identify the relationships between vehicle weight and classification data for use in estimating weight and length distributions at AVC data collection sites.

#### *8.1.2 Calibrating Microscopic Traffic Simulation Models to Account for CMVs*

In order to accurately reflect the weight distribution of CMVs, there is a need to develop a methodology to calibrate microscopic traffic simulation models to account for these vehicles.

An overview of the microscopic traffic simulation aspect of the calibration methodology was outlined in Section 5, with a proposed automated calibration procedure identified in Section 6. The purpose of Section 5 was to discuss the parameters available in microscopic traffic simulation models to address the needs of both passenger cars and CMVs. First, a conceptual calibration methodology that explicitly included microscopic traffic simulation input by vehicle type was proposed. This method was used to identify both spatial and temporal changes, by vehicle type. It was determined in this analysis that to adequately model traffic conditions using microscopic traffic simulation models, the model must be calibrated, or adjusted, such that it accurately reflected the specific components of the system being analyzed. This analysis further identified calibration by vehicle composition as an important aspect of this process, as well as a necessity to meet the need to develop a methodology to model CMVs using these models.

To apply the concepts of the calibration methodology and to begin the process of developing a methodology to calibrate microscopic traffic simulation models to account for CMVs, an application using the CORSIM model was introduced. Although the application in this dissertation is specific to the CORSIM model, the concepts identified can be applied to any microscopic traffic simulation model. Two freeway test networks in Houston, Texas, were used in the analysis. The methodology outlined included calibration of three primary categories of parameters: 1) maximum non-emergency deceleration by vehicle type; 2) speed and acceleration characteristics by vehicle type; and 3) fleet distribution characteristics. The deceleration, speed, and acceleration characteristics of the model were calibrated based on observed distributions of vehicle fleet, with most models providing adequate ranges for these parameters. It was determined for this application that the fleet distribution characteristics were the most important characteristics for calibration to adequately account for the effects of CMVs, while the deceleration and acceleration characteristics utilized default parameter settings, according to the calibrated fleet distribution.

The fleet distribution characteristics were calibrated based on the results of Section 4, with specific application of these results to the simulation model provided in Section 5. This analysis provided a calibrated vehicle distribution table as well as operating characteristics based on the calibrated weight and spacing parameters of the vehicle fleet. Site-specific AVC data were utilized to obtain an accurate representation of the CMV traffic within the network, with the weight and spacing characteristics developed in Section 4 used to calibrate the model. The

resulting CMV distribution and calibration parameters provided an opportunity to analyze the traffic stream using a distribution developed from observed data within the corridor.

The need to develop a methodology to calibrate microscopic traffic simulation models to account for CMVs was continued in Section 6 with the development of an automated calibration methodology for use with the simulation model. This analysis utilized previous automated calibration research and built upon this research to provide an automated calibration methodology to accommodate CMV calibration using microscopic traffic simulation models. The automated calibration methodology used in this analysis was the GA code based on the principles of natural selection and genetics. The GA calibration code was written in the Perl language and was originally developed at the TTI TransLink<sup>®</sup> Research Center (9, 123). The code was modified from its original state to include additional calibration parameters to account for CMVs and was also modified to include two car-following headway distribution algorithms, developed as part of this analysis. These two distributions utilized either a truncated lognormal or truncated normal distribution to assign a mean and standard deviation to the distribution of car-following headways, and to subsequently generate car-following parameters based on this distribution. The simulation output results of these two models were compared with a random distribution assignment, as well as default parameters. This analysis identified all three distributions as effective alternatives at modeling the observed conditions based on the objective function. The lognormal and normal distributions, however, provided several advantages over the random assignment that were not apparent from the results: 1) a statistical distribution of individual driver characteristics (both passenger car and CMV) that can be generated from the mean and variance; 2) a reduction in the amount of redundancy in the calibration parameters because this alternative only required two parameters (mean and standard deviation), rather than 10; and 3) a simplification of the process. Based on the lognormal distribution of car-following headway parameters, a sensitivity analysis of all other parameters in the automated calibration methodology, and a calibrated vehicle fleet, the parameter set was calibrated based on base calibration parameters, as well as base plus vehicle type parameters. In both cases, the model was also calibrated using site-specific vehicle fleet data, thus developing the methodology to account for CMVs using microscopic traffic simulation models.

### 8.1.3 Sensitivity Analysis of CMV Impacts

The final need identified in Section 1 was the need to generate accurate disaggregate input data for use in CMV infrastructure, travel time, and emissions analyses. This was accomplished in Section 7 by testing the proposed microscopic traffic simulation approach and performing sensitivity analyses of the objective function, delay, and emissions results. The sensitivity analyses included a comparison of the calibrated model identified in Section 6, with five alternative models exhibiting different combinations of calibrated and default inputs.

The first step in the analysis of Section 7 was a verification of the simulated vehicle distributions to ensure that the models were simulating the distributions as input and to identify the output distributions of the model. This step was critical in evaluating the infrastructure impacts from the model results. To analyze these impacts, an extraction program was developed to read the disaggregate vehicle results from the simulation output files and then extract individual vehicles from the simulation. This process provides a stream of traffic information that can be used as input to bridge and pavement design models and to estimate the impacts of the vehicle distribution on the infrastructure. Although the model developed in this application does not specifically analyze the infrastructure impacts, the output from the calibrated microscopic traffic simulation model can be used as input to structural analysis tools for this analysis.

Detailed sensitivity analyses were also conducted in Section 7 to compare the calibrated model with the five alternatives mentioned. This analysis identified the impacts of travel time (i.e., volume, delay), as well as emissions. It was assumed for this analysis that the results output by the calibrated simulation model represented “baseline” conditions. This assumption was based on the background behind the calibrated model, and the calibration based on volume and travel time of observed conditions. The results of the objective function analysis indicated that the volume MAER varied from 0.086 to 0.115 (33.7 percent increase) from the base model to a model that included the default parameter set and calibrated distribution, to 0.086 to 0.088 (2.3 percent increase) between the base model and a model that included the calibrated parameter set and a distribution of all semi-trailer medium load CMVs. The travel time MAER results were similar, with the fitness function analysis again providing the worst-case scenario (14.1 percent decrease) between the base model and a model that included the default parameter set and the calibrated distribution. The results of this analysis suggested that the calibration of the parameter set was more critical than the calibration of the vehicle distribution. It was

hypothesized in this analysis, however, that the calibrated distribution, the default distribution, and the vehicle distribution that includes all semi-trailer medium load CMVs portray similar aggregate operating characteristics for the vehicle fleet, as demonstrated by their consistency to provide similar results.

The delay sensitivity analysis also provided similar results, with the delay for the default condition increasing 3.85 percent over the base calibrated parameter set, indicating that the calibrated model provides slightly better overall delay results than the default parameter set, while simulating volume and travel time results more accurately than the default conditions. Again the worst case conditions occur between the base model and the model that includes the default parameter set and calibrated distribution, as the delay per vehicle mile increased by 28.2 percent from 0.78 to 1.0 minutes of delay per vehicle mile.

The final sensitivity analysis performed was that of emissions. The results of this analysis indicated that the emissions output from the base alternative most closely matched the emissions output from the default parameter set and calibrated distribution, as well as the calibrated parameter set, semi-trailer full load truck distribution. This is contrary to the results of the travel time and delay analysis, indicating that the emissions output results place more emphasis on vehicle distribution than on the parameter set. This is not surprising given the emphasis placed by the emissions model on vehicle composition. It is apparent from the emissions analysis results that the calibrated distribution results provide lower overall emissions output results, and therefore the calibration of the distribution is important in maintaining accurate emissions reporting for alternatives.

## **8.2 Conclusions**

The primary question that is answered through this research is: “Can CMV attributes including weight, distribution, velocity, and acceleration be accurately portrayed using standard microscopic traffic simulation models?” Based on the analysis conducted in this dissertation the answer is a qualified yes. The qualifications are that the output is only as accurate as the underlying microscopic traffic simulation model and the input calibration data.

The research presented in this dissertation outlines the methodology to account for these vehicles and is comprised of five primary steps:

1. analyze CMV weight and length distributions to form relationships and develop a database of CMV characteristics;
2. identify calibration parameters available to accommodate CMVs in a given microscopic traffic simulation model;
3. utilize CMV characteristics identified in step 1 and the microscopic traffic simulation model parameters identified in step 2 to develop a site-specific distribution of CMVs in the analysis network;
4. utilize an automated methodology to calibrate the parameter set to match observed volume and travel time conditions; and
5. utilize the parameter set for existing and future analyses.

As identified in the methodology, the first step is an analysis of CMV weight and length distributions from reliable data on the characteristics of these vehicles. The application in this dissertation included a detailed analysis of the WIM data collection sites in the state of Texas. An alternative to this would be analyses of weigh station records combined with volume and classification data from adjacent ATR and/or AVC sites, respectively. The second step in the methodology is to identify the calibration parameters available to accommodate CMVs for any given microscopic traffic simulation model. The application utilized in this dissertation was that of CORSIM, where specific vehicle fleet parameters are available for calibration of CMVs. These parameters can be identified in any representative microscopic traffic simulation model and utilized in the analysis. The final steps in the analysis are to utilize an automated calibration methodology to calibrate the parameter set to match observed conditions and then utilize this parameter set for future analyses. It was observed throughout the analysis that the parameter set was site specific, with different parameter sets identified for different corridors and time periods analyzed. This is hypothesized to be a result of the driver characteristics on varying roadway and congestion levels, overall roadway characteristics, and interaction of the calibration parameters based on the level of congestion on the network.

In summary, the main contributions of this research are:

1. an analysis of the impacts of CMVs in the state of Texas, the application of which can be applied to any state;

2. the development of a methodology to identify relationships between data collection sites (i.e., WIM, AVC), such that the data collected at WIM sites can be used to estimate weight and length distributions at AVC sites, increasing the total number of representative sites for critical design, operations, and planning applications;
3. utilization of an automated calibration approach to analyze the effects of CMVs in the traffic stream;
4. provision of an alternative methodology to model the distribution of car-following sensitivity factors in microscopic traffic simulation models using lognormal and normal distributions; and
5. development of an overall methodology for CMV analysis that, although it was applied to a series of highway networks, can be applied to a variety of network alternatives.

These contributions can be applied to a variety of circumstances to improve the calibration of microscopic traffic simulation models, particularly with respect to CMVs.

### **8.3 Future Research**

Although the research presented in this dissertation provides several contributions to the transportation literature in the area of CMV analysis and microscopic traffic simulation, there are, however, still a number of topics to be addressed associated with this research.

First, the research performed in this dissertation has limited its application to the CORSIM microscopic traffic simulation model, which is arguably the most widely used microscopic traffic analysis tool in the United States. It is recommended, however, that the proposed methodology be applied to additional microscopic traffic simulation models including TRANSIMS, VISSIM, PARAMICS, and others. In addition to applying the methodology to additional microscopic traffic simulation models, the methodology is also recommended to be applied to additional networks, including application in both rural and urban freeway corridors, as well as non-freeway networks. This application would provide an opportunity to evaluate the application of the proposed methodology at a variety of network and congestion levels, thus clarifying some of the sensitivity analysis results and providing an opportunity to make more detailed recommendations on the application of the methodology.

An additional area of research associated with this analysis is the application of OD estimation and the relationship between the OD characteristics of passenger cars and CMVs in

the traffic stream. As was identified throughout this dissertation, the OD estimate for CMVs is generally assumed to be different than that of automobile traffic although it is rarely treated this way. In this research a sensitivity analysis of both CORSIM default OD and synthetic AVI OD was conducted; however, the OD characteristics for passenger cars and CMVs were unchanged on both a system-wide and a link-specific basis. The focus of this analysis was the weight and spacing characteristics of the model and calibration parameters associated with these characteristics, rather than the OD characteristics of the vehicles. An area of future research, therefore, would be to further analyze the OD characteristics of CMVs and utilize this analysis to re-examine the impacts on both a system-wide and a link-specific basis.

The analysis in this dissertation examines the distribution of car-following sensitivity factors and their impact on overall calibration success. Car-following sensitivity factors are only one of many distributions that could be analyzed in microscopic traffic simulation models. Additional distributions should be analyzed, specifically distributions of output results using different parameter sets or random number seeds. The analysis performed in this dissertation did not vary the random number seed within the CORSIM model. Rather, these numbers were kept constant to analyze only the results of the parameter calibration. A further analysis of the distribution of output results using multiple random number seeds as input to the model and/or multiple calibration parameter sets would provide insight into the overall distribution of results.

Finally, one fundamental question that still remains to be answered when calibrating microscopic traffic simulation models, particularly in high-fidelity models such as CORSIM, is the number of parameters necessary for calibration. It was identified throughout the analysis that a number of calibrated parameter sets provided similar results in terms of overall MAER and fitness value, leading to a need to explore the relationship between the parameter sets. In addition, several calibration parameters can be measured in the field, thus eliminating the need to provide automated calibration results for these parameters and introducing an opportunity to input these values, while calibrating for the remaining parameter values. The flexibility to choose the parameters for calibration versus the parameters with fixed values is recommended for further study.

## REFERENCES

1. NAFTA at Eight, A Foundation for Economic Growth. Office of the United States Trade Representative.  
[http://www.ustr.gov/naftareport/nafta8\\_brochure-eng.pdf](http://www.ustr.gov/naftareport/nafta8_brochure-eng.pdf). Accessed July 11, 2002.
2. The US and Mexico at a Glance. United States Embassy in Mexico.  
<http://www.usembassy-mexico.gov/eataglance1.htm>. Accessed July 10, 2002.
3. NAFTA Free Trade Commission: Joint Statement. Canadian Department of Foreign Affairs and International Trade.  
[http://www.dfait-maeci.gc.ca/nafta-alena/Joint\\_Statement-en.asp](http://www.dfait-maeci.gc.ca/nafta-alena/Joint_Statement-en.asp). Accessed July 10, 2002.
4. Bloomberg, L., and J. Dale. Comparison of VISSIM and CORSIM Traffic Simulation Models on a Congested Network. In *Transportation Research Record 1727*, TRB, National Research Council, Washington, DC, 2000, pp. 52–60.
5. Milam, R. T., and F. Choa. Recommended Guidelines for the Calibration and Validation of Traffic Simulation Models. Fehr and Peers Transportation Consultants.  
[http://www.fehrandpeers.com/publications/papers/traff\\_simulation.pdf](http://www.fehrandpeers.com/publications/papers/traff_simulation.pdf). Accessed July 10, 2002.
6. Druitt, S. An Introduction to Microsimulation. *Traffic Engineering and Control*, Vol. 39, No. 9, September 1998, pp. 480–483.
7. Hellinga, B. R. Requirements for the Calibration of Traffic Simulation Models. University of Waterloo Department of Civil Engineering.  
<http://www.civil.uwaterloo.ca/bhelling/publications/CSCE-1998-calibration.pdf>. Accessed July 10, 2002.
8. Hall, F. L., L. Bloomberg, N. M. Rouphail, B. Eads, and A. D. May. Validation Results for Four Models of Oversaturated Freeway Facilities. In *Transportation Research Record 1710*, TRB, National Research Council, Washington, DC, 2000, pp. 161–170.
9. Kim, K. *Optimization Methodology for the Calibration of Transportation Network Micro-Simulation Models*. Ph.D. dissertation, Texas A&M University, College Station, 2002.
10. *Transportation Statistics Annual Report 2000*. BTS01-02U.S. Department of Transportation, Bureau of Transportation Statistics, Washington, DC, 2001.

11. 1990–2001 Truck Crossings into Mexico from Texas. Texas A&M International University, Texas Center for Border Economic and Enterprise Development.  
<http://texascenter.tamui.edu/bbi/bridge/truck/tksthyr.htm>. Accessed October 14, 2002.
12. 1990–2001 Truck Crossings into Texas from Mexico. Texas A&M International University, Texas Center for Border Economic and Enterprise Development.  
<http://texascenter.tamui.edu/bbi/bridge/truck/tknthyr.htm>. Accessed October 14, 2002.
13. 1990–2001 Vehicle Crossings into Texas from Mexico. Texas A&M International University, Texas Center for Border Economic and Enterprise Development.  
<http://texascenter.tamui.edu/bbi/bridge/vehicle/vhnthyr.htm>. Accessed October 14, 2002.
14. 1990–2001 Vehicle Crossings into Mexico from Texas. Texas A&M International University, Texas Center for Border Economic and Enterprise Development.  
<http://texascenter.tamui.edu/bbi/bridge/vehicle/vhsthyr.htm>. Accessed October 14, 2002.
15. *A Policy on Geometric Design of Highways and Streets*. American Association of State Highway and Transportation Officials, Washington, DC, 2001.
16. Taragin, A. Effect of Length of Grade on Speed of Motor Vehicles. In *Proceedings HRB*, Vol. 25, HRB, National Research Council, Washington, DC, 1945, pp. 342–353.
17. Willey, W. E. Survey of Uphill Speeds of Trucks on Mountain Grades. In *Proceedings HRB*, Vol. 29, HRB, National Research Council, Washington, DC, 1949, pp. 304–310.
18. Huff, T. S., and F. H. Scrivner. Simplified Climbing-Lane Design Theory and Road-Test Results. In *Bulletin 104*, HRB, National Research Council, Washington, DC, 1955, pp. 1–11.
19. Schwender, H. C., O. K. Normann, and J. O. Granum. New Method of Capacity Determination for Rural Roads in Mountainous Terrain. In *Bulletin 167*, HRB, National Research Council, Washington, DC, 1957, pp. 10–37.
20. Gillespie, T. *Methods for Predicting Truck Speed Loss on Grades*. Report FHWA/RD-86/059. FHWA, U.S. Department of Transportation, McLean, VA, 1986.
21. Fancher, Jr., P. S., and T. D. Gillespie. *NCHRP Synthesis of Highway Practice 241: Truck Operating Characteristics*. TRB, National Research Council, Washington, DC, 1997.

22. Eisele, W. L. *Estimating Travel Time Mean and Variance Using Intelligent Transportation Systems Data for Real-Time and Off-Line Transportation Applications*. Ph.D. dissertation. Texas A&M University, College Station, 2001.
23. Eisele, W. L., and L. R. Rilett. *Examining Information Needs for Efficient Motor Carrier Transportation by Investigating Travel Time Characteristics and Logistics*. Report SWUTC/01/473700-00005-1. Texas Transportation Institute, Southwest Region University Transportation Center, Texas A&M University, College Station, 2001.
24. Fry, G. T., P. B. Keating, L. R. Rilett, J. L. Farr, and J. E. Elliott. Advanced Simulation and Fatigue Analysis of Steel Highway Bridge Structures. In *Proceedings of the First International Conference on Steel and Composite Structures*, Association for International Cooperation and Research in Steel-Concrete Composite Structures (ASCCS), Pusan, Korea, 2001, pp. 1103–1110.
25. Rilett, L. R., B. G. Hutchinson, and R. C. G. Haas. Cost Allocation Implications of Flexible Pavement Deterioration Models. In *Transportation Research Record 1215*, TRB, National Research Council, Washington, DC, 1989, pp. 31–42.
26. Rilett, L. R., K. Kim, and B. Raney. Comparison of Low-Fidelity TRANSIMS and High-Fidelity CORSIM Highway Simulation Models with Intelligent Transportation System Data. In *Transportation Research Record 1739*, TRB, National Research Council, Washington, DC, 2000, pp. 1–8.
27. Rilett, L. R. Transportation Planning and TRANSIMS Microsimulation Model. In *Transportation Research Record 1777*, TRB, National Research Council, Washington, DC, 2001, pp. 84–91.
28. Lee, C. E., and N. Souny-Slitine. *Final Research Findings on Traffic-Load Forecasting Using Weigh-in-Motion Data*. Report TX-98/987-7, Center for Transportation Research, The University of Texas at Austin, 1998.
29. Lee, C. E., and J. E. Garner. *Collection and Analysis of Augmented Weigh-in-Motion Data*. Report TX-99/987-8. Center for Transportation Research, The University of Texas at Austin, 1996.
30. *Traffic Data and Analysis Manual*. Texas Department of Transportation, Austin, 2001.

31. Middleton, D., J. A. Crawford, T. B. Carlson, A. S. Cothron, D. Jasek, and E. D. Sepulveda, Jr. *Evaluation of TxDOT's Traffic Data Collection and Load Forecasting Process*. Report FHWA/TX-01/1801-1. Texas Transportation Institute, Texas A&M University, College Station, 2001.
32. Estimates of Commercial Motor Vehicles Using the Southwest Border Crossings. U.S. Department of Transportation, Federal Motor Carrier Safety Administration. <http://www.fmcsa.dot.gov/Pdfs/Dist/VehicleCounts18Apr01.pdf>. Accessed September 25, 2003.
33. Burke, D., T. Lomax, D. Schrank, R. Duarte, and M. Hodgson. *Transportation Aspects of the Maquiladora Industry Located on the Texas/Mexico Border*. Report TX-92/2034-2F. Texas Transportation Institute, Texas A&M University, College Station, 1992.
34. June 20, 2002, News Release: New TTI Study Documents Increasing Traffic Congestion, Confirming Latest Census Findings of Lengthening Commutes. The Road Information Program (TRIP). <http://www.tripnet.org/national/nnrTRIPsAnalysisistoTTIReport062002.htm>. Accessed June 25, 2002.
35. Mannering, F. L., and W. P. Kilareski. *Principles of Highway Engineering and Traffic Analysis*. John Wiley and Sons, Inc., New York, 1990.
36. Mannering, F. L., and W. P. Kilareski. *Principles of Highway Engineering and Traffic Analysis*, 2<sup>nd</sup> ed. John Wiley and Sons, Inc., New York, 1998.
37. St. John, A. D., and D. R. Kobett. *NCHRP Report 185: Grade Effects on Traffic Flow Stability and Capacity*. TRB, National Research Council, Washington, DC, 1978.
38. *Traffic Engineering Handbook*, 5<sup>th</sup> ed. (J. L. Pline, ed.). Institute of Transportation Engineers, Washington, DC, 1999.
39. *Traffic Engineering Handbook*, 4<sup>th</sup> ed. (J. L. Pline, ed.). Prentice-Hall, Inc., Englewood Cliffs, NJ, 1992.
40. *A Policy on Geometric Design of Highways and Streets*. American Association of State Highway and Transportation Officials, Washington, DC, 1994.
41. *Transportation and Traffic Engineering Handbook*, 2<sup>nd</sup> ed. (W. S. Homburger, ed.). Prentice-Hall, Inc., Englewood Cliffs, NJ, 1982.
42. *A Policy on Geometric Design of Highways and Streets*. American Association of State Highway and Transportation Officials, Washington, DC, 1990.

43. *Traffic Engineering Handbook*, 2<sup>nd</sup> ed. (H. K. Evans, ed.). Institute of Traffic Engineers, New Haven, CT, 1950.
44. Gazis, D., R. Herman, and A. Maradudin. The Problem of the Amber Signal Light in Traffic Flow. *Operations Research*, Vol. 8, No. 1, January–February 1960, pp. 112–132.
45. Parsonson, P. S., and A. Santiago. Traffic-Signal Change Period Must Be Improved. *Public Works*, Vol. 112, No. 9, September 1981, pp. 110–113.
46. Williams, W. L. Driver Behavior During the Yellow Interval. In *Transportation Research Record 644*, TRB, National Research Council, Washington, DC, 1977, pp. 75–78.
47. Wortman, R. H., and J. S. Matthias. Evaluation of Driver Behavior at Signalized Intersections. In *Transportation Research Record 904*, TRB, National Research Council, Washington, DC, 1983, pp. 10–20.
48. Wortman, R. H., J. M. Witkowski, and T. C. Fox. Traffic Characteristics During Signal Change Intervals. In *Transportation Research Record 1027*, TRB, National Research Council, Washington, DC, 1985, pp. 4–6.
49. Chang, M. S., C. J. Messer, and A. Santiago. Evaluation of Engineering Factors Affecting Traffic Signal Change Interval. In *Transportation Research Record 956*, TRB, National Research Council, Washington, DC, 1984, pp. 18–21.
50. Olson, P. L., D. E. Cleveland, P. S. Fancher, L. P. Kostyniuk, and L. W. Schneider. *NCHRP Report 270: Parameters Affecting Stopping Sight Distance*. TRB, National Research Council, Washington, DC, 1984.
51. Harwood, D. W., J. M. Mason, W. D. Glauz, B. T. Kulakowski, and K. Fitzpatrick. *Truck Characteristics for Use in Highway Design and Operation, Volume I: Research Report*. Report FHWA-RD-89-226. Midwest Research Institute, Kansas City, MO, 1990.
52. *A Policy on Geometric Design of Highways and Streets*. American Association of State Highway and Transportation Officials, Washington, DC, 1984.
53. *Geometric Design and Operational Considerations for Trucks. An Informational Report of the Institute of Transportation Engineers* (K. Fitzpatrick, chair). Institute of Transportation Engineers, Washington, DC, 1992.

54. Fambro, D. B., K. Fitzpatrick, and R. J. Koppa. *NCHRP Report 400: Determination of Stopping Sight Distances*. TRB, National Research Council, Washington, DC, 1997.
55. *Traffic Monitoring Guide*. FHWA, U.S. Department of Transportation Office of Highway Policy Information, Washington, DC, 2001.
56. *Highway Capacity Manual*. TRB, National Research Council, Washington, DC, 2000.
57. May, A. D. *Traffic Flow Fundamentals*. Prentice-Hall, Inc., Englewood Cliffs, NJ, 1990.
58. McShane, W. R., and R. P. Roess. *Traffic Engineering*. Prentice-Hall, Inc., Englewood Cliffs, NJ, 1990.
59. Mimbel, L. E. Y., and L. A. Klein. Summary of Vehicle Detection and Surveillance Technologies Used in Intelligent Transportation Systems. Southwest Technology Development Institute (SWTDI) at New Mexico State University (NMSU). [http://www.nmsu.edu/Research/traffic/public\\_html/Publications/VC/vdst.pdf](http://www.nmsu.edu/Research/traffic/public_html/Publications/VC/vdst.pdf). Accessed September 17, 2003.
60. Hallenbeck, M., and S. Kim. *Final Technical Report for Task A: Truck Loads and Flows*. Report WA-RD 320.3. Washington State Department of Transportation, Seattle, WA, 1993.
61. Hallenbeck, M., M. Rice, B. Smith, C. Cornell-Martinez, and J. Wilkinson. *Vehicle Volume Distributions by Classification*. Report FHWA-PL-97-025. FHWA, U.S. Department of Transportation, Washington, DC, 1997.
62. *Standard Specification for Highway Weigh-in-Motion (WIM) Systems with User Requirements and Test Methods*. ASTM Designation: E 1318-02. American Society for Testing and Materials (ASTM), West Conshohocken, PA, 2002.
63. Garber, N. J., and L. A. Hoel. *Traffic and Highway Engineering*. West Publishing Company, St. Paul, MN, 1988.
64. The AASHO Road Test, Report 5, Pavement Research. In *Highway Research Board Special Report 61E*, HRB, National Research Council, Washington, DC, 1962, pp. 1–242.
65. Van Til, C. J., B. F. McCullough, B. A. Vallerga, and R. G. Hicks. *NCHRP Report 128: Evaluation of AASHTO Interim Guides for Design of Pavement Structures*. TRB, National Research Council, Washington, DC, 1972.

66. Carmichael III, R. F., F. L. Roberts, P. R. Jodahi, H. J. Treybig, and F. N. Flinn. *Effects of Changes in Legal Load Limits on Pavement Costs: Volume 1—Development of Evaluation Procedure*. Report FHWA-RD-78-98, FHWA, U.S. Department of Transportation, Washington, DC, 1978.
67. *Regulation of Weights, Lengths, and Widths of Commercial Motor Vehicles*. Special Report 267. TRB, National Research Council, Washington, DC, 2002.
68. *Federal Size Regulations for Commercial Motor Vehicles*. Publication No. FHWA-MC-96-03. FHWA, U.S. Department of Transportation, Washington, DC, 1996.
69. *Bridge Formula Weights*. Publication No. FHWA-MC-94-007. FHWA, U.S. Department of Transportation, Washington, DC, 1994.
70. *The U.S. Department of Transportation's Comprehensive Truck Size and Weight Study: Volume I Summary Report*. Publication No. FHWA-PL-00-029 (Volume I). FHWA, U.S. Department of Transportation, Washington, DC, 2000.
71. Klebe, F. Meeting the Revised Requirements of the ASTM 1318-02 Standard Specification for Highway Weigh-in-Motion (WIM) Systems. Mettler Toledo. <http://www.mtwim.com/ASTM%201318%20White%20Paper%20-%208-5-02.pdf>. Accessed May 28, 2003.
72. Bushman, R., and A. J. Pratt. Weigh In Motion Technology—Economics and Performance. International Road Dynamics, Inc. [http://www.ird.ca/english/pdf/tech\\_ppr/wim\\_comparison.pdf](http://www.ird.ca/english/pdf/tech_ppr/wim_comparison.pdf). Accessed May 29, 2003.
73. *Specifications, Tolerances, and Other Technical Requirements for Weighing and Measuring Devices, National Institute of Standards and Technology (NIST) Handbook 44, 2003 Edition* (T. L. Grimes, R. Suiter, and J. Williams, eds.). U.S. Government Printing Office, Washington, DC, 2002.
74. McCall, B., and W. C. Vodrazka, Jr. *State's Successful Practices Weigh-in-Motion Handbook*. Center for Transportation Research and Education (CTRE), Ames, IA, 1997.
75. McDonnell, A. H. *Installation and Evaluation of Weigh-in-Motion Utilizing Quartz-Piezo Sensor Technology*. Division of Research, Connecticut Department of Transportation, Hartford, CT, 1998.
76. Livingston, R. A. FHWA Fiber-Optics Research Program: Critical Knowledge for Infrastructure Improvement. *Public Roads*, Vol. 63, No. 1, July/August 1999, pp. 13–19.

77. Weigh-in-Motion Technology Comparisons, January 2001 Technical Brief. International Road Dynamics, Inc.  
[http://www.ird.ca/english/pdf/tech\\_ppr/wim\\_tech\\_compare.pdf](http://www.ird.ca/english/pdf/tech_ppr/wim_tech_compare.pdf). Accessed May 29, 2003.
78. *WIM Scale Calibration: A Vital Activity for LTPP Sites*. Publication No. FHWA-RD-98-104. FHWA, U.S. Department of Transportation, Washington, DC, 1998.
79. Cunagin, W. *NCHRP Report 3-39: Evaluation and Calibration Procedures for Weigh-in-Motion Systems*. TRB, National Research Council, Washington, DC, 1993.
80. Papagiannakis, A. T., K. Senn and H. Huang. *NCHRP Report 3-39(2): On-Site Evaluation and Calibration Procedures for Weigh-in-Motion Systems*. TRB, National Research Council, Washington, DC, 1995.
81. Gonzalez, A., A. T. Papagiannakis, and E. J. O'Brien. Evaluation of an Artificial Neural Network Technique Applied to Multiple-Sensor Weigh-in-Motion Systems. In *Transportation Research Board 82<sup>nd</sup> Annual Meeting Compendium of Papers* (CD-ROM), TRB, National Research Council, Washington, DC, 2003.
82. Papagiannakis, A. T. Calibration of Weigh-in-Motion Systems Through Dynamic Vehicle Simulation. *Journal of Testing and Evaluation*, Vol. 25, No. 2, March 1997, pp. 197–204.
83. Scheaffer, R. L., W. Mendenhall III, and R. L. Ott. *Elementary Survey Sampling*, 5<sup>th</sup> ed. Duxbury Press, Belmont, CA, 1996.
84. Mardia, K. V., J. T. Kent, and J. M. Bibby. *Multivariate Analysis*. Academic Press, New York, 1979.
85. Breiman, L., J. H. Friedman, R. A. Olshen, and C. J. Stone. *Classification and Regression Trees*. Chapman and Hall/CRC Press, Inc., Boca Raton, FL, 1998.
86. Hawkins, D. M. FIRM: Formal Inference-Based Recursive Modeling. *The American Statistician*, Vol. 45, No. 2, May 1991, p. 155.
87. Pearson, K. On Lines and Planes of Closest Fit to Systems of Points in Space. *Philosophical Magazine*, Vol. 2, Series 6, 1901, pp. 559–572.
88. Hotelling, H. Analysis of a Complex of Statistical Variables into Principal Components. *Journal of Educational Psychology*, Vol. 24, 1933, pp. 417–441.
89. Hotelling, H. Simplified Calculation of Principal Components. *Psychometrika*, Vol. 1, 1936, pp. 27–35.

90. Bryant, E. H., and W. R. Atchley. *Multivariate Statistical Methods: Within-Group Covariation*. Halsted Press, Stroudsburg, PA, 1975.
91. Jolliffe, I. T. *Principal Component Analysis*. Springer-Verlag, Inc., New York, 1986.
92. Cureton, E. E., and R. B. D'Agostino. *Factor Analysis: An Applied Approach*. Lawrence Erlbaum Associates, Hillsdale, NJ, 1983.
93. Kaiser, H. F. The Application of Electronic Computers to Factor Analysis. *Educational and Psychological Measurement*, Vol. 20, 1960, pp. 141–151.
94. Jolliffe, I. T. Discarding Variables in a Principal Component Analysis, I: Artificial Data. *Applied Statistics*, Vol. 21, 1972, pp. 160–173.
95. Cattell, R. B. The Scree Test for the Number of Factors. *Journal of Multivariate Behavior Research*, Vol. 1, 1966, pp. 245–276.
96. *SPSS<sup>®</sup> Base 10.0 User's Guide*. SPSS, Inc., Chicago, IL, 1999.
97. Morgan, J. N., and J. A. Sonquist. Problems in the Analysis of Survey Data and a Proposal. *Journal of the American Statistical Association*, Vol. 58, 1963, pp. 415–434.
98. Sonquist, J. A., and J. N. Morgan. *The Detection of Interaction Effects*. Institute for Social Research, University of Michigan, Ann Arbor, 1964.
99. Sonquist, J. A. *Multivariate Model Building: The Validation of a Search Strategy*. Institute for Social Research, University of Michigan, Ann Arbor, 1970.
100. Sonquist, J. A., E. L. Baker, and J. N. Morgan. *Searching for Structure*, rev. ed. Institute for Social Research, University of Michigan, Ann Arbor, 1973.
101. *JMP<sup>™</sup> Version 5 User's Guide*. SAS Institute, Inc., Cary, NC, 2002.
102. *CORSIM User's Guide (Software Help Menu)*. FHWA, U.S. Department of Transportation, Washington, DC, 2001.
103. *TRANSIMS: TRansportation ANalysis SIMulation System, Version: TRANSIMS 3.0*. Los Alamos National Laboratory, Los Alamos, NM, 2002.
104. Nagel, K., P. Stretz, M. Pieck, S. Leckey, R. Donnelly, and C. L. Barrett. *TRANSIMS Traffic Flow Characteristics*. Report LA-UR 97-3531. Los Alamos National Laboratory, Los Alamos, NM, 1998.
105. *VISSIM 3.60 User Manual*. PTV Planung Transport Verkehr AG, Karlsruhe, Germany, 2001.
106. VISSIM Traffic/Transit Simulation Model. Innovative Transportation Concepts, Inc. <http://www.itc-world.com/vissim.htm>. Accessed August 27, 2002.

107. Wiedemann, R. *Simulation des Verkehrsflusses*. Schriftenreihe des Instituts für Verkehrswesen, Heft 8, Universität (TU), Karlsruhe, Germany, 1974.
108. Lieberman, E., and A. K. Rathi. Traffic Simulation. Oak Ridge National Laboratory, Center for Transportation Analysis.  
<http://www-cta.ornl.gov/cta/research/trb/Chap10.pdf>. Accessed July 10, 2002.
109. May, A. D., N. Roupail, L. Bloomberg, F. Hall, and T. Urbanik. Freeway Systems Research Beyond the HCM2000. In *Transportation Research Board 80<sup>th</sup> Annual Meeting Compendium of Papers* (CD-ROM), TRB, National Research Council, Washington, DC, 2001.
110. Goldberg, D. E. *Genetic Algorithms in Search, Optimization, and Machine Learning*. Addison-Wesley Publishing Company, Inc., Reading, MA, 1989.
111. Holland, J. H. *Adaptation in Natural and Artificial Systems*. University of Michigan Press, Ann Arbor, 1975.
112. Foy, M. D., R. F. Benekohal, and D. E. Goldberg. Signal Timing Determination Using Genetic Algorithms. In *Transportation Research Record 1365*, TRB, National Research Council, Washington, DC, 1992, pp. 108–115.
113. Hadi, M. A., and C. E. Wallace. Hybrid Genetic Algorithm to Optimize Signal Phasing and Timing. In *Transportation Research Record 1421*, TRB, National Research Council, Washington, DC, 1993, pp. 104–112.
114. Abu-Lebdeh, G., and R. F. Benekohal. Development of Traffic Control and Queue Management Procedures for Oversaturated Arterials. In *Transportation Research Record 1603*, TRB, National Research Council, Washington, DC, 1997, pp. 119–127.
115. Park, B., C. J. Messer, and T. Urbanik II. Traffic Signal Optimization Program for Oversaturated Conditions: Genetic Algorithm Approach. In *Transportation Research Record 1683*, TRB, National Research Council, Washington, DC, 1999, pp. 133–142.
116. Park, B., C. J. Messer, and T. Urbanik II. Enhanced Genetic Algorithm for Signal-Timing Optimization of Oversaturated Intersections. In *Transportation Research Record 1727*, TRB, National Research Council, Washington, DC, 2000, pp. 32–41.
117. Park, B., and M. Chang. Realizing the Benefits of Adaptive Signal Control at an Isolated Intersection. In *Transportation Research Record 1811*, TRB, National Research Council, Washington, DC, 2002, pp. 115–121.

118. Fwa, T. F., W. T. Chan, and C. Y. Tan. Genetic-Algorithm Programming of Road Maintenance and Rehabilitation. *Journal of Transportation Engineering*, Vol. 112, No. 3, May/June 1996, pp. 246–253.
119. Liu, C. L., A. Hammond, and Y. Itoh. Maintenance Strategy Optimization of Bridge Decks Using Genetic Algorithm. *Journal of Transportation Engineering*, Vol. 123, No. 2, March/April 1997, pp. 91–100.
120. Ge, Y. E., H. M. Zhang, and W. H. K. Lam. Network Reserve Capacity Under Influence of Traveler Information. *Journal of Transportation Engineering*, Vol. 129, No. 3, May/June 2003, pp. 262–270.
121. Tom, V. M., and S. Mohan. Transit Route Network Design Using Frequency Coded Genetic Algorithm. *Journal of Transportation Engineering*, Vol. 129, No. 2, March/April 2003, pp. 186–195.
122. Pattnaik, S. B., S. Mohan, and V. M. Tom. Urban Bus Transit Route Network Design Using Genetic Algorithm. *Journal of Transportation Engineering*, Vol. 124, No. 4, July/August 1998, pp. 368–375.
123. Kim, K., and L. R. Rilett. Genetic-Algorithm-Based Approach for Calibrating Microscopic Simulation Models. In *2001 IEEE Intelligent Transportation Systems Conference Proceedings*, Institute of Electrical and Electronics Engineers (IEEE), Oakland, CA, 2001, pp. 698–704.
124. Cheu, R. L., X. Jin, K. C. Ng, Y. L. Ng, and D. Srinivasan. Calibration of FRESIM for Singapore Expressway Using Genetic Algorithm. *Journal of Transportation Engineering*, Vol. 124, No. 6, November/December 1998, pp. 526–535.
125. Ma, T., and B. Abdulhai. Genetic Algorithm-Based Optimization Approach and Generic Tool for Calibrating Traffic Microscopic Simulation Parameters. In *Transportation Research Record 1800*, TRB, National Research Council, Washington, DC, 2002, pp. 6–15.
126. Chu, L., and X. Yang. Optimization of the ALINEA Ramp-metering Control Using Genetic Algorithm with Micro-simulation. In *Transportation Research Board 82<sup>nd</sup> Annual Meeting Compendium of Papers* (CD-ROM), TRB, National Research Council, Washington, DC, 2003.
127. *Genetic Algorithms in Engineering Systems* (A. M. S. Zalzal and P. J. Fleming, eds.). The Institution of Electrical Engineers, London, United Kingdom, 1997.

128. Chambers, L. *Practical Handbook of Genetic Algorithms: Applications, Volume I*. CRC Press, Inc., Boca Raton, FL, 1995.
129. Dasgupta, D., and Z. Michalewicz. *Evolutionary Algorithms in Engineering Applications*. Springer-Verlag, Inc., New York, 1997.
130. TxDOT Trivia and General Facts. Texas Department of Transportation. <http://www.dot.state.tx.us/insdtdot/geninfo.htm?pg=facts>. Accessed September 17, 2003.
131. Lee, C. E., and N. I. Al-Rashid. *A Portable Scale for Weighing Vehicles in Motion*. Report 54-1F. Center for Highway Research, The University of Texas at Austin, 1968.
132. Machemehl, R. B., C. E. Lee, and C. M. Walton. *Truck Weight Surveys by In-Motion Weighing*. Report CFHR 3-10-74-181-1F. Center for Highway Research, The University of Texas at Austin, 1975.
133. Texas Legal Size and Weight Limits. Texas Department of Transportation. <http://www.dot.state.tx.us/mcd/onestop/size&weight.htm>. Accessed February 26, 2003.
134. *SPSS® Base 10.0 Applications Guide*. SPSS, Inc., Chicago, IL, 1999.
135. *Data Desk® 6.1*. Data Description, Inc., Ithaca, NY, 1997.
136. Montgomery, D. C., and G. C. Runger. *Applied Statistics and Probability for Engineers*, 2<sup>nd</sup> ed. John Wiley and Sons, Inc., New York, 1999.
137. Neter, J., M. H. Kutner, C. J. Nachtsheim, and W. Wasserman. *Applied Linear Statistical Models*, 4<sup>th</sup> ed. Richard D. Irwin, Inc., Chicago, IL, 1996.
138. Brown, M. B., and A. B. Forsythe. Robust Tests for the Equality of Variances. *Journal of the American Statistical Association*, Vol. 69, 1974, pp. 264–267.
139. Welch, B. L. On the Comparison of Several Means: An Alternative Approach. *Biometrika*, Vol. 38, 1951, pp. 330–336.
140. *SPSS® Interactive Graphics 10.0*. SPSS, Inc., Chicago, IL, 1999.
141. Steinberg, D., M. Golovnya, and D. Tolliver. *CART for Windows User Guide*. Salford Systems, San Diego, CA, 2002.
142. Rilett, L. R., and K. Kim. Automatic Calibration of Surface Transportation Demand and Supply Models Using ITS Data. In *Proceedings of the 9<sup>th</sup> World Congress on Transport Research* (CD ROM), Seoul, Korea, 2001.

143. Dixon, M. P. *Incorporation of Automatic Vehicle Identification Data Into the Synthetic OD Estimation Process*. Ph.D. dissertation. Texas A&M University, College Station, 2000.
144. Dixon, M. P., and L. R. Rilett. Real-Time Origin-Destination Estimation Using Automatic Vehicle Identification Data. In *Transportation Research Board 79<sup>th</sup> Annual Meeting Compendium of Papers* (CD-ROM), TRB, National Research Council, Washington, DC, 2000.
145. TSIS-CORSIM Did You Know? University of Florida, McTrans Center for Microcomputers in Transportation.  
<http://www-mctrans.ce.ufl.edu/featured/TSIS/Didyouknow.htm>. Accessed July 5, 2003.
146. Wicks, D. A., and E. B. Lieberman. *Development and Testing of INTRAS, a Microscopic Freeway Simulation Model Vol. 1 Program Design, Parameter Calibration and Freeway Dynamics Component Development*. Report FHWA/RD-80/106. FHWA, U.S. Department of Transportation, Washington, DC, 1980.
147. Halati, A., H. Lieu, and S. Walker. CORSIM—Corridor Traffic Simulation Model. In *Traffic Congestion and Traffic Safety in the 21<sup>st</sup> Century: Challenges, Innovations, and Opportunities*, American Society of Civil Engineers (ASCE), Chicago, IL, 1997, pp. 570–576.
148. Khan, S., P. Maini, and K. Thanasupsin. Car-Following and Collision Constraint Models for Uninterrupted Traffic: Reexamination Using High-Precision Global Positioning System Data. In *Transportation Research Record 1710*, TRB, National Research Council, Washington, DC, 2000, pp. 37–46.
149. Rakha, H., and B. Crowther. Comparison and Calibration of FRESIM and INTEGRATION Steady-State Car-Following Behavior. *Transportation Research Part A, Policy and Practice*, Vol. 37A, No. 1, January 2003, pp. 1–27.
150. Aycin, M. F., and R. F. Benekohal. Comparison of Car-Following Models for Simulation. In *Transportation Research Record 1678*, TRB, National Research Council, Washington, DC, 1999, pp. 116–127.
151. Skabardonis, A. Simulation of Freeway Weaving Areas. In *Transportation Research Record 1802*, TRB, National Research Council, Washington, DC, 2002, pp. 115–124.

152. Rakha, H., and B. Crowther. Comparison of Greenshields, Pipes, and Van Aerde Car-Following and Traffic Stream Models. In *Transportation Research Record 1802*, TRB, National Research Council, Washington, DC, 2002, pp. 248–262.
153. *Highway Capacity Manual*. U.S. Department of Commerce, Bureau of Public Roads, Washington, DC, 1950.
154. *Traffic Engineering Handbook*, 3<sup>rd</sup> ed. (J. E. Baerwald, ed.). Prentice-Hall, Inc., Englewood Cliffs, NJ, 1965.
155. Pignataro, L. J. *Traffic Engineering: Theory and Practice*. Prentice-Hall, Inc., Englewood Cliffs, NJ, 1973.
156. Mei, M., and A. G. R. Bullen. Lognormal Distribution for High Traffic Flows. In *Transportation Research Record 1398*, TRB, National Research Council, Washington, DC, 1993, pp. 125–128.
157. Taieb-Maimon, M., and D. Shinar. Minimum and Comfortable Driving Headways: Reality Versus Perception. *Human Factors*, Vol. 43, No. 1, Spring 2001, pp. 159–172.
158. *A Policy on Geometric Design of Rural Highways*. American Association of Highway Officials, Washington, DC, 1965.
159. Glennon, J. C., and C. A. Joyner. *Re-Evaluation of Truck Climbing Characteristics for Use in Geometric Design*. Report 134-2. Texas Transportation Institute, Texas A&M University, College Station, 1969.
160. Botzow, H. Level-of-Service Concept for Evaluating Public Transport. In *Transportation Research Record 519*, TRB, National Research Council, Washington, DC, 1974, pp. 73–84.
161. Frankel, J., L. Alvarez, R. Horowitz, and P. Li. Safety Oriented Maneuvers for IVHS. *Vehicle System Dynamics*, Vol. 26, No. 4, October 1996, pp. 271–299.
162. Daou, A. On Flow Within Platoons. *Australian Road Research, Journal of the Australian Road Research Board*, Vol. 2, No. 7, March 1966, pp. 4–13.
163. Greenberg, I. The Log-Normal Distribution of Headways. *Australian Road Research, Journal of the Australian Road Research Board*, Vol. 2, No. 7, March 1966, pp. 14–18.
164. Baras, J. S., A. J. Dorsey, and W. S. Levine. Estimation of Traffic Platoon Structure from Headway Statistics. *IEEE Transactions on Automatic Control*, Vol. AC-24, No. 4, August 1979, pp. 553–559.

165. Mei, M., and A. G. R. Bullen. Lognormal Distribution for High Traffic Flows. In *Transportation Research Record 1398*, TRB, National Research Council, Washington, DC, 1993, pp. 125–128.
166. Casella, G., and R. L. Berger. *Statistical Inference*. Wadsworth and Brooks/Cole Advanced Books and Software, Pacific Grove, CA, 1990.
167. Ang, A. H-S., and W. H. Tang. *Probability Concepts in Engineering Planning and Design: Volume I Basic Principles*. John Wiley and Sons, Inc., New York, 1975.
168. *TRAFVU File Description Document, Version 1.2*. Contract No. DTFH61-95-C-00125. ITT Industries, Inc., Systems Division, Colorado Springs, CO, 2001.
169. *Modeling Mobile Source Emissions*. National Research Council, National Academy Press, Washington, DC, 2000.
170. *Comprehensive Modal Emissions Model (CMEM), version 2.0 User's Guide*. University of California, Riverside, Center for Environmental Research and Technology, 2000.
171. Barth, M., C. Malcolm, T. Younglove, and N. Hill. Recent Validation Efforts for a Comprehensive Modal Emissions Model. In *Transportation Research Record 1750*, TRB, National Research Council, Washington, DC, 2001, pp. 13–23.
172. *2001 ATR Vehicle Classification and Border Trends Report (CD-ROM)*. Texas Department of Transportation, Transportation Planning and Programming Division, Austin, 2002.
173. *1997 Vehicle Classification Report*. Texas Department of Transportation, Transportation Planning and Programming Division, Austin, 1999.
174. *1998 Vehicle Classification Report*. Texas Department of Transportation, Transportation Planning and Programming Division, Austin, 1999.
175. *1999 Vehicle Classification Report*. Texas Department of Transportation, Transportation Planning and Programming Division, Austin, 2000.

**APPENDIX A**

**GLOSSARY OF FREQUENTLY USED TERMS AND ACRONYMS**

## **A.1 Frequently Used Terms**

**A\_OD:** Synthetic origin-destination methodology generated using AVI data and input in the CORSIM model.

**AM Peak Period:** The analysis time period from 7:00 a.m. to 8:00 a.m.

**C\_OD:** CORSIM origin-destination methodology, generated internally to the CORSIM model.

**Calibration:** The process in which the model parameters are adjusted such that the model accurately reflects specific components of the system being modeled.

**CORSIM:** CORridor SIMulation software package developed by the Federal Highway Administration (FHWA). Consists of an integrated set of two microscopic traffic simulation models, NETSIM and FRESIM. NETSIM represents the traffic on urban streets while FRESIM provides a representation of traffic on freeways.

**Genetic Algorithm (GA):** A search method based on the mechanics of natural selection and natural genetics. GAs utilize the genetic rules of reproduction, crossover, and mutation to generate populations that include the best parameters to meet the fitness objective

**Mean Absolute Error Ration (MAER):** A statistical measure used to determine the difference between simulated and observed data.

**Off Peak Period:** The analysis time period from 2:00 p.m. to 3:00 p.m.

**PM Peak Period:** The analysis time period from 5:00 p.m. to 6:00 p.m.

**Weigh-in-Motion (WIM):** “the process of measuring the dynamic tire forces of a moving vehicle and estimating the corresponding tire loads of the static vehicle.”

## A.2 Acronyms

**TABLE A.1 List of Frequently Used Acronyms**

<b>Acronym</b>	<b>Title</b>
AADT	Annual Average Daily Traffic
AADTT	Annual Average Daily Truck Traffic
AASHTO	American Association of State Highway and Transportation Officials
ACR	Accumulative Count Recorder
AID	Automatic Interaction Detection
A_OD	AVI Origin-Destination
ASTM	American Society for Testing and Materials
ATMS	Advanced Traffic Management System
ATR	Automatic Traffic Recorder
AVC	Automatic Vehicle Classification
AVI	Automatic Vehicle Identification
AVMT	Annual Vehicle Miles of Travel
BTS	Bureau of Transportation Statistics
Caltrans	California Department of Transportation
CART	Classification and Regression Trees
cdf	Cumulative Distribution Function
CMEM	Comprehensive Modal Emissions Model
CMV(s)	Commercial Motor Vehicle(s)
CO	Carbon Monoxide
C_OD	CORSIM Origin-Destination
CSN	County Station Number
DPS	Department of Public Safety
DVDT	Average Daily Vehicle Distance Traveled
ESAL	Equivalent Single-Axle Load
FHWA	Federal Highway Administration
FIRM	Formal Inference-Based Recursive Modeling
GA	Genetic Algorithm
GATT	General Agreement on Tariffs and Trade
GVW	Gross Vehicle Weight
HC	Hydrocarbons
HOV	High Occupancy Vehicle
HPMS	Highway Performance Monitoring System
ILD	Inductive Loop Detectors
INTRAS	INtegrated TRAffic Simulation
ISTEA	Intermodal Surface Transportation Efficiency Act of 1991
ITE	Institute of Transportation Engineers
ITS	Intelligent Transportation System
IVHS	Intelligent Vehicle Highway System
LCV	Longer Combination Vehicle
LDV	Light Duty Vehicle

TABLE A.1 Continued

Acronym	Title
LTPP	Long Term Pavement Performance
LW	Bending Plate WIM Site
MAER	Mean Absolute Error Ratio
MC	Manual Classification
MPO	Metropolitan Planning Organization
NAFTA	North America Free Trade Agreement
NCHRP	National Cooperative Highway Research Program
NIST	National Institute of Standards and Technology
NN	National Network
NO <sub>x</sub>	Nitrogen Oxides
OD	Origin-Destination
<i>P</i>	Population Size
<i>P<sub>c</sub></i>	Crossover Probability
PCA	Principal Component Analysis
PC(s)	Principal Component(s)
pdf	Probability Density Function
<i>P<sub>m</sub></i>	Probability of Mutation
PZ	Piezoelectric WIM Site
RE	Relative Error
SA	Simplex Algorithm
SHRP	Strategic Highway Research Program
STAA	Surface Transportation Assistance Act
<i>T</i>	Maximum number of Iterations or Generations
TEA-21	Transportation Equity Act for the 21 <sup>st</sup> Century
TMG	Traffic Monitoring Guide
TMIP	Travel Model Improvement Program
TPP	Transportation Planning and Programming Division
TRANSIMS	TRansportation ANalysis SIMulation System
TRB	Transportation Research Board
TSIS	Traffic Software Integration System
TT	Travel Time
TTI	Texas Transportation Institute
TxDOT	Texas Department of Transportation
USDOT	U.S. Department of Transportation
VID	Video Imaging Detection
VMT	Vehicle Miles of Travel
WIM	Weigh-in-Motion

**APPENDIX B**  
**PRELIMINARY ANALYSIS RESULTS**

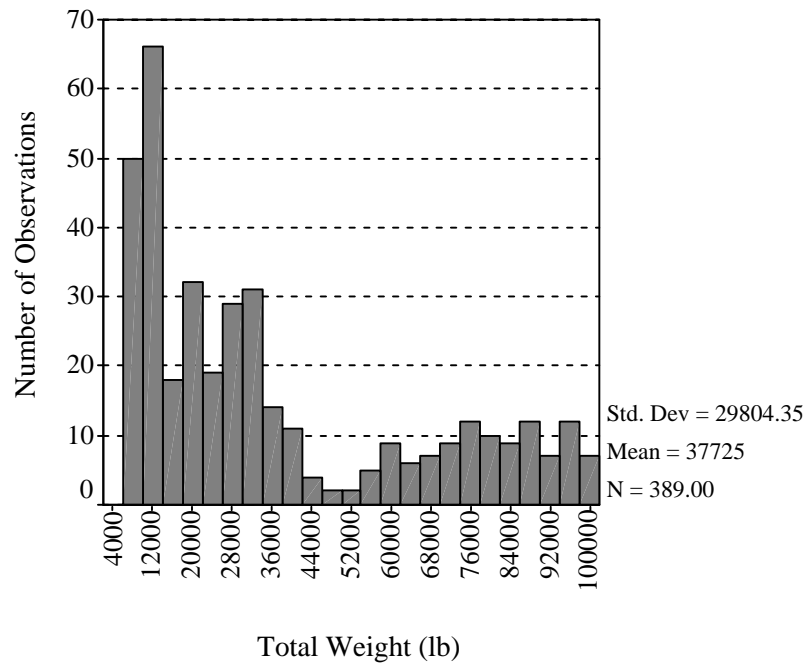


**FIGURE B.1 PZ-071 total weight distribution**

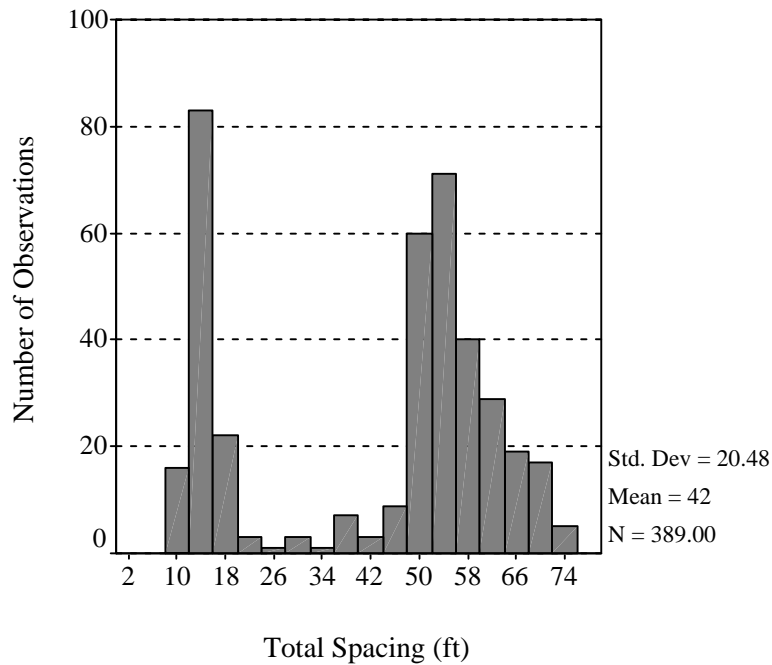


**FIGURE B.2 PZ-071 total spacing distribution**

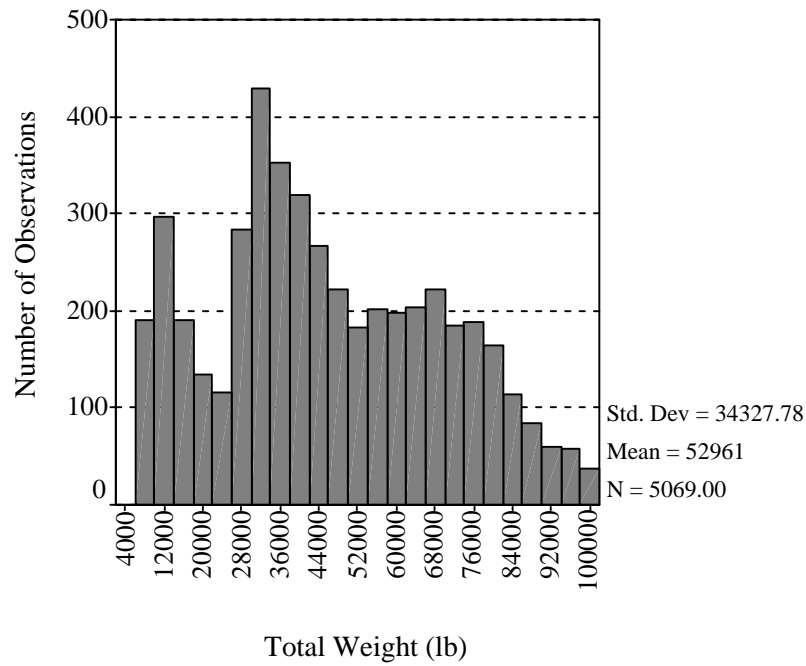


**FIGURE B.3 PZ-074 total weight distribution**

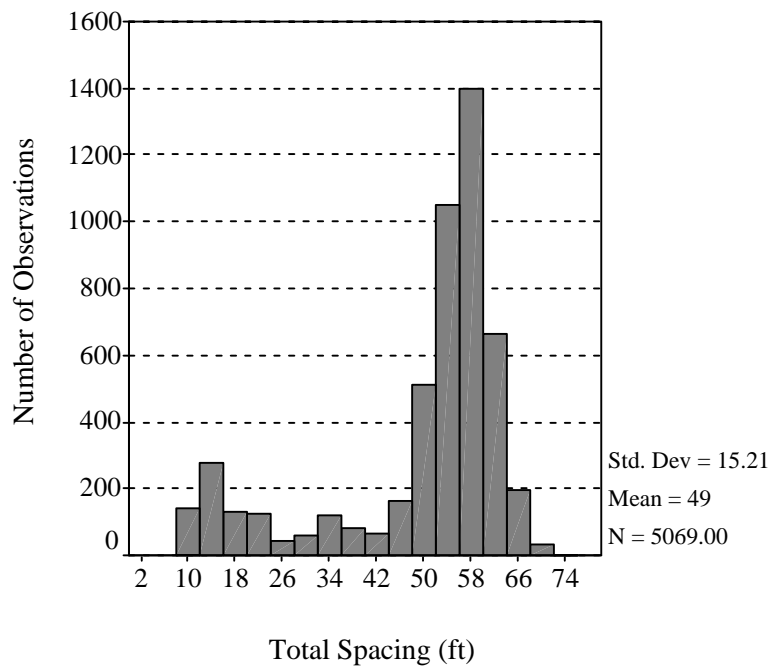


**FIGURE B.4 PZ-074 total spacing distribution**

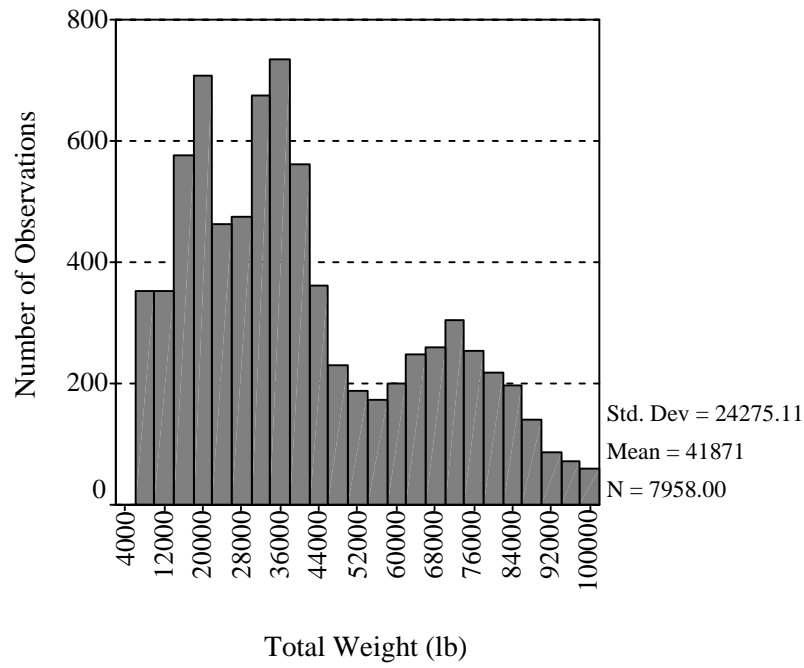


**FIGURE B.5 PZ-181 total weight distribution**

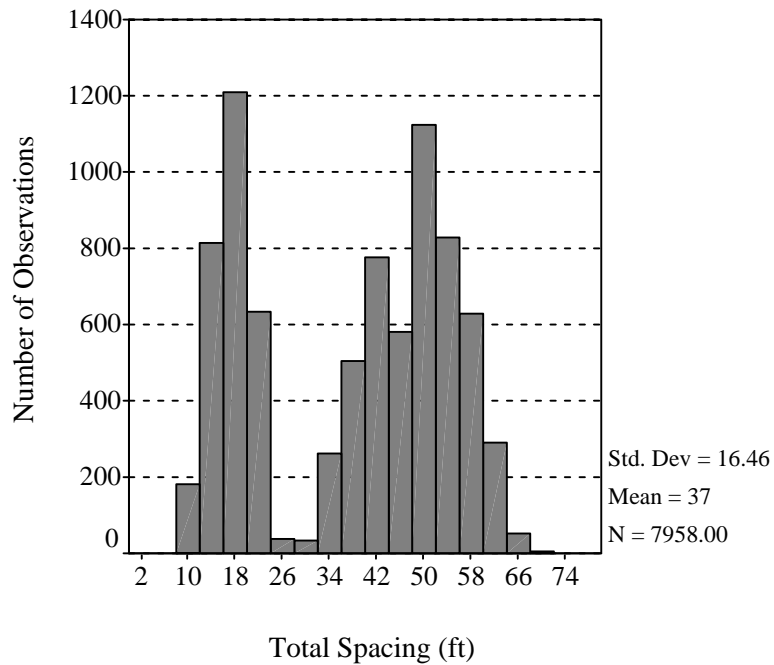


**FIGURE B.6 PZ-181 total spacing distribution**

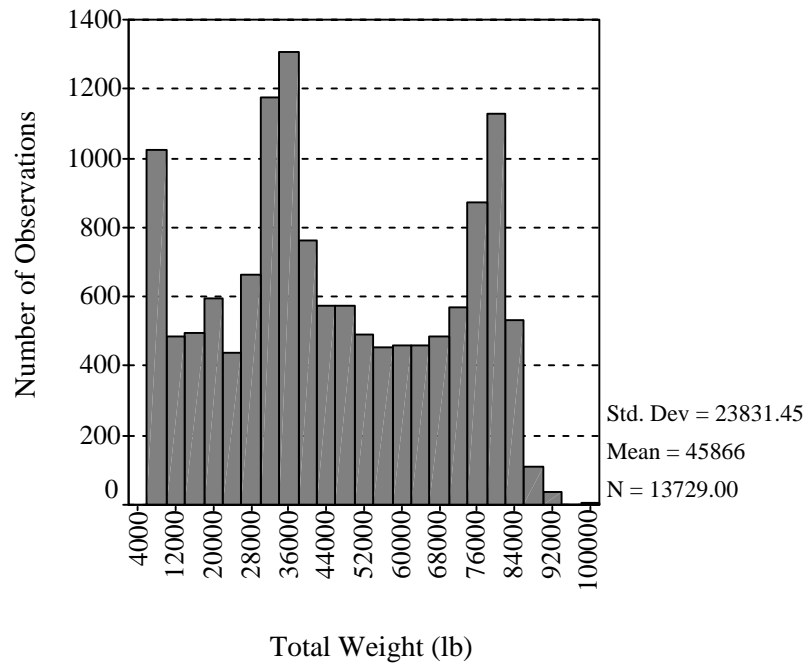


**FIGURE B.7 PZ-502 total weight distribution**

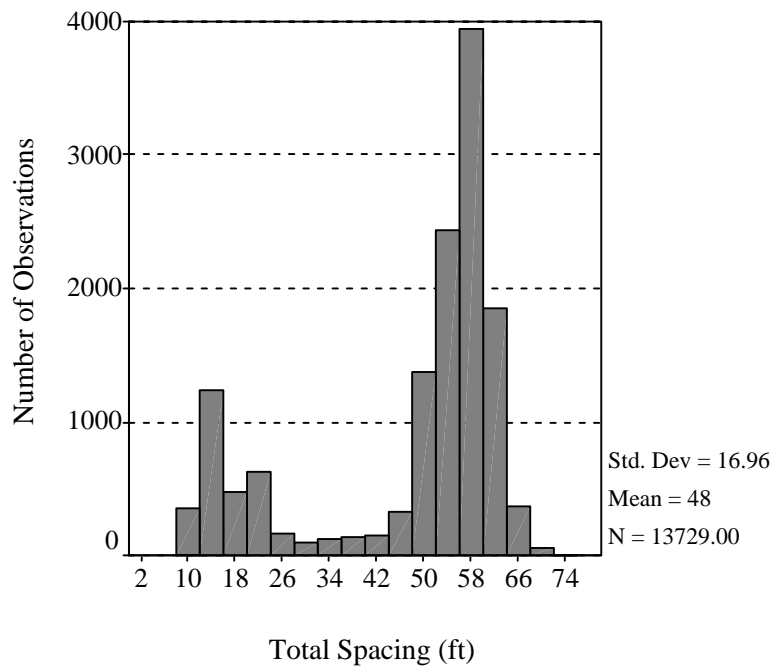


**FIGURE B.8 PZ-502 total spacing distribution**

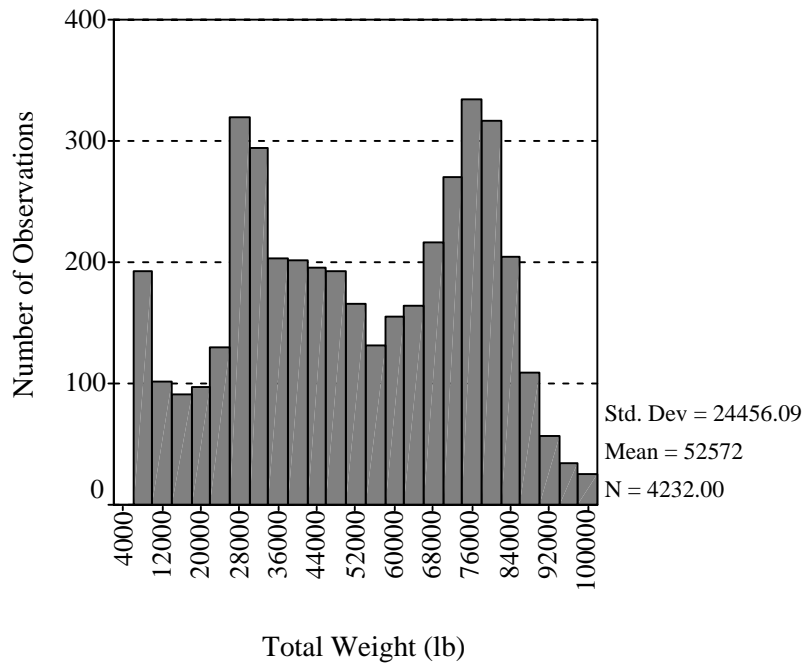


**FIGURE B.9 PZ-518 total weight distribution**

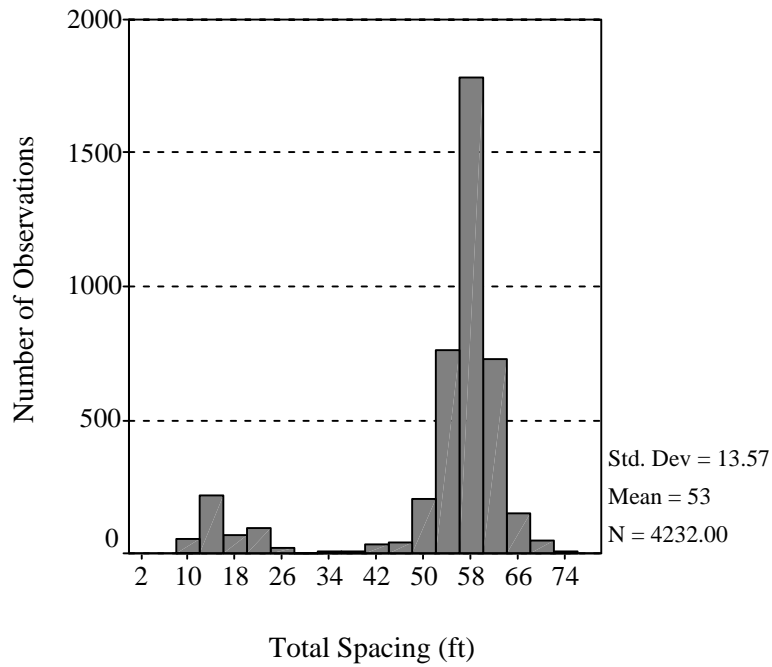


**FIGURE B.10 PZ-518 total spacing distribution**

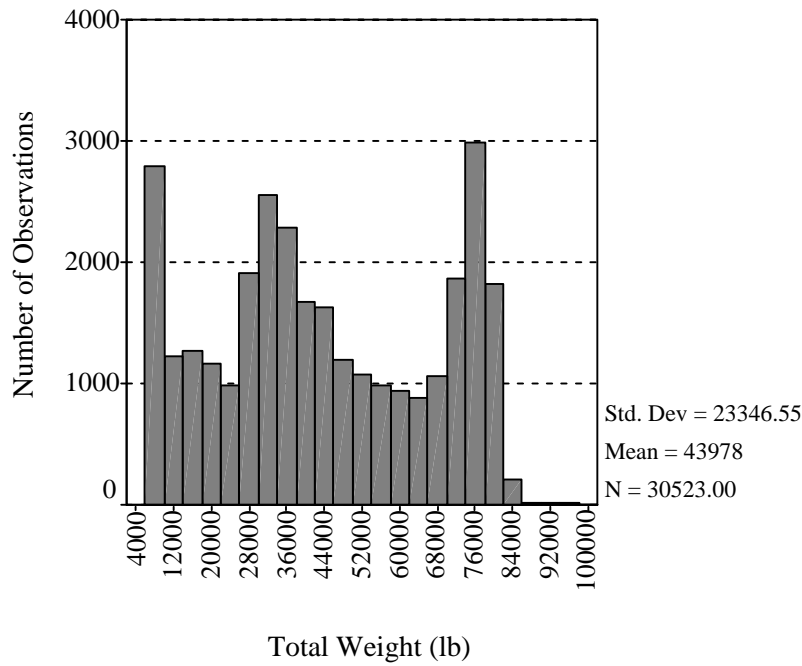


**FIGURE B.11 LW-512 total weight distribution**

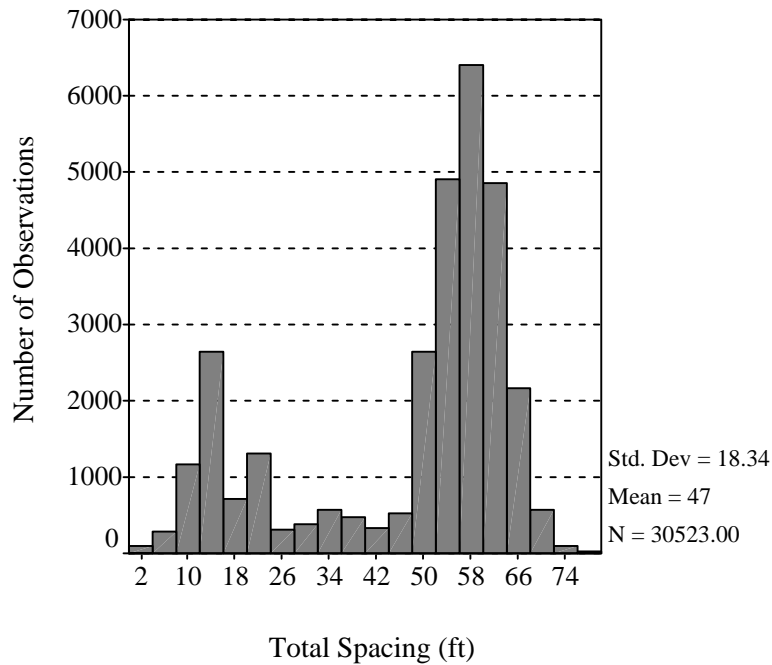


**FIGURE B.12 LW-512 total spacing distribution**

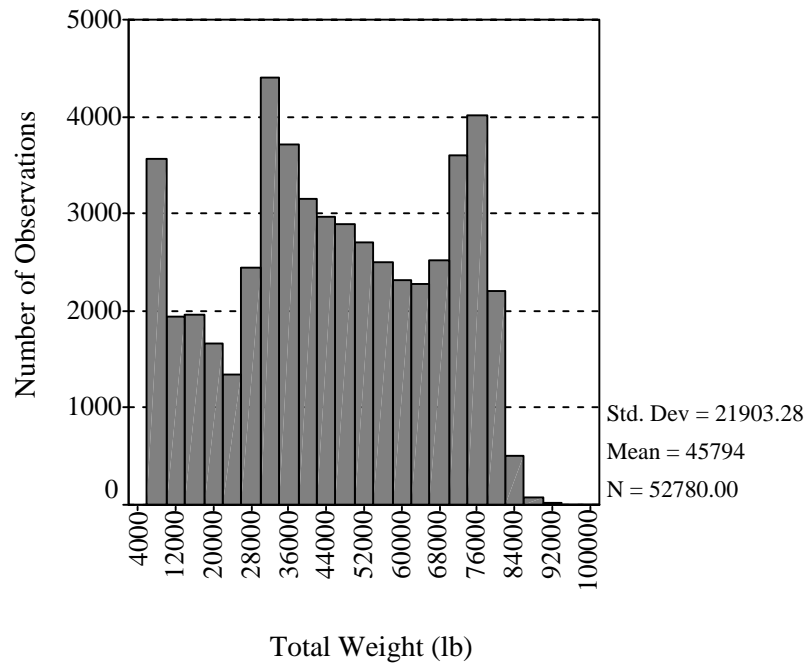


**FIGURE B.13 LW-513 total weight distribution**

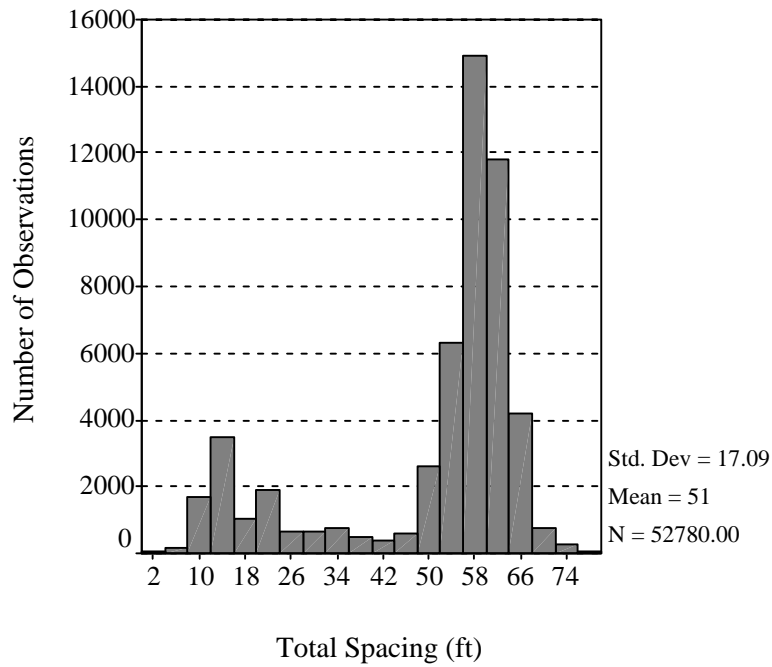


**FIGURE B.14 LW-513 total spacing distribution**

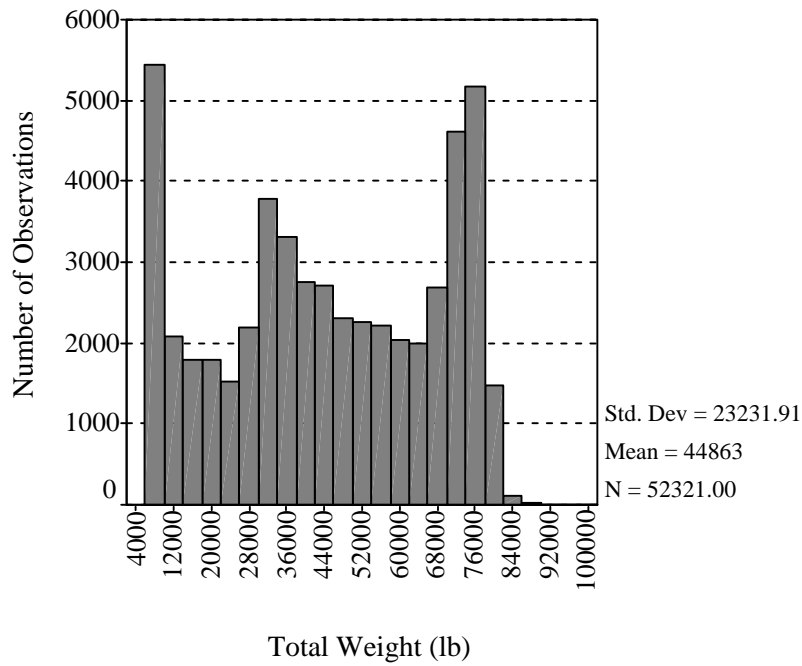


**FIGURE B.15 LW-516 total weight distribution**

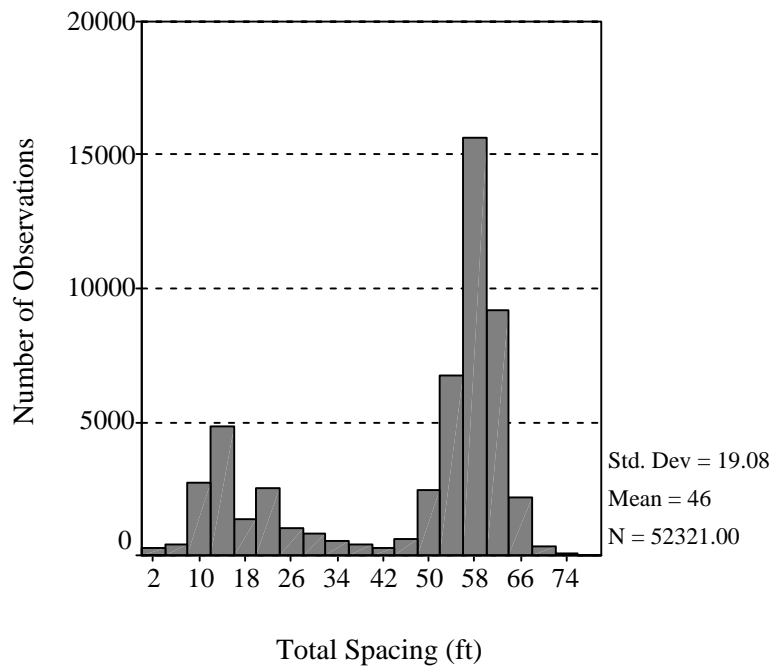


**FIGURE B.16 LW-516 total spacing distribution**

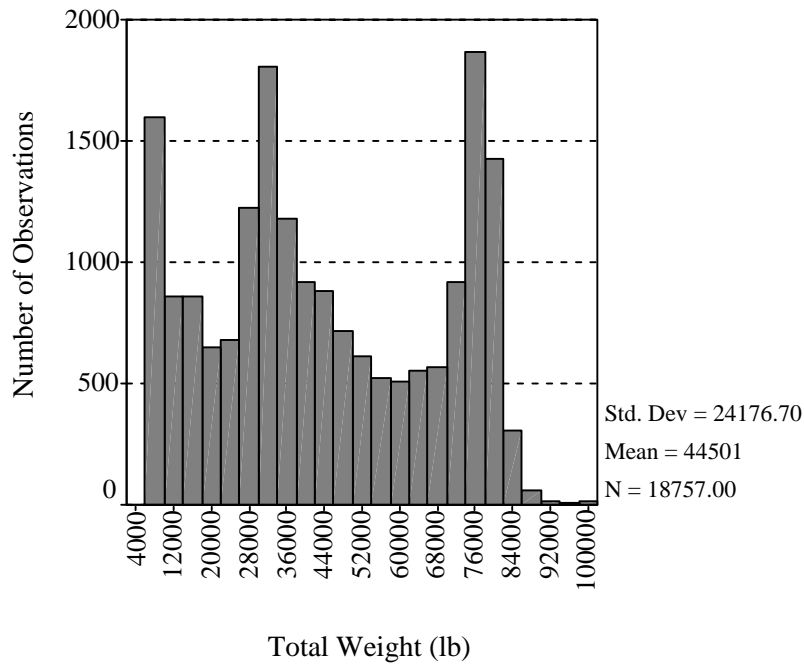


**FIGURE B.17 LW-522 total weight distribution**

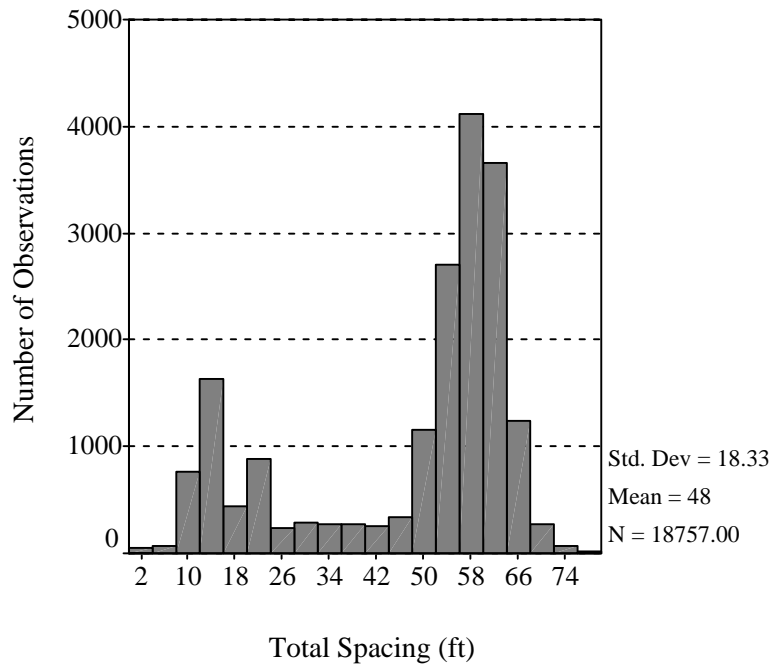


**FIGURE B.18 LW-522 total spacing distribution**

**APPENDIX C**  
**STATISTICAL ANALYSIS RESULTS**

## C.1 Preliminary PCA Analysis Results

**TABLE C.1 Preliminary PCA Component Score Coefficient Matrix**

	Component				
	1	2	3	4	5
Total Weight (lb)	0.139	0.003	-0.009	-0.069	-0.030
Axle A Weight (lb)	0.116	-0.015	-0.042	-0.091	0.042
Axle B Weight (lb)	0.117	-0.016	-0.058	-0.046	-0.050
Axle C Weight (lb)	0.135	-0.013	-0.033	-0.028	-0.037
Axle D Weight (lb)	0.132	-0.008	0.003	-0.027	-0.035
Axle E Weight (lb)	0.131	-0.011	-0.012	-0.105	-0.012
Axle F Weight (lb)	0.016	0.152	0.465	-0.129	0.057
Axle G Weight (lb)	0.010	0.240	-0.048	-0.084	-0.323
Axle H Weight (lb)	0.009	0.238	-0.080	-0.066	-0.276
Axle I Weight (lb)	0.005	0.176	-0.181	0.130	0.444
Axles A to B Spacing (ft)	0.067	-0.032	-0.112	-0.239	0.157
Axles B to C Spacing (ft)	0.037	-0.001	0.056	0.691	-0.179
Axles C to D Spacing (ft)	0.118	-0.025	-0.028	-0.105	0.078
Axles D to E Spacing (ft)	0.087	0.010	0.130	0.390	-0.051
Axles E to F Spacing (ft)	0.012	0.102	0.509	-0.063	0.246
Axles F to G Spacing (ft)	0.007	0.206	-0.095	0.000	-0.089
Axles G to H Spacing (ft)	0.007	0.218	-0.108	-0.004	-0.110
Axles H to I Spacing (ft)	0.004	0.141	-0.172	0.171	0.569
Total Spacing (ft)	0.127	-0.005	0.048	0.147	0.049

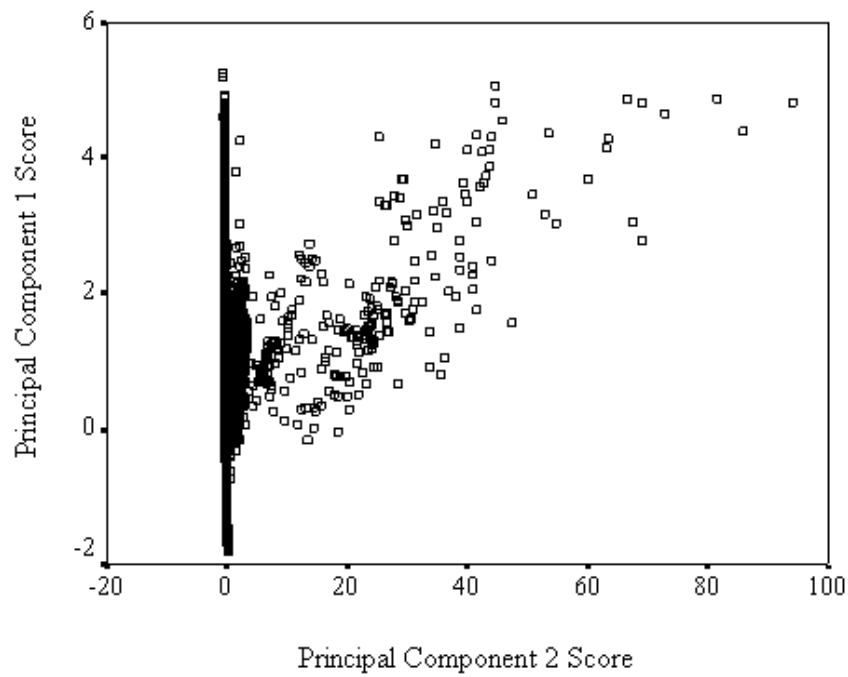


**FIGURE C.1** Preliminary analysis PC one score versus PC two score

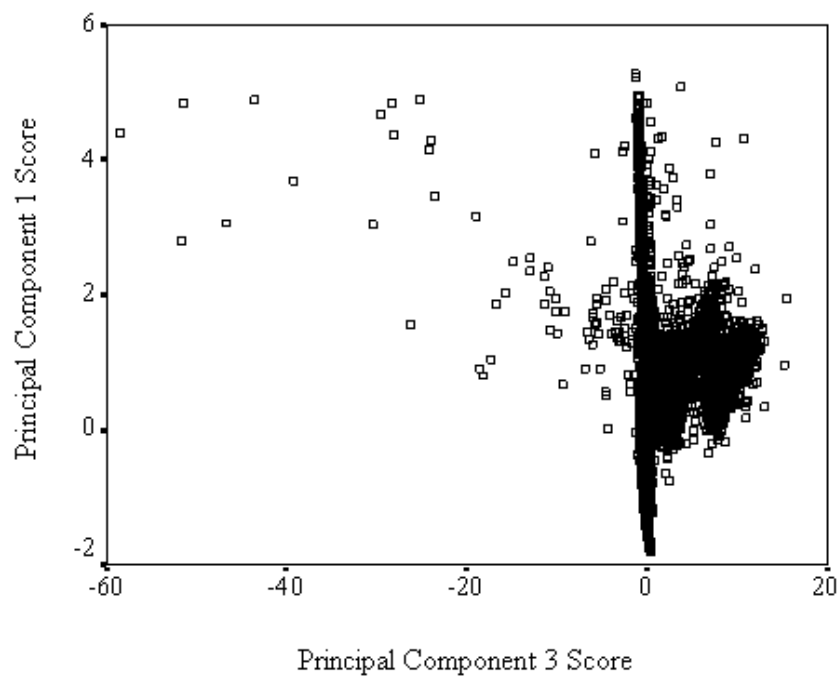


**FIGURE C.2** Preliminary analysis PC one score versus PC three score

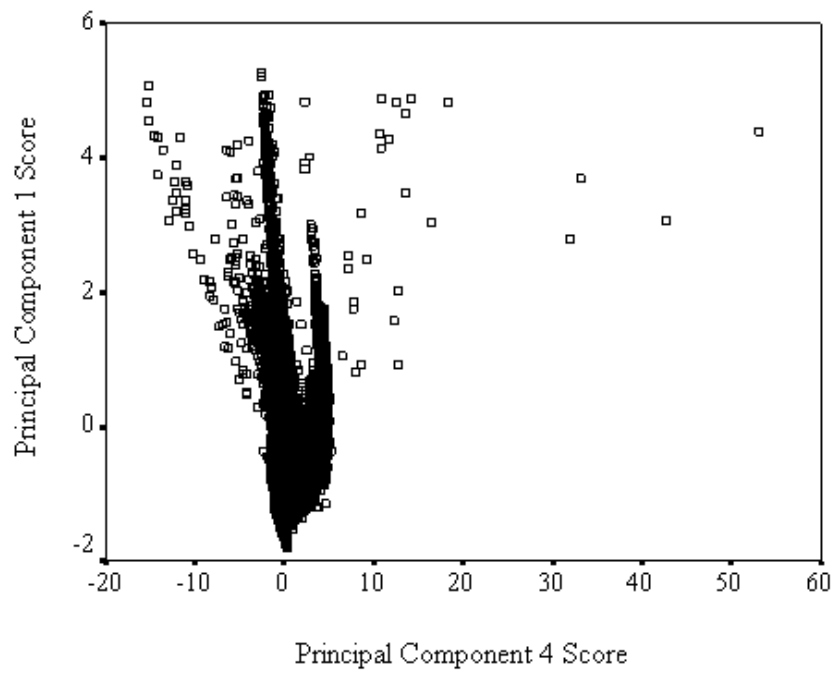


**FIGURE C.3** Preliminary analysis PC one score versus PC four score

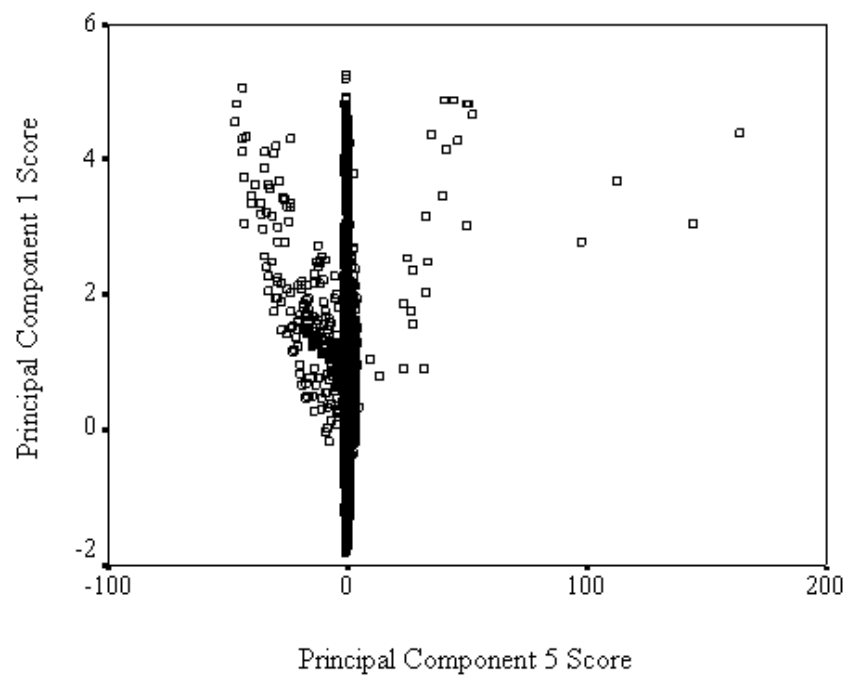


**FIGURE C.4** Preliminary analysis PC one score versus PC five score

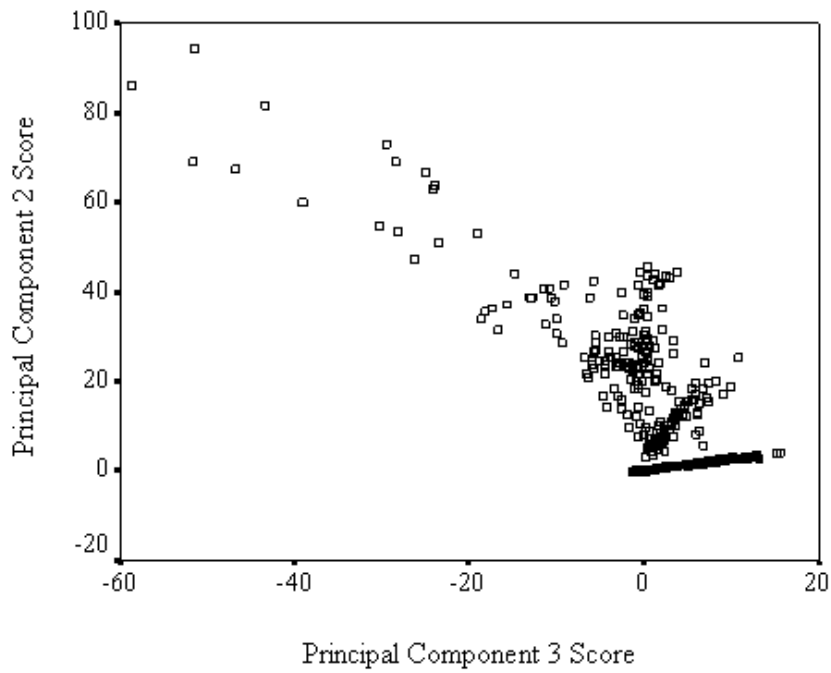


**FIGURE C.5** Preliminary analysis PC two score versus PC three score

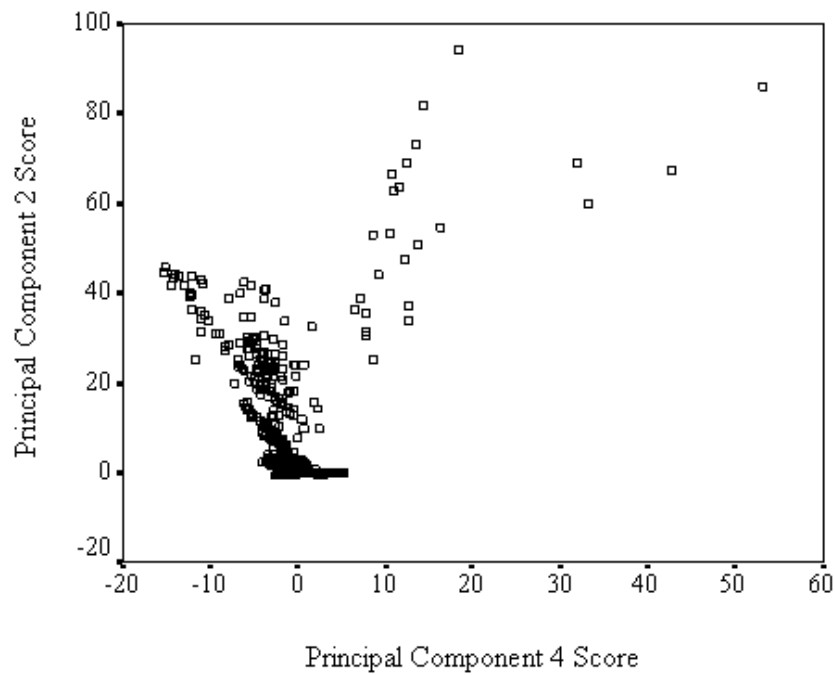


**FIGURE C.6** Preliminary analysis PC two score versus PC four score

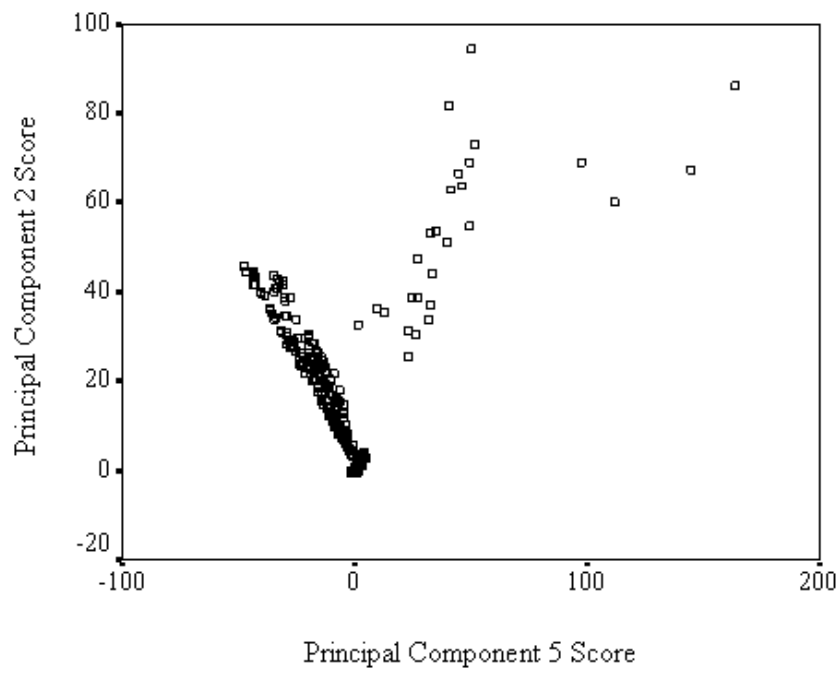


**FIGURE C.7** Preliminary analysis PC two score versus PC five score

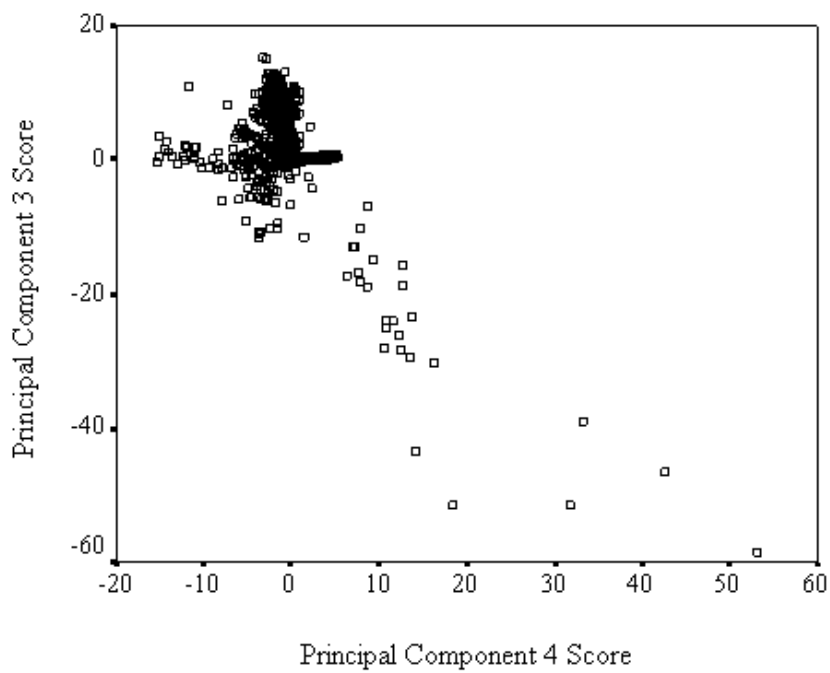


**FIGURE C.8** Preliminary analysis PC three score versus PC four score

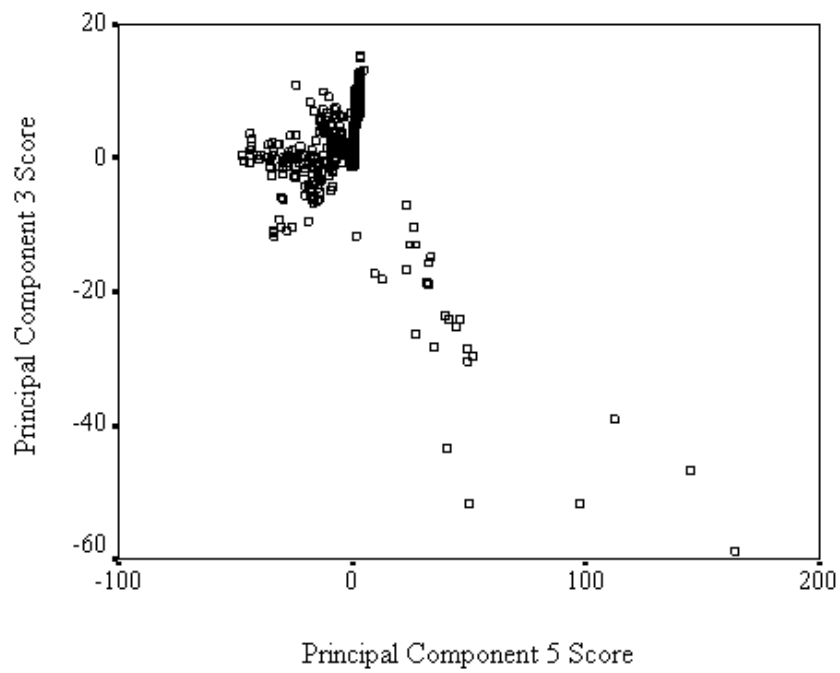


**FIGURE C.9** Preliminary analysis PC three score versus PC five score

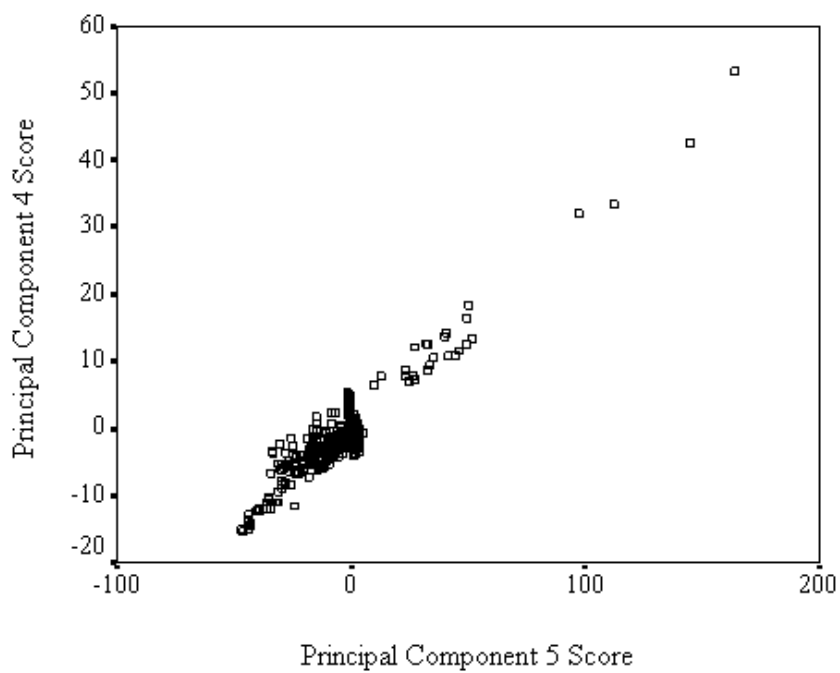


**FIGURE C.10** Preliminary analysis PC four score versus PC five score

## C.2 Spatial Analysis of Data

**TABLE C.2 Reduced Data Component Score Coefficient Matrix**

	Component		
	1	2	3
Total Weight (lb)	0.205	0.020	-0.034
Axle A Weight (lb)	0.094	-0.088	0.150
Axle B Weight (lb)	0.195	0.060	-0.020
Axle C Weight (lb)	0.198	0.016	-0.025
Axle D Weight (lb)	0.195	0.021	-0.062
Axle E Weight (lb)	0.195	0.004	-0.076
Axles A to B Spacing (ft)	0.029	-0.137	0.463
Axles B to C Spacing (ft)	-0.016	0.347	0.065
Axles C to D Spacing (ft)	0.022	-0.327	0.128
Axles D to E Spacing (ft)	-0.001	0.337	0.185
Total Spacing (ft)	0.024	0.065	0.575

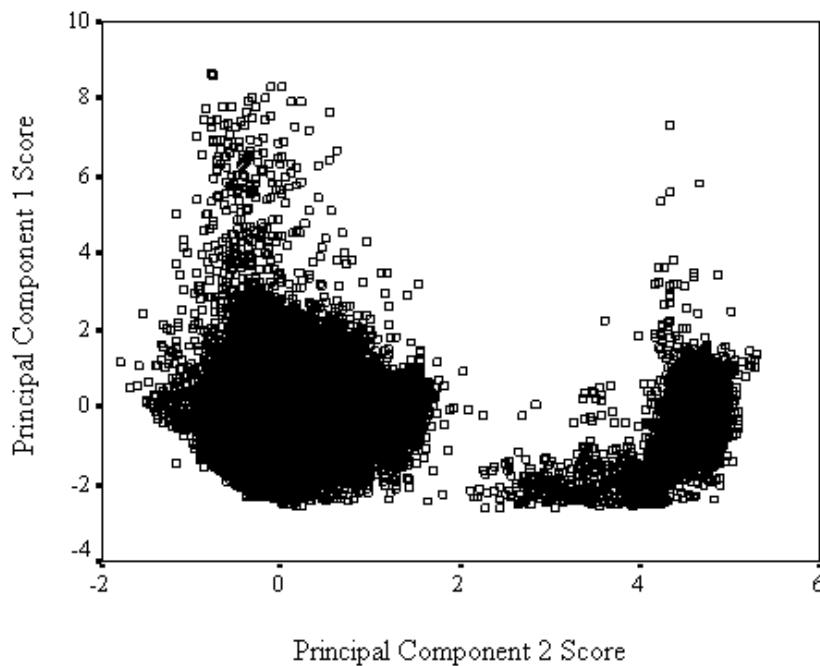


**FIGURE C.11 Spatial data analysis PC one score versus PC two score**

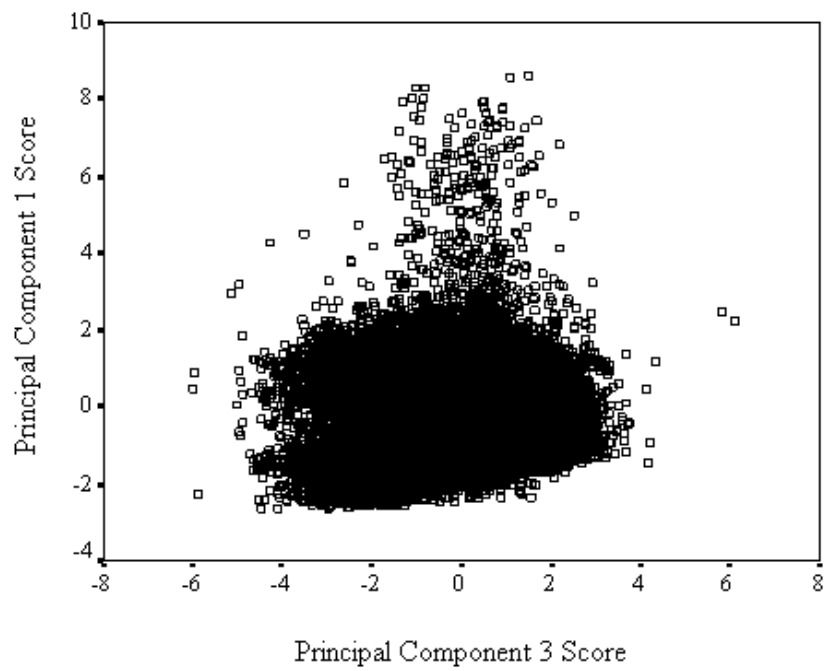


**FIGURE C.12** Spatial data analysis PC one score versus PC three score

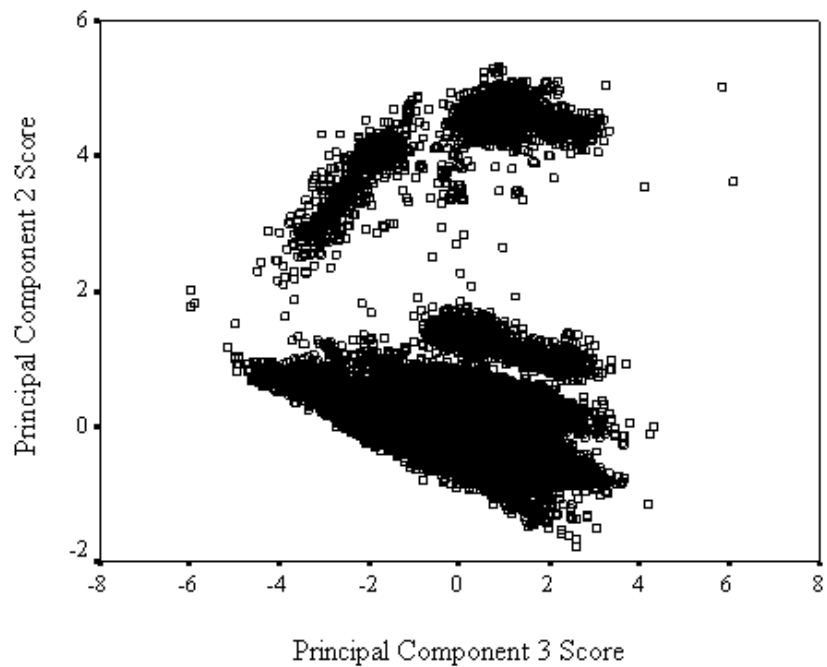


**FIGURE C.13** Spatial data analysis PC two score versus PC three score

**TABLE C.3 Spatial Data Analysis Pairwise Comparison Analysis Results**

(I) Site	(J) Site	Mean Diff. (I – J)	Std. Error	Sig.	95% Confidence Int.	
					Lower Bound	Upper Bound
PZ-071	PZ-074	-7,868.12*	1,276.09	0.000	-11,947.80	-3,788.45
	PZ-181	1,889.40	1,273.30	1.000	-2,181.38	5,960.17
	PZ-502	-954.34	1,252.28	1.000	-4,957.91	3,049.23
	PZ-518	-4,109.09*	1,277.13	0.047	-8,192.08	-26.09
	LW-512	-802.85	1,245.21	1.000	-4,783.80	3,178.11
	LW-513	-34.90	1,241.78	1.000	-4,004.90	3,935.10
	LW-516	-1,995.72	1,242.01	1.000	-5,966.43	1,975.00
	LW-522	-998.55	1,249.25	1.000	-4,992.41	2,995.32
PZ-074	PZ-071	7,868.12*	1276.09	0.000	3,788.45	11,947.80
	PZ-181	9,757.52*	429.68	0.000	8,383.82	11,131.22
	PZ-502	6,913.78*	362.68	0.000	5,754.29	8,073.27
	PZ-518	3,759.04*	440.88	0.000	2,349.53	5,168.54
	LW-512	7,065.28*	337.45	0.000	5,986.46	8,144.10
	LW-513	7,833.23*	324.57	0.000	6,795.56	8,870.89
	LW-516	5,872.41*	325.43	0.000	4,832.01	6,912.80
	LW-522	6,869.58*	352.05	0.000	5,744.06	7,995.10
PZ-181	PZ-071	-1,889.40	1,273.30	1.000	-5,960.17	2,181.38
	PZ-074	-9,757.52*	429.68	0.000	-11,131.22	-8,383.82
	PZ-502	-2,843.74*	352.76	0.000	-3,971.51	-1,715.97
	PZ-518	-5,998.49*	432.76	0.000	-7,382.02	-4,614.95
	LW-512	-2,692.24*	326.76	0.000	-3,736.90	-1,647.59
	LW-513	-1,924.30*	313.45	0.000	-2,926.40	-922.19
	LW-516	-3,885.12*	314.33	0.000	-4,890.05	-2,880.18
	LW-522	-2,887.95*	341.82	0.000	-3,980.77	-1,795.13
PZ-502	PZ-071	954.34	1,252.28	1.000	-3,049.23	4,957.91
	PZ-074	-6,913.78*	362.68	0.000	-8,073.27	-5,754.29
	PZ-181	2,843.74*	352.76	0.000	1,715.97	3,971.51
	PZ-518	-3,154.74*	366.32	0.000	-4,325.86	-1,983.63
	LW-512	151.50	231.69	1.000	-589.22	892.22
	LW-513	919.45*	212.51	0.001	240.06	1,598.83
	LW-516	-1,041.37*	213.81	0.000	-1,724.93	-357.82
	LW-522	-44.20	252.49	1.000	-851.43	763.02
PZ-518	PZ-071	4,109.09*	1,277.13	0.047	26.09	8,192.08
	PZ-074	-3,759.04*	440.88	0.000	-5,168.54	-2,349.53
	PZ-181	5,998.49*	432.76	0.000	4,614.95	7,382.02
	PZ-502	3,154.74*	366.32	0.000	1,983.63	4,325.86
	LW-512	3,306.24*	341.35	0.000	2,214.93	4,397.55
	LW-513	4,074.19*	328.63	0.000	3,023.54	5,124.84
	LW-516	2,113.37*	329.48	0.000	1,060.02	3,166.72
	LW-522	3,110.54*	355.80	0.000	1,973.04	4,248.04

TABLE C.3 Continued

(I) Site	(J) Site	Mean Diff. (I - J)	Std. Error	Sig.	95% Confidence Int.	
					Lower Bound	Upper Bound
LW-512	PZ-071	802.85	1,245.21	1.000	-3,178.11	4,783.80
	PZ-074	-7,065.28*	337.45	0.000	-8,144.10	-5,986.46
	PZ-181	2,692.24*	326.76	0.000	1,647.59	3,736.90
	PZ-502	-151.50	231.69	1.000	-892.22	589.22
	PZ-518	-3,306.24*	341.35	0.000	-4,397.55	-2,214.93
	LW-513	767.95*	165.81	0.000	237.84	1,298.05
	LW-516	-1,192.87*	167.48	0.000	-1,728.31	-657.44
	LW-522	-195.70	214.68	1.000	-882.04	490.63
LW-513	PZ-071	34.90	1,241.78	1.000	-3,935.10	4,004.90
	PZ-074	-7,833.23*	324.57	0.000	-8,870.89	-6,795.56
	PZ-181	1,924.30*	313.45	0.000	922.19	2,926.40
	PZ-502	-919.45*	212.51	0.001	-1,598.83	-240.06
	PZ-518	-4,074.19*	328.63	0.000	-5,124.84	-3,023.54
	LW-512	-767.95*	165.81	0.000	-1,298.05	-237.84
	LW-516	-1,960.82*	139.74	0.000	-2,407.57	-1,514.07
	LW-522	-963.68*	193.82	0.000	-1,583.29	-344.01
LW-516	PZ-071	1,995.72	1,242.01	1.000	-1,975.00	5,966.43
	PZ-074	-5,872.41*	325.43	0.000	-6,912.80	-4,832.01
	PZ-181	3,885.12*	314.33	0.000	2,880.18	4,890.05
	PZ-502	1,041.37*	213.81	0.000	357.82	1,724.93
	PZ-518	-2,113.37*	329.48	0.000	-3,166.72	-1,060.02
	LW-512	1,192.87*	167.48	0.000	657.44	1,728.31
	LW-513	1,960.82*	139.74	0.000	1,514.07	2,407.57
	LW-522	997.17*	195.25	0.000	372.96	1,621.38
LW-522	PZ-071	998.55	1,249.25	1.000	-2,995.32	4,992.41
	PZ-074	-6,869.58*	352.05	0.000	-7,995.10	-5,744.06
	PZ-181	2,887.95*	341.82	0.000	1,795.13	3,980.77
	PZ-502	44.20	252.49	1.000	-763.02	851.43
	PZ-518	-3,110.54*	355.80	0.000	-4,248.04	-1,973.04
	LW-512	195.70	214.68	1.000	-490.63	882.04
	LW-513	963.65*	193.82	0.000	344.01	1,583.29
	LW-516	-997.17*	195.25	0.000	-1,621.38	-372.96

\*Denotes that the mean difference is significant at the 95 percent (0.05) level.

### C.3 Final Results—FHWA Classification

**TABLE C.4 AM Peak Period Final Distributions**

	<b>N</b>	<b>Minimum</b>	<b>Maximum</b>	<b>Mean</b>	<b>Std. Dev.</b>
Total Weight (lb)	18,968	8,000	139,600	44,238.47	23,806.23
Axle A Weight (lb)	18,968	2,200	19,800	9,272.84	2,656.99
Axle B Weight (lb)	18,968	1,700	32,600	10,787.96	4,691.01
Axle C Weight (lb)	15,243	800	29,100	10,895.06	4,500.87
Axle D Weight (lb)	13,941	900	28,200	10,625.29	4,978.90
Axle E Weight (lb)	12,798	1,300	28,500	11,030.15	4,961.87
Axle F Weight (lb)	352	900	20,800	8,917.61	4,053.15
Axle G Weight (lb)	1	17,000	17,000	17,000.00	-
Axle H Weight (lb)	1	16,700	16,700	16,700.00	-
Total Spacing (ft)	18,968	11.0	95.4	46.21	18.56
Axles A to B Spacing (ft)	18,968	10.0	37.6	15.88	2.90
Axles B to C Spacing (ft)	15,243	3.0	45.0	6.51	6.60
Axles C to D Spacing (ft)	13,941	2.1	44.5	28.82	8.89
Axles D to E Spacing (ft)	14,798	2.3	41.0	5.32	3.75
Axles E to F Spacing (ft)	352	3.5	24.2	17.23	7.71
Axles F to G Spacing (ft)	1	14.5	14.5	14.50	-
Axles G to H Spacing (ft)	1	4.7	4.7	4.70	-

**TABLE C.5 Group A Final Distributions—AM Peak Period**

	<b>N</b>	<b>Minimum</b>	<b>Maximum</b>	<b>Mean</b>	<b>Std. Dev.</b>
Total Weight (lb)	3,635	8,000	42,700	12,656.40	5,713.12
Axle A Weight (lb)	3,635	2,700	15,100	5,481.76	1,898.74
Axle B Weight (lb)	3,635	1,900	32,600	7,174.64	4,123.91
Total Spacing (ft)	3,635	11.0	23.5	14.66	3.02
Axles A to B Spacing (ft)	3,635	11.0	23.5	14.66	3.02

**TABLE C.6 Group B Final Distributions—AM Peak Period**

	<b>N</b>	<b>Minimum</b>	<b>Maximum</b>	<b>Mean</b>	<b>Std. Dev.</b>
Total Weight (lb)	2,529	8,500	72,400	28,820.09	12,298.18
Axle A Weight (lb)	2,529	3,100	19,700	8,699.41	3,177.18
Axle B Weight (lb)	2,529	2,100	31,900	10,095.57	5,169.55
Axle C Weight (lb)	2,439	800	29,100	7,572.78	4,641.58
Axle D Weight (lb)	1,137	900	28,200	6,054.09	3,763.15
Total Spacing (ft)	2,529	13.3	62.4	32.89	12.04
Axles A to B Spacing (ft)	2,529	10.0	37.6	15.90	3.78
Axles B to C Spacing (ft)	2,439	3.0	45.0	13.87	11.62
Axles C to D Spacing (ft)	1,137	2.1	42.1	8.04	9.42

**TABLE C.7 Group C Final Distributions—AM Peak Period**

	<b>N</b>	<b>Minimum</b>	<b>Maximum</b>	<b>Mean</b>	<b>Std. Dev.</b>
Total Weight (lb)	12,804	10,900	139,600	56,249.87	18,056.37
Axle A Weight (lb)	12,804	2,200	19,800	10,462.37	1,371.62
Axle B Weight (lb)	12,804	1,700	32,500	11,950.52	4,164.50
Axle C Weight (lb)	12,804	800	24,500	11,527.91	4,184.64
Axle D Weight (lb)	12,804	1,300	28,100	11,031.22	4,869.69
Axle E Weight (lb)	12,798	1,300	28,500	11,030.15	4,961.87
Axle F Weight (lb)	352	900	20,800	8,917.61	4,053.15
Axle G Weight (lb)	1	17,000	17,000	17,000.00	-
Axle H Weight (lb)	1	16,700	16,700	16,700.00	-
Total Spacing (ft)	12,804	22.5	95.4	57.79	5.20
Axles A to B Spacing (ft)	12,804	10.0	24.4	16.22	2.56
Axles B to C Spacing (ft)	12,804	3.2	38.4	5.11	3.74
Axles C to D Spacing (ft)	12,804	2.3	44.5	30.66	6.02
Axles D to E Spacing (ft)	12,798	2.3	41.0	5.32	3.75
Axles E to F Spacing (ft)	352	3.5	24.2	17.23	7.71
Axles F to G Spacing (ft)	1	14.5	14.5	14.50	-
Axles G to H Spacing (ft)	1	4.7	4.7	4.70	-

**TABLE C.8 Midday Peak Period Final Distributions**

	<b>N</b>	<b>Minimum</b>	<b>Maximum</b>	<b>Mean</b>	<b>Std. Dev.</b>
Total Weight (lb)	57,711	8,000	137,700	41,367.70	22,531.88
Axle A Weight (lb)	57,711	1,600	24,800	9,296.14	2,604.44
Axle B Weight (lb)	57,711	1,100	31,300	9,999.65	4,561.38
Axle C Weight (lb)	47,483	600	29,100	9,927.96	4,486.23
Axle D Weight (lb)	43,305	700	30,000	9,392.73	4,996.61
Axle E Weight (lb)	39,721	800	31,200	9,843.59	5,038.67
Axle F Weight (lb)	537	700	23,700	8,253.07	4,582.76
Axle G Weight (lb)	2	13,300	14,200	13,750.00	636.40
Axle H Weight (lb)	2	12,600	15,800	14,200.00	2,262.74
Total Spacing (ft)	57,711	11.0	98.5	46.96	18.02
Axles A to B Spacing (ft)	57,711	10.0	38.3	16.25	2.89
Axles B to C Spacing (ft)	47,483	2.3	44.1	6.11	5.96
Axles C to D Spacing (ft)	43,305	2.1	45.5	29.61	8.44
Axles D to E Spacing (ft)	39,721	2.3	39.8	4.89	2.72
Axles E to F Spacing (ft)	537	3.4	23.6	9.40	7.97
Axles F to G Spacing (ft)	2	14.5	30.9	22.70	11.60
Axles G to H Spacing (ft)	2	4.0	4.7	4.35	0.50

**TABLE C.9 Group A Final Distributions—Midday Peak Period**

	<b>N</b>	<b>Minimum</b>	<b>Maximum</b>	<b>Mean</b>	<b>Std. Dev.</b>
Total Weight (lb)	9,963	8,000	40,100	12,400.01	5,150.80
Axle A Weight (lb)	9,963	2,600	16,700	5,457.30	1,767.19
Axle B Weight (lb)	9,963	1,400	28,000	6,942.71	3,764.08
Total Spacing (ft)	9,963	11.0	23.6	14.83	3.10
Axles A to B Spacing (ft)	9,963	11.0	23.6	14.83	3.10

**TABLE C.10 Group B Final Distributions—Midday Peak Period**

	<b>N</b>	<b>Minimum</b>	<b>Maximum</b>	<b>Mean</b>	<b>Std. Dev.</b>
Total Weight (lb)	8,012	8,100	83,900	26,324.51	11,482.70
Axle A Weight (lb)	8,012	2,100	24,800	8,380.69	3,240.44
Axle B Weight (lb)	8,012	1,300	27,800	9,214.93	5,052.17
Axle C Weight (lb)	7,747	600	26,700	6,695.39	4,319.47
Axle D Weight (lb)	3,569	800	22,800	5,062.12	3,290.31
Total Spacing (ft)	8,012	13.5	65.6	32.80	11.67
Axles A to B Spacing (ft)	8,012	10.0	38.3	16.27	4.00
Axles B to C Spacing (ft)	7,747	2.3	44.1	13.10	10.87
Axles C to D Spacing (ft)	3,569	2.1	44.0	8.67	10.40

**TABLE C.11 Group C Final Distributions—Midday Peak Period**

	<b>N</b>	<b>Minimum</b>	<b>Maximum</b>	<b>Mean</b>	<b>Std. Dev.</b>
Total Weight (lb)	39,736	11,200	137,700	51,663.93	18,495.13
Axle A Weight (lb)	39,736	1,600	19,600	10,443.24	1,331.08
Axle B Weight (lb)	39,736	1,100	31,300	10,924.34	4,265.89
Axle C Weight (lb)	39,736	1,300	29,100	10,558.18	4,240.11
Axle D Weight (lb)	39,736	700	30,000	9,781.70	4,939.70
Axle E Weight (lb)	39,721	800	31,200	9,843.59	5,038.67
Axle F Weight (lb)	537	700	23,700	8,253.07	4,582.76
Axle G Weight (lb)	2	13,300	14,200	13,750.00	636.40
Axle H Weight (lb)	2	12,600	15,800	14,200.00	2,262.74
Total Spacing (ft)	39,736	22.1	98.5	57.87	4.84
Axles A to B Spacing (ft)	39,736	10.0	24.9	16.61	2.42
Axles B to C Spacing (ft)	39,736	2.8	39.6	4.75	2.84
Axles C to D Spacing (ft)	39,736	2.5	45.5	31.50	5.00
Axles D to E Spacing (ft)	39,721	2.3	39.8	4.89	2.72
Axles E to F Spacing (ft)	537	3.4	23.6	9.40	7.97
Axles F to G Spacing (ft)	2	14.5	30.9	22.70	11.60
Axles G to H Spacing (ft)	2	4.0	4.7	4.35	0.50

**TABLE C.12 PM Peak Period Final Distributions**

	<b>N</b>	<b>Minimum</b>	<b>Maximum</b>	<b>Mean</b>	<b>Std. Dev.</b>
Total Weight (lb)	23,259	8,000	117,500	42,484.43	23,395.01
Axle A Weight (lb)	23,259	2,000	23,900	9,290.93	2,662.73
Axle B Weight (lb)	23,259	1,500	29,200	10,133.52	4,577.82
Axle C Weight (lb)	18,747	800	24,000	10,327.44	4,437.28
Axle D Weight (lb)	17,288	900	24,900	10,010.01	4,952.40
Axle E Weight (lb)	16,082	1,200	25,200	10,455.21	4,968.95
Axle F Weight (lb)	182	800	20,700	8,167.03	4,416.23
Total Spacing (ft)	23,259	11.0	80.0	46.87	18.62
Axles A to B Spacing (ft)	23,259	10.0	33.1	16.29	2.86
Axles B to C Spacing (ft)	18,747	2.3	43.6	5.89	5.61
Axles C to D Spacing (ft)	17,288	2.3	45.8	30.14	8.13
Axles D to E Spacing (ft)	16,082	2.0	24.6	4.84	2.64
Axles E to F Spacing (ft)	182	3.4	23.9	10.05	8.20

**TABLE C.13 Group A Final Distributions—PM Peak Period**

	<b>N</b>	<b>Minimum</b>	<b>Maximum</b>	<b>Mean</b>	<b>Std. Dev.</b>
Total Weight (lb)	4,406	8,000	42,100	11,660.96	4,718.56
Axle A Weight (lb)	4,406	2,500	16,100	5,229.66	1,613.75
Axle B Weight (lb)	4,406	2,100	28,300	6,431.30	3,482.97
Total Spacing (ft)	4,406	11.0	23.6	14.43	2.86
Axles A to B Spacing (ft)	4,406	11.0	23.6	14.43	2.86

**TABLE C.14 Group B Final Distributions—PM Peak Period**

	<b>N</b>	<b>Minimum</b>	<b>Maximum</b>	<b>Mean</b>	<b>Std. Dev.</b>
Total Weight (lb)	2,768	8,100	71,400	25,731.03	10,912.41
Axle A Weight (lb)	2,768	2,000	23,900	8,410.73	3,178.88
Axle B Weight (lb)	2,768	1,500	25,600	8,980.46	4,957.87
Axle C Weight (lb)	2,662	800	22,600	6,379.71	4,020.98
Axle D Weight (lb)	1,203	1,100	20,200	5,072.24	3,106.66
Total Spacing (ft)	2,768	14.3	68.2	32.28	11.51
Axles A to B Spacing (ft)	2,768	10.0	33.1	16.48	4.21
Axles B to C Spacing (ft)	2,662	2.3	43.6	12.77	10.78
Axles C to D Spacing (ft)	1,203	2.3	44.1	8.13	10.19

**TABLE C.15 Group C Final Distributions—PM Peak Period**

	<b>N</b>	<b>Minimum</b>	<b>Maximum</b>	<b>Mean</b>	<b>Std. Dev.</b>
Total Weight (lb)	16,085	12,500	117,500	53,810.61	18,111.07
Axle A Weight (lb)	16,085	3,400	19,400	10,554.86	1,245.67
Axle B Weight (lb)	16,085	2,300	29,200	11,346.06	4,159.17
Axle C Weight (lb)	16,085	1,500	24,000	10,980.77	4,155.36
Axle D Weight (lb)	16,085	900	24,900	10,379.30	4,866.16
Axle E Weight (lb)	16,082	1,200	25,200	10,455.21	4,968.95
Axle F Weight (lb)	182	800	20,700	8,167.03	4,416.23
Total Spacing (ft)	16,085	23.7	80.0	58.26	4.65
Axles A to B Spacing (ft)	16,085	10.0	24.8	16.77	2.32
Axles B to C Spacing (ft)	16,085	2.9	37.9	4.75	2.90
Axles C to D Spacing (ft)	16,085	2.3	45.8	31.79	4.94
Axles D to E Spacing (ft)	16,082	2.0	24.6	4.84	2.64
Axles E to F Spacing (ft)	182	3.4	23.9	10.05	8.20

**TABLE C.16 Night Peak Period Final Distributions**

	<b>N</b>	<b>Minimum</b>	<b>Maximum</b>	<b>Mean</b>	<b>Std. Dev.</b>
Total Weight (lb)	61,958	8,000	126,700	51,502.63	20,791.56
Axle A Weight (lb)	61,958	2,700	27,700	10,052.34	2,019.92
Axle B Weight (lb)	61,958	1,700	32,800	11,781.95	4,341.91
Axle C Weight (lb)	56,868	900	26,300	11,364.92	4,112.90
Axle D Weight (lb)	53,699	1,000	30,500	11,122.59	4,583.11
Axle E Weight (lb)	51,421	900	36,100	11,308.22	4,661.95
Axle F Weight (lb)	1,455	800	25,300	8,824.19	3,669.08
Total Spacing (ft)	61,958	11.0	79.6	53.20	14.50
Axles A to B Spacing (ft)	61,958	10.0	33.5	16.37	2.95
Axles B to C Spacing (ft)	56,868	2.5	43.4	6.26	6.08
Axles C to D Spacing (ft)	53,699	2.1	45.8	29.76	8.19
Axles D to E Spacing (ft)	51,421	2.0	25.8	5.83	4.67
Axles E to F Spacing (ft)	1,455	3.4	25.5	19.43	6.38

**TABLE C.17 Group A Final Distributions—Night Peak Period**

	<b>N</b>	<b>Minimum</b>	<b>Maximum</b>	<b>Mean</b>	<b>Std. Dev.</b>
Total Weight (lb)	4,849	8,000	45,800	13,046.44	5,873.19
Axle A Weight (lb)	4,849	2,700	17,400	5,694.49	2,022.30
Axle B Weight (lb)	4,849	2,200	32,800	7,351.95	4,210.64
Total Spacing (ft)	4,849	11.0	23.6	15.07	3.34
Axles A to B Spacing (ft)	4,849	11.0	23.6	15.07	3.34

**TABLE C.18 Group B Final Distributions—Night Peak Period**

	<b>N</b>	<b>Minimum</b>	<b>Maximum</b>	<b>Mean</b>	<b>Std. Dev.</b>
Total Weight (lb)	5,687	8,000	69,300	30,346.30	12,182.88
Axle A Weight (lb)	5,687	2,700	21,100	9,310.66	2,941.96
Axle B Weight (lb)	5,687	1,700	27,100	11,140.34	5,606.04
Axle C Weight (lb)	5,446	900	23,100	7,515.00	4,128.40
Axle D Weight (lb)	2,277	1,000	26,500	6,740.40	3,986.87
Total Spacing (ft)	5,687	13.9	64.6	33.56	12.02
Axles A to B Spacing (ft)	5,687	10.0	33.5	17.35	4.61
Axles B to C Spacing (ft)	5,446	2.5	43.4	13.02	12.11
Axles C to D Spacing (ft)	2,277	2.1	44.0	9.33	10.56

**TABLE C.19 Group C Final Distributions—Night Peak Period**

	<b>N</b>	<b>Minimum</b>	<b>Maximum</b>	<b>Mean</b>	<b>Std. Dev.</b>
Total Weight (lb)	51,422	11,000	126,700	57,468.75	16,632.61
Axle A Weight (lb)	51,422	2,700	27,700	10,545.30	1,216.03
Axle B Weight (lb)	51,422	2,100	26,800	12,270.65	3,928.51
Axle C Weight (lb)	51,422	1,300	26,300	11,772.66	3,894.44
Axle D Weight (lb)	51,422	1,100	30,500	11,316.63	4,510.37
Axle E Weight (lb)	51,421	900	36,100	11,308.22	4,661.95
Axle F Weight (lb)	1,455	800	25,300	8,824.19	3,669.08
Total Spacing (ft)	51,422	25.0	79.6	58.97	4.78
Axles A to B Spacing (ft)	51,422	10.0	24.8	16.38	2.61
Axles B to C Spacing (ft)	51,422	2.9	39.3	5.54	4.47
Axles C to D Spacing (ft)	51,422	2.3	45.8	30.67	6.77
Axles D to E Spacing (ft)	51,421	2.0	25.8	5.83	4.67
Axles E to F Spacing (ft)	1,455	3.4	25.5	19.43	6.38

**APPENDIX D**  
**MICROSCOPIC TRAFFIC SIMULATION**

### D.1 IH-10 Houston, Texas, Test Network

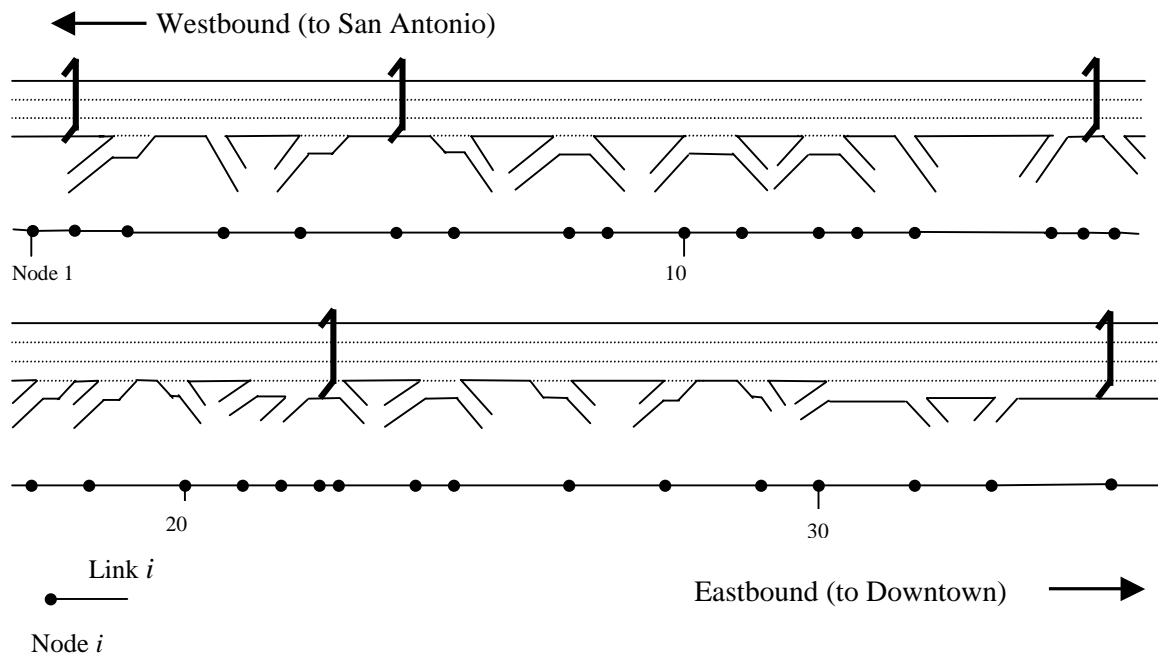


FIGURE D.1 Detailed layout of the IH-10 Houston, Texas, test network

TABLE D.1 Link and Node Data for IH-10 Houston, Texas, Test Network

Node <i>i</i>	Model Node	Attribute	Link <i>i</i>	Length (ft)	Node <i>i</i>	Model Node	Attribute	Link <i>i</i>	Length (ft)
1	11	Mainline	1	635	18	25	On-ramp	18	3,602
2	711	AVI Sta.	2	3,384	19	26	On-ramp	19	1,647
3	12	On-ramp	3	10,089	20	27	Off-ramp	20	1,545
4	13	Off-ramp	4	2,572	21	28	On-ramp	21	2,264
5	14	On-ramp	5	4,811	22	29	On-ramp	22	1,582
6	714	AVI Sta.	6	1,160	23	729	AVI Sta.	23	65
7	15	Off-ramp	7	2,251	24	30	Off-ramp	24	1,854
8	16	On-ramp	8	1,532	25	31	On-ramp	25	1,440
9	17	Off-ramp	9	2,251	26	32	Off-ramp	26	3,294
10	18	On-ramp	10	2,766	27	33	Off-ramp	27	2,057
11	19	Off-ramp	11	2,251	28	34	On-ramp	28	2,779
12	20	On-ramp	12	2,044	29	35	Off-ramp	29	823
13	21	Off-ramp	13	4,104	30	36	On-ramp	30	2,057
14	22	Off-ramp	14	709	31	37	Off-ramp	31	2,887
15	23	On-ramp	15	200	32	38	On-ramp	32	4,128
16	723	AVI Sta.	16	315	33	738	AVI Sta.	33	505
17	24	Off-ramp	17	925	34	39	Mainline	-	-

**TABLE D.2 Observed Link Volume Data for IH-10 Houston, Texas, Test Network**

<b>Link <i>i</i></b>	<b>Attribute</b>	<b>AM Peak</b>	<b>Off Peak</b>	<b>PM Peak</b>
1	Mainline	4,735	3,227	4,149
2	AVI Station	4,735	3,227	4,149
3	On-ramp	5,674	3,796	4,900
4	Off-ramp	4,954	2,960	3,906
5	On-ramp	6,268	4,468	5,549
6	AVI Station	6,268	4,468	5,549
7	Off-ramp	5,770	4,206	5,127
8	On-ramp	6,705	4,450	5,410
9	Off-ramp	6,045	4,106	4,813
10	On-ramp	7,004	5,077	6,069
11	Off-ramp	6,590	4,814	5,532
12	On-ramp	7,328	5,483	6,461
13	Off-ramp	6,487	4,563	5,776
14	Off-ramp	4,698	3,562	3,974
15	On-ramp	5,349	4,208	4,570
16	AVI Station	5,349	4,208	4,570
17	Off-ramp	3,566	3,382	3,727
18	On-ramp	4,455	4,083	4,817
19	On-ramp	5,360	5,085	5,852
20	Off-ramp	4,536	4,406	5,089
21	On-ramp	5,644	5,672	6,249
22	On-ramp	6,402	6,134	6,785
23	AVI Station	6,402	6,134	6,785
24	Off-ramp	6,144	5,156	6,095
25	On-ramp	7,473	5,903	6,935
26	Off-ramp	6,836	5,230	6,237
27	Off-ramp	6,332	4,715	5,645
28	On-ramp	7,577	5,426	6,516
29	Off-ramp	7,458	5,175	6,242
30	On-ramp	9,029	5,818	6,921
31	Off-ramp	8,683	5,103	6,304
32	On-ramp	9,686	5,766	6,954
33	AVI Station	9,686	5,766	6,954

## D.2 US 290 Houston, Texas Test Network

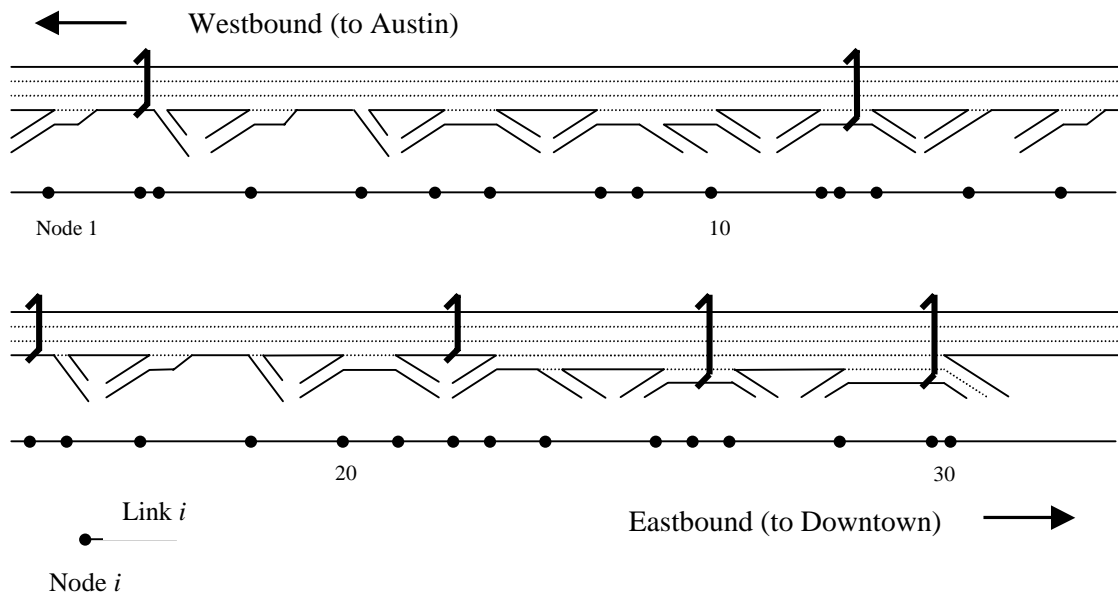


FIGURE D.2 Detailed layout of the US 290 Houston, Texas, test network

TABLE D.3 Link and Node Data for US 290 Houston, Texas, Test Network

Node $i$	Model Node	Attribute	Link $i$	Length (ft)	Node $i$	Model Node	Attribute	Link $i$	Length (ft)
1	10	On-ramp	1	5,238	16	725	AVI Sta.	16	771
2	723	AVI Sta.	2	1,595	17	23	Off-ramp	17	1,399
3	11	Off-ramp	3	301	18	24	On-ramp	18	3,242
4	12	On-ramp	4	2,936	19	25	Off-ramp	19	1,853
5	13	Off-ramp	5	2,751	20	26	On-ramp	20	4,784
6	14	On-ramp	6	5,982	21	27	Off-ramp	21	2,001
7	15	Off-ramp	7	1,880	22	726	AVI Sta.	22	1,774
8	16	On-ramp	8	3,981	23	28	On-ramp	23	5,634
9	17	Off-ramp	9	1,980	24	29	Off-ramp	24	2,159
10	18	Off-ramp	10	4,646	25	30	On-ramp	25	4,488
11	19	On-ramp	11	1,716	26	727	AVI Sta.	26	634
12	724	AVI Sta.	12	591	27	31	Off-ramp	27	1,262
13	20	Off-ramp	13	612	28	32	On-ramp	28	2,402
14	21	On-ramp	14	1,584	29	728	AVI Sta.	29	1,968
15	22	On-ramp	15	5,280	30	33	Off-ramp	30	117

**TABLE D.4** Observed Link Volume Data for US 290 Houston, Texas, Test Network

<b>Link <i>i</i></b>	<b>Attribute</b>	<b>AM Peak</b>
1	On-ramp	4,765
2	AVI Station	4,765
3	Off-ramp	4,210
4	On-ramp	5,844
5	Off-ramp	5,139
6	On-ramp	5,880
7	Off-ramp	5,491
8	On-ramp	6,939
9	Off-ramp	6,254
10	Off-ramp	4,440
11	On-ramp	5,396
12	AVI Station	5,396
13	Off-ramp	3,490
14	On-ramp	4,048
15	On-ramp	4,922
16	AVI Station	4,922
17	Off-ramp	4,626
18	On-ramp	5,400
19	Off-ramp	4,731
20	On-ramp	5,593
21	Off-ramp	4,850
22	AVI Station	4,850
23	On-ramp	6,299
24	Off-ramp	5,858
25	On-ramp	6,968
26	AVI Station	6,968
27	Off-ramp	6,094
28	On-ramp	7,161
29	AVI Station	7,161
30	Off-ramp	7,161

### D.3 IH-10 Houston, Texas, CORSIM Input File (AM Peak Period)

**TABLE D.5 IH-10 Houston, Texas, CORSIM Input File (AM Peak Period)**

```

FRESIM Model of I-10 EB Houston, Texas                                00
AM Peak - AVI OD - Calibration Model - 3% Trucks                    I10AAC3.trf 00
Record Types 50 and 71 calibrated based on actual conditions        00
Grant Schultz                                07 102003 TTI TransLink    0001 01
      1    0      60      7981      21      80700      7781      7581 02
3600                                          04
                                          0I10AAC 05
8011 11 711      0 3                                1          19
8112 112 12      1 1                                1          19
8114 114 14      1 1                                1          19
8116 116 16      1 1                                1          19
8118 118 18      1 1                                1          19
8120 120 20      1 1                                1          19
8123 123 23      1 1                                1          19
8125 125 25      1 1                                1          19
8126 126 26      1 1                                1          19
8128 128 28      1 1                                1          19
8129 129 29      1 1                                1          19
8131 131 31      1 1                                1          19
8134 134 34      1 1                                1          19
8136 136 36      1 1                                1          19
8138 138 38      1 1                                1          19
      11 711 12 6350 3                                1          19
      711 12 13 33840 3                                1          19
      12 13 14100890 3 91 810 92 154                1 9          19
      13 14 714 25720 3                                1          19
      14 714 15 48110 3 91 525                        1          19
      714 15 16 11600 3 92 181                        1 9          19
      15 16 17 22510 3                                1          19
      16 17 18 15320 3 93 1532                        1 9          19
      17 18 19 22510 3                                1          19
      18 19 20 27660 3 93 2766                        1 9          19
      19 20 21 22510 3                                1          19
      20 21 22 20440 3 93 2044                        1 9          19
      21 22 23 41040 3 92 80                          1 9          19
      22 23 723 7090 3                                1          19
      23 723 24 2000 3 91 200                          1          19
      723 24 25 3150 3 92 80                          1 9          19
      24 25 26 9250 3                                1          19
      25 26 27 36020 3 91 174                          1 9          19
      26 27 28 16470 3 91 150 92 174                1 9          19
      27 28 29 15450 3                                1          19
      28 29 729 22640 4 91 150                        1          19
      29 729 30 15820 4 91 150                        1          19
      729 30 31 650 3 92 65                          1 9          19
      30 31 32 18540 3                                1          19
      31 32 33 14400 3 93 1440                        1 9          19
      32 33 34 32940 3 92 80                          1 9          19
      33 34 35 20570 3                                1          19
      34 35 36 27790 3 91 150 92 86                  1 9          19
      35 36 37 8230 3                                1          19
      36 37 38 20570 4 91 150 92 80                  1 9          19
      37 38 738 28870 4                                1          19
      38 738 39 41280 4 91 150                        1 9          19
      738 398039 5050 4                                1          19
      112 12 13 3611 1                                9          19

```

**TABLE D.5** Continued

114	14	714	5971	1	9	19
116	16	17	2691	1	9	19
118	18	19	3051	1	9	19
120	20	21	2001	1	9	19
123	23	723	3181	1	9	19
125	25	26	6331	1	9	19
126	26	27	6761	1	9	19
128	28	29	4001	1	9	19
129	29	729	2101	1	9	19
131	31	32	2101	1	9	19
134	34	35	1311	1	9	19
136	36	37	1741	1	9	19
138	38	738	2661	1	9	19
13	1138113		6201	1	1	19
15	1158115		5251	1	1	19
17	1178117		4921	1	1	19
19	1198119		2001	1	1	19
21	1218121		4761	1	1	19
22	1228122		7551	1	1	19
24	1248124		6331	1	1	19
27	1278127		4921	1	1	19
30	1308130		2101	1	1	19
32	1328132	16401	1	1	1	19
33	1338133	1311	1	1	1	19
35	1358135	2101	1	1	1	19
37	1378137	1801	1	1	1	19
8011	11	0	0	0	31060	20
8112	112	0	0	0	31060	20
8114	114	0	0	0	31060	20
8116	116	0	0	0	31060	20
8118	118	0	0	0	31060	20
8120	120	0	0	0	31060	20
8123	123	0	0	0	31060	20
8125	125	0	0	0	31060	20
8126	126	0	0	0	31060	20
8128	128	0	0	0	31060	20
8129	129	0	0	0	31060	20
8131	131	0	0	0	31060	20
8134	134	0	0	0	31060	20
8136	136	0	0	0	31060	20
8138	138	0	0	0	31060	20
11	711	0	0	0	31065	20
711	12	0	0	0	31065	20
12	13	0	0	0	31065	5500
13	14	0	0	0	31065	20
14	714	0	0	0	31065	20
714	15	0	0	0	31065	5971
15	16	0	0	0	31065	20
16	17	0	0	0	31065	1100
17	18	0	0	0	31065	20
18	19	0	0	0	31065	2500
19	20	0	0	0	31065	20
20	21	0	0	0	31065	1100
21	22	0	0	0	31065	2500
22	23	0	0	0	31065	20
23	723	0	0	0	31065	20
723	24	0	0	0	31065	2500
24	25	0	0	0	31065	20
25	26	0	0	0	31065	20
26	27	0	0	0	31060	1600
27	28	0	0	0	31060	20
28	29	0	0	0	31060	20

TABLE D.5 Continued

29	729	0	0	0	31060		20	
729	30	0	0	0	31060	2500	20	
30	31	0	0	0	31060		20	
31	32	0	0	0	31060	1400	20	
32	33	0	0	0	31060	2500	20	
33	34	0	0	0	31060		20	
34	35	0	0	0	31060	2500	20	
35	36	0	0	0	31060		20	
36	37	0	0	0	31060	2000	20	
37	38	0	0	0	31060		20	
38	738	0	0	0	31060		20	
738	39	0	0	0	31060		20	
112	12	0	0	0	31060		20	
114	14	0	0	0	31060		20	
116	16	0	0	0	31060		20	
118	18	0	0	0	31060		20	
120	20	0	0	0	31060		20	
123	23	0	0	0	31060		20	
125	25	0	0	0	31060		20	
126	26	0	0	0	31060		20	
128	28	0	0	0	31060		20	
129	29	0	0	0	31060		20	
131	31	0	0	0	31060		20	
134	34	0	0	0	31060		20	
136	36	0	0	0	31060		20	
138	38	0	0	0	31045		20	
13	113	0	0	0	31045		20	
15	115	0	0	0	31045		20	
17	117	0	0	0	31045		20	
19	119	0	0	0	31045		20	
21	121	0	0	0	31045		20	
22	122	0	0	0	31045		20	
24	124	0	0	0	31045		20	
27	127	0	0	0	31045		20	
30	130	0	0	0	31045		20	
32	132	0	0	0	31045		20	
33	133	0	0	0	31045		20	
35	135	0	0	0	31045		20	
37	137	0	0	0	31045		20	
12	13	144954	113	720			25	
714	15	165770	115	498			25	
16	17	186045	117	660			25	
18	19	206590	119	414			25	
20	21	226487	121	841			25	
21	22	234698	122	1789			25	
723	24	253566	124	1783			25	
26	27	284536	127	824			25	
729	30	316144	130	258			25	
31	32	336836	132	637			25	
32	33	346332	133	504			25	
34	35	367458	135	119			25	
36	37	388683	137	346			25	
27	28	1	1	1544			32	
29	729	2	1	15802000			32	
35	36	1	1	820			32	
8011	114735	3			33	33	34	50
8112	112	939	3		100			50
8114	1141314	3			100			50
8116	116	935	3		100			50
8118	118	959	3		100			50
8120	120	738	3		100			50
8123	123	651	3		100			50



**TABLE D.5** Continued

116	24	33	74
116	27	15	74
116	30	2	74
116	32	4	74
116	33	3	74
116	35	1	74
116	37	2	74
118	19	0	74
118	21	0	74
118	22	0	74
118	24	33	74
118	27	15	74
118	30	2	74
118	32	4	74
118	33	3	74
118	35	1	74
118	37	2	74
120	21	0	74
120	22	0	74
120	24	33	74
120	27	15	74
120	30	2	74
120	32	4	74
120	33	3	74
120	35	1	74
120	37	2	74
123	24	33	74
123	27	15	74
123	30	2	74
123	32	4	74
123	33	3	74
123	35	1	74
123	37	2	74
125	27	0	74
125	30	5	74
125	32	11	74
125	33	9	74
125	35	2	74
125	37	6	74
126	27	0	74
126	30	5	74
126	32	11	74
126	33	9	74
126	35	2	74
126	37	6	74
128	30	5	74
128	32	11	74
128	33	9	74
128	35	2	74
128	37	6	74
129	30	4	74
129	32	11	74
129	33	9	74
129	35	2	74
129	37	6	74
131	32	0	74
131	33	0	74
131	35	0	74
131	37	0	74
134	35	0	74
134	37	0	74
136	37	0	74

**TABLE D.5** Continued

11	100	4000	170
711	735	4000	195
112	3772	3900	195
12	4119	4000	195
13	14208	4000	195
113	14820	3900	195
114	16191	3900	195
14	16780	4000	195
714	21591	4000	195
15	22751	4000	195
115	23266	3900	195
116	24765	3900	195
16	25015	4000	195
17	26560	4000	195
117	27046	3900	195
118	28536	3900	195
18	28824	4000	195
19	31608	4000	195
119	31776	3900	195
120	33694	3900	195
20	33867	4000	195
21	35924	4000	195
121	36389	3900	195
22	40041	4000	195
122	40780	3900	195
123	40461	3900	195
23	40763	4000	195
723	40923	4000	195
24	41278	4000	195
124	41903	3900	195
125	41578	3900	195
25	42203	4000	195
126	45154	3900	195
26	45823	4000	195
27	47470	4000	195
127	47952	3900	195
128	48626	3900	195
28	49015	4000	195
129	51094	3900	195
29	51279	4000	195
729	52861	4000	195
30	52926	4000	195
130	53111	3900	195
131	54595	3900	195
31	54780	4000	195
32	56220	4000	195
132	57857	3900	195
33	59514	4000	195
133	59599	3900	195
134	61486	3900	195
34	61571	4000	195
35	64350	4000	195
135	64535	3900	195
136	65031	3900	195
36	65173	4000	195
37	67230	4000	195
137	67380	3900	195
138	69871	3900	195
38	70117	4000	195
738	74245	4000	195
39	74750	4000	195
1			210

**APPENDIX E**  
**SENSITIVITY ANALYSIS RESULTS**

### E.1 IH-10 Houston, Texas, Test Network—Constant Growth Analysis

**TABLE E.1 S157, IH-610, 0.7 Miles West of IH-45, AADT Percent Variation by Year**

YEAR	AADT	Previous Year												
		1988	1989	1990	1991	1992	1993	1994	1995	1996	1997	1998	1999	2000
1988	152,298													
1989	159,963	5.0												
1990	162,546	6.7	1.6											
1991	165,144	8.4	3.2	1.6										
1992	163,236	7.2	2.0	0.4	-1.2									
1993	168,508	10.6	5.3	3.7	2.0	3.2								
1994	173,736	14.1	8.6	6.9	5.2	6.4	3.1							
1995	178,882	17.5	11.8	10.1	8.3	9.6	6.2	3.0						
1996	186,653	22.6	16.7	14.8	13.0	14.3	10.8	7.4	4.3					
1997	190,431	25.0	19.0	17.2	15.3	16.7	13.0	9.6	6.5	2.0				
1998	196,650	29.1	22.9	21.0	19.1	20.5	16.7	13.2	9.9	5.4	3.3			
1999	197,239	29.5	23.3	21.3	19.4	20.8	17.1	13.5	10.3	5.7	3.6	0.3		
2000	199,061	30.7	24.4	22.5	20.5	21.9	18.1	14.6	11.3	6.6	4.5	1.2	0.9	
2001	190,821	25.3	19.3	17.4	15.5	16.9	13.2	9.8	6.7	2.2	0.2	-3.0	-3.3	-4.1

#### E.1.1 Growth Rate Calculation

$$\text{Average Straight Line Growth 1988 to 2001} = \frac{25.3\%}{13 \text{ years}} = 1.95 \text{ percent per year.}$$

**TABLE E.2 2010 Link Volume Data for IH-10 Houston, Texas, Test Network**

Link <i>i</i>	AM Peak	Off Peak	Link <i>i</i>	AM Peak	Off Peak	Link <i>i</i>	AM Peak	Off Peak
1	6,061	4,131	12	9,380	7,018	23	8,195	7,852
2	6,061	4,131	13	8,303	5,841	24	7,864	6,600
3	7,263	4,859	14	6,013	4,559	25	9,565	7,556
4	6,341	3,789	15	6,847	5,386	26	8,750	6,694
5	8,023	5,719	16	6,847	5,386	27	8,105	6,035
6	8,023	5,719	17	4,564	4,329	28	9,699	6,945
7	7,386	5,384	18	5,702	5,226	29	9,546	6,624
8	8,582	5,696	19	6,861	6,509	30	11,557	7,447
9	7,738	5,256	20	5,806	5,640	31	11,114	6,532
10	8,965	6,499	21	7,224	7,260	32	12,398	7,380
11	8,435	6,162	22	8,195	7,852	33	12,398	7,380

## VITA

**GRANT GEORGE SCHULTZ**  
 Brigham Young University  
 Department of Civil and Environmental Engineering  
 368 Clyde Building  
 Provo, Utah 84602

### Education

Ph.D., Civil Engineering, Texas A&M University, December 2003  
 M.S., Civil Engineering, Brigham Young University, April 1995  
 B.S., Civil Engineering, Brigham Young University, April 1994

### Selected Academic Awards/Honors

SWUTC Regional Outstanding Doctoral Student, 2002  
 SWUTC Ph.D. Student of the Year in Transportation, Texas A&M University, 2002  
 Eno Transportation Foundation Leadership Development Training Fellow, 2002  
 Academic Excellence Award Recipient, Texas A&M University, 2002-2003  
 American Public Transportation Foundation (APTF) Jack R. Gilstrap Scholarship, 2001  
 APTF Continuing Student Scholarship, 2002-2003  
 President, Institute of Transportation Engineers Student Chapter, Texas A&M University, 2002  
 Outstanding Student, Institute of Transportation Engineers District 9 (TexITE), 2002  
 Advanced Institute in Transportation Ph.D. Fellowship, Texas A&M University, 2001-2002

### Research Experience

Graduate Research Assistant, Texas Transportation Institute, January 2001 to December 2003  
 Graduate Research Assistant, Brigham Young University, September 1994 to May 1995

### Professional Experience

The Sear-Brown Group, Salt Lake City, Utah, July 1996 to December 2000  
 Keller Associates, Inc., Boise, Idaho, May 1995 to July 1996  
 Utah Department of Transportation, Salt Lake City, Utah, April 1994 to September 1994

### Honor Society and Professional Memberships

Sigma Xi, The Scientific Research Society, Texas A&M University, Associate Member  
 Chi Epsilon, National Civil Engineering Honor Society, Texas A&M University, Member  
 Tau Beta Pi, National Engineering Honor Society, Brigham Young University, Member  
 Golden Key National Honor Society, Brigham Young University, Member  
 Institute of Transportation Engineers (ITE), Member  
 American Society of Civil Engineers (ASCE), Associate Member

### Professional Registration

Professional Engineer (P.E.), Utah License #: 98-264949-2202  
 Professional Traffic Operations Engineers (PTOE), Transportation Certification Board, #530